Dissertation

Quasiparticle pictures and graphs - from perturbative to non-perturbative linked-cluster expansions

by
Kris Cöster
from Kleve

submitted for the degree of
Doctor rerum naturalium (Dr. rer. nat.)
of the Faculty of Physics, TU Dortmund University

Dortmund, December 2015

Contact to the author: kris.coester@tu-dortmund.de

First reviewer: Dr. Kai P. Schmidt
Second reviewer: Prof. Dr. Frithjof Anders

Contents

Publikationen

Teilpublikationen:

- Tao Hong, K. P. Schmidt, K. Coester, F. F. Awwadi, M. M. Turnbull, Y. Qiu, J. A. Rodriguez-Rivera, M. Zhu, X. Ke, C. P. Aoyama, Y. Takano, Huibo Cao, W. Tian, J. Ma, R. Custelcean, H. D. Zhou, and M. Matsuda
  Magnetic ordering induced by interladder coupling in the spin-1/2 Heisenberg two-leg ladder antiferromagnet C9H18N2CuBr4
  Physical Review B **89**, 174432 (2014)

- K. Coester, S. Clever, F. Herbst, S. Capponi, and K.P. Schmidt, A generalized perspective on non-perturbative linked-cluster expansions
  European Physics Letters **110**, 20006 (2015), Editors choice

- K. Coester and K.P. Schmidt, Optimizing linked-cluster expansions by white graphs
  Physical Review E **92**, 022118 (2015)

Liste weiterer Publikationen:

- M. Powalski, K. Coester, R. Moessner, and K. P. Schmidt, Disorder by disorder and flat bands in the kagome transverse field Ising model
  Physical Review B **87**, 054404 (2013)

- K. Coester, W. Malitz, S. Fey, and K.P. Schmidt, Quantum disorder and local modes of the fully-frustrated transverse field Ising model on a diamond chain
  Physical Review B **88**, 184402 (2013)

- D.G. Joshi, K. Coester, K. P. Schmidt, and Matthias Vojta, Non-linear bond-operator theory and 1/d expansion for coupled-dimer magnets I: Paramagnetic phase
  Physical Review B **91**, 094404 (2015)

Abstract

A fundamental principle in condensed matter physics is the effective description in terms of quasiparticles. The high-energy part of the system is accounted for by renormalized properties of the quasiparticles, providing both, an accurate description and interpretation of the relevant low-energy physics. We consider two classes of methods suited to provide effective quasiparticle descriptions in the thermodynamic limit: (non-perturbative) linked-cluster expansions ((N)LCEs) and continuous unitary transformations (CUTs). We focus specifically on the combination of both methods, providing a different perspective and solutions to existing challenges.
LCEs provide high-order series expansions in a perturbation parameter, by combining effective Hamiltonians determined on finite clusters. We introduce a white-graph expansion for the method of perturbative continuous unitary transformations when implemented as an LCE. The essential idea behind an expansion in white graphs is to perform an optimized bookkeeping during the calculation by exploiting the model-independent effective Hamiltonian in second quantization and the associated inherent cluster additivity. This approach is shown to be especially well suited for microscopic models with many coupling constants, since the total number of relevant graphs is drastically reduced. The white-graph expansion is exemplified for a two-dimensional quantum spin model, illustrating its efficiency.
In NLCEs, the perturbative treatment of finite clusters is replaced by a numerical exact (block) diagonalization. While LCEs are restricted due to their perturbative nature, the non-perturbative variant is not. In graph-based continuous unitary transformations (gCUTs), the block diagonalization is achieved by a non-perturbative CUT performed on finite clusters. The central objective of this thesis is a modification of the gCUT scheme, allowing to treat two kinds of major issues, denoted by pseudo and genuine decay, occuring for NLCEs due to the non-perturbative treatment of clusters.
Indeed, one finds surprising effects caused by the non-perturbative renormalization. In particular, we identify a fundamental challenge for any non-perturbative approach based on finite clusters resulting from the reduced symmetry on graphs, most importantly the breaking of translational symmetry when targeting the properties of excited states. This can be traced back to the appearance of intruder states in the low-energy spectrum, which represent a major obstacle in quasi-degenerate perturbation theory. Here, a generalized notion of cluster additivity is introduced, which is used to formulate an optimized scheme of gCUTs, allowing to solve and to physically understand this major issue. Most remarkably, our improved scheme demands to go beyond the paradigm of using the exact eigenvectors on graphs. We demonstrate that the modified scheme is correct in the non-perturbative regime.
Even at quantum criticality, the scheme gives valid results. To determine the critical behavior, one must rely on extrapolation schemes. We introduce a generic approach to extract critical properties from sequences of numerical data which is directly relevant for NLCEs. The scheme is applied to the quantum phase transition between the dimerized and the isotropic spin 1/2 Heisenberg chain.
Finally, we investigate a scenario where the gapped quasiparticle excitation is not stable for all momenta, i.e., the one-particle mode merges with the continuum for certain momenta and one observes quasiparticle decay. In this case, intruder states merging with the low-energy spectrum on finite clusters represent genuine physics of the system. Again, a proper renormalization on

finite clusters satisfies the generalized cluster additivity. Our adjusted renormalization approach performed on finite clusters does not necessarily lead to a full decoupling of the quasiparticle subspaces and the remaining interactions are part of the effective description. The resulting effective Hamiltonian can be analyzed to describe quasiparticle decay in the thermodynamic limit. The modified scheme is applied to four-leg spin 1/2 Heisenberg ladders, providing insights into the spectral properties.
Overall, this thesis presents several important developments for the derivation of effective quasiparticle pictures in quantum spin models via perturbative and non-perturbative LCEs, opening various opportunities for future investigations.

Kurze Zusammenfassung

Ein fundamentales Prinzip in der Physik kondensierter Materie ist die effektive Beschreibung anhand von Quasiteilchen. Dem Hochenergie-Anteil des Systems wird durch renormalisierte Eigenschaften der Quasiteilchen Rechnung getragen, was sowohl zu einer akkuraten Beschreibung als auch zu einer direkten Interpretation der relevanten Niederenergiephysik führt. Zwei Methodenklassen stehen im Zentrum dieser Arbeit: (nicht-perturbative) linked-cluster Enwicklungen {*Englisch:* (non-perturbative) linked-cluster expansions ((N)LCEs)} und kontinuierliche unitäre Transformationen {*Englisch:* continuous unitary transformations (CUTs)}. Ziel dieser Arbeit ist es, durch die Kombination beider Methodenklassen einen neuen Blickwinkel und Lösungen aktueller Problemfelder zu bieten.
Durch Kombinationen effektiver Hamiltonians, die auf endlichen Clustern bestimmt werden, lässt sich in LCEs eine Hochordnungsreihentwicklung bestimmen. Wir führen für die Anwendung der perturbativen kontinuierlichen unitären Transformationen im Rahmen einer LCE eine Weiß-Graph Entwicklung ein. Die grundlegende Idee einer solchen Entwicklung ist eine optimierte Buchhaltung während der Rechnung. Hierbei werden der modellunabhängige effektive Hamiltonian in zweiter Quantisierung und die damit verknüpfte Cluster-Additivität direkt ausgenutzt. Wir zeigen, dass dieser Ansatz besonders dann effizient ist, wenn das mikroskopische Modell mehrere Kopplungskonstanten aufweist, da sich dadurch die Zahl der relevanten Graphen drastisch reduzieren lässt. Die Weiß-Graph Entwicklung und deren Effizienz werden anhand eines zwei-dimensionalen Quanten-Spin Modells verdeutlicht.
In NLCEs wird die perturbative Berechnung auf endlichen Graphen durch eine nicht-perturbative (Block)-Diagonalisierung ersetzt. Daher ist diese Entwicklung nicht durch einen perturbativen Parameter beschränkt. Bei graphen-basierten kontinuierlichen unitären Transformationen {*Englisch:* graph-based continuous unitary transformations (gCUTs)} wird die Blockdiagonalisierung durch eine nicht-perturbative CUT erreicht. Nicht-perturbative Effekte führen hierbei zu zwei Problemfeldern, dem künstlichen und dem echten Zerfall. Die zentrale Zielsetzung dieser Arbeit ist es, die gCUT-Methode derart zu modifizieren, dass beide Fälle behandelt werden können.
Durch die nicht-perturbative Renormierung enstehen erstaunliche Effekte. Wir zeigen ein grundlegendes Problem bei der Bestimmung von Eigenschaften angeregter Zustände auf, das durch die gebrochene Translationssymmetrie entsteht. Dies lässt sich auf Zustände, sogenannte Eindringlinge, im Niederenergiespektrum zurückführen, was ein wesentliches Problem in quasi-entarteter Störungsrechnung darstellt. Ein verallgemeinertes Konzept der Cluster-Additivität wird eingeführt, mittels dessen sich dieses Problem lösen und auch physikalisch verstehen lässt. Bemerkenswerterweise ist es hierbei nötig, sich über das Paradigma exakter Eigenvektoren auf Graphen hinwegzusetzen. Es wird gezeigt, dass das modifizierte Schema selbst im nicht-perturbativen Regime korrekte Ergebnisse liefert.
Selbst bei Quanten-Kritikalität liefert das neue Schema valide Resultate. Um kritisches Verhalten bestimmen zu können, müssen Extrapolations-Methoden verwendet werden. Wir führen einen allgemeinen Ansatz zur Bestimmung kritischer Eigenschaften aus numerischen Sequenzen, wie sie in NLCEs vorliegen, ein. Dieses neue Schema wird zur Bestimmung des Quanten-Phasen-Übergangs zwischen der dimerisierten und der isotropen Spin 1/2 Heisenberg-Kette angewendet.
Zum Schluss untersuchen wir den Fall eines Systems mit Anregungslücke, dessen Quasiteilchen

Anregung nicht für alle Impulse stabil ist, d.h., die Ein-Teilchen Mode mischt in das Mehrteilchen-Kontinuum für bestimmte Impulse und es entsteht Quasiteilchen-Zerfall. In diesem Fall spiegeln die Eindringlinge im Niederenergiespektrum echte Physik wider. Wiederum genügt eine angemessene Renormalisierung der verallgemeinerten Cluster-Additivität. Der angepasste Renormalisierungs-Ansatz führt nun nicht mehr zu einer Entkopplung der Quasiteilchen-Unterräume und die verbleibende Wechselwirkung ist Teil der effektiven Beschreibung. Der entstehende effektive Hamiltonian kann analysiert werden, um Quasiteilchen-Zerfall im thermodynamischen Limes zu beschreiben. Der so modifizierte Ansatz wird für die Spin 1/2 Vierbein-Leiter verwendet, um die spektralen Eigenschaften zu bestimmen.
Zusammengefasst werden in dieser Arbeit verschiedene wichtige Entwicklungen zur Bestimmung von effektiven Quasiteilchen-Bildern in Quanten-Spin Modellen mittels perturbativer und nicht-perturbativer LCEs dargestellt. Hierdurch eröffnen sich vielfältige Möglichkeiten für zukünftige Untersuchungen.

Chapter 1

Introduction

When your only tool is a hammer, everything looks like a nail.

- Daniel Dennett

A fundamental challenge in condensed matter theory is the description of strongly-correlated quantum lattice models. Here, correlations and collective behavior play a central role making it notoriously hard to find an adequate description. Besides the development of analytical tools, these challenges lead to a large treasure of strong numerical tools, which represent a central cornerstone of condensed matter physics by now. Experiments, analytical approaches and numerical techniques cannot be considered as independent branches since they continuously stimulate and complement each other. Therefore, progress in the vast research field of condensed matter physics stems from the combined approach of experiment, analytical descriptions and numerical tools, producing a mutual momentum steadily pushing the limits of our overall understanding of nature.

In physics, a central notion is constituted by the broad concept of quasiparticles, going back to a work by Landau in 1957 [1]. Landau's work initially aimed at the description of liquid ^{3}He at low temperatures via quasi-free fermions with renormalized parameters due to the interaction. The so-called Fermi liquid theory was soon realized to be applicable to other interacting fermion systems, most notably the electrons in a metal. The description of metals by Fermi liquids is so powerful that metals deviating from this behavior are even referred to as non-Fermi liquids [2]. Most importantly, Landau's approach introduces a groundbreaking notion where the collective excitations of the microscopic models can be understood as dressed versions of elementary excitations without interactions. Necessarily, the ground state of the system must be adiabatically connected to the interaction free system. The characterization of low-energy physics, i.e., the ground state, elementary excitations etc., in terms of these quasiparticles is of central importance in condensed matter physics and beyond. If this characterization succeeds, the fundamental mechanisms determining the corresponding physics of the system are understood. Famous examples of this concept in condensed matter physics are for instance lattice vibrations called phonons [3, 4], excitons in semiconductors [5], magnons [6, 7] and triplons [8–10] in quantum magnets as well as orbitons in Mott insulators [11].

This concept and interpretation is primarily associated with perturbative and analytical approaches like diagrammatic techniques, spin wave theory [6, 7] or bond operators [8, 9]. In contrast, numerical techniques often provide plain data of a target quantity which must be interpreted thereafter. This category applies for instance to exact diagonalization, quantum Monte Carlo (QMC) simulations [12, 13] or density matrix renormalization group [14] (DMRG). However, there are numerical techniques where the quasiparticle picture constitutes the starting point of the numerical approach. Such a biased foundation is connected to an unambiguous interpretation of the resulting data in terms of these quasiparticles. Consequently, both classes of approaches can be viewed as complementary tools. In a broader sense, each numerical technique has individual strengths and advantages but also biases, limitations and blind spots.

Consequently, a large arsenal of advanced complementary numerical tools is clearly desirable. In this thesis, we focus on methodological developments of numerical tools yielding effective quasiparticle Hamiltonians in terms of hardcore bosons. For demanding parameter regimes, especially when the quasiparticle picture becomes indistinct, an adequate description via quasiparticles becomes both challenging and interesting in any regard.
By construction, the quasiparticle picture becomes indistinct at quantum criticality. An effective quasiparticle description of the system close to or even at quantum criticality is very demanding, but allows to characterize quantum phase transitions.
Another fascinating scenario where the quasiparticle picture is eroded is the so-called spontaneous quasiparticle decay. Quasiparticle decay was first predicted [15] and experimentally observed [16, 17] for superfluid ^{4}He. Here, an energy-momentum threshold exists where the quasiparticle description breaks down, i.e., the single-particle pole is absent in the Green's function for certain momenta $k > k_c$.
Indeed, similar behavior exists for quantum lattice models. Here, the discrete (bosonic) elementary excitation enters the multi-particle continuum leading to quasiparticle decay for the corresponding momenta, which can be experimentally observed in one-dimensional [18–21] or two-dimensional [22–26] systems. Theoretical approaches to describe quasiparticle decay in quantum magnets range from Fermi's golden rule [27], diagrammatic techniques [28–31], Bethe Ansatz [32], and specifically designed quasiparticle renormalization techniques [33]. These methods are suited to provide a description in terms of the decaying quasiparticle inside the continuum and differ conceptually from other techniques, which can also be applied in this scenario like exact diagonalization techniques [34], quantum Monte Carlo analysis [35] or high-order series expansions [36, 37].
To derive an effective quasiparticle description in challenging regimes defined by quantum-phase transitions or quasiparticle decay, further development of the current numerical approaches is desirable. At the core of our consideration lay two techniques, each applicable for the description in terms of quasiparticles in form of sophisticated effective quasiparticle Hamiltonians: (Numerical) linked-cluster expansions ((N)LCEs) and continuous unitary transformations (CUTs).
CUTs, introduced in 1994 by Wegner [38], are perfectly suited for this purpose since they provide a generic and systematic scheme to perform a unitary transformation, allowing, inter alia, to derive effective Hamiltonians.
Generically, the quasiparticle picture used in the effective description is constituted by one part of the Hamiltonian while the other part can be viewed as a perturbation, coupling the different quasiparticle (QP) channels. The CUT continuously decouples the QP channels which 'dresses' the quasiparticles resulting in an effective description. The decoupled QP blocks can be investigated separately, allowing for an intuitive understanding of the underlying physics in terms of these dressed quasiparticles. Such an effective Hamiltonian provides convenient access to complicated quantities, i.e., one-particle dispersions [39], multi-particle interactions (bound states) and dynamical correlation functions [10, 40–43].
By construction, the application of such a CUT is non-trivial and requires the introduction of reasonable truncations, resulting in different variants of CUTs [39, 44–48]. In contrast to the other CUT variants, both approaches applied in this thesis involve the calculation on finite clusters which is the natural link to (N)LCEs.
In LCEs, high-order series expansions of various physical quantities can be derived directly in the thermodynamic limit by performing calculations on finite systems. The applications of high-order series expansion range from zero-temperature properties like the ground-state energy [49, 50], order parameters, or entanglement entropies [51] to high-temperature expansions, which give access to thermodynamic quantities [52]. Interestingly, it took until 1996 to set up similar expansions for the physical properties of elementary excitations like one-particle dispersions

[53], two-particle interactions [54, 55] or dynamical correlation functions [56, 57], i.e., physical properties which are of direct importance for the interpretation of inelastic neutron or inelastic light scattering experiments.
The usefulness of high-order series expansions is limited due to its perturbative nature. It is therefore desirable to reflect on non-perturbative linked-cluster expansions (NLCEs) [58–62]. The essential idea behind all NLCEs is a non-perturbative treatment of clusters, achieved via an exact (block) diagonalization, yielding results in the thermodynamic limit after an appropriate embedding procedure. Indeed, many exciting developments have been achieved in this direction recently, e.g., the derivation of effective low-energy spin models [46, 63, 64], the calculation of entanglement entropies [65] or the extension to time-dependent quantities out of equilibrium [66, 67]. Recently, NLCEs are introduced to study many-body localization transitions in a disordered system with continuous non-perturbative disorder [68]. Overall, NLCEs are a strong tool for the investigation of quantum lattice models with a vast range of applications without finite-size effects.
The methods applied in this thesis combine the concepts of CUTs and (N)LCEs: The perturbative variant of this approach is given by perturbative continuous unitary transformations (pCUTs) [39] but implemented as an LCE, in other words, the (normal-ordered) effective Hamiltonian is determined on finite clusters via pCUTs and the results are combined to gain the result in the thermodynamic limit.
The non-perturbative variant is called graph-based continuous unitary transformations (gCUTs) introduced by Yang and Schmidt [46] in 2011. Here, the CUT is solved non-perturbatively on finite clusters via a numerical integration on matrix level, yielding an effective cluster-dependent Hamiltonian. Analogously, these results are combined to constitute the effective Hamiltonian in the thermodynamic limit.
The underlying CUT separates the considered approaches from all other (N)LCE approaches in literature. The leading principle of this thesis is to exploit the properties provided by the CUT to develop optimized versions of LCEs/pCUTs and NLCEs/gCUTs, respectively.
Generically, all numerical tools exhibit a systematic truncation parameter, e.g. the perturbation order in high-order series expansions or the considered system sizes in exact diagonalization techniques and NLCE approaches. The size of this parameter is a measure for the fluctuations taken into account and more accuracy is gained by increasing the respective truncation parameter. Consequently, a significant increase in this truncation parameter is a major objective of further developments of a given method. Indeed, developments in this direction represent one central route pursued in this thesis concerning specifically pCUTs/LCEs. The efficiency of all (perturbative) LCEs is based on a topological identification process: If subclusters of the infinite lattice can be mapped onto each other by a simple renumeration of sites, these clusters are topologically identical. Obviously, it suffices to restrict the calculation to topological distinct clusters (graphs), resulting, specifically for more than one dimension, in an extremely effective calculation process.
However, if multiple couplings are present, these couplings inhibit topological equivalence. In these cases, especially relevant for experimental realizations with several coupling constants, the maximally available order is significantly reduced. In this thesis, we introduce another kind of graph expansion, a so-called *white-graph expansion*, which overcomes the latter limitation to a great extent by a fundamental reorganization of the calculation process [69].

Due to the rather recent invention, the room for understanding and developments is considerably larger for NLCEs and gCUTs in particular. In gCUTs, substantial progress is achieved by introducing an efficient truncation scheme on finite clusters. This practically doubles the maximal number of manageable supersites, which represents a remarkable improve-

ment with respect to the exponential scaling of the Hilbert space. Yet, in NLCEs, more decisive and fundamental challenges exist.
One challenge concerns the extrapolation techniques. Powerful extrapolation schemes, corresponding to an extrapolation to an infinite order in the perturbation parameter, exist in the established field of high-order series expansion. These extrapolation schemes represent sophisticated resummation techniques allowing to extract critical properties like critical points and, most importantly, critical exponents. In contrast, NLCEs and all non-perturbative methods provide sequences of data points. While first extrapolation schemes are applied for NLCEs [62, 65], to the best of our knowledge, no similar extrapolation scheme for the extraction of critical exponents is available. That is, no access to these fundamental physical quantities exist. We propose a new extrapolation scheme for NLCE techniques and similar methods. In this scheme, the numerical data points are mapped to a series expansion in a pseudo perturbation parameter. As a result, one can implement the standard series expansion techniques, which gives, as we argue, access to critical points as well as critical exponents.
Both developments aim at a direct or indirect enhancement of the fluctuations included in the final results, which is of obvious interest for all numerical tools. However, this strategy is not a panacea, because it is essential that the *proper* fluctuations are considered. While this statement may appear mundane, the implementation is surprisingly non-trivial. This particularly refers to the derivation of an effective description in terms of quasiparticles in NLCE approaches: while the quasiparticle picture is sharp and well-defined for small values of the couplings, this identification can become ambiguous for larger values of the couplings if there exists an energetic overlap between different quasiparticle sectors on finite clusters. Then, only non-perturbative renormalizations of the initial Hamiltonian are capable of separating the quasiparticle subspaces on finite cluster. The fundamental challenges associated with these scenarios require a reconsideration of the underlying core concepts of NLCE approaches. Remarkably, the nature of such an energetic overlap can be two-kind, leading to two quite distinct central issues:
i) As a core component, all LCEs share that the physical system on clusters has a reduced symmetry compared to the infinite system, e.g. the translational symmetry is broken by construction. For the perturbative LCEs, the full symmetry is nevertheless restored after embedding and exactly the same fluctuations present in the thermodynamic limit are taken into account. However, as we demonstrate in this thesis, this inherent symmetry reduction represents a fundamental challenge for any non-perturbative approach based on finite clusters when calculating excitation energies of elementary excitations. Namely, intruder states enter the low-energy spectrum leading to a break down of the standard approach. This challenge is solved by an adapted version of gCUTs [70]. Fascinatingly, this generalization requires not to use the exact eigenvectors on graphs, revealing once more the non-trivial connection between finite systems and the thermodynamic limit in quantum many-body systems.
ii) A fundamentally different scenario is present if the energetic overlap observed on finite clusters is genuine, i.e., it corresponds to quasiparticle decay in the thermodynamic limit and represents physics of the system. This overlap demands a modified renormalization approach on finite clusters. In 2011, Fischer and Uhrig introduced a CUT suited to describe the system by means of an effective Hamiltonian in terms of the decaying quasiparticles [33]. Our objective is the implementation of a similar approach relying on NLCEs. While the CUT implemented by Fischer and Uhrig is applied in operator space, in gCUTs, the CUT is performed on finite clusters on matrix level. This leads to different challenges but also opportunities, which arise for the treatment of quasiparticle decay via NLCEs. This allows to provide a complementary perspective on this issue.

This thesis is structured as follows:
In chapter 2, the basics of the methods under consideration are described. First, we introduce a setup, defining the objectives of the effective descriptions. Then, we describe (N)LCEs and CUTs, providing insights into the underlying concepts of both approaches.
In chapter 3, we discuss pCUTs, focussing on the implementation of pCUT as an LCE. On this basis, we introduce the white-graph expansion, designed to provide high-order series expansions if multiple couplings are present, which is demonstrated by an application to a two-dimensional system.
In chapter 4, we discuss the gCUT-method which builds the center of the thesis. First, we discuss the general gCUT scheme, suited to describe systems if no decay on clusters is present and introduce an efficient truncation scheme. On this basis, we discuss the treatment of both pseudo and genuine decay on finite clusters by following the notion of generalized cluster additivity, which we introduce. In addition to that, a novel extrapolation technique for NLCEs is presented and these various developments are demonstrated in the applications.
Finally, we provide a conclusion of the work covered in this thesis in chapter 5.

Chapter 2

Basics of the applied methods

In this chapter, the basics of the methods used in this thesis are discussed. First, we are going to introduce a setup describing the general structure of the systems under consideration combined with the objectives of our methods.

2.1 The setup

We consider a generic quantum lattice Hamiltonian $\mathcal{H}$ at zero temperature. By decomposing the original lattice into a superlattice of supersites, one can always rewrite *exactly* $\mathcal{H}$ as [71]

$$\mathcal{H} = \mathcal{H}_0 + \sum_{j=1}^{N_\lambda} \lambda_j \mathcal{V}^{(j)} \quad . \tag{2.1}$$

Here, a supersite might be a spin, two linked spins like a dimer, or any other finite set of linked sites which can be easily diagonalized. Then, the unperturbed part of $\mathcal{H}$ is diagonal in supersites i of the lattice. While the perturbative approach used in this thesis is restricted to an equidistant spectrum of a supersite, the non-perturbative variant is not. A generalization to non-equidistant spectra is straightforward.
In the following, we assume the local spectrum to be equidistant. Then,

$$\begin{aligned} \mathcal{H}_0 &= E_0 + \sum_{i,\alpha} \hat{f}^\dagger_{i,\alpha} \hat{f}_{i,\alpha} \\ &= E_0 + \mathcal{Q} \quad , \end{aligned} \tag{2.2}$$

where E_0 denotes a constant and the sum over α runs over all excited local degrees of freedom. The operator $\mathcal{Q}$ counts the number of excitations which are viewed as quasiparticles with different flavors α. This interpretation in terms of quasiparticles is fundamental for the approach because the objective is to transfer the quasiparticle picture defined by $\mathcal{H}_0$ to the full Hamiltonian $\mathcal{H}$. By construction, the approach is only well defined as long as no quantum phase transition occurs as a function of $\{\lambda_i\}$ and it is only capable of detecting second-order phase transitions. We begin our considerations for the Hamiltonian and continue with the spectral density of observables.

2.1.1 Effective Hamiltonian

In the following, the full Hamiltonian $\mathcal{H}$ is expressed and understood in terms of these quasiparticles. The unperturbed ground state $|\text{ref}\rangle$ is interpreted as the vacuum and is given as the product state $|\text{ref}\rangle \equiv |0\rangle \dots |0\rangle$ with $|0\rangle$ being the lowest state of a supersite. Accordingly, $\hat{f}^\dagger_{i,\alpha}|\text{ref}\rangle$ creates a local excitation of type α on supersite i.

Supersites interact via the perturbation $\mathcal{V} \equiv \sum_j \lambda_j \mathcal{V}^{(j)}$. The sum over j runs over all N_λ perturbation parameters λ_j. The different operators $\mathcal{V}^{(j)}$ build the bonds of the lattice, so that one can assign a different "color" for each perturbation parameter λ_j. Keeping in mind the applications, it is reasonable to restrict the discussion to Hamiltonians where the perturbation $\mathcal{V}$ couples two supersites. A generalization to perturbations which couple an arbitrary number of supersites is straightforward. Furthermore, if the different colors of the links are not of direct relevance, the different perturbation parameters λ_j are substituted by a single perturbation parameter λ.
One can rewrite Eq.(2.1) as

$$\mathcal{H} = \mathcal{H}_0 + \sum_{n=-N}^{N} T_n \quad , \tag{2.3}$$

so that $[\mathcal{Q},T_n] = nT_n$. Physically, the operator $T_n \equiv \sum_j \lambda_j T_n^{(j)}$ corresponds to all operators where the change of energy quanta with respect to $\mathcal{H}_0$ is exactly n. The maximal (finite) change in energy quanta is called $\pm N$. Generically, $\mathcal{H}$ is expressed in normal-ordered form with respect to $\mathcal{H}_0$ as $\mathcal{H} = \mathcal{H}_\mathrm{c} + \mathcal{H}_\mathrm{nc}$ using annihilation (creation) operators $\hat{f}_{i,\alpha}^{(\dagger)}$

$$\mathcal{H}_\mathrm{c} = E_0(\lambda) + \sum_{i,j,\alpha,\beta} a_{i,j}^{\alpha\beta}(\lambda)\, \hat{f}_{i,\alpha}^\dagger \hat{f}_{j,\beta} + \mathrm{h.c.} + \ldots \tag{2.4}$$

$$\mathcal{H}_\mathrm{nc} = \sum_{i,j,\alpha,\beta} \Gamma_{i,j}^{\alpha\beta}(\lambda)\, \hat{f}_{i,\alpha}^\dagger \hat{f}_{j,\beta}^\dagger + \mathrm{h.c.} + \ldots \,, \tag{2.5}$$

where dots refer to other particle-conserving (non-conserving) terms in $\mathcal{H}_\mathrm{c}$ ($\mathcal{H}_\mathrm{nc}$), consisting of more than two operators. The goal is then to derive a renormalized particle-conserving Hamiltonian $\mathcal{H}_\mathrm{eff} = \tilde{\mathcal{H}}_\mathrm{c}$ accounting for the influence of $\mathcal{H}_\mathrm{nc}$ quantitatively.

$$\mathcal{H}_\mathrm{eff} = \tilde{E}_0(\lambda) + \sum_{i,j,\alpha,\beta} \tilde{a}_{i,j}^{\alpha\beta}(\lambda)\, \hat{\tilde{f}}_{i,\alpha}^\dagger \hat{\tilde{f}}_{j,\beta} + \mathrm{h.c.} + \ldots \tag{2.6}$$

The approximation is introduced by the truncations necessary to determine the relevant operator coefficients of the effective Hamiltonian. The quality of this approximation defines essentially the applicability of these approaches.
Note, that the normal ordering of the operators decomposes the effective Hamilton operator $\mathcal{H}_\mathrm{eff}$ as

$$\mathcal{H}_\mathrm{eff} = \mathcal{H}_{\mathrm{eff},0} + \mathcal{H}_{\mathrm{eff},1} + \mathcal{H}_{\mathrm{eff},2} + \mathcal{H}_{\mathrm{eff},3} + \ldots, \tag{2.7}$$

where $\mathcal{H}_{\mathrm{eff},n}$ is an n-particle irreducible operator irrelevant for the $(n-1)$-QP channel. The prefactors of operators not relevant for the QP-channels under consideration are therefore not calculated.
The quasiparticle conservation of the effective Hamiltonian implies a direct interpretation and intuitive understanding of the physics in terms of these quasiparticles. Note that these particles can be viewed as dressed versions of the particles defined by the unperturbed Hamiltonian.
The effective Hamiltonian of the form Eq.(2.6) represents a substantial simplification, since fundamental quantities like a one-particle dispersion can be determined straightforwardly. The Hamiltonian separates into different particle-blocks because the associated degrees of freedom are already integrated out and each QP channel can be investigated separately; the many-body problem is reduced to an effective few-body problem.
The underlying assumption behind the effective description is that the desired low-energy is

dominated by the low-particle physics. If this is the case, it suffices to restrict the considerations to a rather small number of quasiparticles n. Typical QP channels considered range from $n = 0$ to $n = 3$. The accurate derivation of the relevant operator coefficients but also the analysis of the QP channels become more complex with increasing n.
The zero-particle state defines the ground state and the ground-state energy $E_0(\lambda)$ is directly provided by the effective Hamiltonian.
The analysis of higher QP channels is performed in Fourier space. The one-particle states of Eq.(2.6) are essentially, i.e., up to the flavor α and the localization within the unit cell, defined by the momentum. Typically, this enables an analytical solution of the one-particle subspace. On the contrary, the multiple-particle subspaces are typically analyzed by subsequent numerical analysis. The n-particle states are essentially defined by the total momentum and $(n-1)$ relative distances between the particles. The maximally manageable relative distances define the quality of the analysis which can become unsatisfactory for larger values of n.

2.1.2 Effective spectral densities

A strength of this approach is that the simplification to effective few-body problems also applies for spectral densities defining experimentally relevant static and dynamic structure factors. To this end, the associated observables must be included in the mapping-procedure. These observables carry a momentum $\boldsymbol{k}$ defined by the general form

$$\mathcal{O}(\boldsymbol{k}) = \frac{1}{\sqrt{\mathcal{N}}} \sum_j \exp(\mathrm{I}\boldsymbol{k}\boldsymbol{r}_j)\mathcal{O}_{\boldsymbol{r}_j} \tag{2.8}$$

where $\boldsymbol{r}_j$ defines the location where the observable $\mathcal{O}_{\boldsymbol{r}_j}$ acts and $\mathcal{N}$ refers to the number of unit cells. The observable is expressed by the annihilation (creation) operators of the initial Hamiltonian

$$\mathcal{O}(\boldsymbol{k}) = \frac{1}{\sqrt{\mathcal{N}}} \sum_{i,j,\alpha,\beta} b_{i,j}^{\alpha\beta}(\lambda,\boldsymbol{k})\, \hat{f}_{i,\alpha}^\dagger \hat{f}_{j,\beta} + \text{h.c.} + \ldots + \frac{1}{\sqrt{\mathcal{N}}} \sum_{i,j,\alpha,\beta} \Upsilon_{i,j}^{\alpha\beta}(\lambda,\boldsymbol{k})\, \hat{f}_{i,\alpha}^\dagger \hat{f}_{j,\beta}^\dagger + \text{h.c.} + \ldots \tag{2.9}$$

consisting in general of QP-conserving and non-conserving parts. To perform calculations within the effective description, the observable must be expressed in the *same* operators as the effective Hamiltonian:

$$\mathcal{O}_{\text{eff}}(\boldsymbol{k}) = \frac{1}{\sqrt{\mathcal{N}}} \sum_{i,j,\alpha,\beta} \tilde{b}_{i,j}^{\alpha\beta}(\lambda,\boldsymbol{k})\, \hat{f}_{i,\alpha}^\dagger \hat{f}_{j,\beta} + \text{h.c.} + \ldots + \frac{1}{\sqrt{\mathcal{N}}} \sum_{i,j,\alpha,\beta} \tilde{\Upsilon}_{i,j}^{\alpha\beta}(\lambda,\boldsymbol{k})\, \hat{f}_{i,\alpha}^\dagger \hat{f}_{j,\beta}^\dagger + \text{h.c.} + \ldots \tag{2.10}$$

Note that the effective observables are in general not quasiparticle conserving.
Therefore, the normal ordering decomposes the effective observable $\mathcal{O}_{\text{eff}}$ as

$$\mathcal{O}_{\text{eff}} = \mathcal{O}_{\text{eff},0,0} + \mathcal{O}_{\text{eff},0,1} + \mathcal{O}_{\text{eff},0,2} + \mathcal{O}_{\text{eff},0,3} + \ldots \tag{2.11}$$

$$+ \mathcal{O}_{\text{eff},1,0} + \mathcal{O}_{\text{eff},1,1} + \mathcal{O}_{\text{eff},1,2} + \mathcal{O}_{\text{eff},1,3} + \ldots \tag{2.12}$$

$$+ \ldots \quad ,$$

where $\mathcal{O}_{\text{eff},\Delta m,n}$ is an n-particle irreducible operator changing the number of particles by Δm. The spectral density of the observable at zero temperature can be calculated by the momentum and energy resolved spectral density

$$I(\boldsymbol{k},\omega) = -\frac{1}{\pi}\mathrm{Im}\left(G^{\mathcal{O},+}(\boldsymbol{k},\omega)\right) \tag{2.13}$$

with the zero-temperature Green's function

$$G^{\mathcal{O},+}(\boldsymbol{k},\omega) = \langle\hat{0}|\mathcal{O}^\dagger(k)\frac{1}{\omega-(\mathcal{H}-\tilde{E}_0)+\mathrm{I}\cdot 0^+}\mathcal{O}(k)|\hat{0}\rangle \quad . \tag{2.14}$$

Here, $|\hat{0}\rangle$ denotes the ground state of the system. The calculation of this structure factor can be performed for the effective system by

$$I_{\mathrm{eff}}(\boldsymbol{k},\omega) = -\frac{1}{\pi}\mathrm{Im}\left(\langle\widetilde{\mathrm{ref}}|\mathcal{O}^\dagger_{\mathrm{eff}}(k)\frac{1}{\omega-(\mathcal{H}_{\mathrm{eff}}-\tilde{E}_0)+\mathrm{I}\cdot 0^+}\mathcal{O}_{\mathrm{eff}}(k)|\widetilde{\mathrm{ref}}\rangle\right) \tag{2.15}$$

$$= \sum_n -\frac{1}{\pi}\mathrm{Im}\left(\langle\widetilde{\mathrm{ref}}|\mathcal{O}^\dagger_{\mathrm{eff},n,0}(k)\frac{1}{\omega-(\mathcal{H}_{\mathrm{eff},n}-\tilde{E}_0)+\mathrm{I}\cdot 0^+}\mathcal{O}_{\mathrm{eff},n,0}(k)|\widetilde{\mathrm{ref}}\rangle\right) \tag{2.16}$$

$$= \sum_n I_n^{\mathcal{O}}(\boldsymbol{k},\omega) \tag{2.17}$$

Here, $|\widetilde{\mathrm{ref}}\rangle$ denotes the ground state in the effective description, i.e, the (dressed) reference state. The spectral density decomposes into spectral densities $I_n^{\mathcal{O}}(\boldsymbol{k})$ of the n-QP channel which can be investigated independently.
The analysis of the spectral density is performed in Fourier space and becomes more complex with increasing n. The one-particle spectral density takes the form

$$I_n^{\mathcal{O}}(\boldsymbol{k},\omega) = \sum_m |A_{\boldsymbol{k},m}|^2\delta\big(\omega-\omega_m(\boldsymbol{k})\big) \quad , \tag{2.18}$$

where the sum runs over all one-particle bands $\omega_m(\boldsymbol{k})$ numerated by m. For quasiparticle sectors $n>1$, the effective spectral density can be investigated via a Lanczos analysis and a continued fraction analysis [72].
We waive a detailed discussion of the effective Hamiltonian in Fourier space and the Lanczos and a continued fraction analysis, because it does not advance the understanding significantly. Instead, we refer the well-disposed reader to any of the numerous works [29, 73, 74].

2.1.3 Energetic overlap

Finally, we would like to briefly present limits of the presented approach and possible solutions. The approach is well-justified and works well when the considered particle sectors are energetically well separated. However, the quality of the approximation can become poor in the more demanding case when the QP sectors are energetically very close. Then, interactions between the different QP sectors become considerable and the approximation of operator sequences can become poor.
In the more severe cases, QP sectors do overlap energetically and the separation of these QP channels is not possible; the quasiparticle picture begins to dissipate. One observes spontaneous quasiparticle decay. The term spontaneous is often used to emphasize that this phenomenon occurs at $T=0$ and is separated from the thermal broadening observed for finite temperatures [75–77]. However, since we consider only systems at $T=0$, the term is dropped in the following.
To illustrate a standard scenario of quasiparticle decay, we consider a Hamiltonian of the form

$$\mathcal{H} = \mathcal{H}_{\mathrm{sym}} + \zeta\mathcal{H}_{\mathrm{asym}} \quad , \tag{2.19}$$

with

$$\mathcal{H}_{\mathrm{sym}} = \mathcal{H}_0 + \lambda\sum_{n=-N,n\ \mathrm{even}}^{N} T_n \tag{2.20}$$

$$\mathcal{H}_{\mathrm{asym}} = \lambda \sum_{n=-N, n \text{ odd}}^{N} T_n \quad . \tag{2.21}$$

For the special case $\zeta = 0$, the absence of terms connecting the even and the odd number of quasiparticles results in parity conservation. This property generically can be traced back to a symmetry of the system which is broken by $\mathcal{H}_{\mathrm{asym}}$. In these situations, it is possible that the QP sectors are energetically well separated for $\mathcal{H}_{\mathrm{sym}}$ only due to the symmetry. Then, small values of ζ lead to an instant overlap of the QP sectors and the challenge is to define a justified continuation of the effective description in these cases, specifically for the one quasiparticle sector. Let us stress, that symmetry breaking is only one of the mechanism leading to quasiparticle decay [78], however, also with regard to the applications, we focus the discussion on this scenario.

A solution in this case is provided by an approach introduced by Fischer and Uhrig in [33]. To maintain a valid effective description in these cases, non-conserving terms must be left in the effective Hamiltonian defining remaining QP-block interactions. As a result, the QP channels cannot be analysed separately. The maximal number of QPs included in the analysis define a truncation affecting also the lower-QP channels.
This kind of approach was first implemented by Fischer and Uhrig where only the $(m = 0)$-irreducible operators are decoupled from the remainder. The one-particle sector is analysed simultaneously with the two-particle and three-particle sector via a Lanczos algorithm to determine spectral densities. Inspired by this scheme, we choose a similar approach and develop it further in the context of NLCEs. In our approach, the CUT on finite clusters is designed to separate all states which do not overlap energetically and only states which overlap energetically remain coupled. As a consequence, the scheme is also suited to describe quasiparticle-continuum level-repulsion.
With this, we conclude the presentation of the setup and the objectives of the method. Several approaches exist to derive an effective Hamiltonian of the form Eq.(2.6) and the corresponding effective observables Eq.(2.10).
One route is provided by CUTs, i.e., the Hamiltonian is continuously transformed to the effective Hamiltonian via a generator scheme driving the transformation. The different variants of CUTs are essentially classified by the truncation scheme applied.
Another route can be understood in the context of (N)LCE, i.e., the effective Hamiltonian in the thermodynamic limit is composed of effective Hamiltonians derived on finite clusters. The methods applied in this thesis are love children of both approaches. Therefore, it is reasonable to expand on (N)LCE and CUT approaches first before introducing the approaches in detail.

2.2 Linked-cluster expansions and non-perturbative linked-cluster expansions

This section provides an introduction to linked-cluster expansions (LCEs), yielding high-order series expansions in a perturbation parameter and the non-perturbative extensions called non-perturbative linked-cluster expansions or numerical linked-cluster expansions (NLCEs). For further reading we refer to detailed introductions to LCEs in [79] or [80]. A short introduction to NLCEs can be found in [62].
The general concept behind any LCE and NLCE is to decompose physical quantities in the thermodynamic limit into a sum of reduced contributions from finite linked clusters. This principle is based on the linked-cluster theorem. The linked-cluster theorem is not a theorem

in a rigorous sense and is understood very broadly as a concept. The standard approach to many-body perturbation theory is an expansion in terms of connected space-time perturbation theory diagrams analogous to Feynman diagrams in quantum field theory. Here, however, the term linked cluster refers to a spatially connected lattice and we define a cluster of the infinite system as a finite subset of supersites and their linking bonds.
For (N)LCEs, the linked-cluster theorem is a consequence of the so-called cluster additivity which builds the basis for the subtraction scheme essential to LCEs and NLCEs. To make the term cluster additivity more tangible for the moment: It simply means that the target quantity on a disconnected cluster splits into the sum of connected clusters.
LCEs and NLCEs exhibit a rich spectrum of applications showing that (N)LCEs are a highly versatile approach. The reason for this lies in the simple requirements for these approaches; the quantities of interest in the thermodynamic limit must exist on finite clusters. Consequently, (N)LCEs will probably also be applicable for many other challenges in the future. LCEs rely on a small expansion parameter not present in NLCE approaches. In this sense, NLCEs are less restricted than LCEs.
We begin this chapter with a quick review of the historical background and the developments of LCEs and NLCEs. Afterwards, the important concept of cluster additivity is discussed in detail.

2.2.1 Historical background

In the following, we are going to present the historical background of (a) LCEs and (b) NLCEs. The objective is to give insights into the application area and the status of the current literature. Specifically, open problems addressed in this thesis are pointed out.

Linked-cluster expansions

High-order series expansions are an important tool in statistical physics. Typically, the linked-cluster theorem is used to determine the correct expression of physical quantities up to high orders in a perturbation parameter by performing calculations on finite linked clusters. Historically, such LCEs date back to the 1950's and 1960's [81–84], where high-temperature series for extensive thermodynamic quantities have been determined. Similarly, extensive zero-temperature ground-state properties like the ground-state energy or susceptibilities can be calculated via LCEs as first proposed by Nickel in 1980 and implemented by Marland in 1981 [49]. Further progress has been made steadily over the years [50, 52, 85, 86]. The targeted quantities are extensive and therefore the cluster additivity lying at the core of all LCEs is trivially fulfilled. This property allows to compute these quantities per site for an infinite system by combining the reduced quantities of linked clusters. The reduced contribution of a cluster is obtained by subtracting reduced contributions of all subclusters to avoid double counting. Consequently, a reduced contribution corresponds to the fluctuations which are specific to a given cluster.
For non-extensive quantities like excitation energies, however, LCEs are more complicated and for a long time the calculation of an energy gap was only achieved by a deficient scheme which also needed *unlinked* clusters [52]. It took until 1996 when Gelfand set up a true linked-cluster expansion for a one-particle dispersion [53]. Gelfand realized that quantum fluctuations of the vacuum have to be subtracted from one-particle hopping amplitudes to perform proper linked-cluster expansions. Yet, unrealized at that time, this approach in terms of similarity transformations on graphs violates the cluster additivity and is therefore inapplicable when

the ground state and the targeted excitation-subspace are characterized by identical quantum numbers. In 2000, it has been shown that the use of orthogonal transformations on graphs restores the cluster additivity and therefore allows for a consistent calculation of many-particle excitation energies [54, 55, 79].
At the same time, an alternative route to linked-cluster expansions has been established by the method of pCUTs [39], allowing for the calculation of high-order series expansions for many-particle excitation energies as well as spectral densities [87]. In contrast to the other approaches mentioned above, in pCUTs, a quasiparticle conserving effective Hamiltonian in second quantization is derived model-independently. The method requires that the unperturbed part of the Hamiltonian has an equidistant spectrum and that the system is bounded from below. Interestingly, this method fulfills the cluster additivity by construction. In recent years, pCUTs were indeed used as linked-cluster expansions, i.e. a full graph decomposition has been implemented to calculate relevant matrix elements. Important examples are the derivation of effective low-energy spin models for the Hubbard model on the triangular and honeycomb lattice [63, 88], the calculation of the one-magnon gap for the fully-frustrated transverse field Ising model on the triangular and kagome lattice [89], the treatment of topological phase transitions of perturbed non-Abelian string-net models on the honeycomb lattice [90, 91], or the determination of the one-triplon dispersion of coupled Heisenberg dimers on hypercubic lattices for arbitrary dimension [92]. Overall, linked-cluster expansions constitute an efficient tool with a vast variety of applications.
The numerical power of all (perturbative) linked-cluster approaches, especially in more than one dimension, relies on a full graph decomposition. To this end, the lattice is divided into small subclusters on which the actual calculations are carried out. Afterwards, results in the thermodynamic limit are obtained by embedding the finite-cluster results into the infinite system properly.
Let us consider two different subclusters of the lattice. If a simple renumeration of the sites maps the Hamiltonian of the first cluster to the Hamiltonian of the second cluster, these clusters are called topologically equivalent. Obviously, the calculation can be restricted to topologically distinct clusters called graphs, yielding a highly efficient approach.
However, the number of topologically relevant graphs grows exponentially with the order of the series expansion as well as with the total number of different coupling constants. Consequently, it becomes very hard to reach sufficiently high orders for problems with several expansion parameters. This is especially relevant for the comparison with experimental data where typically different coupling strengths are important and have to be determined.
In this chapter, we introduce a new kind of graph expansion, a so-called *white-graph expansion*, which overcomes the latter limitation to a great extent [69]. The white-graph expansion benefits directly from the underlying framework provided by the effective pCUT Hamiltonian in second quantization.
This short outlook concludes the perturbative part of the historical overview. The second part deals with the non-perturbative counter-part of the LCE approach.

Non-perturbative Linked Cluster Expansions

The essential idea behind all NLCEs is a non-perturbative treatment of graphs, achieved via an exact (block) diagonalization, yielding results in the thermodynamic limit after an appropriate embedding procedure.
Interestingly, the underlying idea can be traced back to 1984 introduced by Irving and Hamer as a so-called exact linked-cluster expansion (ELCE). Irving and Hamer simply replaced the series expansion of the ground-state energy per cluster by the corresponding numerical exact

value for this cluster [50]. In principle, it is possible to modify all high-order series expansions via LCEs in this fashion. However, the power of this concept remained unheeded for some time but received more attention recently and many exciting developments have been achieved in this direction.
NLCEs can be used to obtain temperature-dependent properties of quantum lattice models [58–62], where the main advantage of NLCEs compared to the standard perturbative high-temperature expansions is the lack of a small parameter in the series. Consequently, it is possible to access arbitrarily low temperatures for models with short-range correlations.
Furthermore, the approach can be extended to determine time-dependent quantities out of equilibrium accessible directly in the thermodynamic limit [66, 67]. In addition to that, NLCEs are applied to a system with random disorder, extracting several thermodynamic properties in a disordered average [93]. Additionally, NLCEs can be used as a tool to calculate the bipartite entanglement entropies [65]. Here, NLCEs are shown to be one of the few methods capable of accurately calculating universal properties of arbitrary Renyi entropies at higher dimensional critical points.
Recently, NLCEs are introduced as an accurate tool to study many-body localization transition in a disordered system with continuous non-perturbative disorder [68]. Furthermore, a combination of NLCE techniques with density matrix renormalization group calculations is also successfully applied [94]. The general idea to combine NLCEs with other numerical methods is an interesting and quite promising route.
Distinct from the calculation of extensive quantities is the derivation of effective low-energy models via NLCEs as considered in this thesis. Here, degrees of freedom are separated in order to gain a renormalized effective description of the system. First approaches in this direction can be traced back to the derivation of low-energy Hamiltonians by contractor renormalization group (CORE) [95–97]. Historically, this method is related to the real-space renormalization group approaches. In contrast, another approach for the derivation of effective low-energy Hamiltonians via NLCEs are gCUTs which can be understood in the context of CUTs [46].
Both NLCE schemes are successfully applied for the derivation of effective low-energy spin models, yielding convergent results in the non-perturbative regime [63]. The methods are based on a (block) diagonalization on finite clusters, defining a renormalized effective low-energy model on the cluster. The effective models on the finite clusters are embedded into the lattice to obtain the effective low-energy model in the thermodynamic limit. The underlying assumption of this renormalization is a separation of degrees of freedom on the finite cluster. As we describe in the course of this thesis, this assumption is not always justified.
Following this historical summary, we well focus on the core concept of (N)LCE approaches, the cluster additivity.

2.2.2 Cluster additivity

Let us call two clusters A and B disconnected, if they do not have any (super)sites in common and there is no bond linking (super)sites from cluster A and B. For a disconnected cluster $C = A \cup B$, any operator/quantity defined on this cluster $\mathcal{M}^C$ is called *cluster additive* if it can be expressed as

$$\mathcal{M}^C \coloneqq \mathcal{M}^A \otimes \mathbb{1}^B + \mathbb{1}^A \otimes \mathcal{M}^B \,, \tag{2.22}$$

so that $\mathcal{M}^C$ splits into a part associated with the Hilbert space $\mathfrak{H}^A$ ($\mathfrak{H}^B$) of subcluster A (B). The reduced contribution of $\mathcal{M}^C$ is gained by the subtraction of subgraph contributions. If Eq.(2.22) is fulfilled, the subtraction of the subclusters located in A (B) cancel exactly with

$\mathcal{M}^A \otimes \mathbb{1}^B$ ($\mathbb{1}^A \otimes \mathcal{M}^B$). Hence, the reduced contribution of $\mathcal{M}^C$ vanishes, i.e., it vanishes for all disconnected clusters and the expansion can be carried out considering linked clusters only. The Hamiltonian $\mathcal{H}^C$ is cluster additive by definition since there is no link connecting sites from cluster A and cluster B. As a consequence, the ground-state energy itself obeys Eq.(2.22) implying a proper LCE for the ground-state energy. Moreover, the same holds for all extensive quantities.
This is less trivial when targeting quantities of an effective low-energy model. Obviously, it is essential that the effective Hamiltonian is cluster additive. While the cluster additivity of the effective Hamiltonian seems almost evident, there are indeed scenarios where some approaches may yield effective Hamiltonians which are not cluster additive.
Given a cluster additive effective Hamiltonian, it demands a proper interpretation of the matrix elements calculated on the graphs and the corresponding extraction of the coefficients. This extraction process corresponds to a normal ordering of the operators drawn from the matrix elements. By construction, only normal-ordered operators obey the cluster additivity. In order to determine these normal-ordered operator on a given cluster, matrix elements of lower particle-states must be subtracted. This rather technical procedure is described in the appendix [A.1].

Cluster additivity of the effective low-energy Hamiltonian

It seems physically intuitive that the effective Hamiltonian is cluster additive, because the clusters A and B are physically separated systems which should be reflected in the effective description. Contrary to this intuition, the cluster additivity is not trivially fulfilled. However, for pCUTs, the effective Hamiltonian is indeed always cluster additive which naturally arises from the flow equation approach. In CUTs, the effective Hamiltonian is derived by the integration of the flow equation $\partial_l \mathcal{H}(\ell) = [\eta(\ell),\mathcal{H}(\ell)]$. The initial Hamiltonian $\mathcal{H}(\ell = 0)$ is transformed continuously to an effective Hamiltonian given by $\mathcal{H}(\ell = \infty)$. The approach is discussed in detail in [2.3].
Let us assume

$$\mathcal{H}(\ell)^C = \mathcal{H}(\ell)^A \otimes \mathbb{1}^B + \mathbb{1}^A \otimes \mathcal{H}(\ell)^B \quad . \tag{2.23}$$

Using the generator scheme applied in pCUTs (see Eq.(2.41)) or the other standard generator scheme (see Eq.(2.35)), Eq.(2.23) directly implies

$$\eta(\ell)^C = \eta(\ell)^A \otimes \mathbb{1}^B + \mathbb{1}^A \otimes \eta(\ell)^B \tag{2.24}$$

and one finds, using Eq.(2.23) and Eq.(2.24),

$$\partial_l \mathcal{H}(\ell)^A \otimes \mathbb{1}^B + \mathbb{1}^A \otimes \partial_l \mathcal{H}(\ell)^B = [\mathcal{H}(\ell),\eta(\ell)]^C \tag{2.25}$$

$$= [\mathcal{H}(\ell),\eta(\ell)]^A \otimes \mathbb{1}^B + \mathbb{1}^A \otimes [\mathcal{H}(\ell),\eta(\ell)]^B. \tag{2.26}$$

The flow equation splits into a flow on cluster A and a flow on cluster B. The initial Hamiltonian $\mathcal{H}(\ell = 0)$ is cluster additive by definition. Consequently, the effective Hamiltonian $\mathcal{H}_{\text{eff}}$ derived by the flow equation is indeed *always* cluster additive if Eq.(2.24) is fulfilled. Moreover, the same argumentation can be applied for the effective observables O_{eff} derived via:

$$\partial_l O(\ell)^A \otimes \mathbb{1}^B + \mathbb{1}^A \otimes \partial_l O(\ell)^B = [O(\ell),\eta(\ell)]^C \tag{2.27}$$

$$= [O(\ell),\eta(\ell)]^A \otimes \mathbb{1}^B + \mathbb{1}^A \otimes [O(\ell),\eta(\ell)]^B. \tag{2.28}$$

Interestingly, to the best of our knowledge, this proof of the cluster additivity does not exist in current literature. For pCUTs, one can proof that the structure of the effective Hamiltonian originates from nested operators, guaranteeing a proper linked-cluster expansion [98]. However, the latter *results* from the cluster additivity property above.
While the cluster additivity of the effective Hamiltonian results naturally from the CUT approach, this is different for other (N)LCE approaches.
A different route of approaches can be grouped under the term matrix perturbation theory. The initial calculation in this field was performed by Gelfand in 1996 [53]. It is based on a similarity transformation S applied to the initial Hamiltonian to derive an effective Hamiltonian. Therefore, the effective Hamiltonian exhibits the same eigenvalues order by order as the initial Hamiltonian. For the systems investigated in Ref.[53], the excitations are protected by a quantum number from the ground state. Thus, the Hamiltonian separates into two blocks, where the excitation is located on cluster A (B). As a consequence, there are no hopping elements from cluster A to cluster B, ensuring the cluster additivity of this approach.
If, however, the excited states are not protected by a quantum number from the ground state, one obtains indeed hopping elements from cluster A to cluster B and the approach does not work. There are two related approaches, namely a 'two-block' orthogonal transformation and a 'multi-block' orthogonal transformation, designed to address this challenge [79]. The so-called 'two-block' orthogonal transformation is computationally efficient but is still found to fail in some cases. While the reasons for this are not yet fully understood, one can rely on the computationally more demanding 'multiblock' orthogonal transformation which seems to work in all relevant cases.
The same subtleties are also present for the derivation of effective models via NLCEs. Here, two methods are currently available in the literature [46, 95]. The cluster additivity of the effective Hamiltonian in the gCUT procedure relies essentially on the interplay of the commutator in the flow equation Eq.(2.31) and the generator at use. While the quasiparticle generator schemes obey Eq.(2.24), this is not guaranteed for modifications of the standard scheme. Note, that the *same* generator scheme must be used on every graph to achieve a consistent subtraction.
The other NLCE approach for deriving effective low-energy models is the contractor-renormalization group (CORE). Former CORE applications involved the description of connected range-N interactions in a truncated Hilbert space [95–97].
Additionally, an effective quasiparticle description as outlined in 2.1 can also be achieved via CORE [99]. To the best of our knowledge, there is no investigation of the cluster additivity of the CORE approach in literature. The CORE procedure is discussed in the appendix A.2 focussing on the cluster additivity for both application fields. It is found, that the description of the connected range-N interactions in a truncated Hilbert space might violate the cluster additivity. However, this issue can be resolved by changing the orthogonalization procedure involved in the calculation. It might be interesting to investigate if this improves the results of CORE.
The derivation of quasiparticle descriptions requires, again, the separation of the ground state and the corresponding excitations via a quantum number. This is consistent with the perturbative LCE approaches, since the diagonalization-projection process in CORE can be viewed as a similarity transformation on the cluster. The unitary transformation in gCUTs is more costly but provides more information.
Finally, it should be noted that cluster additivity is sufficient for perturbative LCEs only. For non-perturbative NLCEs, a generalization of this concept is necessary in order to avoid non-perturbative artifacts leading to a breakdown of this method [70]. The generalization is introduced in 4.2.1.
With this, the fundamental concepts of (N)LCEs are explained. Next, we describe the underlying

principles of CUTs, finishing the basics of the procedure.

2.3 Continuous Unitary Transformations

Unitary transformations can be used to change the basis of a system in order to find a simpler and better suited description of the problem. A textbook example of such a unitary transformation is the bosonic Bogoliubov transformation arising in linear spin-wave theory of quantum antiferromagnets [6]. Clearly, finding such a transformation a priori is not always possible and one alternative route are continuous unitary transformations (CUTs), which were proposed by Wegner [38] in 1994. A similar approach was proposed independently by Głazek and Wilson [100] during the same period.
CUTs represent a *schematic* way of performing a unitary transformation to find an effective description of the system. The CUTs map the initial Hamiltonian $\mathcal{H}$ by

$$\mathcal{H}(\ell) = U^\dagger(\ell)\, \mathcal{H}\, U(\ell) \tag{2.29}$$

to the transformed Hamiltonian $\mathcal{H}(\ell)$. As indicated by the name, the unitary transformation $U(\ell)$ depends on the *continuous* flow parameter ℓ. Here, $\mathcal{H}(\ell = 0) = \mathcal{H}$ corresponds to the initial system and $\mathcal{H}_{\text{eff}} := \mathcal{H}(\ell = \infty)$ is the resulting effective system. In this thesis, we associate $\mathcal{H}_{\text{eff}} = \tilde{\mathcal{H}}_{\text{nc}}$, i.e., the effective Hamiltonian corresponds to the desired effective description in terms of quasiparticles.
The transformation is driven by the antihermitian generator $\eta(\ell)$:

$$\partial_l U(\ell) = \eta(\ell) U(\ell) \quad . \tag{2.30}$$

The generator is defined by a scheme of the general form $\eta(\ell) = \eta[\mathcal{H}(\ell)]$. Combining Eq.(2.29) and Eq.(2.30) leads to the so-called flow equation

$$\partial_l \mathcal{H}(\ell) = [\eta(\ell), \mathcal{H}(\ell)] \quad , \tag{2.31}$$

which must be solved in order to obtain the effective Hamilton operator. So for a given model and generator scheme, the challenge of finding the effective description by means of a unitary transformation is transferred to the integration/solution of the flow equation, building therefore the centerpiece of all CUT methods.
During the flow, the Hamiltonian defines the next infinitesimal transformation to be performed on itself by the indicated feedback structure via the generator scheme $\eta(\ell) = \eta[\mathcal{H}(\ell)]$. It is essential that the generator scheme leads to a convergent flow, i.e., fix points of the differential equation defined by $\lim_{\ell\to\infty}[\eta(\ell), \mathcal{H}(\ell)] = 0$.
Note that the generator scheme applied in the CUT defines the shape of the effective Hamiltonian to a certain extent. If the targeted low-energy physics is energetically well separated from the remainder, well-engineered generator schemes are available in the literature [39, 101]. If, however, both subspaces do overlap energetically, modifications of the quasiparticle generator schemes are required which is subject of ongoing investigations [33, 70, 102] and is also one of the main focuses of this thesis.
Analogously to the Hamiltonian, one can transform observables in order to describe experimentally accessible quantities such as dynamical correlation functions. The associated observable O must be transferred to the same basis, which implies

$$\partial_l \mathcal{O}(\ell) = [\eta(\ell), \mathcal{O}(\ell)] \quad , \tag{2.32}$$

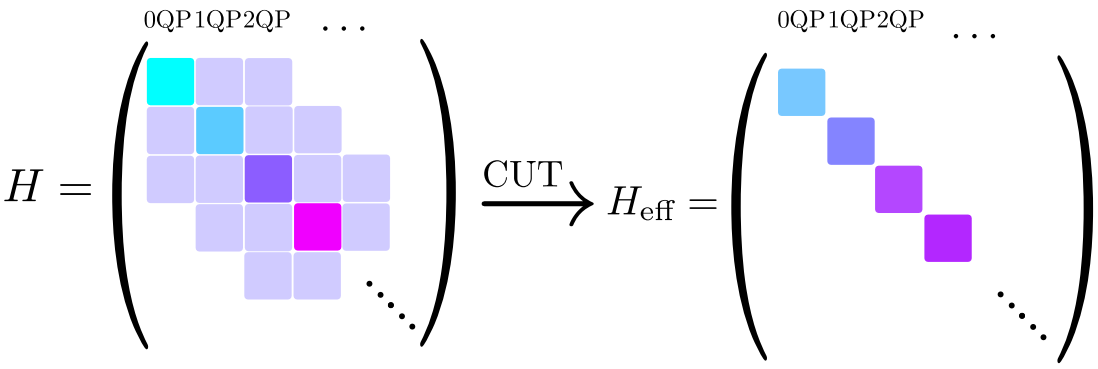

Figure 2.1: Left: Schematic representation of the initial Hamiltonian. The colored blocks are block diagonal with respect to the number of quasiparticles. Off diagonal matrix elements are represented by grey blocks. Each block couples to a finite number of different blocks resulting in an initial band diagonality. Right: The resulting Hamiltonian derived via CUTs is block diagonal with respect to the number of quasiparticles. The colour coding indicates the admixture of bare particles in the vacuum of the effective system.

where $\mathcal{O}(\ell = 0)$ corresponds to the initial observable and $\mathcal{O}_{\text{eff}} := \mathcal{O}(\ell = \infty)$ is the observable within the effective description. Since the generator depends on the Hamiltonian, it is typically reasonable to perform both integrations simultaneously.
We conclude that the CUT method provides a perfect tool for the applications described in section 2.1. Unfortunately, for a given generator scheme, the solution of the flow equations Eq.(2.31) and Eq.(2.32) is highly non-trivial. In general, the commutator produces new terms which are not contained in the original Hamiltonian, resulting in an infinite set of coupled differential equations. This is the reason why one has to introduce an adequate truncation scheme which represents the main task of this method, leading to a variety of approaches. In short, the crucial points of this method are the choice of the generator scheme, yielding a proper low-energy description, and of a truncation scheme, capturing the relevant (low-energy) physics of the system.
It should be mentioned that the application fields of flow equations go beyond the scope of this brief overview. Flow equations find applications inter alia in the description of real time dynamics [103, 104] or in the effective description in k-space for gapless bosonic excitations [48, 105] or are applied to the Kondo model [106–108].
In the following, we are going to restrict the discussion to the scenario described in section 2.1, i.e., the derivation of effective low-energy models at $T = 0$ with an underlying (local) quasiparticle picture. For the applications under consideration, there are, essentially, two generator schemes (and their modifications) in use. We briefly discuss the properties of the two main generator schemes on matrix level independently of the CUT variant in the next section. Thereafter, the different CUT variants - classified by the way the flow equation is solved and the associated truncation scheme - are discussed.

2.3.1 Generator schemes

The aim of the CUT is to transform a Hamiltonian of the system to an effective Hamiltonian via the integration of the flow equation Eq.(2.31). Our objective is the derivation of an effective description in terms of quasiparticles implying that the effective Hamiltonian is block diagonal

with respect to the number of quasiparticles. The convergence can therefore be determined by the sum over the squares of the non-block diagonal elements, also called residual off-diagonality (ROD) [44]:

$$\mathrm{ROD} := \sum_{i,j} |\mathcal{H}_{\mathrm{nc,ij}}|^2 \tag{2.33}$$

$$= \mathrm{Tr}\left(\mathcal{H}_{\mathrm{nc}}\right)^2 \quad . \tag{2.34}$$

Consequently, any valid generator scheme under consideration must satisfy $\lim_{\ell\to\infty} \mathrm{ROD}(\ell) = 0$. It may be added that the ROD is not only relevant for the investigation of generator schemes. In applications, the flow equation is integrated numerically and the integration can be terminated if the ROD falls below a threshold value. Furthermore, the behavior of the ROD during the flow can give indications of the underlying physics.
The initial Hamiltonian is band diagonal because only a finite number of particles is created (annihilated) by the perturbation. The CUT rotates away the elements connecting different particle sectors restoring the quasiparticle picture given by the unperturbed Hamiltonian. The particles of the effective system represent the actual particles of the system and can be viewed as dressed versions of the bare particles defined by the initial system. The procedure is schematically shown in figure 2.1.
In the following, we investigate this property for the two main generator schemes used in this field on matrix level. A scheme providing a generalization to infinite systems is discussed in Ref.[109]. To this end, we choose an initial basis which is block diagonal with respect to the number of particles defined by $\mathcal{H}_0$. In other words, the particle conserving part of the Hamiltonian $\mathcal{H}_{\mathrm{c}}(\ell)$ is block diagonal.
An important quantity during the integration is given by the eigenvalues of the different particle blocks during the flow. Let $\varepsilon_i^m(\ell)$ be the i-th eigenenergy of the m-particle block of $\mathcal{H}_{\mathrm{c}}(\ell)$. For $\ell = 0$, the energies are determined by the contributions of the initial block-diagonal elements. This corresponds exactly to the contributions included in first-order perturbation theory and so $\varepsilon_i^m(\ell = 0)$ can simply be identified with the eigenenergies provided by first-order perturbation theory in λ.
During the flow, the renormalization effects of the different blocks are continuously incorporated. Since the effective Hamiltonian is quasiparticle conserving and connected to the initial Hamiltonian via a unitary transformation, the eigenvalues $\varepsilon_i^m(\ell = \infty)$ can be identified with the actual eigenvalues of the system (neglecting truncation errors). This reflects the more general concept that each n-particle block can be investigated separately recovering the correct physics. While the possible values of $\varepsilon_i^m(\ell = \infty)$ must recover the spectrum of the system, it is not specified which eigenvalues are connected to which particle block. Hence, the development of the subblock energies with ℓ is an essential characteristic of a generator scheme. These diagonal elements are of crucial importance for the quality of the effective model and the challenges addressed in this thesis. The following discussion of the generator schemes focuses on the ROD in combination with the behaviors of the subblock energies ε_i^m.

Wegner generator

The generator scheme originally proposed by Wegner [38] is given by

$$\eta^{\mathrm{W}} = [\mathcal{H}_{\mathrm{d}}, \mathcal{H}_{\mathrm{nd}}] = [\mathcal{H}_{\mathrm{d}}, \mathcal{H}], \tag{2.35}$$

where $\mathcal{H}_{\mathrm{d}}$ refers to the diagonal and $\mathcal{H}_{\mathrm{nd}}$ to the non-diagonal part of the Hamiltonian. This generator scheme achieves, up to degeneracies, a full diagonalization up to degeneracies; for

the considered block diagonalization the term diagonal can be redefined with respect to the number of quasiparticles, i.e., all quasiparticle conserving terms are viewed as diagonal.
For the sake of simplicity, we discuss the original scheme while all statements can be generalized to the modified generator scheme achieving the block diagonalization. In a given basis (defined by the eigenstates of the initial Hamiltonian) the Hamilton operator is now considered in matrix representation and the Wegner generator reads

$$\eta^{\mathrm{W}}_{i,j} = \sum_k \varepsilon_i \delta_{i,k} h_{k,j} - \sum_k h_{i,k} \varepsilon_k \delta_{k,j} \tag{2.36}$$

$$= (\varepsilon_i - \varepsilon_j) h_{i,j} \quad , \tag{2.37}$$

where $\varepsilon_i = h_{i,i}$ refers to the diagonal elements at a given value ℓ. For the generator scheme aiming at block diagonalization, these elements can be identified with the subblock energies ε_i^m in the corresponding basis as defined above.
To proof that the generator scheme indeed leads to a full diagonalization up to degeneracies, one can examine the sum over the squares of the non-diagonal elements [38]. By investigating the trace of $\mathcal{H}^2_{\mathrm{nd}}$, one ends up with

$$-\sum_{k,i\neq k} \partial_l |h_{i,k}|^2 = 2 \sum_{k,i} \left(\varepsilon_k - \varepsilon_i\right)^2 h_{k,i} h_{i,k} \quad . \tag{2.38}$$

The square of the absolute values of the off-diagonal elements never increases and decreases with ℓ as long as the right side is not zero. If $\varepsilon_k \neq \varepsilon_i$ ($\varepsilon_i^m \neq \varepsilon_j^n$) for all elements, a full diagonalization (block-diagonalization) is performed. Contrary, non-diagonal elements which connect states with the same diagonal elements do not have to vanish. In practice, the transformation becomes numerically unstable and demanding when the difference between two diagonal elements becomes very small.
Another fundamental consequence is that the order of the diagonal energies cannot be switched during the flow:

$$\varepsilon_i(\ell = 0) < \varepsilon_j(\ell = 0) \Rightarrow \varepsilon_i(\ell = \infty) < \varepsilon_j(\ell = \infty) \tag{2.39}$$

$$\varepsilon_i^m(\ell = 0) < \varepsilon_j^n(\ell = 0) \Rightarrow \varepsilon_i^m(\ell = \infty) < \varepsilon_j^n(\ell = \infty). \tag{2.40}$$

This implies that a change in the order of the initial diagonal elements as a function of λ leads to an abrupt change of the effective Hamiltonian which is physically deeply unsatisfying. A change in the order of the initial diagonal elements does *not* correspond to a drastic change of the physics. The initial diagonal elements represent only the first-order perturbation theory, fully ignoring the renormalization via interactions of the different quasiparticle blocks. The interaction between different particle blocks is generically repulsive and the first-order perturbation theory typically overestimates the energetic overlap. For this reason, we consider this class of generator schemes to be unfavorable for the considered applications.
Another inconvenience arises from the fact that the band diagonality of the initial Hamiltonian is not conserved during the flow. That is, interactions not present in the initial system are generated and the Hamiltonian loses its simple structure. Both issues are absent in the generator scheme discussed in the following.

Quasiparticle generator

In 1997, Stein introduced a new generator scheme aiming at the derivation of a block diagonal effective low-energy Hamiltonian for the Hubbard model [101]. Stein's ansatz allows a strong

coupling expansion for the Hubbard model and can be viewed retrospectively as the first introduction of the quasiparticle generator restricted to a specific set up.
In order to introduce a generator scheme which keeps the band diagonality, a new generator performing a full diagonalization of matrices was proposed by Mielke in 1998 [110]. Mielke proved several properties of this generator scheme including the conservation of the band diagonality during the flow. Even though no degenerate subspaces are decoupled, the scheme is closely related to the approach introduced by Stein.
Finally, Stein's approach was extended and generalized in 1999 by Knetter and Uhrig with the so-called quasiparticle conserving generator η^Q [39]. This generator scheme relies on a quasiparticle picture defining the generator elements. Using η^Q, Knetter and Uhrig provided the possibility to derive high-order series expansions when the unperturbed Hamiltonian $\mathcal{H}_0$ is equidistant and the system is bounded from below.
All these generators can be viewed to be variants of an identical scheme. For these generator schemes, the band diagonality of the initial Hamiltonian is conserved, and, most importantly, the order of the diagonal energies of the effective system is not defined by the order of the initial eigenvalues [33, 111]. This generator scheme builds the basis for all the applications in this thesis and will be discussed next.
Let $\mathcal{Q}$ be the operator counting the number of excitations, i.e., $\mathcal{Q}|i\rangle = q_i|i\rangle$ if $|i\rangle$ is a q_i-particle state. One defines the generator scheme in the eigenbasis of Q as

$$\eta^Q_{i,j} = \mathrm{sgn}(q_i - q_j)\mathcal{H}_{i,j} \quad , \tag{2.41}$$

where q_i denotes the number of quasiparticles of state i. For a system bounded from below, one can proof that the final Hamiltonian obeys $[\mathcal{Q},\mathcal{H}(\infty)] = 0$, i.e., the number of elementary excitations is a conserved quantity after the transformation and the quasiparticle picture is restored [39].
The ℓ-dependence during the CUT lies in analogy to the time dependence within the Heisenberg picture in the operators while the states are static. Thus, arbitrary operators $\mathcal{A}$ transform via $\mathcal{A}(\ell) = U^\dagger(\ell)\mathcal{A}U(\ell)$. However, the operator $\mathcal{Q}$ yields the interpretation of the states which are static. Therefore, the operator is *not* transformed by the CUT and one can simply identify $Q(\ell) = Q(\ell = 0)$.
This means that the definition of a quasiparticle is transformed during the CUT. The particles for $\ell = 0$ can be identified with the particles of the initial Hamiltonian Eq.(2.5) while the particles for $\ell = \infty$ can be identified with the dressed particles of the effective Hamiltonian Eq.(2.6).
In the following, we discuss the behavior of the subblock energies. If the ground state is unique, this generator scheme maps the zero-particle state, i.e., the vacuum, to the ground state of the system [111].
The proof can be generalized showing that this generator scheme transforms the Hamiltonian in such a way that all subblock energy eigenvalues are ascending by their QP number, i.e., $m < n$ directly implies $\varepsilon^m_i(\ell = \infty) < \varepsilon^n_j(\ell = \infty)$ [33].
This sorting of the eigenvalues is the main difference of this generator scheme when compared to the Wegner generator scheme where the order of the initial subblock eigenvalues is equivalent to the order of the eigenvalues of the final effective Hamiltonian. This follows from the fact that the ROD never increases with ℓ for the Wegner generator scheme. Consequently, the ROD can indeed increase with ℓ for the quasiparticle generator scheme which indicates that subblock energies of different quasiparticle blocks are sorted by the generator.
Note that the states are only sorted within subspaces of the Hilbert space having the same quantum numbers. Specifically, the maximum of the one-particle dispersion can be energetically above the minimum of the multi-particle continuum if these points are located at different

momenta. For each momentum one can identify the one-particle state with the lowest energy. This sorting often reflects a physical intuition since one identifies the lowest energies of the system with the lowest number of excitations. However, subtleties exist when QP subspaces overlap energetically and it is no longer possible to separate the degrees of freedom. A standard example for this would be the decay of the one-particle mode in the continuum for certain momenta. Then, the quasiparticle generator defines the minimum of a given momenta as the one-particle mode. This rigorous identification can cause a break down of this approach for non-perturbative truncations. Nevertheless, an adapted generator scheme where for example the corresponding elements in the generator are eliminated can provide a possible remedy [33]. Obviously, the number of possible modifications is manifold and a major challenge addressed in this thesis is the definition of a suited systematic and appropriate modification.
Following this brief discussion of the main generator schemes, we give an overview over the different CUT variants in literature, completing the chapter of the CUT approach.

2.3.2 Variants of continuous unitary transformations

For clarity, we briefly recapitulate the set up and objectives. We start with a Hamiltonian Eq.(2.5) which defines a quasiparticle picture. Our aim is to derive a quasiparticle conserving Hamiltonian such, that the relevant low-energy physics can be understood in terms of these particles. One way of deriving such an effective Hamiltonian is by means of the CUT method relying on the generator schemes discussed above. In order to perform the CUT, one must solve the flow equation Eq.(2.31). To this end truncations are inevitably involved since the commutator generates new terms implying an infinite set of coupled differential equations. Different approaches for the solution of the flow equation exist, defining the different CUT variants. These different variants will be discussed in the following, putting the methods developed during this thesis in context of the existing literature.

Perturbative continuous unitary transformations

Given the initial Hamiltonian Eq.(2.1), a perturbative truncation seems natural. Indeed, this ansatz was one of the first computationally demanding approaches [39]. For the so-called perturbative continuous unitary transformations (pCUTs), the Hamiltonian $\mathcal{H}$ and the generator η^Q are expanded to a certain order in the perturbation parameter λ and the flow equation is solved model-independently. All terms up to a given order in λ are taken into account, so no truncation error is made up to this order. However, this method is restricted to an equidistant spectrum of $\mathcal{H}_0$, limiting its applications.
The resulting Hamiltonian can be determined model-independently. Yet, as a consequence, the Hamiltonian is not normal-ordered and the desired model dependent low-energy physics has to be extracted in a second step. This step involves the calculation on finite clusters which is the natural link to LCEs. Herein lies the actual art and different approaches are possible. Since the pCUT method is applied in this thesis, it is discussed in detail in chapter 3.

Self-similar continuous unitary transformations

Another approach is given by the self-similar continuous unitary transformations (sCUTs). The Hamiltonian is kept in a self-similar form defined by a truncated basis of (normal-ordered) operators $\hat{o}_i$ selected in the beginning of the calculation [45, 112, 113]. The Hamiltonian and

the generator are then described as linear combinations of these operators:

$$\mathcal{H}(\ell) = \sum_i g_i(\ell)\hat{o}_i \quad . \tag{2.42}$$

Operators generated by the commutator not included in the basis are neglected. Therefore, the flow equation Eq.(2.31) defines a finite set of differential equations for the coefficients $g_i(\ell)$ of the basis operators:

$$\partial_l g_i(\ell) = \sum_{j,k} a_{i,j,k} g_j(\ell) g_k(\ell) \quad . \tag{2.43}$$

The differential equation system is then solved numerically. The truncation scheme is therefore on the level of operators kept in the basis. It can be chosen for instance by the locality of the operators, i.e., all operators involving lattice sites with a distance larger than $d_{\max}$ are neglected. Furthermore, the number of excitations affected by the operator is another possible truncation. One problem of this approach is that typically several truncations are introduced simultaneously which aggravates the problem of a well-controlled truncation.
It should be noted, that recently a promising truncation scheme for sCUT approaches in momentum-space is introduced in Ref.[48]. Here, a schematic truncation is provided by scaling arguments.

Enhanced perturbative continuous unitary transformations

The essential idea of enhanced perturbative continuous unitary transformations (epCUT) is to enhance the application of perturbative continuous unitary transformations to non-equidistant spectra in $\mathcal{H}_0$ [47]. To this end, the flow equation is solved - similar to sCUTs - numerically and on the operator level. The objective is to gain series expansions for the desired target quantity, e.g. the ground-state energy or a one-particle dispersion. The coefficients $g_i(\ell)$ are therefore not a single number but are replaced by a series expansion. The truncation is introduced in the coefficients $a_{i,j,k}$ with respect to the recoupling effect to the target quantities concerning the order of the expansion parameter. Hence, one applies a truncation of the differential equation system with respect to the expansion parameter rather than a truncation of the operator basis as it is done in the sCUT approach. Although the results for equidistant spectra in $\mathcal{H}_0$ are equivalent to the results produced by pCUTs, the realization of this method differs fundamentally and in this respect the method is more closely affiliated with the sCUT methods.

Directly evaluated enhanced perturbative continuous unitary transformations

Directly evaluated enhanced perturbative continuous unitary transformations (deepCUT) [47] were developed as a by-product of the implementation of epCUTs. One can use the perturbative truncation of epCUT to set up a finite set of coupled differential equations, evaluate them for a certain value of the perturbation parameter λ and solve these equations. This scheme is called deepCUT and turns out to be a robust extrapolation of the perturbative results [47, 102]. In contrast to the sCUT methods, this approach has a well-controlled truncation parameter making this scheme more robust and powerful. The method has been successfully applied to the Ionic Hubbard model on a chain [114, 115] and in two dimensions [116]. This method represents the strongest method in this lineage.

graph-based continuous unitary transformations

Clearly separated from these approaches, where the flow equation is solved on the operator level, are the graph-based continuous unitary transformations (gCUTs) introduced in 2011 by Yang and Schmidt [46]. Here, the flow-equation is solved on finite clusters and the result in the thermodynamic limit is obtained by a summation of the finite-cluster results. The Hamiltonian on a finite system can be represented by a matrix, so that, in principle, the flow-equation can be solved without any truncation error. Hence, the error of the approximation is induced only by the finite spatial range of the fluctuations taken into account. This method represents the main focus of this thesis and is discussed in 4.

Let us close this chapter with some final remarks about CUTs. The perturbative truncation applied in pCUTs or epCUTs yields unique results and no artifacts of the specific truncation scheme or the CUT method are present. However, depending on the parameter regime, this may be different for CUTs based on truncations which are not purely perturbative. In a parameter regime where the quasiparticle subspaces are energetically well separated, all approaches work well and no artifacts are present. In parameter regimes where this is not the case, the description is by construction more demanding.
As mentioned above, a sorting of the eigenvalues can cause the ROD to increase indicating an energetic overlap of the subspaces. For sCUT and deepCUT, this may even result in divergencies of the ROD which prohibits the derivation of an effective model in these scenarios. Solutions are based on modifications of the standard quasiparticle generator scheme avoiding the sorting property to some extent:
Firstly, one can simply eliminate all terms in the generator which couple the one-particle mode with the other QP channels. Renormalization effects of these terms are considered to be small and are included in a second evaluation process where the coupled one- two- and three-particles subspaces are diagonalized simultaneously in a numerical fashion [33].
Secondly, one can apply a variational determination of the generator elements in order to prevent a divergence of the ROD [102]. In this scheme, the quasiparticle blocks are (almost) completely decoupled.
For gCUTs, the problem of divergencies of the ROD is avoided since the flow equation is solved on a finite system and no divergencies can appear. However, artifacts of this approach manifest in convergence problems with the cluster sizes. As described in 2.2, these problems arise when the low-energy subspace overlaps energetically with the remainder and the possible nature of this overlap is twofold. Firstly, the overlap is characterized as genuine decay if the energetic overlap on finite clusters corresponds to an energetic overlap in the thermodynamic limit. This situation is similar to the scenario described above for sCUT and deepCUT.
Secondly, the overlap can be characterized as pseudo decay if it is only caused by the broken translational invariance of the finite cluster. This is an artifact inherent to all NLCE approaches and not present for sCUT and deepCUT. Consequently, a solution of this artifact is even more mandatory.
The idea is to develop modifications the standard quasiparticle generator in order to treat pseudo and genuine decay. A full decoupling of the subspaces on the finite clusters is in both scenarios not desired. Consequently, a variational approach in form of [102] is not taken into consideration. In contrast to [33], it is also not sufficient to eliminate all terms in the generator which couple the one-particle mode with the remainder, since renormalization effects are substantial. Consequently, a modification must eliminate *certain* elements from the generator.

The golden thread of this thesis is to exploit attributes provided by CUT calculations in order to address the challenges arising in the (N)LCE scheme.

This is done for the perturbative variant pCUT and the non-perturbative counterpart gCUT in different ways. Firstly, we are going to describe the combination of pCUTs with LCEs to define a new scheme called white-graph expansion, allowing an efficient calculation for systems with multiple coupling types [69].
Secondly, the continuous transformation during the flow is utilized to implement modified generator schemes which address both pseudo and genuine decay within the gCUT scheme. The understanding and treatment of pseudo decay represents major progress for NLCEs in general. The conceptual ideas allow to identify and fully eliminate these artificial effects [70]. The treatment of genuine decay via NLCEs breaks new ground for this approach. A reasonable continuation of the results in the parameter regime showing genuine decay is introduced. Consequently, these developments for the gCUT scheme represent the main achievement of this thesis.

Chapter 3

Perturbative Continuous Unitary Transformations

In this chapter, we describe the combination of LCEs and pCUTs to set up a new kind of graph expansion, so-called *white-graph expansion*. The content of this chapter is already published in Ref. [117] and Ref.[69].

Perturbative continuous unitary transformations are an effective tool for the calculation of high-order series expansions. In contrast to other tools for calculating high-order series expansions like LCEs via matrix perturbation theory [79] or the enhanced version called epCUT [47], the method is restricted to an equidistant spectrum in $\mathcal{H}_0$. The method can be applied to calculate one-particle dispersions [39], multi-particle interactions, spectral properties like spectral densities and dynamic structure factors [10, 40–43] or effective spin models [88].
The application consists essentially of two steps: i) the perturbative order-by-order solution of the flow equation Eq.(2.31) yielding an effective Hamiltonian and effective observables. ii) a non-trivial extraction of the effective low-energy physics.
The first step depends only on the structure of the perturbation, namely, how many particles at most are created (annihilated) by the perturbation. In this sense, the obtained solution is model independent.
However, this generality comes at the price of a complex model dependent extraction process because the effective operators are not normal-ordered, i.e., the desired matrix elements have to be extracted in a separate step. The real challenge lies in the second step which introduces the model-dependent physics and therefore typically represents the bottle-neck of the calculations.
The extraction process is based on the linked-cluster theorem which allows the determination of matrix elements in the thermodynamic limit by applying the effective operators to *finite* clusters. At the end of this process a normal-ordered low-energy Hamiltonian is obtained.
Essentially, two approaches are possible: in the standard straight-forward approach the calculation can be carried out on a single sufficiently large cluster, see e.g. [10, 39, 40, 118, 119]. The advantage of this approach is that the implementation is straightforward and details of the operator structure are irrelevant for the general scheme.
For two or more dimensions, this approach is typically unfavorable because one runs into memory problems and a full cluster decomposition is the method of choice [88–91]. It is then even possible to use this idea and determine quantities in arbitrary dimensions [92].
Let us also mention that a hybrid, a decomposition into rectangular clusters, has been also successfully introduced for the pCUT method recently[98]. A rectangular cluster expansion seems to be especially well suited for non-perturbative extensions of linked-cluster expansions, since a typical length scale can be assigned to each rectangular graph, which is much less trivial when performing a full graph decomposition [65, 70].
The computational efficiency of the full cluster decomposition is based on a topological identification process, namely, fluctuations which correspond to the same graph can be identified

with each other. As a result, only a small subset of topologically distinct fluctuations must be calculated, resulting, especially for more than one dimension, in an extremely effective calculation process. However, if multiple couplings are present, these couplings inhibit topological equivalence. In these cases, especially relevant for experimental realizations with several coupling constants, the maximally available order is significantly reduced (see e.g. Ref.[120]). In this chapter, we introduce a new scheme, a so-called white-graph expansion, addressing this issue relying on a reordering of the calculation process.[1]
In the following, we start with a brief review of the solution of the flow equation, which builds the basis of every pCUT approach. Then, we discuss the extraction of the low-energy physics from the resulting effective Hamiltonian, leading naturally to the concept of a full graph decomposition. Finally, we introduce the white-graph expansion as applied in this thesis followed by an application to a two-dimensional quantum spin 1/2 model of coupled XXZ-ladders.

3.1 Perturbative solution of the flow equation

Continuous unitary transformations are a tool for the derivation of effective low-energy models. The transformation is driven by the so-called flow equation Eq.(2.31) which can in general only be solved by introducing a truncation scheme. In this chapter, we describe the perturbative solution of the flow equation [39] yielding the correct effective Hamiltonian for a given order. It should be noted, that the scheme can only be applied if $\mathcal{H}_0$ is equidistant and bounded from below.
Here, the flow equation Eq.(2.31) is solved via the perturbative ansatz

$$\mathcal{H}(\{\lambda_j\};\ell) = \mathcal{H}_0 + \sum_{\sum_j k_j = k}^{\infty} \lambda_1^{k_1} \dots \lambda_{N_\lambda}^{k_{N_\lambda}} \sum_{|\underline{m}|=k} F(\ell;\underline{m}) T(\underline{m}), \tag{3.1}$$

implying, according to Eq.(2.41),

$$\eta^Q(\{\lambda_j\};\ell) = \sum_{\sum_j k_j = k}^{\infty} \lambda_1^{k_1} \dots \lambda_{N_\lambda}^{k_{N_\lambda}} \sum_{|\underline{m}|=k} F(\ell;\underline{m}) \mathrm{sgn}\left(M(\underline{m})\right) T(\underline{m}). \tag{3.2}$$

The following notations have been introduced

$$\underline{m} = (m_1, m_2, \dots, m_k) \tag{3.3}$$
$$m_i \in \{0, \pm 1, \pm 2, \dots, \pm N\} \tag{3.4}$$
$$|\underline{m}| = k \tag{3.5}$$
$$T(\underline{m}) = T_{m_1} T_{m_2} T_{m_3} \dots T_{m_k} \tag{3.6}$$
$$M(\underline{m}) = \sum_{i=1}^{k} m_i. \tag{3.7}$$

This ansatz leads to recursive differential equations for the real functions $F(l;\underline{m})$ with the initial conditions $F(0,\underline{m}) = 1$ for $|\underline{m}| = 1$ and $F(0,\underline{m}) = 0$ for $|\underline{m}| > 1$. Due to the structure of the recursive equations, they can be solved in principal analytically. The calculation of the

[1] It should be noted, that this concept corresponds to an idea already introduced in the authors Diploma thesis [121]. However, the final intellectual step of separated white-graph results is introduced here, providing a considerably faster evaluation process and a new perspective.

analytic functions F can be performed on a computer up to a certain order $n_{\max}$ limited by the computation time and the memory usage only. The solution leads to an effective Hamiltonian of the form

$$\mathcal{H}_{\text{eff}}(\{\lambda_j\}) = \mathcal{H}_0 + \sum_{\sum_j k_j = k}^{\infty} \lambda_1^{k_1} \dots \lambda_{N_\lambda}^{k_{N_\lambda}} \sum_{|\underline{m}|=k} \sum_{\sum_i m_i = 0} C(\underline{m}) T(\underline{m}), \tag{3.8}$$

with $C(\underline{m}) \in \mathbb{Q}$. The restriction $\sum_i m_i = 0$ reflects the particle-conserving property of the final Hamiltonian. The summands can be viewed as virtual fluctuations of the new dressed particles defined by the effective Hamiltonian.

In a similar manner one can calculate other physical quantities with pCUT [87]. To this end, the same unitary transformation has to be applied to any observable $\mathcal{O}$ of interest

$$\frac{\partial \mathcal{O}(\{\lambda_j\};\ell)}{\partial \ell} = [\eta^{\mathcal{Q}}(\{\lambda_j\};\ell), \mathcal{O}(\{\lambda_j\};\ell)]. \tag{3.9}$$

Using the perturbative ansatz

$$\begin{aligned} \mathcal{O}(\{\lambda_j\};\ell) \quad = \quad & \sum_{\sum_j k_j = k}^{\infty} \lambda_1^{k_1} \dots \lambda_{N_\lambda}^{k_{N_\lambda}} \\ & \sum_{i=1}^{k+1} \sum_{|\underline{m}|=k} G(\ell;\underline{m},i) \mathcal{O}(\underline{m};i) \end{aligned} \tag{3.10}$$

with

$$\mathcal{O}(\underline{m};i) := T_{m_1} \dots T_{m_{i-1}} \mathcal{O} T_{m_i} \dots T_{m_k} \quad , \tag{3.11}$$

one obtains recursive differential equations for the functions $G(\ell;\underline{m},i)$. The final result is given by

$$\begin{aligned} \mathcal{O}_{\text{eff}}(\{\lambda_j\}) \quad = \quad & \sum_{\sum_j k_j = k}^{\infty} \lambda_1^{k_1} \dots \lambda_{N_\lambda}^{k_{N_\lambda}} \\ & \sum_{i=1}^{k+1} \sum_{|\underline{m}|=k} \tilde{C}(\underline{m};i) \mathcal{O}(\underline{m};i), \end{aligned} \tag{3.12}$$

with $\tilde{C}(\underline{m},i) = G(\ell=\infty;\underline{m},i) \in \mathbb{Q}$. In contrast to the effective Hamiltonian, effective observables are *not* quasiparticle conserving.

The coefficients $C(\underline{m})$ and $\tilde{C}(\underline{m};i)$ are independent of the model and can be straightforwardly applied to all the problems matching the requirements of the pCUT method. This generality is only possible at the expense of the second model-dependent extraction process described next for the effective Hamiltonian $\mathcal{H}_{\text{eff}}$. The treatment of effective observables can be done in complete analogy.

3.2 Perturbative continuous unitary transformations as a linked-cluster expansion

Since the effective operators like $\mathcal{H}_{\text{eff}}$ are not normal-ordered, matrix elements defining the effective model are not directly accessible. In order to calculate the desired matrix elements, the

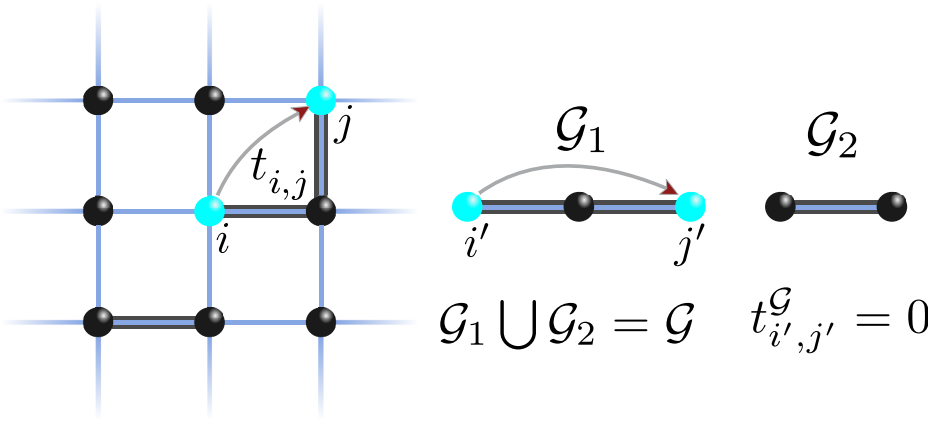

Figure 3.1: All fluctuations involving the highlighted links are pooled together in this representation. The overall contribution of these fluctuations to the hopping element $t_{i,j}$ in the thermodynamic limit (left panel) can be identified with a reduced contribution of a disconnected cluster (right panel) vanishing due to the linked cluster theorem. The figure is taken from Ref.[69].

effective Hamiltonian $\mathcal{H}_{\text{eff}}$ can be applied to a finite cluster yielding the correct contributions in the thermodynamic limit for a given order and matrix element. This crucial property results from the linked cluster theorem which states that only linked processes have an overall contribution to cluster additive quantities. The cluster additivity of the effective Hamiltonian results directly from the CUT approach (see 2.2.2).
We restrict the discussion to Hamiltonians where the perturbation couples always two supersites. The coupling between supersites is represented by a link in the cluster and the operator can be decomposed as

$$T_n = \sum_l \tau_{n,l} \quad , \tag{3.13}$$

where $\tau_{n,l}$ affects only the two supersites which are connected by the link l in the effective lattice. In other words, the operator $\tau_{n,l}$ acts on the link l. The sum runs over all links of the lattice. Inserting this decomposition into Eq.(3.8) yields

$$\begin{aligned} \mathcal{H}_{\text{eff}}(\{\lambda_j\}) \quad = \quad & \mathcal{H}_0 + \sum_{\sum_j k_j = k}^{\infty} \lambda_1^{k_1} \dots \lambda_{N_\lambda}^{k_{N_\lambda}} \cdot \\ & \sum_{|\underline{m}|=k} \sum_{\sum_i m_i = 0} C(\underline{m}) \sum_{l_1 \dots l_k} \tau_{m_k,l_1} \dots \tau_{m_k,l_k} \end{aligned} \tag{3.14}$$

In practice, however, the Hamiltonian is applied using Eq.(3.8). Each summand of order k can be understood as a virtual fluctuation involving the links $l_1 \dots l_k$. The links form a pattern which can be assigned to a cluster consisting of these links and adjacent sites. If the fluctuation pattern corresponds to a disconnected cluster, the overall contributions annihilate each other and such fluctuation patterns can be discarded, see also figure 3.1.

If the links (and the adjacent sites) form a connected cluster C, the process is called linked

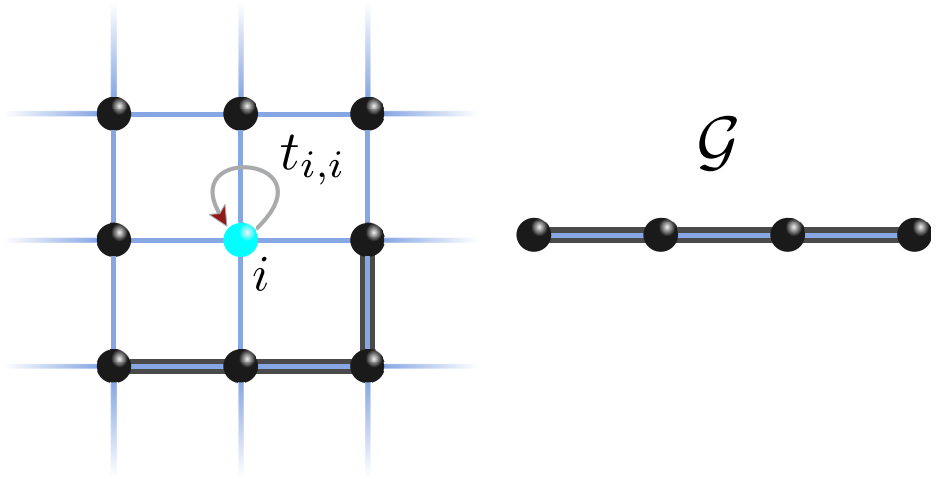

Figure 3.2: The fluctuation pattern indicated by the highlighted links corresponds to fluctuations associated with the vacuum. These fluctuations are irrelevant for the local one-particle hopping element $t_{i,i}$ in the thermodynamic limit (left panel). The figure is taken from Ref.[69].

and the Hamiltonian can be rewritten as a sum over these linked clusters

$$\mathcal{H}_{\text{eff}}(\{\lambda_j\}) = \mathcal{H}_0 + \sum_{\sum_j k_j = k}^{\infty} \lambda_1^{k_1} \dots \lambda_{N_\lambda}^{k_{N_\lambda}} \sum_{|\underline{m}|=k \sum_i m_i = 0} \sum_{C_k} C(\underline{m}) \sum_{l_1 \dots l_k, l_1 \bigcup l_2 \dots l_k = C_k} \tau_{m_k,l_1} \dots \tau_{m_k,l_k}. \tag{3.15}$$

Note that there are also fluctuation patterns which correspond to a lower QP channel since not all excitations are involved in the fluctuation as illustrated in figure 3.2. These fluctuations cancel via the subtraction scheme required for the normal ordering (see A.1).

A linked-cluster expansion arises therefore naturally from the pCUT approach. The simplest approach is to design a sufficiently large cluster which incorporates all the relevant linked fluctuations of a desired order and to carry out the calculation on this single cluster. Yet, the calculation based on this approach still incorporates a lot of unlinked processes resulting in an unnecessary computational overhead. Furthermore, these processes are kept in the memory during the calculation which usually defines the highest possible order.

It is therefore typically favorable to use a full cluster decomposition. To this end the contribution of (small) clusters is calculated by applying $\mathcal{H}_{\text{eff}}$ to all clusters determining the corresponding matrix elements which requires a minimal memory usage. Contributions of smaller subclusters have then to be subtracted in order to gain the reduced contributions of the cluster and to avoid double counting of fluctuations. Hence, after the subtraction, every link l_j in Eq.(3.15) is involved at least once.

The matrix elements in the thermodynamic limit are then determined by summing up all the reduced contributions of these subclusters. The efficiency of this approach is based on the identification of clusters by means of the topology which implies that the calculation can be restricted to a much smaller set of topologically distinct clusters called graphs.

3.2.1 Generating relevant graphs

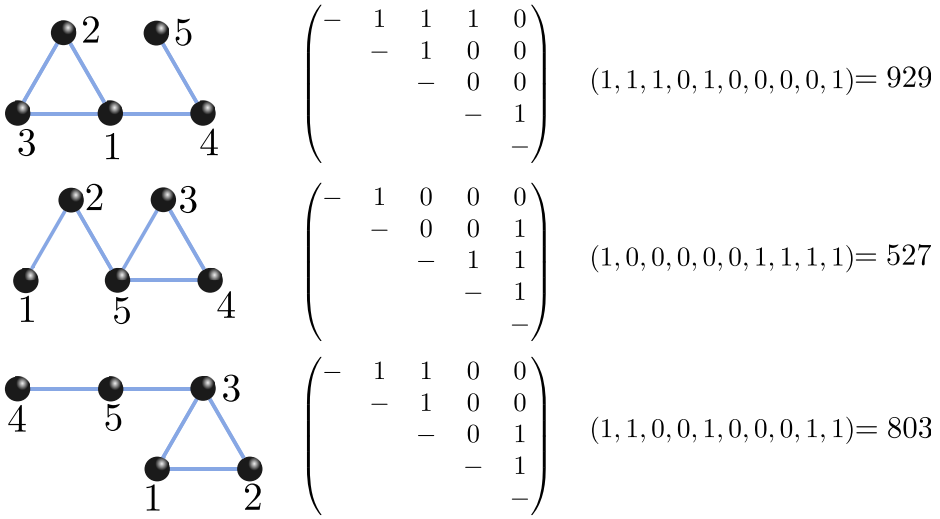

Figure 3.3: Three different labelings of the same graph are depicted with the corresponding adjacency matrices and the resulting keys. The first labeling corresponds to the canonical labeling and the resulting key is the graph key. The figure is taken from Ref.[69].

In the following, we briefly outline the underlying concepts of the topological identification by means of a canonical labeling. The identification process is oriented on the details given in Ref.[79].

First, we consider a system where all (super)sites are coupled by identical undirected bonds. In this case, a cluster is fully determined by an (arbitrary) numeration of the sites and the bonds linking the sites. A cluster of n sites can be represented by an $n \times n$ adjacency matrix $m_{i,j}$ with

$$m_{ij} = \begin{cases} 1, & \text{if sites } i \text{ and } j \text{ are connected by a bond} \\ 0, & \text{else.} \end{cases} \tag{3.16}$$

Two clusters are called topologically equivalent, if a simple renumeration of the sites yields the same adjacency matrix in both cases. Obviously, it is sufficient to restrict the calculation to topologically distinct clusters (graphs) because the results can easily be mapped via a relabeling.

In order to identify clusters as topologically equivalent, it is reasonable to introduce a canonical labeling which is distinct from other labelings. To this end, one identifies the off-diagonal elements $m_{i,j}$ $(i < j)$ as the binary bits of an integer number with the order $(m_{1,2}, m_{1,3}, \ldots m_{1,n} \ldots m_{n-1,n})$ serving as a key. The labeling which maximizes this key corresponds to the canonical labeling and defines the graph, see also figure 3.3 for examples. If two clusters are topologically equivalent, they are assigned to the same graph. In practice, it is necessary to find the labeling which maximizes the key efficiently. We do not go into technical details for the implementation. For further reading we refer to Ref.[79].

Using the graph key, it is possible to schematically produce the required connected graphs by successively adding links to a given set of graphs. Furthermore, the number of graphs relevant for the calculation can be additionally reduced. Obviously, it is sufficient to include only graphs

that can be embedded into the lattice under consideration, i.e. if the lattice contains clusters corresponding to this graph.

By construction, the reduced contribution of a graph of n links starts at most at order n. Hence, for a given order n, only connected graphs of up to n links have to be considered. Depending on the problem, further selection rules can help to reduce the number of relevant graphs because the presence of conserved quantities might result in further constraints for a given order.

3.2.2 Calculation on graphs

The next step is to perform the actual calculation on graphs, i.e. $\mathcal{H}_{\text{eff}}$ is evaluated to determine the relevant low-energy matrix elements. For the implementation, one typically chooses the eigenbasis of $\mathcal{Q}$, i.e. every basis state can be identified with a defined distribution of bare excitations. During the application of the operator sequences in $\mathcal{H}_{\text{eff}}$ the intermediate states are represented as linear combinations of these basis states

$$|\Psi\rangle = \sum_j \alpha_j |j\rangle \quad . \tag{3.17}$$

The basis states $|j\rangle$ are represented by integer numbers where the information of the basis states is encoded bitwise in the bit representation of an integer as known for instance from exact diagonalization. In this basis, the action of the operators in Eq.(3.13) affects only a small number of bits allowing for a fast access and modifications via bitwise operations.

Compared to the dimension of the full Hilbert space, the number of terms in an intermediate state is small. Therefore, it is useful to use associative arrays consisting of a key (the state represented by an integer) and an associated value (the coefficient α_j represented by a rational number). This is also illustrated in figure 3.4(a).

The desired matrix elements are then given as series expansions with rational coefficients. In order to gain cluster additive quantities for the embedding, the normal ordering is applied, followed by the subtraction of subclusters contributions.

3.2.3 Graph embedding

Finally, the graphs are embedded into the infinite lattice, i.e. all realizations of a given graph on the lattice are produced recovering all the clusters in Eq.(3.15) via the appropriate relabeling. The contributions of the cluster additive quantities are added up accordingly. Note that the contributions of all linked clusters in Eq.(3.15) are incorporated while the actual calculation is performed on a massively smaller subset of topologically distinct clusters. The embedding procedure is straightforward and technical details of the implementation can be found in Ref.[79].

Typically, the bottleneck of the calculation is defined by the derivation of the effective model on the graphs via pCUTs. Hence, the efficiency of this approach is based on the identification of clusters and the associated reduction of the number of clusters involved in the calculations.

3.3 White-graph expansion

Up to now, we have described the essential steps to set up a linked-cluster expansion with the pCUT method. This standard scheme becomes inefficient when the physical system possesses many linktypes corresponding to perturbation parameters λ_j, which is for example relevant when fitting experimental data with microscopic calculations. These linktypes function as

another topological attribute which can be incorporated in the usual scheme by generalizing $m_{i,j} \in \{0,1 \dots n\}$ for n linktypes. Clearly, this leads to an exponential growth of relevant graphs needed for the calculation. However, as we demonstrate in the following, one can circumvent this inconvenience by a so-called white-graph expansion.

The underlying principle of the white-graph expansion is to ignore the different linktypes (colors) for the topological classification of the clusters. The white-graph number is simply defined using Eq.(3.16) and the calculation is restricted to topologically distinct clusters in this sense. However, the contributions of clusters in Eq.(3.15) *cannot* be gained by a simple mapping of the sites because the contributions do differ depending on the color pattern of the links. To this end, additional information is tracked during the pCUT calculation on the single graphs allowing to restore the contribution of each cluster exactly from the calculation on white graphs.

3.3.1 The calculation on white graphs

The additional bookkeeping can be interpreted as an enhanced or generalized monomial; additional values $\boldsymbol{n}$ are assigned to the links to keep track of the relevant information. The latter can be comprised in a single object $M(\boldsymbol{n})$ which can be viewed as a generalized monomial. The choice of $M(\boldsymbol{n})$ is problem-dependent and must be adjusted for each application. If the links differ only with respect to the coupling strength, it is sufficient to track how often each link was active in the operator sequence applied to the current state. For more complex problems, more information must be tracked and this approach may become unfavorable in scenarios where a lot of linktypes are involved and the non-zero matrix elements differ greatly between the linktypes. However, in principle, it is always possible to track the relevant information.

Evaluated for a given link pattern, the generalized monomials must yield an actual polynomial in the multiple perturbation parameters of the different couplings such that the result corresponds exactly to the calculation on a cluster having this very link pattern. This allows for the subsequent evaluation necessary for the embedding procedure.

As indicated by the name, the generalized monomials obey

$$M(\boldsymbol{n_1}) \cdot M(\boldsymbol{n_2}) = M(\boldsymbol{n_1} + \boldsymbol{n_2}) \tag{3.18}$$

and the intermediate states during the calculation are then expressed as linear combinations of these elements:

$$|\Psi\rangle = \sum_{i,j} \alpha_{i,j} M(\boldsymbol{n}_i)|j\rangle \quad . \tag{3.19}$$

Note that the action of an operator in Eq.(3.13) affects the generalized monomials $M(\boldsymbol{n}_i)$ and the state $|j\rangle$ independently; similarly to the action on product wave functions.

As in a standard pCUT set up, it is reasonable to use associative arrays to represent the intermediate states. The information of a generalized monomial can analogously be encoded bitwise. In a naive implementation, the state combined with the generalized monomial defines the key and the associated amplitude $\alpha_{i,j}$ corresponds to the value as visualized in figure 3.4(b).

In an improved implementation, one can make use of the product structure of the generalized monomials as well as of the intermediate states and factorize the representation:

$$|\Psi\rangle = \sum_{j} |j\rangle \left(\sum_{i} \alpha_{i,j} M(\boldsymbol{n}_i) \right) \quad . \tag{3.20}$$

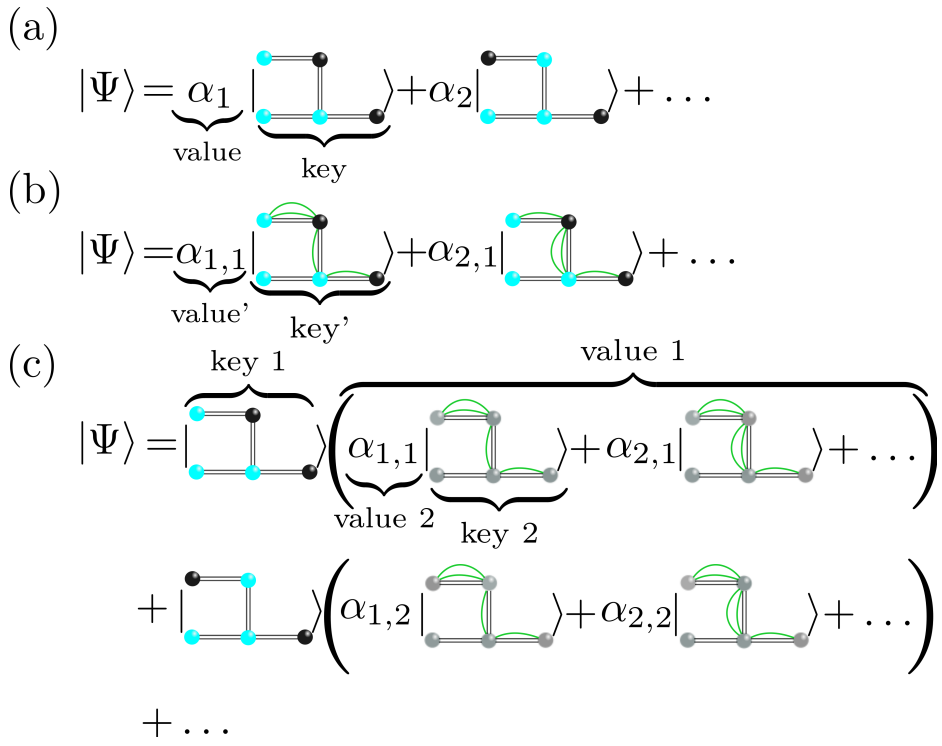

Figure 3.4: (a) The standard representation of intermediate states $|\Psi\rangle$ following Eq.(3.17) so that α_j corresponds to a rational number. (b) Standard calculation on white graphs using the generalized monomials as written in Eq.(3.19). (c) Improved calculation on white graphs following Eq.(3.20) which uses the product structure of the generalized monomials. The figure is taken from Ref.[69].

The effect of the operators on the state $|j\rangle$ can be calculated independently of the effect on the appendant sum of generalized monomials. Consequently, numerous redundant search, comparison, and shift operations are avoided. The implementation of this approach requires two nested containers. The key of the first container is defined by the state $|j\rangle$ while the value is given by a second container. The second container is defined by a key comprising the information of the generalized monomial $M(\boldsymbol{n}_i)$ and the value corresponds to the amplitude $\alpha_{i,j}$ of this generalized monomial and the state. This is illustrated in figure 3.4(c).

For an efficient performance, we recommend a simple modification of this procedure. As shown in subsection 3.2, the reduced contribution of a graph involves each link at least once. This property can help to reduce the computational effort immensely. The objective is to calculate the reduced contribution of a cluster directly without relying on a second subtraction step.

We consider the calculation in order k on a graph consisting of n links. Let $\mu_{i,j}$ denote how often a link j appeared in the operator sequences comprised in the monomial $M(\boldsymbol{n}_i)$. This information is typically tracked anyway and cause no computational overhead. We define

$$\mu_i = \sum_j \tilde{\mu}_{i,j} \quad \text{with} \quad \begin{cases} \tilde{\mu}_{i,j} \equiv \mu_{i,j} - 1, & \text{if } \mu_{i,j} > 1 \\ \tilde{\mu}_{i,j} = 0, & \text{else.} \end{cases} \tag{3.21}$$

One can discard all intermediate generalized monomials $M(\boldsymbol{n}_i)$ where $\mu_i > k - n$.
Evidently, this is specifically relevant if the number of links n is close or equal to the order k, i.e. for graphs with a large number of links. By construction, these graphs represent the majority of graphs making this modification extremely valuable.

Finally, the matrix elements of the Hamiltonian are given as linear combinations of the generalized monomials. The generalized monomials of these matrix elements build the centerpiece of this approach carrying the relevant information for the embedding of the white graphs described in the following.

3.3.2 Embedding white graphs

For the embedding procedure of a standard linked-cluster expansion, all realizations of a given graph on the lattice are produced recovering all the clusters in Eq.(3.15) via the according relabeling and the contributions of the clusters are added up. Analogously for the white-graph embedding, all realizations of a given graph on the lattice are generated. In order to recover the contributions of all clusters in Eq. 3.15, the information of the link pattern must be incorporated in a second evaluation step. The matrix elements on the white graphs are given as sums of generalized monomials. Evaluated for a given link pattern, the generalized monomials yield a polynomial in the multiple perturbation parameters recovering the result of the calculation on a cluster corresponding to the given link pattern. The resulting contributions are added up for all embeddings recovering the correct result in the thermodynamic limit.

3.4 Coupled two-leg XXZ Heisenberg ladders

In order to illustrate the functioning and usefulness of a white-graph expansion, we discuss in this section the calculation of one-magnon dispersions for the ordered state of a two-dimensional quantum spin model of coupled two-leg XXZ ladders involving four different perturbation parameters. The microscopic model in terms of spin 1/2 operators reads

$$\mathcal{H} = \sum_{\gamma,\langle i,j\rangle} J_\gamma \left[S_i^{\mathrm{z}} S_j^{\mathrm{z}} + \frac{\lambda}{2} \left(S_i^{\mathrm{x}} S_j^{\mathrm{x}} + S_i^{\mathrm{y}} S_j^{\mathrm{y}} \right) \right] \tag{3.22}$$

and is depicted in figure 3.5(I). The different couplings J_γ correspond to rung (leg) exchange J_{rung} (J_{leg}) of the two-leg ladders, the inter-ladder exchange J_{int}, and a spin-anisotropy λ. This Hamiltonian was recently shown to be relevant for the quantum magnet $C_9H_{18}N_2CuBr_4$ displaying long-range Néel order and gapped magnon excitations [117]. The structure is illustrated in figure 3.5(II). We exploit the white-graph expansion to set up a high-order series expansion for the one-magnon dispersion. This allows to determine the exchange couplings of the system to be $J_{\mathrm{leg}} = 0.60(2)$ meV, $J_{\mathrm{rung}} = 0.64(9)$ meV, $J_{\mathrm{int}} = 0.19(2)$ meV with the spin-anisotropy $\lambda = 0.93(2)$, according to inelastic neutron-scattering measurements [117].
To calculate the one-magnon dispersion, we perform a sublattice rotation to obtain a ferromagnetic reference state for the Ising case $\lambda = 0$, which transforms Eq. (3.22) to

$$\mathcal{H} = \sum_{\gamma,\langle i,j\rangle} J_\gamma \left[-S_i^{\mathrm{z}} S_j^{\mathrm{z}} - \frac{\lambda}{2} \left(S_i^{+} S_j^{+} + S_i^{-} S_j^{-} \right) \right]. \tag{3.23}$$

We then introduce hardcore-boson operators $\hat{a}_\nu^\dagger$ and $\hat{a}_\nu$ ($\hat{b}_\nu^\dagger$ and $\hat{b}_\nu$), which create and annihilate a magnon at site A (B) of rung ν above the ferromagnetic reference state, obtaining the

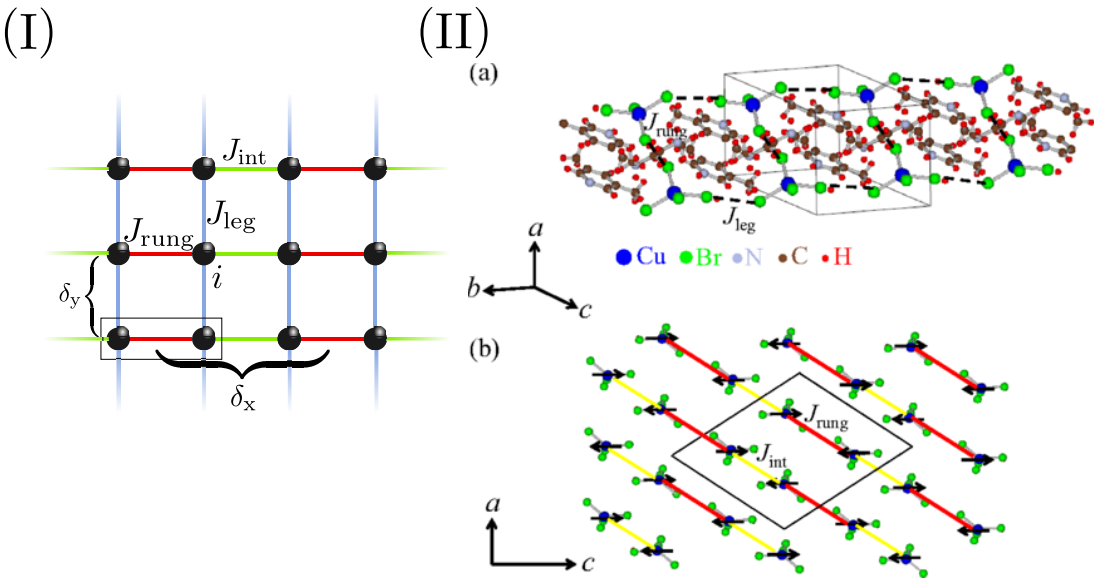

Figure 3.5: (I) Illustration of the quantum spin model of coupled two-leg XXZ ladders. Filled circles represent quantum spin 1/2 which are linked by various solid lines illustrating the different exchange couplings $J_{\rm rung}$, $J_{\rm leg}$, and $J_{\rm int}$. The black box shows the two-site unit cell of the system corresponding to the rungs of the ladder and δx (δy) refers to the distance between two neighboring rungs belonging to different (same) ladders. (II) (a) Crystal structure of $C_9H_{18}N_2CuBr_4$, in which the ladder chain extends along the b axis. Outlined is a nuclear unit cell. (b) Projection onto a plane perpendicular to the b axis, showing the proposed interladder couplings. Different lines stand for the different bonds. Red and yellow lines indicate the intraladder coupling $J_{\rm rung}$ and interladder coupling $J_{\rm int}$, respectively. Black arrows indicate the directions of the spins. The parallelogram is a projection of a magnetic unit cell. Figure (I) is taken (up to adjustments of notation) from Ref.[70] and figure (II) is taken from Ref.[117].

hardcore-boson Hamiltonian

$$\begin{aligned}\frac{\mathcal{H}}{\tilde{J}} &= -\frac{N}{2}+\sum_{\nu}\left(\hat{n}_{\nu}^{(a)}+\hat{n}_{\nu}^{(b)}\right)\\ &\quad+\sum_{\nu}\left[T_{\nu,0}+\lambda\left(T_{\nu,-2}+T_{\nu,+2}\right)\right] \quad ,\end{aligned} \tag{3.24}$$

where $\tilde{J}=J_{\rm leg}+(J_{\rm rung}+J_{\rm int})/2$, N is the number of unit cells, $\hat{n}_{\nu}^{(a)}=\hat{a}_{\nu}^{\dagger}\hat{a}_{\nu}$, and $\hat{n}_{\nu}^{(b)}=\hat{b}_{\nu}^{\dagger}\hat{b}_{\nu}$. The sums are taken over all rungs. The operators $T_{\nu,n}$, with $T_{\nu,-2}=T_{\nu,+2}^{\dagger}$, are given by

$$\begin{aligned}T_{\nu,0} &= -x_{\rm rung}\hat{n}_{\nu}^{(a)}\hat{n}_{\nu}^{(b)}-x_{\rm int}\hat{n}_{\nu}^{(b)}\hat{n}_{\nu+\delta x}^{(a)}\\ &\quad-x_{\rm leg}\left(\hat{n}_{\nu}^{(a)}\hat{n}_{\nu+\delta y}^{(a)}+\hat{n}_{\nu}^{(b)}\hat{n}_{\nu+\delta y}^{(b)}\right)\end{aligned} \tag{3.25}$$

and

$$\begin{aligned}T_{\nu,+2} &= -x_{\rm rung}\hat{a}_{\nu}^{\dagger}\hat{b}_{\nu}^{\dagger}-x_{\rm int}\hat{b}_{\nu}^{\dagger}\hat{a}_{\nu+\delta x}^{\dagger}\\ &\quad-x_{\rm leg}\left(\hat{a}_{\nu}^{\dagger}\hat{a}_{\nu+\delta y}^{\dagger}+\hat{b}_{\nu}^{\dagger}\hat{b}_{\nu+\delta y}^{\dagger}\right) \quad ,\end{aligned} \tag{3.26}$$

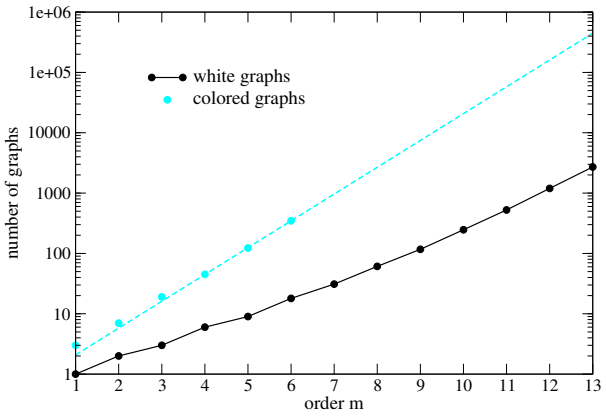

Figure 3.6: The number of white (colored) graphs are shown as filled black (cyan/grey) circles as a function of the perturbative order m for the model of coupled two-leg XXZ Heisenberg ladders. The dashed cyan/grey curve represents a fit $a \exp(b\, m)$ through the data points corresponding to colored graphs. The figure is taken from Ref.[69].

where $x_\gamma = J_\gamma/\tilde{J}$, and δx (δy) is the distance between two neighboring rungs belonging to different ladders (the same ladder).

At this point let us replace $x_\gamma \to \tau x_\gamma$ with $\tau \in [0,1]$ so that $\tau = 1$ corresponds to our physical system Eq.(3.24) and $\tau = 0$ functions as a well defined starting point for perturbation theory. Indeed, the resulting Hamiltonian can be rephrased as

$$\frac{\mathcal{H}}{\tilde{J}} \;=\; \mathcal{H}_0 + \tau \sum_{n\in\{-2,0,2\}} T_n \quad , \tag{3.27}$$

which corresponds exactly to Eq.(2.1) and meets all criteria relevant to apply the pCUT method as described above: i) The unperturbed Hamiltonian at $\tau = 0$ is equidistant, ii) the unperturbed spectrum is bounded from below, and iii) the perturbation is decomposed in T_n operators. One can therefore map Eq.(3.27) to an effective model, $\mathcal{H}_{\text{eff}}$, which conserves the number of magnons. The one-magnon sector $\mathcal{H}^{(1)}_{\text{eff}}$, which is of our interest here, corresponds to an effective hopping Hamiltonian for the magnons in real space and is therefore fully determined by the one-magnon hopping amplitudes. The corresponding one-magnon sector $\mathcal{H}^{(1)}_{\text{eff}}$ can then be simplified by a Fourier transformation to

$$\mathcal{H}^{(1)}_{\text{eff}} = \sum_{\boldsymbol{k}} \left(\omega^\alpha(\boldsymbol{k}) \alpha^\dagger_{\boldsymbol{k}} \alpha_{\boldsymbol{k}} + \omega^\beta(\boldsymbol{k}) \beta^\dagger_{\boldsymbol{k}} \beta_{\boldsymbol{k}} \right) \quad , \tag{3.28}$$

where $\omega^\alpha(\boldsymbol{k})$ and $\omega^\beta(\boldsymbol{k})$ denote the two one-magnon branches stemming from the two-site unit cell. Here, we have determined both one-magnon branches by series expansion up to 13th order in all parameters τx_γ. At this order one has to treat 2709 white graphs in total. Clearly, the number of graphs with color is many orders of magnitude larger and a related calculation is well beyond any realistic set up. This is further highlighted in figure 3.6 where the number of colored and white graphs is displayed against the perturbative order m. Since the different linktypes differ only with respect to their coupling strengths, the additional information $\boldsymbol{n}$ tracked during the calculation on white graphs must incorporate how many times each link is

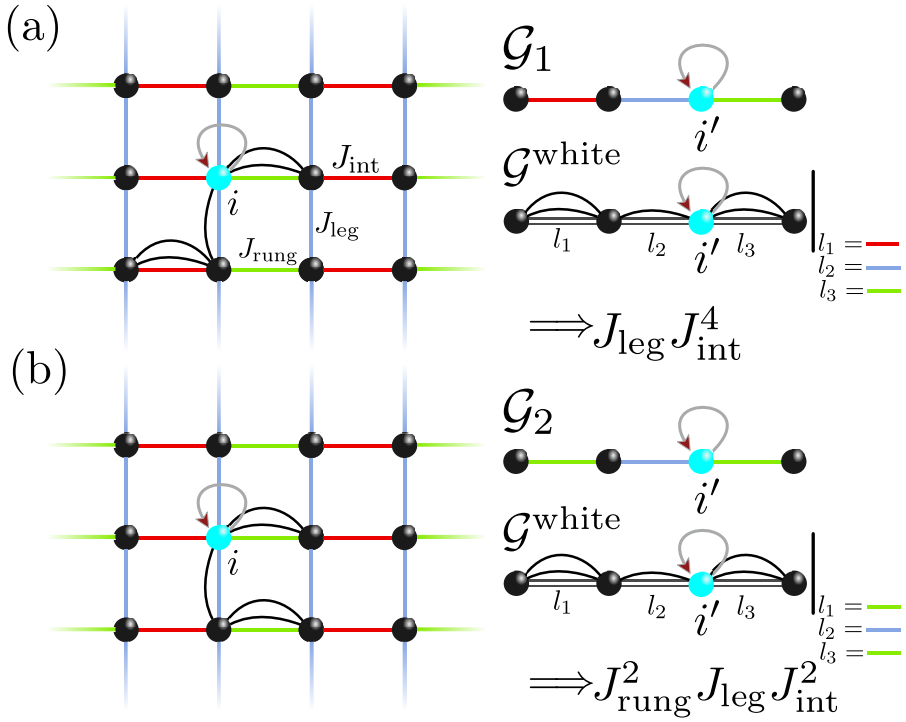

Figure 3.7: Illustration of two different fluctuation patterns contributing to the local one-particle hopping element $t_{i,i}$ in the thermodynamic limit (left panel) for the quantum spin model of coupled two-leg XXZ ladders. The solid lines correspond to the different exchange couplings $J_\perp$, $J_\parallel$, and $J_{\rm int}$. The occurrence of a link in Eq.(3.15) is visualized by an arc defining the fluctuation pattern. All fluctuations with this pattern are pooled together in this representation. Both fluctuations are associated with topologically distinct graphs $\mathcal{G}_1$ and $\mathcal{G}_2$ (right panel) solely because their colorings are different. Decomposing the results of the calculation with respect to the fluctuation pattern allows to gain both contributions by embedding a single white graph $\mathcal{G}^{\rm white}$ and 'evaluating' the resulting coloring. The evaluation yields polynomials in the different perturbation parameters J_γ. The figure is (up to adjustments of notation) taken from Ref.[69].

acted on by the perturbation parameters J_γ. This is in fact identical to the approach where *all* links of a graph have different coupling constants and the result is given as a multi-variable polynomial. Finally, during the embedding procedure, the coupling constants of the graph are matched with the ones of the specific graph realizations on the lattice. This is visualized for the local one-particle hopping element $t_{i,i}$ in figure 3.7. Let us stress that the results for the one-magnon dispersions are given analytically in all physical parameters $x_\perp$, $x_\parallel$, $x_{\rm int}$, and λ. Scanning through a large variety of parameter sets, which is often needed when fitting experimental data, is then straightforward as long as convergence in τ up to $\tau = 1$ is given: the values for the different couplings just have to be inserted into the analytical expression.

Physically, the series in τ do converge well for small values of λ. First, both limits $\tau = 0$ and $\lambda = 0$ have exactly the same ground state as well as the same one-magnon excitations. Only the multi-magnon energies differ. Second, quantum fluctuations are strongly suppressed for small λ and/or τ. We find that bare series in τ are quantitatively converged up to $\tau = 1$

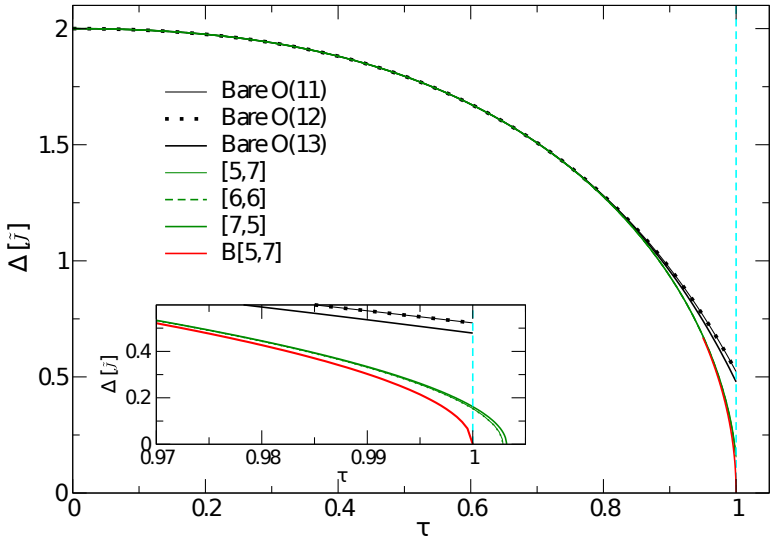

Figure 3.8: One-magnon gap $\Delta/\tilde{J}$ as a function of τ for the isotropic square lattice $J_{\text{leg}} = J_{\text{rung}} = J_{\text{int}} = \lambda = 1$ for different bare series and different (biased) DlogPadé extrapolants. *Inset*: Zoom close to $\tau = 1$. The figure is taken from Ref.[69].

for $\lambda \lesssim 0.8$. For larger values of λ, one has to rely on extrapolation schemes like DlogPadé extrapolation (see Ref.[122] or discussion in section 4.3).
This is especially true for the most demanding case of the one-magnon low-energy gap $\Delta \equiv \min_{\boldsymbol{k}} \left(\omega^{\alpha}(\boldsymbol{k}),\omega^{\beta}(\boldsymbol{k})\right)$ at $\lambda = 1$. In DlogPadé extrapolation one constructs various extrapolants $[L,M]$ where L (M) denotes the order of the numerator (denominator) and one requires $L + M = m - 1$ where m denotes the maximal perturbative order. In the case of a physical phase transition, the DlogPadé extrapolation displays poles which allows to deduce the critical exponent $z\nu$ for every extrapolant $[L,M]$. The quality of the DlogPadé extrapolation can be further improved when the location of a quantum critical point is known exactly. This is true in our case since the only physical point of the expansion is $\tau = 1$. For this case one can bias the DlogPadé extrapolation. This yields extrapolants $B\,[L,M]$ having a pole at $\tau = 1$ by construction. In the following, we exemplify a typical behavior of Δ for the isotropic Heisenberg model on the square lattice with $J_{\text{leg}} = J_{\text{rung}} = J_{\text{int}} = \lambda = 1$. This isotropic point is known to have gapless Goldstone bosons due to the breaking of $SU(2)$ symmetry in the long-range ordered Néel ground state. One therefore expects that the one-magnon gap Δ is gapped for all values $\tau < 1$ and vanishes at $\tau = 1$. As outlined in Refs. [123, 124], the quantum critical behavior is mean-field like, i.e. one has critical exponents $\nu = 1/2$ and $z = 1$. Our results for the one-magnon gap are displayed in figure 3.8. The bare series is reliable up to $\tau \lesssim 0.85$ predicting an unphysical gap for $\tau = 1$.

This situation is strongly improved using DlogPadé extrapolation. Essentially all extrapolants show a pole close to $\tau \approx 1$. Taking all $[L,M]$ of highest order $L + M = 12$ with $L \geq 3$ and $L \geq 3$, the average pole is found at $\tau_0 = 1.004$ with an average critical exponent $z\nu \approx 0.52$ very close to the expected value $1/2$. The quality of the extrapolation gets even better when biasing the extrapolants such that they exhibit a pole at exactly $\tau = 1$. In this case one finds an average critical exponent $z\nu \approx 0.499$. Overall, we therefore find quantitative agreement even in the most demanding quantum critical regime using our high-order series expansion. Let us

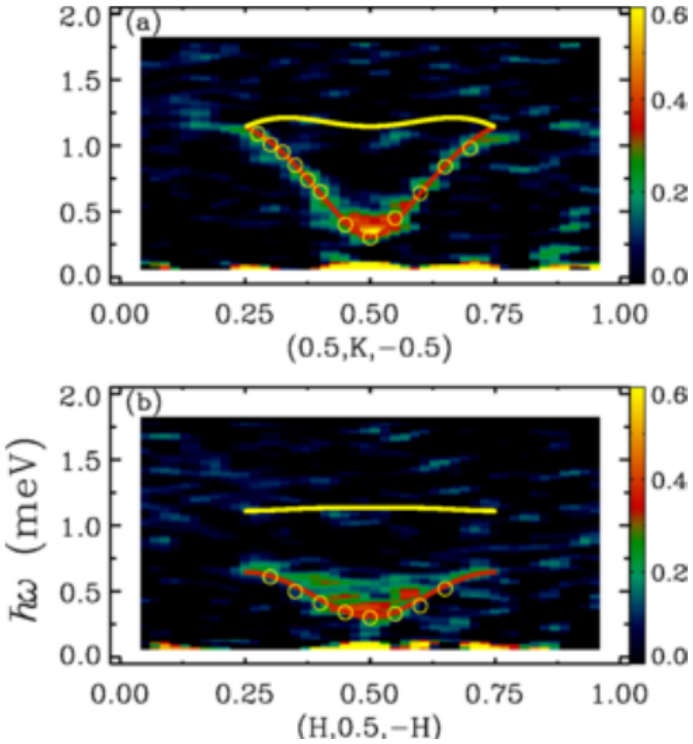

Figure 3.9: False-color map of the measured spectra along the ladders and perpendicular to the ladders along. Red and yellow lines show the fit of the one-magnon dispersion. The figure is taken from Ref.[117].

stress that similarly well converged results can be directly deduced in all parts of the (large) parameter space.
This is especially important in comparison to experiment. Unfortunately, DlogPadé extrapolations do not provide good approximations for the whole momentum axis. Therefore, we perform Padé extrapolations of $\omega_\alpha^2(\boldsymbol{k})$ and $\omega_\beta^2(\boldsymbol{k})$. The reason for casting $\omega_\alpha^2(\boldsymbol{k})$ and $\omega_\beta^2(\boldsymbol{k})$, instead of $\omega_\alpha(\boldsymbol{k})$ and $\omega_\beta(\boldsymbol{k})$, as Padé approximants is that the one-magnon energy gap $\Delta = \omega(0,0)$ of a square-lattice antiferromagnet vanishes at $\lambda = 1$ with a square-root singularity [123, 124]. In other words Δ^2 is a linear function of λ close to the critical point. This behavior of Δ^2 is ensured by expressing $\omega_\alpha^2(\boldsymbol{k})$ as a Padé approximant.

To compare the calculation with the experimental data of the inelastic neutron-scattering measurements, we (i) shift the two magnon dispersions $\omega_\alpha(\boldsymbol{k})$ and $\omega_\beta(\boldsymbol{k})$ by $\boldsymbol{k} = (0,\pi)$ and (ii) fold the resulting dispersions into the reduced BZ in the y direction, because the unit cell of the Néel-ordered state comprises four sites before the sublattice rotation. We choose the exchange constants J_γ and the spin-anisotropy λ such that the calculated curves lie within experimental error bars. The results are in excellent agreement with the observed dispersions, as shown in figure 3.9.
Finally, we want to remark, that the one-magnon physics in this parameter regime can*not* be captured adequately by a simple leading-order calculations and it requires advanced technical tools to obtain sufficiently accurate results. In addition to that, only analytical series-expansion

results allow for a fast scanning of the large parameter space, showing clearly the uitility of the white-graph expansion.

3.5 Conclusions

In this chapter we have introduced the so-called white-graph expansion for the method of perturbative continuous unitary transformations when implemented as a linked-cluster expansion. The essential idea behind this expansion is an optimal bookkeeping during the calculation on graphs which is possible due to the presence of the model-independent effective pCUT Hamiltonian in second quantization. Our approach is especially useful when the microscopic model under consideration has several expansion parameters. This case usually represents a major challenge for any kind of linked-cluster expansion due to the proliferating number of linked graphs. Indeed, each expansion parameter corresponds to a distinct color in the graph expansion. The white-graph expansion overcomes this challenge to a great extent, since the actual calculation is performed on white graphs and the coloring is done after the calculation as a final step.
We are strongly convinced that this white-graph expansion is useful in many situations, e.g. microscopic models in three dimensions or systems with long-rang interactions being notoriously complicated for linked-cluster expansions. Finally, it would be interesting whether other types of linked-cluster expansions like for example Takahashi's degenerate perturbation theory [125] or matrix perturbation theory [79] can be also reformulated as a white-graph expansion.
The white-graph expansion relies on the utilization of the underlying CUT framework to set up a modified LCE scheme. In the next chapter, we discuss the exploitation of the underlying CUT framework, to define a modified NLCE approach.

Chapter 4

Graph-based Continuous Unitary Transformations

In this chapter we focus on the combination of CUTs (see also 2.3) with the underlying concepts of NCLEs (see also 2.2). This approach, introduced by Yang and Schmidt in 2011, is called graph-based continuous unitary transformations (gCUTs) and provides a scheme to derive effective low-energy models if at least one degree of freedom is gapped [46].
On the one hand, gCUTs can be interpreted as a schematic real-space truncation scheme for CUTs. On the other hand, gCUTs can be viewed as an NLCE where the quantities of interest are derived on finite clusters by a CUT and then embedded into the lattice to gain the result in the thermodynamic limit. Using this method, a smooth derivation of the quantities, which is inherent to CUTs, is combined with a physically intuitive real-space truncation of NLCEs.
The objectives of this chapter are twofold: (i) The general gCUT scheme is presented where the focus is laid on technical developments and findings going beyond the initial gCUT scheme introduced in [46]. (ii) Following this, the quasiparticle generator scheme is modified to address the challenges arising from non-perturbative renormalization on clusters. Namely, the scheme is modified to treat both, pseudo decay (see 4.2.3 and genuine decay (see 4.2.4).

4.1 General scheme

In this section, we are going to present the general scheme which is applicable if neither pseudo nor genuine decay is present during the calculation. We are going to start by introducing a recipe for gCUTs to highlight the main steps of the approach. Afterwards, these steps are elaborated on, introducing further improvements.

4.1.1 Recipe

A recipe for applying gCUTs is described in the following and is presented in the style of the CORE algorithm given in [96]. Both methods differ only with respect to the derivation of the effective model on the finite cluster. While CORE relies on an exact diagonalization of the low-energy spectrum followed by projection operations into the desired subspace, gCUTs are based on a CUT applied to finite clusters.
The recipe for gCUTs reads:

- Choose a small cluster (e.g., rung, plaquette, triangle, etc.) and diagonalize it. These small clusters build the supersites and impose the quasiparticle picture. The lowest state of these effective sites is identified with the absence of a quasiparticle while the excitations are identified with the presence of a quasiparticle on the respective supersite. (see also 2.1.)

- Choose a consistent and systematic pattern of clusters consisting of up to N supersites which cover the whole lattice for $N \to \infty$. Topologically equivalent clusters can be identified with each other.
- For each cluster $\mathcal{C}$ do:
  - Represent the Hamiltonian $\mathcal{H}^{\mathcal{C}}$ and observables $\mathcal{O}^{\mathcal{C}}$ as matrices in a suited (truncated) basis
  - Perform the CUT with a suited generator scheme via numerical integration of the flow equation Eq.(2.31): $\mathcal{H}^{\mathcal{C}} \xrightarrow{\text{CUT}} \mathcal{H}^{\mathcal{C}}_{\text{eff}}$
  - Extract the low-energy Hamiltonian $\hat{\tilde{h}}^{\mathcal{C}}$ on the cluster. Lower QP channels must be subtracted (see appendix A.1)
  - Perform the *same* transformation for observables and identify the low-energy part of the observables $\hat{\tilde{o}}_{\mathcal{C}}$ accordingly
  - Determine the reduced contributions of the cluster by subtracting the reduced contributions of all connected subclusters:

$$\hat{h}_{\mathcal{C}} = \hat{\tilde{h}}_{\mathcal{C}} - \sum_{\mathcal{C}_{\text{sub}}} \hat{h}_{\mathcal{C}_{\text{sub}}} \tag{4.1}$$

$$\hat{o}_{\mathcal{C}} = \hat{\tilde{o}}_{\mathcal{C}} - \sum_{\mathcal{C}_{\text{sub}}} \hat{o}_{\mathcal{C}_{\text{sub}}} \quad . \tag{4.2}$$

- Finally, the effective Hamiltonian and the effective observable are given by a cluster expansion

$$H^{\text{gCUT}}_{\text{eff}} = \sum_{\mathcal{C}} \hat{h}_{\mathcal{C}}$$
$$O^{\text{gCUT}}_{\text{eff}} = \sum_{\mathcal{C}} \hat{o}_{\mathcal{C}} \quad ,$$

  where the sum runs over all clusters $\mathcal{C}$ of the lattice. The sum implies that all the operator coefficients are added up defining the effective Hamiltonian (effective observables) in the thermodynamic limit of the form Eq.(2.6) (Eq.(2.10)).

- Bon appetit!

This recipe builds the basic framework for any gCUT calculation. As always, the devil is in the details.
First, the systematic pattern of clusters chosen for the cluster expansion does affect the quality of the expansion severely. The optimal pattern is problem dependent and still a question of ongoing research [65, 126].
Second, the truncation of the basis is essential for reaching sufficiently large graph lengths. While the first gCUT calculations were carried out using the full untruncated basis [46, 63], we introduce truncation schemes, allowing to reach significantly larger cluster sizes. The truncations are described in 4.1.3 and have been applied recently for the derivation of effective spin models [64].
Lastly, the flow equation on each cluster must be solved relying on a suited generator scheme. The development of suited generator schemes to treat pseudo decay and genuine decay represents the main focus of this thesis and is addressed in detail in 4.2.3 and 4.2.4.
If neither pseudo nor genuine decay is present, the standard quasiparticle generator scheme

Eq.(2.41) represents a well-engineered generator scheme. However, in order to introduce truncations, a moderate modification of the scheme is advisable.
It is useful to continue by first describing the matrix representation of the Hamiltonian and the observables to build the basis for further discussion.

4.1.2 Matrix representation

In gCUTs, the Hamiltonian is represented on matrix level which depends on the basis chosen for the representation. In the following, we want to discuss the choices of the basis suited for the calculations. These choices of the basis are not separated from the choice of the generator scheme. The definition of the generator scheme sets constraints for the choice of the possible bases. As indicated above, the applications rely on modifications of the quasiparticle generator. The matrix representation given in Eq.(2.41) requires that each basis state of the initial system is an eigenstate of $\mathcal{Q}$.
In order to extract the prefactors of the effective hopping operators after the CUT, it is appropriate that these prefactors are identical to the matrix elements of the low-energy block. This implies, oftentimes, that the basis states building the low-energy block after the CUT must be eigenstates of the operators $\tilde{n}_{i,\alpha} = \tilde{f}^\dagger_{i,\alpha}\tilde{f}_{i,\alpha}$, i.e., the states can be identified with a defined pattern of excitations.
It seems natural to build the whole basis in this fashion because the matrix elements of the initial Hamiltonian in this basis are directly provided by the representation of the Hamiltonian of the form Eq.(2.5). Indeed, the first calculations were performed in this basis [46, 63]. We refer to this basis choice as the *standard basis*.
However, to perform the CUT, the valid subspace of different bases in accordance with Eq.(2.41) is defined by the constraint that each basis state is an eigenstate of $\mathcal{Q}$. A unitary transformation U_{block} transfers within this subspace, if $\mathcal{Q} = U^\dagger_{\text{block}}\mathcal{Q}U_{\text{block}}$. One finds

$$\tilde{\mathcal{H}}(\ell) = U^\dagger_{\text{block}}\mathcal{H}(\ell)U_{\text{block}} \tag{4.3}$$

$$\tilde{\eta}(\ell) = U^\dagger_{\text{block}}\eta(\ell)U_{\text{block}} \tag{4.4}$$

$$\partial_\ell\mathcal{H}(\ell) = [\mathcal{H}(\ell),\eta(\ell)] \tag{4.5}$$

$$\Rightarrow \partial_\ell\tilde{\mathcal{H}}(\ell) = [\tilde{\mathcal{H}}(\ell),\tilde{\eta}(\ell)] \quad , \tag{4.6}$$

with $\tilde{\eta}(\ell) = \eta[\tilde{\mathcal{H}}(\ell)]$ i.e., the identical generator scheme can be applied relying on the transformed Hamiltonian. Most importantly, $\tilde{\mathcal{H}}_{\text{eff}} = U^\dagger_{\text{block}}\mathcal{H}_{\text{eff}}U_{\text{block}}$, which means that the results gained in different bases are connected by the corresponding unitary transformation and are therefore equivalent. Furthermore, one finds for the residual off-diagonality (ROD)

$$\text{ROD} := \sum_{i,j,q_i\neq q_j} |\mathcal{H}_{ij}(\ell)|^2 = \text{Tr}\left(\mathcal{H}^2_{\text{nc}}\right) \tag{4.7}$$

$$= \text{Tr}\left(\tilde{\mathcal{H}}^2_{\text{nc}}\right) = \sum_{i,j,q_i\neq q_j} |\tilde{\mathcal{H}}_{ij}(\ell)|^2 \quad . \tag{4.8}$$

In other words, the ROD is equivalent for any of these bases and one is free to transform between them. It is even possible to change the basis during the flow if it is appropriate.
In all these possible bases, the particle conserving part of the Hamiltonian $\mathcal{H}_{\text{c}}(\ell)$ is block diagonal. As discussed in 2.3, the eigenvalues of these subblocks serve as crucial characteristics of the transformation. Consequently, the basis which diagonalizes the subblocks defined by $\mathcal{H}_{\text{c}}(\ell)$ is specifically relevant. We refer to this basis as *subblock basis*. Note that this basis choice

is ℓ-dependent and therefore requires a change of basis during the flow.
The freedom of choice with respect to the basis for the matrix representation is an essential property allowing, inter alia, to make use of the spatial symmetries by transforming to a suited basis (see 4.1.4) or to introduce truncation schemes as discussed in the following.

4.1.3 Truncation of the basis

In the following, we introduce a systematic and efficient truncation scheme for the basis. Without any form of truncation, matrices of the size $D_{\mathfrak{H}} \times D_{\mathfrak{H}}$ must be treated, where $D_{\mathfrak{H}}$ denotes the dimension of the considered Hilbert space. Then, the integration of the flow equation has generally order $D_{\mathfrak{H}}^2$ memory complexity and order $D_{\mathfrak{H}}^3$ time complexity. In contrast, CORE relies on an exact diagonalization for the low-energy spectrum. Consequently, memory and time complexity are of order $D_{\mathfrak{H}}$ and significantly larger system sizes can be treated via CORE. gCUTs rely on a CUT on each cluster, which yields more information compared to the similarity transformation applied in CORE. As a result and in contrast to CORE, gCUTs are applicable if the excitations are not protected by a quantum number from the ground state (see 2.2.2). Still, if both methods are applicable, they yield comparable results making this gap in length scales of the clusters unsatisfying. This suggests that the information necessary to set up the effective model via the CUT should mostly be contained in a small proportion of the basis. The idea of a truncation of the basis is to utilize this fact to reduce the size of these matrices in order to reach cluster sizes comparable to CORE.

Generator scheme $\eta^{\mathrm{QP},m}$

In initial applications, the whole Hilbert space was considered without any form of truncation [46, 63]. One reason for this is the robust straight-forward implementation of CUTs via the standard basis. Furthermore, the generator scheme η^{QP} in matrix representation imposes that each basis state has a defined number of quasi particles (see Eq.(2.41)). This complicates possible truncation schemes furthermore and causes unfavorable restrictions. However, one can avoid these constraints by relying on a slightly modified generator scheme.
Typically, one is only interested in the low-energy block and therefore it is sufficient to decouple the desired low-energy physics from the remainder. To this end, one can introduce a new generator $\eta^{\mathrm{QP},m}$ which only decouples the $(n \leq m)$-particle blocks while the $(n > m)$-particle blocks are not decoupled.
The corresponding modification is simple; all states with more than m particles are reinterpreted as $(m+1)$-particle states:

$$\eta_{i,j}^{\mathrm{QP},m} = (\tilde{q}_i - \tilde{q}_j) h_{i,j} \quad \text{with} \begin{cases} \tilde{q}_i = q_i, & \text{if } q_i \leq m \\ \tilde{q}_i = m+1, & \text{else.} \end{cases} \tag{4.9}$$

Indeed, this generator scheme yields valid results for the targeted $(n \leq m)$-particle block and the results are even identical to the results gained via η^{QP}. A proof for this property is given in Ref. [33].
We remark that, in contrast to sCUT approaches, the different generators will always yield the same transformation because the CUT is performed on matrix level on a finite cluster. Interestingly, for $m = 0$, the generator can be identified with a generator scheme defined by Dawson et al. [127].

A related modification of the quasiparticle generator scheme has been developed for sCUT and deepCUT approaches [29, 33, 102, 113, 116]. The generator scheme is denoted by $\hat{\eta}_{m:n}$ and is constructed with the same underlying principle that only the m lowest quasiparticle subspaces are decoupled.
Following the discussion given in [33], we stress that both schemes are not identical. The generator scheme $\eta^{\mathrm{QP},m}$ applied in gCUTs is naturally defined on the level of matrix elements. In contrast, $\hat{\eta}_{m:n}$ is defined with respect to normal-ordered operators, i.e., elements within higher quasiparticle channels associated with $(n \leq m)$-particle irreducible operators are additionally considered. The generator scheme $\hat{\eta}_{m:n}$ is designed to prevent divergencies during the numerical integration.
In contrast, the purpose of $\eta^{\mathrm{QP},m}$ is to facilitate possible truncations. Any linear combination of $(n > m)$ particle states is a valid basis state, which is clearly a favorable position for any truncation scheme.

Block-Lanczos truncation

The objective of the truncation is to approximate the low-energy matrix elements of the effective Hamiltonian as good as possible by a truncated basis. Let the low-energy states of the unperturbed Hamiltonian $\mathcal{H}_0$ be denoted by $\{|n^0\rangle\}$. Necessarily, these low-energy states must be included in the basis since they build the low-energy matrix. As a consequence, these states must be the starting point of any truncation.
The importance of a possible basis state is then defined by the influence of this state on the low-energy matrix *after* the CUT. To estimate this influence *before* the CUT, one can investigate the matrix elements of the initial Hamiltonian. It is reasonable to view the size of the matrix elements between the basis states with the low-energy states $\{|n^0\rangle\}$ as a measure for the importance of these states. Note that two states can be coupled indirectly via multiple matrix elements. Taking this criterion as an underlying principle to set up the basis leads to a block-Lanczos like truncation.
We want to construct the basis successively maximizing the size of the matrix elements. The states $\{|\tilde{n}^1\rangle\} \equiv \{H|n\rangle\}$ maximize this overlap via construction. The states can be orthonormalized to the states $\{|n^0\rangle\}$ via Gram-Schmidt $\{|\tilde{n}^1\rangle\} \to \{|n^1\rangle\}$ and included in the basis. Then, the matrix elements of the remaining states not included in the current basis with $\{|n^0\rangle\}$ vanish. These states only couple indirectly via $\{|n^1\rangle\}$.
The same argumentation can now be applied to the states $\{|n^1\rangle\}$ and so on. Interestingly, this scheme can be viewed as a variant of a scheme known as the block Lanczos algorithm with the states $\{|n^0\rangle\}$ as starting vectors [128].

$$\begin{aligned} \{|\tilde{n}^i\rangle\} &\equiv \{H|n^i\rangle\} \\ \{|\tilde{n}^{i+1}\rangle\} &\xrightarrow{\text{Gram Schmidt}} \{|n^{i+1}\rangle\} \\ i &\to i+1 \quad . \end{aligned}$$

This is repeated until a cut-off $i = i_{\max}$ or a maximal basis size $d_{\max}$ is reached. The resulting Hamiltonian is sketched in figure 4.1 (a). If the norm after orthogonalization is beyond a threshold $\varepsilon_{\mathrm{GS}}$ for a basis state, it is advisable to discard the state from the basis ($\varepsilon_{\mathrm{GS}} = 10^{-11}$). Furthermore, it is expedient to perform the Gram-Schmidt orthonormalization multiple times to ensure orthogonality.
The procedure builds up the basis systematically and in each step the size of the relevant matrix elements is maximized. Also, the quality of the truncation is regulated by a single parameter,

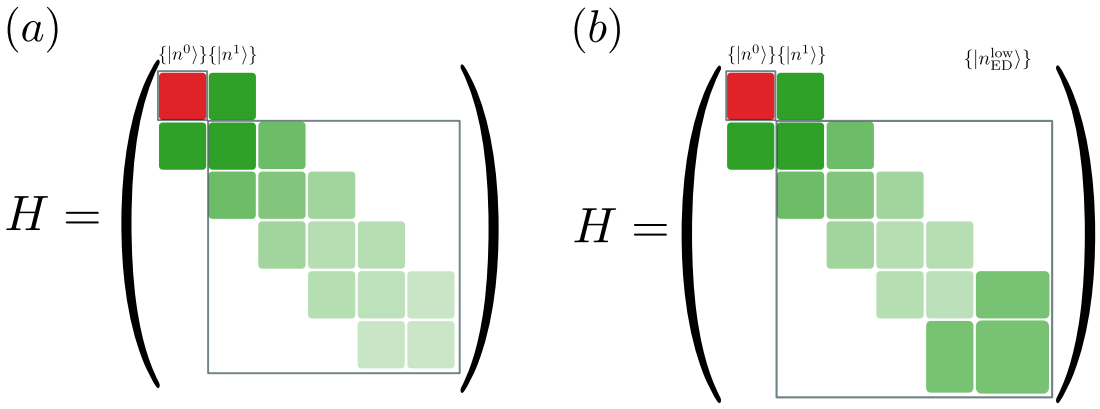

Figure 4.1: Schematic representation of the truncated bases. The color coding indicates the importance of the states with respect to the result of the effective low-energy model. (*a*) Basis generated via the block-Lanczos algorithm. The importance of the different states decreases with the depth of the Lanczos algorithm. (*b*) The basis generated via the block-Lanczos algorithm additionally expanded by the accurate low-energy states $\{|n_{\mathrm{ED}}^{\mathrm{low}}\rangle\}$, which are typically of significant importance.

which allows for direct convergence tests.
As a further beneficial characteristic, the states $\{|n^i\rangle\}$ obey the symmetries shared by both $\{|n^0\rangle\}$ and the Hamiltonian. The implementation of symmetries is discussed in detail in 4.1.4.

Extended block Lanczos truncation

The block-Lanczos truncation scheme already represents a valid truncation scheme. However, it is crucial for the effective low-energy model that the corresponding low-energy states are captured accurately in the basis. While this works rather well when the system is in the perturbative regime, the accuracy of this approach can become unsatisfying in the non-perturbative regime. This affects specifically the approximation of the high-energetic low-energy states.
This issue can be addressed by additionally including the m lowest states of the full Hamiltonian $\mathcal{H}$ to the basis in order to incorporate an accurate low-energy spectrum. The low-energy eigenstates $\{|n_{\mathrm{ED}}^{\mathrm{low}}\rangle\}$ can be gained via standard exact diagonalization (ED) algorithms, such as a restarted iterative version of block-Lanczos algorithm described above, Davidson algorithm [129] or Jacobi-Davidson algorithm [130]. The low-energy eigenspectrum is determined up to an accuracy $\varepsilon_{\mathrm{ED}} = 10^{-11}$. The states $\{|n_{\mathrm{ED}}^{\mathrm{low}}\rangle\}$ are included via Gram Schmidt orthonormalization in the basis generated by the block-Lanczos algorithm. The resulting truncation scheme is sketched in figure 4.1 (b).
In this scheme, the eigenvalues within the low-energy matrix are accurate and not affected by increasing d_{max}. Instead, increasing d_{max} corresponds to a unitary transformation within the decoupled low-energy block. In other words, the states $\{|n^i\rangle\}$, with $i > 0$, only affect *how* the states $\{|n^0\rangle\}$ are transformed by the CUT to the low-energy states, suggesting a faster convergence with d_{max} in comparison with the pure block-Lanczos approach described above.
Let n_{low} denote the number of low-energy states. On the one hand, it is advisable to choose $m > n_{\mathrm{low}}$ because the low-energy subspace may overlap with the remainder and accuracy is generally improved. On the other hand, the accurate determination of the low-energy eigenstates

is computationally costly. In applications, we choose $m = \lfloor \frac{3}{2} n_{\text{low}} \rfloor$.
Finally, it should be noted that it is useful to perform the ED for the low-energy spectrum *before* the generation of the basis via the block-Lanczos scheme. During the ED procedure, maximally m_{ED} vectors are stored where m_{ED} is larger than m by a significant factor. Therefore, the maximal number of states which are stored simultaneously, i.e., the overall memory usage, is minimized by performing the ED for the low-energy spectrum first.
In summary, relying on a slightly modified generator scheme, the truncated basis is generated via a block-Lanczos algorithm starting with the low-energy states of the unperturbed Hamiltonian. More accuracy is gained by additionally including the lowest energy states of the full Hamiltonian.

4.1.4 Symmetries

In the following we are going to discuss the incorporation of symmetries in the gCUT scheme, where the focus is laid on the implementation of the truncation scheme discussed in 4.1.3. The Hamiltonian of the finite cluster often possesses certain symmetries and therefore conserved quantities. It is typically suggestive to exploit these conserved quantities for any numerical procedure, because the implementation of the symmetries usually helps to reduce memory complexity, time complexity and numerically stabilizes the procedure.
The gCUT procedure on a single cluster essentially splits into two different parts. A first part where the Hamiltonian (and the observables) are generated in a truncated basis and a second part where the flow equation is solved by numerical integration. The memory usage of the procedure is determined by the first part of the gCUT calculation and can be drastically reduced by implementing symmetries.
Furthermore, the computational effort is substantially reduced for both parts of the calculation. While the implementation of the second part is not directly affected by the implementation of symmetries, the size of the relevant matrices can be considerably reduced. Equally relevant, the procedure is stabilized by the incorporation of symmetries.
States from symmetry sectors not associated with the low-energy model do not contain relevant information. However, they can affect the stability of the procedure because defective eigenvalues mix with the low-energy spectrum. Even though the matrix elements between the symmetry sector of the targeted low-energy subspace and the other symmetry sectors should be zero in principle, these interactions can become significant during the numerical integration. For this reason alone, the implementation of symmetries is advisable in gCUTs.
The implementation of symmetries concerns most importantly how the states are represented in a symmetrized basis and how the action of the Hamiltonian in this basis is determined. Furthermore, the considered observables and the extraction process of the low-energy physics must be adjusted as described subsequently.

Symmetrized basis state representation

The truncation scheme described in 4.1.3 consists basically of the same steps which are involved in ED techniques. In these respects, the implementation of the scheme is closely oriented to the implementation of these techniques. This includes specifically the exploitation of symmetries. The following discussion focuses mainly on the basic concepts to motivate and explain the underlying structure of the implementation. For further reading we refer to Ref. [131].
The main task is to effectively combine the numerical representation of the states in a symmetrized basis and the calculation of the action of the Hamiltonian, which is defined in the standard basis.
The action of the Hamiltonian of the basis states represented in the standard basis can be

calculated very efficiently. To this end, we consider a system where the local Hilbert space of a supersite has dimension $d_{\text{loc}} = 2^n$, $n \in \mathbb{N}$.[1]
Consequently, n bits suffice to specify the state of a supersite. In the standard basis, a basis state of a cluster consisting of m supersites is than defined by $(n \cdot m)$ bits. Therefore, each basis state can be represented by an integer number. Using the bit representation, the action of the terms in the Hamiltonian affects only a small number of bits allowing for a fast access and modifications via bitwise operations.
The numerical representation of basis vectors via vectors of size 2^{nm} is straightforward. One simply identifies the index of the vector with the integer-representation of the state and the value defines the corresponding amplitude.
The objective is to transfer the numerical representation of the states and the rapid evaluation of the terms in the Hamiltonian in the standard basis to the symmetric basis. Symmetries for the systems under consideration are:

- magnetization conservation: S^z_{tot} constant,
- spatial reflection symmetry: parity conserved,
- full $SU(2)$ spin symmetry: S^2_{tot} conserved $\rightarrow$ spin inversion symmetry.

Among these symmetries, the first two are implemented routinely in ED programs. The full $SU(2)$ symmetry is in general rather hard to implement. However, for the calculations under consideration the provided $SU(2)$ symmetry allows to study the $S^z_{\text{tot}} = 0$ channel only. Consequently, a global spin inversion which maps $S^z \rightarrow -S^z$ can be exploited. This symmetry splits the representations with even total spin (symmetric) and odd total spin (anti-symmetric).
Let d_{sym} denote the size of the subspace defined by the exploited symmetries and accordingly d_{full} denotes the dimension of the full Hilbert space. In ED, the vectors of the size d_{sym} are typically manageable while the vectors of size d_{full} are not.
First, we consider the total magnetization only. The implementation can be generalized to every additive quantity which is conserved. Each basis state of the standard basis has a defined magnetization and it is straightforward to decide if a state is part of the considered subspace. These states define a vector of size d_{mag}. For these vectors, the identification of the index with the integer-representation, as described for the standard basis, is not possible. However, an additional integer-list of size d_{mag} allows to store the corresponding integer-representation of these indices.
Using these integer-lists, the Hamiltonian can be, in full analogy to the standard basis, applied to the bit-representation of each vector index. In turn, the resulting bit-representations must be assigned to the corresponding indices to define the resulting vector. An effective implementation is non-trivial; naive implementations are either memory efficient and time-consuming (binary search, ordered list of size d_{mag}) or computationally efficient but memory-intense (list of size d_{full}, integer-representation $\hat{=}$ list index).
However, an elegant and very efficient way to determine the index of a bit representation is provided by the so-called Lin tables [132]. The essential idea is that the additive characteristic of the conserved quantity allows to determine the index by dividing the system into (two) small subsystems (two lists of size $d_{\text{full}}^{1/2}$, integer-representation $\hat{=}$ two list indices). In this thesis, the magnetization conservation is treated relying on Lin-tables.

[1] For the dimerized spin 1/2 ladder structures considered in this thesis, this is indeed the case ($n = 2$). In cases where only the inequality $d_{\text{loc}} < 2^n$ can be fulfilled by $n \in \mathbb{N}$, the implementation requires additional bookkeeping.

The remaining symmetries are spatial reflection symmetries and the spin-inversion symmetry. These symmetries are associated with parities in real space and spin-space, respectively. In contrast to the total magnetization S^z_{tot}, the associated subspaces are not defined by a fraction of the original basis, instead, (anti)-symmetrized linear combinations of the original basis states build the subspaces.
The set of basis states of such linear combinations define an orbit. Incorporating additional information, it is possible to restrict the calculation to one representative state per orbit only because the remaining combinations correspond to symmetry operations with known (relative) phase factors. Consequently, the omitted calculations are redundant. In analogy to the characterization of a graph via a canonical labeling (see 3.2.1), the representative can be identified with the state which maximizes the integer representation.
Similar to the discussion above, a list of size d_{sym} can be used to provide the bit representation of each representative for the vector indices. The Hamiltonian is applied to these bit representations yielding in general other bit representations of states which are *not* representatives. In order to define the resulting vector, one must determine the index of the corresponding representative in the resulting vector in combination with possible phase factors and the number of states of this orbit. The latter two represent necessary information to determine the correct results while restricting the calculation to representatives.
It is possible to gain the corresponding representative by applying all the symmetry operations to maximize the integer representation. This naturally gives access to the corresponding phase factor and number of states associated with this orbit. Finally, the index can be determined via a binary search in a list of size d_{sym}. The procedure is memory efficient but computationally costly.
However, in gCUTs it is reasonable to increase the computational efficiency at the expense of memory usage. In standard ED applications, only information about a very small number of extremal eigenvalues and eigenvectors of the eigenproblem is required. Hence, standard ED implementations require to keep $n \sim 10^0 - 10^1$ vectors in the memory at the same time. Consequently, the procedure is sensitive to memory overheads of $O(d_{\text{mag}})$.
This is different for the gCUT scheme where typically $n \sim 10^2 - 10^3$ vectors must be stored simultaneously and rather few spatial symmetries are provided. As a consequence, the overhead which is produced by storing additional lists of size d_{mag} for the corresponding vector index and phase factor is relatively small in gCUTs. Therefore, the bit-representation is transferred via lin-tables to a list index. This list index is used to determine the phase factor, normalization factor and the vector index using additional lists of size d_{mag}.

Additional symmetries

The magnetization, spatial symmetries and spin-flip symmetries are included directly on the level of the states. In contrast, the full $SU(2)$ symmetry is not implemented on the level of the numerical representation of the basis states. However, the symmetry is respected in the sense that the block-Lanczos like approach described in 4.1.3 conserves the symmetries shared by the low-energy states and the Hamiltonian. As a result, the $SU(2)$ symmetry is conserved, up to numerical errors, on the level of the Hamiltonian.
Still, specifically at the determination of the low-energy spectrum for the expanded block-Lanczos scheme, defective eigenstates with other total spin values can enter the low-energy spectrum. This can affect the stability of the integration procedure and it is desirable to discard these eigenstates already during the iteration process of the respective ED algorithm. In principle, one can determine the eigenvalue of S^2_{tot} of the low-energy states to decide if the

state is associated with the considered total spin-channel. Yet, the application of S^2_{tot} includes a lot of terms and is computationally expensive. By applying S_{tot} twice in succession less terms must be calculated in each step but the symmetries of the Hamiltonian are broken by the intermediate step (spin-flip symmetry, S^z_{tot}).
However, a computationally efficient solution is provided by investigating the overlap of these states $\{|n^{\mathrm{low}}_{\mathrm{ED}}\rangle\}$ with the bare low-energy states $\{|n^0\rangle\}$ defined by $\mathcal{H}_0$. The defective eigenstates are assigned to other QP channels and the overlap with the bare low-energy states should vanish. We define

$$\alpha_i = \sum_j |\langle n^{\mathrm{low}}_{\mathrm{ED},i}|n^0_j\rangle|^2, \tag{4.10}$$

where $|n^0_j\rangle$ denotes the j-th bare low-energy state and $|n^{\mathrm{low}}_{\mathrm{ED},i}\rangle$ denotes the i-th low-energy eigenvector obtained via ED. One finds $\alpha_i \gtrsim 10^{-2}$ for the proper eigenstates and $\alpha_i \lesssim 10^{-10}$ for the defective eigenstates. During the iteration procedure determining the exact low-energy spectrum, the states with $\alpha_i < \alpha_c$ ($\alpha_c = 10^{-7}$) are discarded guaranteeing that the incorporated low-energy spectrum of the effective Hamiltonian is determined by the considered symmetry channel only.
To sum up, using additional bookkeeping, the vectors are kept in a symmetrized basis while the action of the Hamiltonian is performed on bit representations with a rapid bitshift operation. Symmetries not already included in the basis states are respected by the block-Lanczos scheme and by additionally defining a critical overlap α_c for the exact eigenvectors.

Observables

The spatial reflection symmetries provided by the cluster split the representation of the Hamiltonian into symmetric and anti-symmetric channels with respect to these symmetries. The gCUT calculation is performed for each symmetry channel separately by using a symmetrized basis. However, in order to calculate experimentally relevant quantities like dynamic structure factors, it is necessary to additionally calculate low-energy matrix elements of effective observables. Also, the treatment of decay via adjusted generator schemes relies on these matrix elements.
Let the relevant observables $\mathcal{O}_j$ be numbered by an index j which indicates the action of the observable on the respective site or link.
The relevant matrix elements relate to $\mathcal{O}_j(\ell)|0\rangle$ where $|0\rangle$ denotes the vacuum and $\mathcal{O}_j(\ell) = U^\dagger(\ell)\mathcal{O}_j U(\ell)$ the transformed observable. Note that the observables $\mathcal{O}_j$ are *not* symmetric. Consequently, the operator basis defined by the observables $\mathcal{O}_j$ is transformed accordingly, such that the observable separates into symmetric and anti-symmetric parts. Then, $\mathcal{O}_{j,\mathrm{sym},n}|0\rangle$ can be assigned a symmetry channel n and the determination of the observable separates into the different channels.

Extraction of the low-energy physics

Finally, one must extract the relevant amplitudes of the hopping operators. These amplitudes are defined in the 'original' unsymmetric low-energy matrix and a corresponding retransformation of the basis must be performed. To this end, it is useful to distinguish between two classes of symmetries.
The first class of symmetries is defined by quantum numbers which have a specified value for the low-energy model itself, e.g., by the total magnetization $S^z_{\mathrm{tot}} = 0$. The physics corresponding

to other quantum numbers is irrelevant for the derivation of the effective model. Possible exceptions are calculations relevant to the subtraction of lower-QP channels (see A.1).
The second class of symmetries divides the low-energy model on the finite cluster into different symmetry sectors, e.g., a reflection symmetry on a cluster splits the low-energy model into a symmetric and anti-symmetric sector. One has to loop over these symmetry channels to extract the relevant information.
Let the states $|i\rangle$ denote the (unsymmetric) low-energy states of the system which define the desired low-energy matrix. These states satisfy the first class of symmetries and not the second class of symmetries.
Let the corresponding (anti)-symmetrized low-energy states of symmetry sector m be denoted by $|i_{\mathrm{sym},m}\rangle$. With this, one finds

$$\langle i|\mathcal{H}|j\rangle = \langle i| \sum_{m,i'} |i'_{\mathrm{sym},m}\rangle\langle i'_{\mathrm{sym},m}|\mathcal{H} \sum_{m',j'} |j'_{\mathrm{sym},m'}\rangle\langle j'_{\mathrm{sym},m'}|j\rangle \tag{4.11}$$

$$= \sum_{m,i',j'} \langle i|i'_{\mathrm{sym},m}\rangle\langle i'_{\mathrm{sym},m}|\mathcal{H}|j'_{\mathrm{sym},m}\rangle\langle j'_{\mathrm{sym},m}|j\rangle \tag{4.12}$$

The CUT calculations are performed in the symmetrized basis for all the relevant symmetry sectors and the results are combined to gain the desired effective result.
Analogously, the operator basis of the considered observables must be desymmetrized.

4.2 Treatment of decay

In this section, we describe the treatment of decay on finite clusters to obtain proper results in the thermodynamic limit. This section builds the central element of this thesis. Fundamental concepts are challenged, new concepts are introduced and at the end of this process, two modified gCUT schemes are defined, suited to treat pseudo and genuine decay.
In the standard terminology, one cannot observe decay on finite clusters, since only well-defined eigenfunctions exist on finite clusters. However, this expression points to an analogy of decay in the thermodynamic limit, namely, an energetic overlap of the different quasiparticle blocks. Since one can always identify the lowest states of the system with the lowest quasiparticle states and fill the basis from below, also the term energetic overlap requires more explanation. Energetic overlap must be defined with respect to a reference point: Here, we consider two different effective quasiparticle blocks of an effective Hamiltonian of the form Eq.(2.6) to overlap energetically, if only a non-perturbative renormalization of the initial Hamiltonian is able to separate the respective quasiparticle channels. Of course, no rigorous line separating perturbative and non-perturbative renormalization effects exists. In the context of gCUTs, this identification line can be reasonably drawn by the flow itself: small values of ℓ are identified with a perturbative renormalization and large values of ℓ are associated with a non-pertubative renormalization.
On the finite cluster, the overlap can be caused by two different effects. If the energetic overlap is just an artifact of the broken translational symmetry, it is referred to as pseudo decay. If, however, the energetic overlap reflects quasiparticle decay on finite clusters, it is referred to as genuine decay. Both situations are physically quite different, yet, we will show that both breakdowns can be understood by the same principles.
In the following, we are going to investigate the reasons for these breakdowns and also present a guideline to solve these issues by a proper generalization of cluster additivity. In particular, we are going to revisit the concept of cluster additivity and we introduce and motivate a mandatory

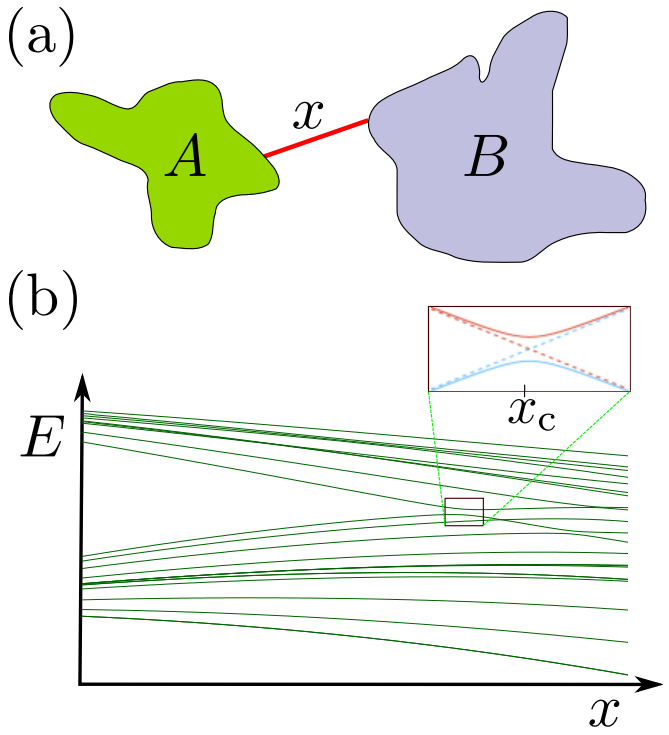

Figure 4.2: (a) Sketch of two clusters A and B which are linked by a single bond of strength x. (b) Sketch of the eigenvalues E as a function of x for the joined system $A + B$ linked by a single bond. (*Inset*) Zoom on the first anti-level crossing. Dashed lines represent the appropriate evolution of eigenvalues respecting the generalized notion of cluster additivity. Both figures are taken from Ref.[70].

generalization of this concept for NLCEs when deriving effective low-energy models. On this basis, the applied gCUT schemes are deduced.

4.2.1 Generalized cluster additivity

Cluster additivity is sufficient to perform an NLCE if the targeted low-energy physics on each cluster is energetically well-separated from the remainder. One can simply rely on an exact (block) diagonalization on finite clusters and combine the finite cluster contributions to gain the result in the thermodynamic limit. By contrast, the treatment of such an overlap demands additional care, because non-perturbative effects play a major role.
For clarification, we consider a cluster C consisting of two subclusters A and B which are linked by only one link of coupling strength x as illustrated in figure 4.2(a). For $x = 0$, the cluster additivity ensures a proper subtraction of all quantities and the reduced contribution vanishes, which is the conceptual starting point. One aims at evaluating the reduced contribution for $x = \lambda$ because this corresponds to the cluster C in the actual calculation.
Any quantity $\mathcal{M}^C$ like the effective Hamiltonian Eq.(2.6) on this cluster $\tilde{\mathcal{H}}_c^C$ takes then the form

$$\mathcal{M}^C = \mathcal{M}^A \otimes \mathbb{1}^B + \mathbb{1}^A \otimes \mathcal{M}^B + \mathcal{M}_x, \tag{4.13}$$

where $\mathcal{M}_x$ gives rise to the reduced contribution of cluster C.
We consider the case of energetic overlap on cluster C. Then, one prototypical evolution of the eigenenergies of $\mathcal{H}^C$ is displayed in figure 4.2(b). One observes two regimes: For small x, the change of eigenvalues and eigenvectors is smooth while, for larger x, there are characteristic anti-level crossings starting from x_c where eigenenergies and eigenvectors change drastically. At each anti-level crossing, the definition of a quasiparticle changes abruptly, i.e., these anti-level crossings can affect $\mathcal{M}^C$ severely in an unphysical fashion. This drastic change in the target quantity $\mathcal{M}^C$ undermines the underlying concept of the subtraction scheme, which can either impede convergence considerably or even lead to a complete breakdown of NLCEs for $\lambda \gtrsim x_\mathrm{c}$. Therefore, one has to generalize the notion of cluster additivity by demanding that any physical quantity $\mathcal{M}^C$ like the effective Hamiltonian $\tilde{\mathcal{H}}_\mathrm{c}^C$ is sufficiently smooth as a function of x for $0 \leq x \leq \lambda$. For a single anti-level crossing at x_c, this can be naturally discussed by focusing on the two involved energy levels as sketched in the zoom of figure 4.2(b). Denoting the two eigenvectors for $x < x_\mathrm{c}$ as $|i\rangle$ and $|j\rangle$, the eigenvectors at (or close to) x_c are entangled superpositions of $|i\rangle$ and $|j\rangle$. Sharp anti-level crossings should now be replaced by true level crossings as indicated by the dashed lines in figure 4.2(c). The dashed lines represent the cured eigen-energies identified with the diagonal elements $\langle i|H|i\rangle$ of the disentangled vectors $|i\rangle$. Depending on the underlying physics, this replacement can be imperative to avoid a complete breakdown of the approach. As a direct consequence, one can*not* use the exact eigenvectors as it is done so far in all implementations of NLCEs.

Pseudo decay

Let us consider a physical system where the one-particle mode is stable, i.e., the one-particle dispersion is below any relevant many-particle continuum for any momentum, and the maximum of the one-particle dispersion is larger than the minimum of the many-particle energies. This happens for instance when the one-particle mode is protected by a symmetry from the two-particle continuum and the relevant continuum is the three-particle continuum as visualized in figure 4.3(a). In addition to that, this occurs if the one-particle gap is sufficiently small, i.e., specifically close to or at quantum phase transitions.
On the open clusters, no energetic separation between one-particle states and multi-particle states is given. The corresponding states are protected by the translational symmetry in the thermodynamic limit which implies that the interaction between these states is zero. Yet, this protection is a priori not at work on open clusters and one expects a finite (and very small) interaction between these states. To gain the proper results in the thermodynamic limit, one has to ignore this interaction, which corresponds exactly to the replacement of anti-level crossings with true level crossings, as discussed above.

For pseudo decay, this replacement is mandatory to avoid artificial entanglement between certain states having different quantum numbers in the thermodynamic limit. In other words, the smooth behavior of all quantities in the thermodynamic limit *must* be reflected by the effective model derived on the finite cluster. If one relies on an effective low-energy model as suggested by adiabatically tracking anti-level crossings, the approach completely breaks down. Finally, it should be noted that the translational invariance is recovered by the embedding procedure and therefore the remaining artificial interactions cancel out and one obtains the decoupled low-energy mode.

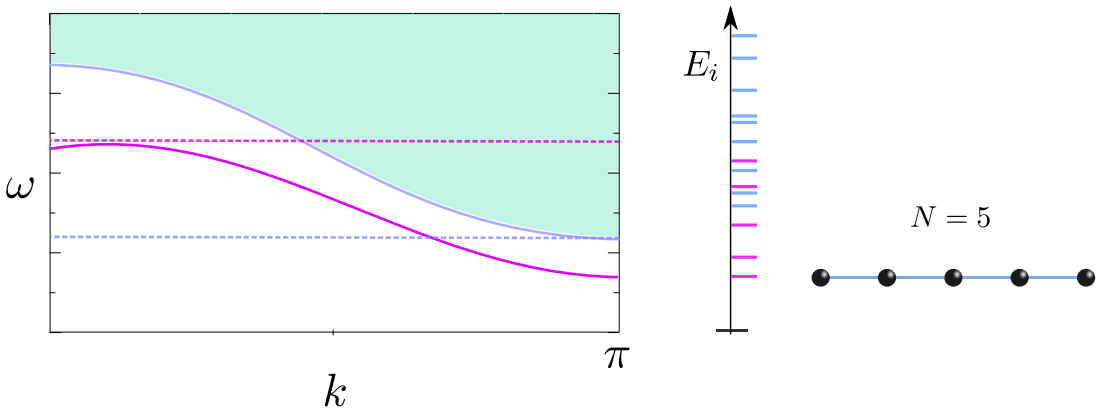

Figure 4.3: (a) Sketch of a one-particle dispersion (solid magenta line) and the three-particle continuum (cyan surface). The maximum of the one-particle dispersion (dashed magenta line) is energetically above the minimum of the three-particle continuum (dashed blue line). (b) Sketch of an open cluster and the corresponding spectrum. The color coding indicates the affiliation to the one-particle and multi-particle states respectively.

Genuine decay

Diametrically opposed to pseudo decay is *genuine* decay on clusters. In these cases, the energetic overlap on finite clusters reflects the energetic overlap also present in the thermodynamic limit. We consider the Hamiltonian of the form Eq.(2.19) and a scenario where the one-particle mode overlaps energetically with the two-triplon continuum for $\zeta = 0$.
Then one can distinguish two different scenarios [28, 29]:
i) If ζ is very small, the situation is clearly associated with quasiparticle decay. Consequently, a suitable effective low-energy model should not decouple the one-particle mode from the continuum.
ii) If ζ is large, the one-particle mode is pushed out of the two-particle continuum, i.e., the effective low-energy model should yield a decoupled one-particle mode.
Naturally, this is also reflected by the physics and the effective low-energy models on the finite cluster. Both scenarios are in accordance with the generalized cluster additivity, which helps to understand possible convergence problems.
The generalized cluster additivity demands that the functions $\mathcal{M}_x$ should be *sufficiently* smooth as a function of x for $0 \leq x \leq \lambda$. If the interaction of the states $|i\rangle$ and $|j\rangle$ is small, the anticrossings are extremely sharp. In these cases, relying on the exact eigenfunctions can yield erratic results and it is physically reasonable to replace the anti-crossings by crossings. In the other limiting case of large ζ, the interactions of the states $|i\rangle$ and $|j\rangle$ are large and the anticrossings can hardly be identified as such. Then it is physically reasonable to use the actual eigenfunctions.
For intermediate scenarios, the situation is less clear. The challenge is to set up a systematic procedure which satisfies the physical intuition of both limiting cases. In contrast to pseudo decay, a rigorous characterization of disentangled states is surely not possible, because a well-defined one-particle mode does not exist in the thermodynamic limit. This means that the continuation of the states is to some extent ambiguous and one must define criteria for this continuation.

Note, that the interblock interactions do not cancel during the embedding procedure since a decoupled one-particle mode does not exist. These remaining elements moderate the decay and lead to a finite broadening of the spectral density inside the continuum.
The remaining challenge is to identify the disentangled states $|i\rangle$ on a cluster. A systematic disentanglement of specific levels involved in artificial anti-level crossings is a priori a very complicated task and it is by far not obvious that a general solution exists. We will show that this is indeed possible by relying on a modified gCUT approach as discussed next, focussing on the underlying ideas and the basic structure of the treatment of decay.

4.2.2 Basic framework

As discussed in 4.2.1, the derivation of effective low-energy models via the standard NLCE schemes is only well-defined/valid if the eigenstates associated with the low-energy model are energetically well beneath the remainder for each cluster involved in the calculation. An energetic overlap of the subspaces on the other hand is identified with decay (pseudo decay or genuine decay) on finite clusters not treated adequately by the standard NLCE schemes relying on an exact (block)-diagonalization.
A guideline to treat both types of decay properly is given by the so-called generalized cluster additivity. This guideline demands the substitution of sharp anti-level crossings by true level crossings implying that one can*not* rely on the exact eigenvectors (see 4.2.1).
In gCUTs, the block-diagonalization on finite clusters is performed via a CUT which is determined by the generator scheme applied. Consequently, the mean to prevent a full block-diagonalization within the gCUT scheme is given by (small) modifications of the quasiparticle generator schemes. Perfectly suited for this purpose as a starting point is the quasiparticle generator Eq.(2.41) designed to achieve a full separation of the different particle-blocks. The quasiparticle generator sorts the subblock eigenvalues with respect to the number of quasiparticles and this sorting property must be avoided if particle subspaces overlap energetically. To this end, one can eliminate certain elements from the generator scheme. If one sets $\eta_{ij}^{\mathcal{Q}} = -\eta_{ji}^{\mathcal{Q}} \equiv 0$, the states i and j are not separated by the CUT leaving a finite matrix element h_{ij} after the CUT. Note, that the matrix elements eliminated from the generator must be ignored in the determination of the ROD in order to define a suited measure of convergence.

The adequate treatment of decay within gCUTs requires to identify the relevant matrix elements and to eliminate them on an appropriate scale in ℓ. This elimination process relies on the implementation of suited weights which helps to define the desired low-energy states. The definition of the respective weights differ for pseudo and genuine decay. However, the general procedure and its underlying concepts are identical for both approaches.
In the following, we discuss these general ideas. First, we identify a region in ℓ suited for the elimination of these matrix elements. Second, we define the basis suited for the elimination process during integration. Building on this, the general procedure is described.

A matter of time

The generator elements are identified and set to zero *during* the flow in order to treat the decay adequately. The identification of the 'right' value of ℓ for the elimination of a matrix elements seems problematic. Fortunately, there exists a region of intermediate values of ℓ, which defines appropriate values for the elimination. This is based on two reasons: i) the decay is caused by small interactions and ii) the CUT naturally separates the decoupling of strongly interacting and weakly interacting states with respect to the ℓ-scale:

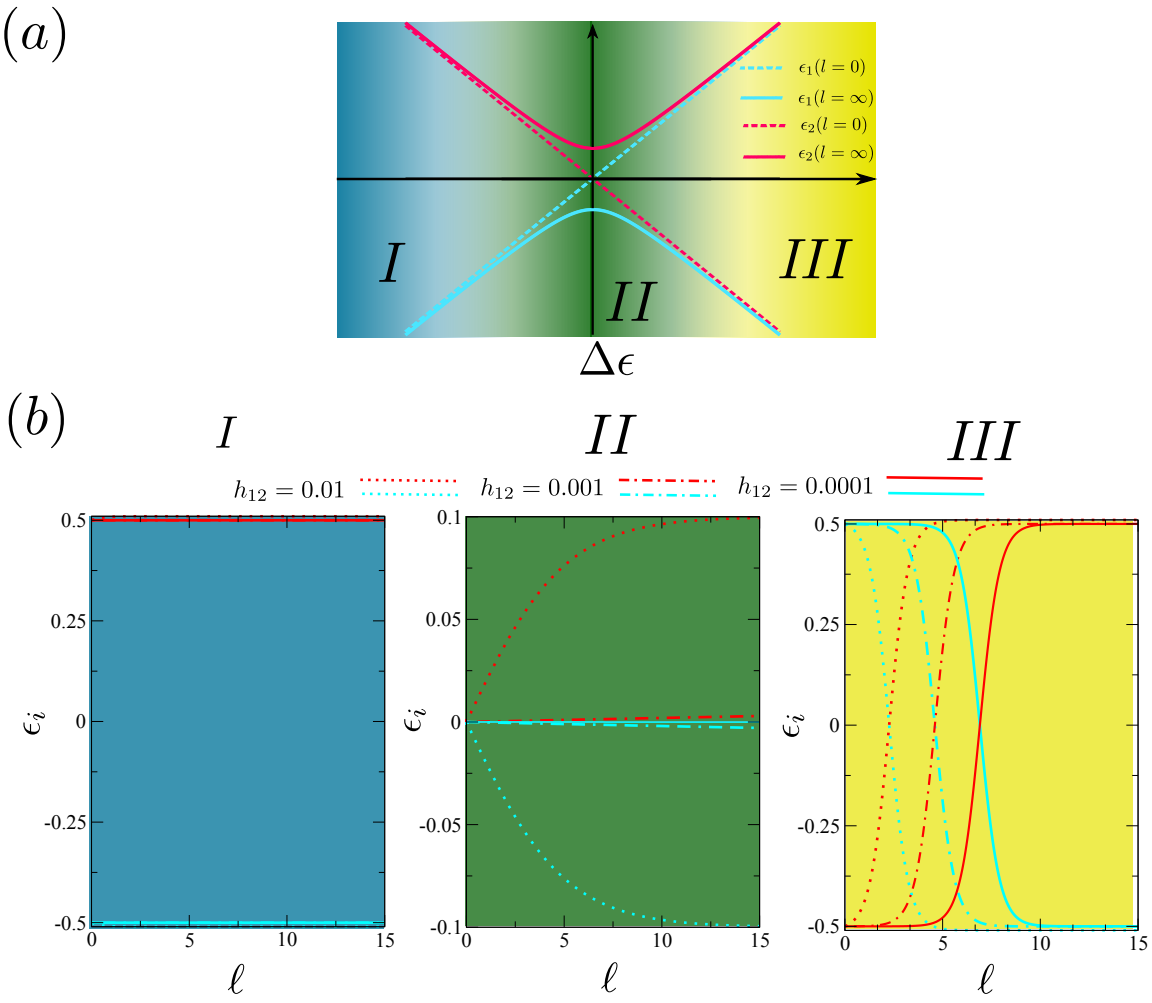

Figure 4.4: (a) Sketch of the initial diagonal elements and the resulting final diagonal elements in dependence of the initial difference $\Delta\varepsilon$. The sketch is divided into three different regions as indicated by the color coding. (b) Three graphs are presented affiliated with the three regions of (a) as indicated by the color coding. Each graph shows the evolution of the diagonal elements $\varepsilon_{1/2}(\ell)$ for a suited value of $\Delta\varepsilon$ and different values of h_{12}.

i) Pseudo decay is just an artifact of the broken translational symmetry. Therefore, the interaction which causes the decay is artificial and expected to be small. In contrast, genuine decay is caused by genuine interactions. Still, the replacement of anti-level crossings by level crossings is only reasonable if these crossings are sharp, i.e., if the corresponding interaction is small. Broad anticrossings caused by large interactions do not represent decay but repulsive inter-block interaction.
ii) For small values of ℓ, the CUT is dominated by large interactions while the larger values of ℓ are dominated by small interactions. In analogy to the anticrossings, the essential properties of

the CUT can be understood by investigating a simple two-level system

$$H = \begin{pmatrix} \varepsilon_1 & h_{12} \\ h_{12} & \varepsilon_2 \end{pmatrix} \quad . \tag{4.14}$$

The CUT is performed using the quasiparticle generator η^{QP} Eq.(2.41):

$$\eta^{\mathrm{QP}} = \begin{pmatrix} 0 & \mathrm{sgn}(q_1-q_2)h_{12} \\ \mathrm{sgn}(q_2-q_1)h_{12} & 0 \end{pmatrix} \quad , \tag{4.15}$$

where $q_1 < q_2$, i.e., we associate ε_1 with a lower QP channel than ε_2. Energy shifts are irrelevant and for convenience we choose $\varepsilon_1 + \varepsilon_2 = 0$ yielding

$$\varepsilon_{1/2}(\ell) = \pm\tfrac{1}{2}\tanh\left(C\ell + \operatorname{arctanh}\left(\frac{\Delta\varepsilon}{C}\right)\right)C \quad , \tag{4.16}$$

with $\Delta\varepsilon = \varepsilon_1(0) - \varepsilon_2(0)$ and $C = \sqrt{4h_{12}(0)^2 + (\Delta\varepsilon)^2}$.
The velocity of the transformation at $\ell = 0$ is given by

$$\partial_l \varepsilon_{1/2}(\ell)|_{\ell=0} = \pm 2h_{12}(0)^2 \quad . \tag{4.17}$$

This indicates already that small interactions are integrated on larger ℓ-scales than large interactions. The development of the diagonal elements $\varepsilon_{1/2}(\ell)$ depends additionally on the initial values $\varepsilon_{1/2}$. To discuss the behavior of the diagonal elements $\varepsilon_{1/2}(\ell)$ with ℓ in more detail, it is reasonable to divide the initial conditions $\varepsilon_{1/2}(\ell = 0)$ into three regions as sketched in figure 4.4 (a)).
Indeed, the resulting (anti-)crossing in figure 4.4(a) relates to the (anti-)crossing depicted in figure 4.2 (b). One can identify the initial condition with the proper disentangled system obtained for intermediate values of ℓ. Then, the artificial entanglement is integrated continuously into the effective description for large values of ℓ.
The three regions differ with respect to the qualitative behavior of $\varepsilon_{1/2}(\ell)$. For each region, the ℓ-dependence of the subblock energies is shown for appropriate initial values $\varepsilon_{1/2}$ and different interaction strengths in figure 4.4 (b). The three regions are qualitatively defined as:
(I) The region before the anticrossing $\left(\varepsilon_1 - \varepsilon_2 \approx -\sqrt{(\varepsilon_1 - \varepsilon_2)^2 + 4h_{12}^2}\right)$: The eigenvalues and the respective diagonal elements are sufficiently similar and the region is already treated adequately by the standard quasiparticle generator scheme.
(II) The region of the anticrossing $\left(\varepsilon_1 \sim \varepsilon_2\right)$: The initial diagonal elements are not similar to the eigenvalues of the system. The interaction results in a level repulsion which is integrated on relatively large ℓ-scales $l \sim \ell_{\mathrm{rep}}$. The overall level repulsion decreases while ℓ_{rep} increases with decreasing interaction strengths.
(III) The region after the anticrossing $\left(\varepsilon_1 - \varepsilon_2 \approx \sqrt{(\varepsilon_1 - \varepsilon_2)^2 + 4h_{12}^2}\right)$: The eigenvalues and the respective diagonal elements are sufficiently similar but the order of the initial diagonal elements is switched. As a result, the quasiparticle generator scheme resorts these eigenvalues. For small values of ℓ, the diagonal elements are relatively constant and than switched at $\ell \sim \ell_{\mathrm{crit}}$ ($\ell_{\mathrm{crit}} < \ell_{\mathrm{rep}}$). The value of ℓ_{crit} increases with decreasing interaction strength.
For the quantum many body systems under consideration, the behavior is of course much more complex. Still, the same basic mechanisms are present and smaller interactions are integrated on larger ℓ-scales than large interactions. Consequently, to treat decay, modifications of the quasiparticle generator scheme relate to the intermediate and large values of ℓ defined by the corresponding value of ℓ_{crit}. Next, we describe an optimal basis chosen for the numerical integration to treat decay.

A matter of perspective

By construction, the modifications of the generator scheme in gCUTs are defined on matrix level and not in terms of coefficients of (normal-ordered) operators as in the sCUT approaches [33, 102]. Consequently, the choice of the basis plays a fundamental role because the generator scheme is defined with respect to the given basis.[2] In one basis, the defective inter-block interaction can be completely incorporated in a single matrix element h_{ij} while the defective part can be distributed over several matrix elements in another basis. In the first case, it is sufficient to simply put a single generator element to zero. This is evidently favorable over the determination of a complicated "equilibrium" as required in the latter case. Note that such a well-suited basis corresponds to a basis of the desired disentangled eigenstates.
In 4.1.2, we introduce the standard basis and the subblock basis which are arguably the two most natural basis choices in gCUTs. In the standard basis, the matrix elements can be identified with coefficients of (not normal-ordered) operators while the subblock basis diagonalizes the QP conserving part $\mathcal{H}_c(\ell)$ of the Hamiltonian providing the subblock energies of the different particle block. The anticrossings are naturally described and understood in terms of eigenenergies. Consequently, the subblock basis is clearly more appropriate for the treatment of decay than the initial standard basis.
The compelling argument for the subblock basis is provided by the CUT itself. As described in 2.3.1, the characteristics of the generator schemes are defined by the development of the subblock energies during the flow. The modifications must be designed to affect the development of these subblock eigenvalues accordingly. Therefore, the subblock basis is the natural basis for the considered modifications.

Conceptual approach

The concept of this approach relies on the combination of the subblock basis with the considerations with regard to the different ℓ scales. For small values of ℓ, the CUT is dominated by large interactions; the defective interactions are small and incorporated at intermediate values of $\ell \sim \ell_{\text{crit}}$. As a result, the CUT can be performed without modifications of the generator scheme up to intermediate value of $\ell = \ell_{\text{switch}}$ with $\ell_{\text{switch}} < \ell_{\text{crit}}$. Then, the large interactions are almost completely incorporated by the CUT and the small interactions causing the decay are not integrated yet. Consequently, the intermediate Hamiltonian is close (yet not sufficiently close) to the proper effective Hamiltonian. At this point, the basis states of the subblock basis are, up to small interactions, eigenstates of the system. The remaining interblock-interactions include specifically defective interactions, i.e, these states are close to the disentangled eigenstates. Therefore, each defective interaction is mainly contained in a single matrix element.
The objective is then to apply a modified generator scheme for $\ell > \ell_{\text{switch}}$, such, that only the remaining proper interactions are integrated out while the defective interactions are not. This is achieved by setting (only) the defective generator elements in the subblock basis to zero. In order to decide whether the according generator elements should be eliminated, one must rely on additional weights and evaluate how the elimination of a generator element affects these weights. However, a large portion of the matrix elements can be excluded a priori by energetic considerations. Only elements associated with region II and region III must be considered. Let

[2] Interestingly, the tensorial optimization described in [102] can also be viewed to rely on other operator bases for the definition of the generator scheme. The resemblance of both overall modification concepts can be interpreted as 'convergent evolution' supporting the current direction.

$\varepsilon_i^n(\ell)$ be the i-th eigenenergy of the n-particle block. If

$$\varepsilon_i^n(\ell) + \Delta_{\text{vicinity}} > \varepsilon_j^m(\ell) \tag{4.18}$$

with $m > n$, the respective interaction between these states can be defective. The parameter $\Delta_{\text{vicinity}} > 0$ must be chosen such, that the elements associated with region II are included, i.e., Δ_{vicinity} is determined essentially by the size of the defective interactions.
All other interactions can be integrated out because they represent either innocuous defective interactions before the anticrossing (region I) or proper interactions also present in the thermodynamic limit.[3]
If Δ_{vicinity} is chosen too small, defective matrix elements associated with region II are not eliminated and if Δ_{vicinity} is chosen too large, possibly wrong elements are eliminated.
In most cases, there exists a relatively large intervall of values Δ_{vicinity} which satisfy both requirements. This can be different if multi-particle continua inducing repulsive interactions become energetically very close.
For $\ell > \ell_{\text{switch}}$, the relevant matrix elements are tested for every Runge Kutta step. Generator elements can either be eliminated or re-activated. Additional modifications like sign-changes or continuous adaptations of these elements are not considered.
It should be noted that the modifications of the generator elements are only applied between the discrete Runge Kutta steps. However, such discretization errors are typically expected to be small. Furthermore, implied by the approach, these errors only relate to relatively small matrix elements having a small effect on the current transformation. Consequently, on expand of the mathematical beauty, we waive a complex correction procedure of these discretization errors.
With this, the basic concepts of the procedure are introduced. Note that the underlying idea behind this approach is that the transformed Hamiltonian is close to the desired effective Hamiltonian at $\ell = \ell_{\text{switch}}$ with $\ell_{\text{switch}} < \ell_{\text{crit}}$. In this sense, we assume ℓ_{crit} to be sufficiently large which defines a limitation of the presented scheme.
For actual applications of the scheme, a rather technical but relevant additional step must be introduced.

Definition of the subblocks in a truncated basis

The truncation scheme introduced in 4.1.3 relies on a slightly modified generator scheme $\eta^{\text{QP},m}$, replacing the physical meaning of the quasiparticle number by a more convenient definition. The unphysical definition of the quasiparticle blocks does not affect the results of the general scheme. However, this can be different for the modifications introduced to treat decay because the quasiparticle subblocks represent relevant physical information. Therefore, the truncated basis must be adjusted accordingly.
The generator scheme $\eta^{\text{QP},m}$ (see Eq.(4.9)) used for the truncation scheme simply redefines the n-particle states with $n > m$ as $(m+1)$-particle states. By applying the scheme analogously, the entire $(m+1)$-particle block is diagonalized.
While the subblock energies $\varepsilon_i^n(\ell)$ behave identical for $n \leq m$ in both generator schemes, the $(m+1)$-particle subblock energies behave fundamentally different. All the interactions of the $(n > m)$-particle states are integrated out instantly by the diagonalization leading to a drastic reduction of the subblock energies. Accordingly, for low values of ℓ these energies represent the lowest energies of the system by far (see figure 4.5(a)).

[3] This gives rise to the interesting conceptual question concerning the treatment of pseudo decay. It is not evident, if the interaction with states associated with different momenta in region I is only harmless, or if the collective influence of these high-energetic states is again proper.

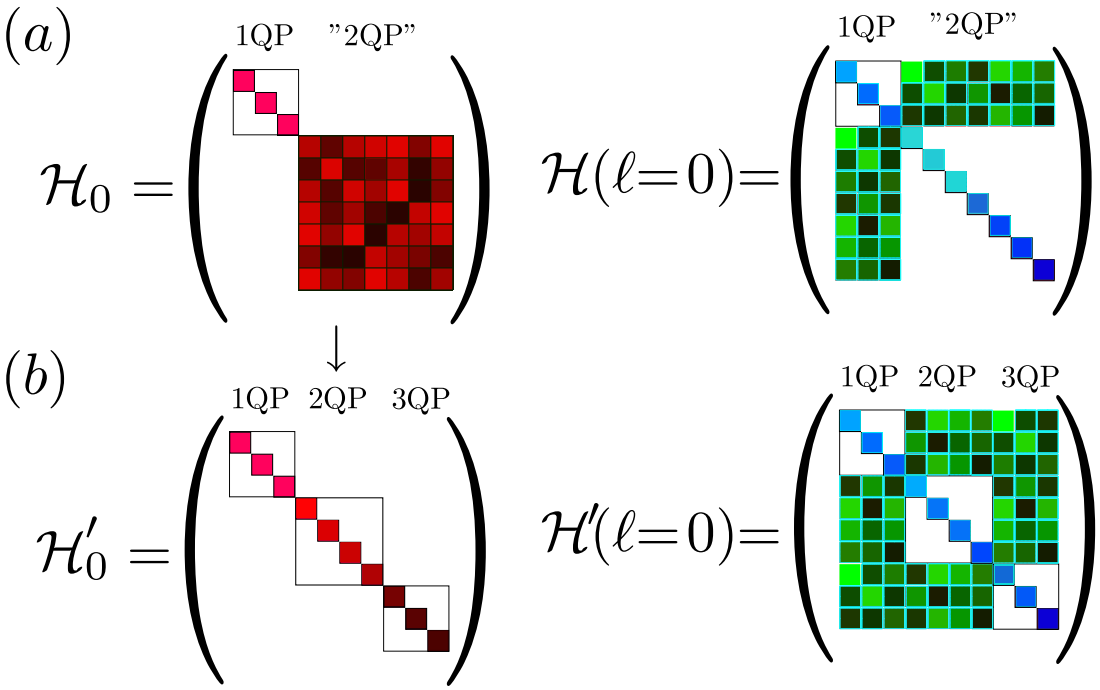

Figure 4.5: Sketch of the different Hamiltonians for $m = 1$. The color coding indicates the size of the matrix elements. (a) The unperturbed Hamiltonian $\mathcal{H}_0$ in the initial basis does not allow to define physical quasiparticle blocks and the entire multi-particle states are simply defined as 2QP states. This results in unphysical subblock energy reduction of the subblock energies for the resulting Hamiltonian $\mathcal{H}(\ell = 0)$ shown on the right. (b) In contrast, the diagonalized unperturbed Hamiltonian $\mathcal{H}'_0$ allows to define the QP blocks by rounding the diagonal elements. The resulting subblock energies for the resulting Hamiltonian $\mathcal{H}'(\ell = 0)$ behave more physical.

While this behavior has only marginal effect if the defective interactions are very small and treatable on large ℓ-scales, this difference can become relevant if the interactions are larger. However, in order to still rely on the truncation scheme introduced in 4.1.3, one can perform a simple basis transformation *before* the CUT to define the particle blocks. In the basis provided by the truncation scheme, the initial unperturbed Hamiltonian $\mathcal{H}_0$ is only diagonal with respect to the low-energy block defined by the states $\{|n^0\rangle\}$. By contrast, the remaining block is non-diagonal with respect to $\mathcal{H}_0$ and it is not possible to define quasiparticle blocks within this basis, but one can simply diagonalize the unperturbed Hamiltonian $\mathcal{H}_0$ to define a better suited basis. Generically, the eigenvalues are not integer numbers. Still, by rounding the eigenvalues for the definition of the particle number, a valid particle-block structure can be restored. Let $\mathcal{H}'_0$ denote the diagonalized unperturbed Hamiltonian. The basis is arranged such that the eigenvalues (diagonal elements) are sorted in ascending order and one defines the QP number of the basis state $|i\rangle$ by rounding the diagonal element:

$$q_i = \left\lfloor \left(\mathcal{H}'_0\right)_{i,i} \right\rceil \quad . \tag{4.19}$$

The procedure is visualized in figure 4.5(b). Most importantly, the Hamiltonian gained via this scheme converges with increasing $d_{\max}$ to the original scheme of the untruncated basis.

This concludes the description of the basic procedure providing the general framework. However, the treatment of decay relies on weights which function as key indicators to decide if a generator element should be eliminated or reactivated. The corresponding weights can be affiliated with the respective symmetries and therefore require a specific definition for pseudo and genuine decay as addressed next.

4.2.3 Pseudo decay

In the following, we want to describe the treatment of pseudo decay relying on the basic procedure described in 4.2.2. To apply this approach, we first introduce suited weights to define the disentangled low-energy states. Followed by a discussion of these weights and their physical interpretation, we address the resulting implementation.

Reduced weights

The artificial anticrossing observed on finite clusters are only caused by the broken translational invariance. The states involved in artificial anticrossings are mainly affiliated with different momenta in the thermodynamic limit which suggests that it is possible to construct a quantity which helps to define the respective states.
Indeed, such a quantity is provided by the reduced n-QP weights. In CORE, the reduced n-QP weight of an eigenstate $|\nu\rangle$ is defined by

$$W_{\nu,n} = \langle \bar{\nu},n|\bar{\nu},n\rangle \tag{4.20}$$

with

$$|\bar{\nu},n\rangle = \underbrace{\left(1 - \sum_{\bar{\mu}} \frac{|\bar{\mu},n\rangle\langle\bar{\mu},n|}{W_{\bar{\mu},n}}\right)}_{\text{Gram Schmidt}} \underbrace{\frac{P_n|\nu\rangle}{\sqrt{\langle\nu|P_n|\nu\rangle}}}_{\text{Normalized projected state}} \quad , \tag{4.21}$$

where P_n projects on the n-particle subspace of the unperturbed Hamiltonian $\mathcal{H}_0$. The sum runs over all eigenstates $|\bar{\mu}\rangle$ associated with the effective n-QP block having a smaller eigenenergy. The determination of the reduced weight consists of two parts. The determination of the (normalized) projection of the state on the n-particle subspace followed by a Gram Schmidt orthogonalization.
This not very intuitive quantity appears in the CORE procedure in the context of exact eigenvectors. To transfer the definition in terms of eigenstates to the gCUT procedure, the eigenstates are replaced by the basis states of the subblock basis and the eigenenergies are replaced by the subblock energies. For each basis state, the sum runs over all subblock basis states of the n-QP block with a sufficiently smaller subblock energy defining an ℓ-dependent weight $W_{\nu,n}(\ell)$. The sum is taken over all n-QP states $|i\rangle$ which satisfy

$$\varepsilon_i^n(\ell) + \Delta_{\text{vicinity}} < \varepsilon_j^m(\ell) \quad , \tag{4.22}$$

where Δ_{vicinity} is introduced to account for the antilevel crossings associated with region II ($m > n$). Note that the basis states must be transferred to the initial basis representation at $\ell = 0$ to perform the proper projection operation because the projection operator refers to *bare* particles. This can be done by additionally tracking the unitary transformation during the CUT.
In the following, we want to discuss the reduced weights addressing the different aspects:

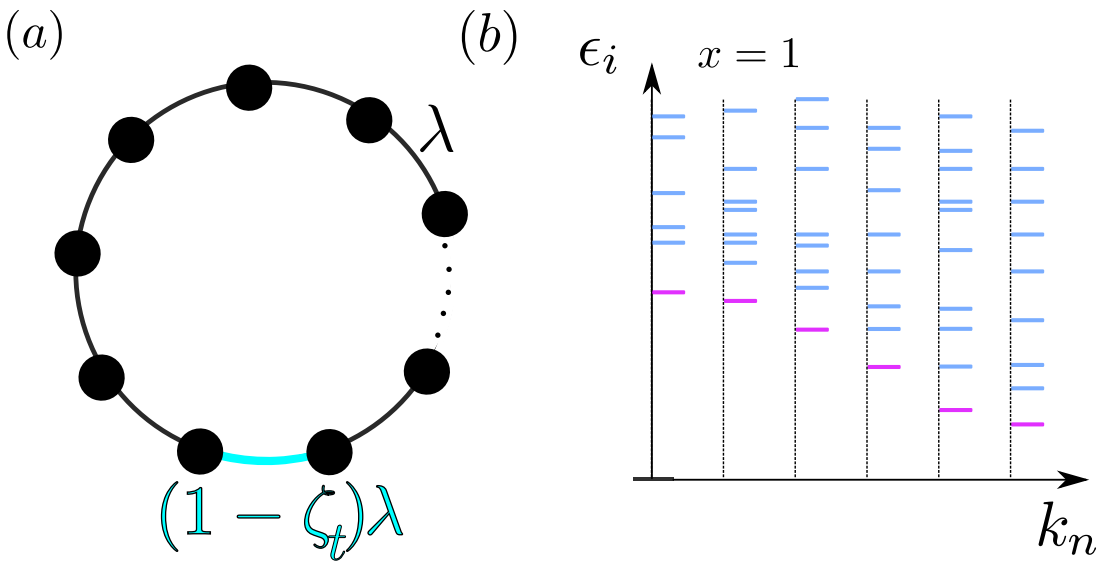

Figure 4.6: (a) Sketch of an open chain with an additional coupling of strength $(1-\zeta_t)\lambda$ which allows to tune between open boundary conditions and periodic boundary conditions. (b) Sketch of the eigenspectrum for $\zeta_t = 0$ in dependence of the discrete momenta k_n. The color coding indicates the affiliation to the one-particle (magenta) or the multi-particle blocks.

i) This quantity naturally arises in the CORE procedure. While there exists no direct physical interpretation of this weight, it can be viewed as a measure of the proportion of new information for the n-QP block provided by the eigenstate $|\nu\rangle$ within the CORE scheme.
Applications show that states with a weight close to zero must be discarded from the procedure to gain proper results [96]. In contrast, the other states typically have a significant larger weight $W_{\nu,n} \sim 1$.
These findings can be interpreted in the context of generalized cluster additivity and a single antilevel crossing as depicted in figure 4.4. A weight close to zero is caused by an artificial anti-level crossing and signals a defective state with a lower eigenenergy (region III). Consequently, if this state is not discarded from the basis, the approach breaks down. In contrast, a weight $W_{\nu,n} \sim 1$ signals a proper eigenstate $|\nu\rangle$ (region I).
Note that region II is not treated adequately by the exact eigenstates of the system and the associated weights are smaller but not close to zero. From the behavior in region I and region III we conclude that the correct linear combination must maximize the weight of the disentangled low-QP state ($W_{\nu,n} \sim 1$) and minimize the reduced weight of the disentangled high-QP state ($W_{\nu,n} \sim 0$). Therefore, the reduced QP weights provide a way to rigorously define the disentangled eigenstates. In gCUTs, the modifications of the generator scheme are designed to serve this objective by adjusting the generator elements accordingly.
ii) To provide more insight into the physical mechanisms behind the properties, we reconsider an open chain on supersites coupled with λ. Here, we additionally introduce a coupling of strength $\lambda_{\text{per}} = (1-\zeta_t)\lambda$ connecting both ends of the chain (see figure 4.6(a)). The parameter ζ_t allows to tune between periodic boundary ($\zeta_t = 0$) and open ($\zeta_t = 1$) boundary conditions. We want to investigate the reduced one-particle weights for this system in a parameter regime with pseudo decay but without genuine decay.

For $\zeta_t = 0$, the translational invariance separates the system into different sectors with respect to the momenta and no pseudo decay occurs. For each momentum sector, no energetic overlap between the low-energy states and the other multi-particles states exists and one can simply identify the lowest eigenstate with the one-particle state of the effective low-energy model (see figure 4.6(b)).
If, however, one does not explicitly label the states with respect to the momentum, an energetic overlap exists in principle. Still, the proper one-particle states can be identified via $W_{\bar{\nu},1}$ because one finds exactly $W_{\bar{\nu},1} = 1$ for the one-particle states and $W_{\bar{\nu},1} = 0$ for all other states. The reason for this is that the projected state $\hat{P}_n|\nu\rangle$ still have a defined momentum which is reflected in the scalar products during the Gram Schmidt orthogonalization. This demonstrates that the reduced weights naturally extract this momentum property.
If we consider small deviations from the fully symmetric systems $\zeta = \varepsilon$, the translational invariance of the system is broken and the proper one-particle states cannot be identified by labeling the states with a momentum. Yet, an identification of the proper one-particle states is still possible relying on the reduced weights. Surprisingly, the empirical data suggest that this identification process can even be transferred to open boundary conditions ($\zeta_t = 1$). The latter implies an interpretation in terms of standing waves.
iii) Next, we consider the system in the perturbative and the $\ell = 0$ limit. In first-order perturbation theory in λ for the eigenenergies, the effective Hamilton operator is given by $\mathcal{H}^{(1)} = \mathcal{H}_0 + \lambda T_0$. The diagonalization of this Hamiltonian corresponds exactly to the subblock description at $\ell = 0$ and the resulting n-particle weights of the n-QP subblock are identical to one. This guarantees the perturbative starting point and suggests a well-controlled behavior of the reduced weights for small values of ℓ.
vi) Finally, it should be noted, that an orientation on the reduced one-particle weights breaks the cluster addivitiy in a rigorous sense, if the ground state is not separated by the one-particle states by a quantum number of the system (see discussion in the appendix A.2). This is never the case in the considered applications. Nevertheless, we investigated this quantity for such cases and find very similar behavior and no problems of this approach are observed. In the authors opinion, this property reflects that the generalized cluster additivity is more complex since it relates to the full cluster and not simply two disconnected clusters. The pure case of two disconnected clusters represents a good intellectual starting point, however, the actual calculations are always performed on connected cluster clusters and the properness of the transformation is decided on these clusters. Specifically a momentum related property can*not* relate to these cases.

Implementation

In the following, we want to describe the implementation of the reduced-weight generator scheme. First, one must define the parameter ℓ_{switch}, defining the point in ℓ, from which the generator element modification is applied. This parameter must be sufficiently large, so that the basis states within the subblock basis are close to the disentangled states. Simultaneously, the parameter must be chosen sufficiently small, so that the influence of the artificial interactions on the effective model is weak. In the case of pseudo decay, the scale of ℓ_{crit} is relatively large. Consequently, a relatively large window of proper values of ℓ_{switch} exists, allowing a plain definition of ℓ_{switch}. The parameter ℓ has the dimension of inverse energy and we simply choose to define ℓ_{switch} as an inverse energy scale. The initial energy scale of the Hamiltonian $\mathcal{H}(\lambda = 0)$ is given by the elementary excitation energy which is normalized to one. Consequently, we simply choose $\ell_{\text{switch}} = 1$. The results obtained in this thesis are robust with respect to ℓ_{switch}. However, if a more accurate definition of ℓ_{switch} is required in future applications, we refer to

the definition in applied in treatment of genuine decay (see 4.2.4).
Let $\tilde{\mathcal{H}}_{\mathrm{BD}}(\ell)$ denote the Hamiltonian in the subblock basis, which is connected to the initial Hamiltonian $\mathcal{H}$ by the transformation of the CUT (which is also represented in the sub-block basis) followed by an ℓ-dependent unitary transformation $U_{\mathrm{BD}}(\ell)$ which diagonalizes the QP blocks:

$$\tilde{\mathcal{H}}_{\mathrm{BD}}(\ell) = U^{\dagger}_{\mathrm{BD}}(\ell)U^{\dagger}(\ell)\mathcal{H}U(\ell)U_{\mathrm{BD}}(\ell) \tag{4.23}$$

The subblock basis state $|\mu\rangle$ in the initial basis are consequently given by

$$|\mu(\ell)\rangle = U^{\dagger}_{\mathrm{BD}}(\ell)U^{\dagger}(\ell)|\mu\rangle \quad . \tag{4.24}$$

To estimate the influence of of the generator element $\eta^{\mathcal{Q}}_{ij}$, one performs a single step of size δ_ℓ with the generator

$$\eta^{\delta}_{i',j'} = -(\delta_{i,i'}\delta_{j,j'} + \delta_{i,j'}\delta_{j,i'})\eta^{\mathcal{Q}}_{i'j'}. \tag{4.25}$$

This revokes the contribution of the element $\eta^{\mathcal{Q}}_{ij}$ in linear order and defines the new transformation

$$U_\delta(\ell) = U(\ell) + U(\ell)\eta^{\delta}\delta_\ell + O(\delta^2_\ell) \quad , \tag{4.26}$$

yielding the corresponding basis states

$$|\mu_\delta(\ell)\rangle = U^{\dagger}_{\mathrm{BD}}(\ell)U^{\dagger}_{\delta}(\ell)|\mu\rangle. \tag{4.27}$$

We consider the case $q_i = n$ and $q_j = m > n$. For the disentangled eigenstates, we expect $W_{i,n} \sim 1$ while $W_{j,n} \sim 0$. Strong deviations from that can be caused by a defective generator element η_{ij} (η_{ji}). Consequently, if $W_{i_\delta,n} > W_{i,n}$ or $W_{j_\delta,n} < W_{j,n}$, the generator element $\eta^{\mathcal{Q}}_{ij}$ is considered defective and is eliminated. If, however,$W_{i_\delta,n} < W_{i,n}$ and $W_{j_\delta,n} > W_{j,n}$, the generator element is reactivated.
As previously mentioned, a detection of possibly critical matrix elements via Eq.(4.18) can become problematic. At quantum criticality, multi-particle continua are on top of the one-particle dispersion. This is also reflected by the physics on the finite cluster. A lot of states merge with the low-energy spectrum and, additionally, states associated with similar momenta become energetically very close. Therefore, a simple distinction between proper and defective interactions candidates by means of $\Delta_{\mathrm{vicinity}}$ can become problematic and it can happen that proper matrix elements are eliminated. Close to quantum criticality, one additionally requires

$$\frac{\left|\langle i(\ell)|\hat{P}_n|j(\ell)\rangle\right|}{\sqrt{\left|\langle i(\ell)|\hat{P}_n|i(\ell)\rangle\langle j(\ell)|\hat{P}_n|j(\ell)\rangle\right|}} > \Delta_{\mathrm{scalar}} \quad , \tag{4.28}$$

with a suited value Δ_{scalar}. If the system is not close to criticality, these values are small, because the states which are energetically close relate to the different momenta. However, if the system is close to quantum criticality, one finds indeed states on the finite cluster, where the overlap is significantly larger. The corresponding matrix elements are genuine and are not to be eliminated. If the overlap is larger than Δ_{scalar}. Next, we describe the treatment of genuine decay.

4.2.4 Quasiparticle decay

The treatment of quasiparticle decay within the gCUT scheme relies on the basic procedure described in section 4.2.2 which requires the definition of generalized weights defining the desired effective low-energy states.
First, we discuss the objective of the modification in the case of quasiparticle decay with respect to the thermodynamic limit and on this basis we introduce a suited weight defined on finite clusters. Subsequently, we present the implementation of the resulting scheme.

Spectral weight

For pseudo decay, the classifying weight is given by the reduced n-particle weight $W_{i,n}$ with $W_{i,n} \sim 1$ ($W_{i,n} \sim 0$), if state $|i\rangle$ is an disentangled m-particle state with $m = n$ ($m > n$).
In genuine decay, the states involved in the anticrossing are associated with the same momentum in the thermodynamic limit and represent in this sense valid continuations of the eigenfunctions. In accordance with that, one finds in these cases for the relevant states $W_{i,n} \sim 1$ for both $m = n$ and $m > n$. Therefore, the reduced n-particle weight is *not* suited in the case of genuine decay. To specify the suited weights in the case of quasiparticle decay, it is useful to define the objective of the modification first and deduce the relevant weight from that.
To this end, we discuss a prototypical scenario associated with genuine decay of the one-particle mode. We consider an initial Hamiltonian of the form Eq.(2.19) for $\zeta = 0$, i.e., the Hamiltonian separates into a channel with an even and odd number of quasiparticles. For simplicity, we consider a one-dimensional system with a single supersite per unit cell and only one flavor of excitations.
We examine a scenario where the one-particle mode is energetically beneath the two-particle continuum for the momentum region $k > k_c$ and energetically inside the two-particle continuum for the other momentum region $k < k_c$. Due to the parity-symmetry, the one-particle mode is stable for the whole momentum axis.

Next, we considere an observable $\mathcal{O}(k)$ which is split into a symmetric ($\mathcal{O}_+$) and an anti-symmetric part ($\mathcal{O}_-$), i.e.,

$$\mathcal{O}_+(k) = \sum_m \hat{\tilde{T}}_m \text{ with } m = 2n_i,\ n_i \in \mathbb{Z} \tag{4.29}$$

$$\mathcal{O}_-(k) = \sum_m \hat{\tilde{T}}_m \text{ with } m = 2n_i + 1,\ n_i \in \mathbb{Z} \quad , \tag{4.30}$$

where $\tilde{T}_n$ ($\tilde{T}_{-n}$) creates (annihilates) n (bare) quasiparticles. Then, the effective spectral density Eq.(2.17) of the one-particle mode $I_1^{\mathcal{O}_-}(k,\omega)$ is given by a (prominent) delta-function while the corresponding spectral density of the two-particle continuum $I_2^{\mathcal{O}_-}(k,\omega)$ is zero. Such a scenario is sketched in figure 4.7 (a). (Correspondingly, $I_2^{\mathcal{O}_+}(k,\omega)$ is finite while $I_1^{\mathcal{O}_+}(k,\omega)$ is zero.)
Next, we introduce a small asymmetry in the Hamiltonian ($\zeta = \varepsilon$) inducing spontaneous quasiparticle decay for the one-particle mode for $k < k_c$. For these momenta, no prominent delta-function exists and, consequently, no distinct definition of a one-particle mode exists either. However, one observes a sharp resonance inside the two-particle continuum (see figure 4.7 (b)). The standard NLCE/CUT approach brutally defines the minimum of the each momentum as the one-particle mode. Not only is this definition physically counter intuitive, but it can also lead to severe convergence problems in NLCE approaches for small values of ζ. This quasi-breakdown of the approach relates to genuine decay on finite clusters. It is physically

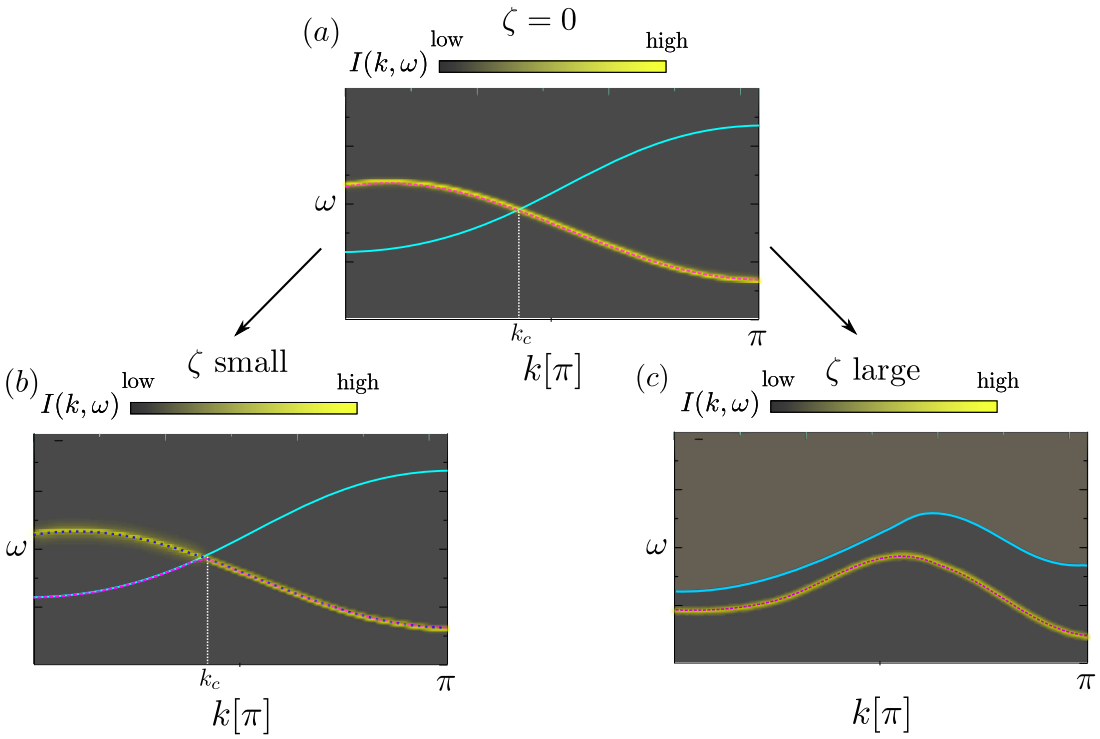

Figure 4.7: Sketch of a one-particle dispersion (dashed magenta line) and the two-particle continuum (solid cyan line). The spectral density $I(k,\omega)$ is represented by the color coding. (a) The one-particle dispersion is protected by a symmetry from the two-particle continuum, i.e., the dispersion is stable for all momenta and the spectral density is given by a delta function (illustrated with finite broadening). (b) The symmetry protecting the one-particle dispersion from the two-particle continuum is broken by a small term in the Hamiltonian. Consequently, for $k < k_c$, the delta-function is replaced by a resonance inside the continuum. The standard approach identifies the minimum for all momenta as the one-particle dispersion (dashed magenta line) while the physical more reasonable continuation of the one-particle dispersion is located at the resonance (dotted blue line). (c) The symmetry protecting the one-particle dispersion from the two-particle continuum is broken by a large term in the Hamiltonian and the one-particle dispersion is pushed out of the continuum.

highly plausible to identify the position of the resonance with the decaying one-particle mode. If we introduce a large asymmetry in the Hamiltonian, the one-particle dispersion is pushed out of the two-particle continuum (see figure 4.7 (c)). The task is to find a consistent continuation of the effective description from $\zeta = 0$ to $\zeta \neq 0$ in both scenarios. Consequently, it is not sufficient to simply ignore the terms associated with ζ in the generator or to apply the standard quasiparticle generator scheme. We want to adjust the CUT performed on finite clusters via systematic modifications of the generator scheme such, that the one-particle mode is located at the resonance if one observes decay *and* corresponds to the one-particle dispersion if it is pushed out of the continuum. In both cases, the one-particle mode is expected to carry a significant amount of spectral weight. Consequently, in is reasonable to assume that this property distincts the one-particle states on finite cluster from the two-particle states on finite cluster. It turns out, that this prototypical scenario can be too simplified, yet, it functions as a reasonable

reference point. The corresponding spectral weight on finite cluster is given by:

$$I_{n,\mathrm{tot}}^{\mathcal{O}_{+/-}^C}(\ell) = \sum_j \sum_{i\in n\mathrm{QP}} |\langle i(\ell)|\mathcal{O}_{j,+/-}^C|0\rangle|^2 \tag{4.31}$$

$$= \sum_{i\in n\mathrm{QP}} I_i^{\mathcal{O}_{+/-}^C}(\ell) \quad . \tag{4.32}$$

Here, $|0\rangle$ denotes the ground state of the system in the initial basis. The first sum runs over the observables where the index j simply numerates the different observables $\mathcal{O}_{j,+/-}^C$ acting on different sites, links etc.. The second sum runs over the n-QP subblock basis states, which are denoted by $|i(\ell)\rangle$. Accordingly, these subblock basis states must be also represented in the initial basis $\big($see Eq.(4.24)$\big)$.

The resulting spectral weight $I_{n,\mathrm{tot}}^{\mathcal{O}_{+/-}^C}(\ell=\infty)$ defines a cluster additive quantity describing the spectral weight captured in the n-particle subspace. For $\zeta\lambda = 0$, one finds $I_{n,\mathrm{tot}}^{\mathcal{O}_{-}^C}(\ell=\infty) = 0$ if the value of n is even and $I_{n,\mathrm{tot}}^{\mathcal{O}_{+}^C}(\ell=\infty) = 0$ if the value of n is odd.

For small values of $\zeta\lambda$, one expects $I_{n,\mathrm{tot}}^{\mathcal{O}_{-}^C}(\ell=\infty) \gg I_{n+1,\mathrm{tot}}^{\mathcal{O}_{-}^C}(\ell=\infty)$ for odd values of n and accordingly $I_{n,\mathrm{tot}}^{\mathcal{O}_{-}^C}(\ell=\infty) \gg I_{n+1,\mathrm{tot}}^{\mathcal{O}_{-}^C}(\ell=\infty)$ for even values of n. Deviations from this indicates quasiparticle decay on finite clusters, i.e., the quantities represent the desired generalized weights.

In particular, to treat decay of the one-particle dispersion inside the two-particle continuum, one investigates $I_{1,\mathrm{tot}}^{\mathcal{O}_{-}^C}(\ell)$ and to treat decay between the two-particle states (two-particle continuum and two-particle bound states) in the three-particle continuum, one relies on $I_{2,\mathrm{tot}}^{\mathcal{O}_{+}^C}(\ell)$.

These spectral weights represent the counterpart to the reduced weights $W_{i,n}$. Indeed, conceptually, both generalized weights stem from considerations of a purely symmetric case ($\zeta = 0$, $\zeta_t = 0$) where they uniquely define the desired states. This identification process via these weights is transferred to $\zeta \neq 0$ and $\zeta_t \neq 0$, respectively. Moreover, the validity of both approaches is perturbatively guaranteed.

However, there are fundamental differences: In the case of pseudo decay, the symmetry is fully restored after the embedding procedure. For quasiparticle decay, this is not the case and the remaining interactions moderate the decay and are accounted for by a subsequent analysis of the coupled QP channels.

Definition of ℓ_{switch}

The transformation is performed without modifications up to $\ell = \ell_{\mathrm{switch}}$ where the large interactions are already integrated out and the eigenfunctions are therefore relatively close to the disentangled eigenfunctions of the desired effective description. Then, the generator elements are modified in order to maximize the corresponding spectral weight in the targeted n-particle subspace.

Note, that it is the CUT integration process which allows to separate defective interactions from proper interactions because they are integrated on different ℓ scales. In this context, proper interactions denote interactions which are large and lead to a level repulsion in the thermodynamic limit. In contrast, defective interactions are considered to be small and induce quasiparticle decay in the thermodynamic limit. We want to prevent these interactions from unphysically affecting the definition of the particle-subspace. Of course, a rigorous definition of these terms is not possible and our classification relies on the respective ℓ-scale of these

interactions, i.e., the classification applied in the scheme is ultimately determined by the definition of ℓ_{switch}. An adequate definition of ℓ_{switch} is therefore of particular importance in the case of genuine decay.

The spectral weight $I^{\mathcal{O}^C_-}_{1,\text{tot}}(\ell)$ is designed to provide a suited definition for this ℓ-scale. The weight increases for small values of ℓ because the bare low-energy states are continuously transformed in the direction of the disentangled low-energy states. These states represent the low-energy states of the system and therefore typically carry a large portion of the overall spectral weight. At $\ell = \ell_{\text{max}}$, $I^{\mathcal{O}^C_-}_{1,\text{tot}}(\ell)$ becomes maximal and decreases for larger values of ℓ, which can be partly attributed to genuine decay. Consequently, we choose $\ell_{\text{switch}} = \ell_{\text{max}}$.

Note that this generator scheme violates the cluster additivity in a rigorous sense, because different values of ℓ_{switch} for different clusters imply that different generator schemes are applied. A cluster additive scheme would be defined by choosing ℓ_{switch} independent of the cluster size, for instance by averaging ℓ_{max} over the different clusters or by defining it as the inverse of a typical energy scale of the considered Hamiltonian. Still, a cluster-adjusted (and symmetry-channel adjusted) ℓ_{switch} is more consistent with the concept that it defines a scale of the current transformation, which can vary from cluster to cluster and symmetry-channel to symmetry-channel respectively.

The scheme applied in this thesis can be improved by defining basis-state dependent values, i.e., the testing procedures are activated for each subblock basis state $|i\rangle$ individually via $\ell_{\text{switch},i}$. A plausbile definition is therefore provided by the maximum of $I_i^{\mathcal{O}^C_-}(\ell)$. Nevertheless, these quantities are not cluster additive either, but one can introduce a cluster additive substitute by

$$\tilde{I}_i^{\mathcal{O}^C_-}(\ell) = |\langle i(\ell)|\mathcal{O}^C_{j,+/-}|0(\ell)\rangle|^2 \quad , \tag{4.33}$$

where $|0(\ell)\rangle$ is the dressed vacuum of the current transformation represented in the initial basis, i.e., $|0(\ell = \infty)\rangle$ is the actual ground state. This quantity will, by construction, decrease at first. Consequently, values of $\ell_{\text{switch},i}$ can be defined by inflection points of these quantities.

It should be noted that such a definition is in principle applicable, but should be treated with care. As we discuss in the applications (see 4.4.1), one observes sharp antilevel crossings in ℓ for the subblock energies and the corresponding basis states. In a short intervall in ℓ, two basis states are essentially interchanged, which leads to pseudo-maxima in $I_i^{\mathcal{O}^C_-}(\ell)$ and $\tilde{I}_i^{\mathcal{O}^C_-}(\ell)$ respectively. Consequently, such artificial maxima must be ignored which requires careful treatment and additional sophisticated checks. We are (so far) not able to resolve this issue.

To implement a simple and robust scheme, we simply define ℓ_{switch} as the maximum of $I^{\mathcal{O}^C_-}_{1,\text{tot}}$, since the total spectral weight is not affected by anti-crossings within a QP channel. This definition reflects a physical intuition and represents a good approximation. In addition to that, it should be noted, that this effect is irrelevant for quasi one-dimensional cluster expansions considered in this thesis, since the final result is only constituted by the two largest clusters of the expansion (see also discussion in Ref.[133]).

Elimination process

The relevant matrix elements are determined relying on Eq.(4.18). Because the defective interactions in genuine decay are not a pure artifacts, one should choose generically larger values for Δ_{vicinity} compared with pseudo decay. The principles of the elimination process are similar to the treatment of pseudo decay, but one focuses on the respective spectral weight and not the reduced QP-weights.

We denote the Hamiltonian in the subblock basis as $\tilde{\mathcal{H}}_{\mathrm{BD}}(\ell)$, connected to the initial Hamiltonian $\mathcal{H}$ by the transformation of the CUT and the subblock diagonalization:

$$\tilde{\mathcal{H}}_{\mathrm{BD}}(\ell) = U_{\mathrm{BD}}^{\dagger}(\ell)U^{\dagger}(\ell)\mathcal{H}U(\ell)U_{\mathrm{BD}}(\ell) \quad . \tag{4.34}$$

The subblock basis state $|\mu\rangle$ in the initial basis are consequently given by

$$|\mu(\ell)\rangle = U_{\mathrm{BD}}^{\dagger}(\ell)U^{\dagger}(\ell)|\mu\rangle. \tag{4.35}$$

We want to investigate the linear contributions of the generator element $\eta_{ij}^{\mathcal{Q}}$. To this end, one performs an infinitesimal step of size δ_ℓ with the generator η^δ defined by

$$\eta^{\delta}_{i',j'} = -(\delta_{i,i'}\delta_{j,j'} + \delta_{i,j'}\delta_{j,i'})\eta^{\mathcal{Q}}_{i'j'} \quad . \tag{4.36}$$

This step revokes the linear contributions of the generator element $\eta_{ij}^{\mathcal{Q}}$ and defines a new transformation

$$U_\delta(\ell) = U(\ell) + U(\ell)\eta^\delta\delta_\ell + O(\delta_\ell^2) \quad , \tag{4.37}$$

yielding the corresponding basis states

$$|\mu_\delta(\ell)\rangle = U_{\mathrm{BD}}^{\dagger}(\ell)U_\delta^{\dagger}(\ell)|\mu\rangle. \tag{4.38}$$

The resulting spectral weight is given by

$$I^{\mathcal{O}^C_{+/-}}_{n,\mathrm{tot},\delta}(\ell) = \sum_j \sum_{i\in n\mathrm{QP}} |\langle i_\delta(\ell)|\mathcal{O}^C_{j,+/-}|0\rangle|^2 \tag{4.39}$$

and one investigates the quantity

$$\Delta I = \frac{I^{\mathcal{O}^C_{+/-}}_{n,\mathrm{tot}}(\ell) - I^{\mathcal{O}^C_{+/-}}_{n,\mathrm{tot},\delta}(\ell)}{\delta_\ell} \tag{4.40}$$

$$= 2\sum_j \sum_{i\in n\mathrm{QP}} \langle i|U(\ell)U_{\mathrm{BD}}(\ell)\mathcal{O}^C_{j,+/-}|0\rangle\langle i|U(\ell)\eta^\delta U_{\mathrm{BD}}(\ell)\mathcal{O}^C_{j,+/-}|0\rangle + O(\delta_\ell) \quad . \tag{4.41}$$

If $\Delta I > \varepsilon_\Delta$, the generator element $\eta_{i,j}$ is eliminated, if $\Delta I < \varepsilon_\Delta$, the generator element is reactivated. A threshold $\varepsilon_\Delta = 10^{-9}$ is just chosen to prevent random activation-elimination sequences. In practice, one calculates $U_{\mathrm{BD}}(\ell)\mathcal{O}^C_{j,+/-}|0\rangle$ first. Because η^δ consists only of two elements, this allows for a fast testing procedure for the matrix elements satisfying Eq.(4.18). As previously mentioned, the identification of possibly defective generator elements via Eq.(4.18) can become problematic. In the considered case, a prototypical scenario is given by level repulsions leading to a depression of the one-particle dispersion, i.e., these interactions are genuine and to not lead to quasiparticle decay. If the two-particle continuum is energetically close to the one-particle dispersion, the corresponding states on the finite clusters are also energetically close. If the matrix elements are falsely eliminated, the resulting one-particle dispersion in the thermodynamic limit is still coupled to the two-particle continuum. However, this effect is treated by the subsequent evaluation process, which renormalizes the one-particle dispersion. If the renormalization is only moderate, the approach is considered to valid. (So far, a counterpart similar Eq.(4.28) is missing in current applications.)

4.3 Extrapolation techniques

In the preceding section, the treatment of pseudo decay is presented. This renders previously infeasible calculations close to or even at quantum criticality possible. Since this regime is associated with a divergence of the correlation length, extrapolation schemes become essential. However, in current literature, effective extrapolation techniques for NLCEs are missing, specifically with regard to critical exponents. In this section, we describe the extrapolation techniques which can be used to extrapolate the results obtained via pCUTs (gCUTs) to infinite order (infinite cluster sizes). First, we give a brief introduction into well-established extrapolation techniques for series expansions. On this basis, we discuss the possibility to apply these techniques to NLCEs.

4.3.1 Series expansion

A decisive feature for high-order series expansions is the presence of powerful extrapolation techniques. For a more detailed overview over this vast topic, we refer the interested reader to a well-written introduction by Guttmann [122].
We consider a series expansion of the form

$$F(\lambda) = \sum_{n\geq 0}^{m} a_n \lambda^n = a_0 + a_1\lambda + a_2\lambda^2 + \dots a_m\lambda^m, \tag{4.42}$$

with $\lambda \in \mathbb{R}$ and $a_i \in \mathbb{R}$. The function $F(\lambda)$ represents an approximant of the actual function $\tilde{F}(\lambda) = \lim_{n\to\infty} F(\lambda)$. Here, $\tilde{F}(\lambda)$ may represent the excitation gap, the entanglement entropy or any other quantity accessible via LCEs. Naturally, depending on the quantity and the value of λ, the approximation can become deficient.
The fundamental idea behind extrapolation schemes is the derivation of extrapolants from $F(\lambda)$. These extrapolants are functions whose form differ from the plain series expansion, which leads to a better approximation, i.e., the form of the extrapolant is generically more suited to mimic the behavior of the actual physical function $\tilde{F}(\lambda)$ than a plain series.
A standard extrapolation scheme is the Padé extrapolation defined by

$$P[L/M]_F := \frac{P_L(\lambda)}{Q_M(\lambda)} = \frac{p_0 + p_1\lambda + \dots + p_L\lambda^L}{q_0 + q_1\lambda + \dots q_M\lambda^M} \quad , \tag{4.43}$$

with $p_i \in \mathbb{R}$ and $q_i \in \mathbb{R}$ and $q_0 = 1$. The latter can be achieved by reducing the fraction. The real coefficients are fully defined by the condition that the Taylor expansion of $P[L/M]_F$ (in λ around $\lambda = 0$) up to order $L + M$ ($L + M \leq m$) recovers the corresponding Taylor expansion of the original series $F(\lambda)$.
Naturally, Padé extrapolants are more versatile than a plain series and are specifically suited for scenarios where a rational function is approximated. Poles of an extrapolant can either reflect physics of the system or they can simply be an artifact of the extrapolation technique. If such a spurious pole is located close to or between $\lambda = 0$ and the considered λ value, the corresponding extrapolant is called *defective* and should be discarded.
There is no single blueprint distinguishing physical and defective poles and this must be decided in the respective context and matched with the expectations. The extrapolation is considered to work if several combinations of L and M yield similar results. Specifically relevant is the convergence of the families defined by $L - M = \text{const}$. Padè extrapolants constitute a valid extrapolation scheme, however, especially close to quantum criticality, the rational functions

fail to capture the characteristic behavior.
In these cases, it is advisable to implement the so-called Dlog-Padé extrapolation, which are applicable to quantities of definite sign like energy gaps or spectral weights. Most importantly, this scheme allows the extraction of critical exponents, i.e., the extrapolants are suited to describe power-law behavior.
If one assumes power-law behavior near a critical value λ_c, the function $\tilde{F}(\lambda)$ close to λ_c is given by

$$\tilde{F}(\lambda) \approx \left(1 - \frac{\lambda}{\lambda_c}\right)^{-\alpha} A(\lambda). \tag{4.44}$$

If $A(\lambda)$ is analytic at $\lambda = \lambda_c$, we can write

$$\tilde{F}(\lambda) \approx \left(1 - \frac{\lambda}{\lambda_c}\right)^{-\alpha} A|_{\lambda=\lambda_c} \left(1 + O(1 - \tfrac{\lambda}{\lambda_c})\right). \tag{4.45}$$

Near the critical value λ_c, the logarithmic derivative is then given by

$$\begin{aligned} \tilde{D}(\lambda) &:= \frac{\mathrm{d}}{\mathrm{d}\lambda} \ln \tilde{F}(\lambda) \\ &= \frac{\tilde{F}'(\lambda)}{\tilde{F}(\lambda)} \\ &\approx \frac{-\alpha}{\lambda - \lambda_c}\{1 + O(\lambda - \lambda_c)\}. \end{aligned} \tag{4.46}$$

In the case of power-law behavior, the logarithmic derivative $\tilde{D}(\lambda)$ is expected to exhibit a single pole. In this case, Padé extrapolations are perfectly suited to approximate $\tilde{D}(\lambda)$. These extrapolants are defined by the corresponding series $D(\lambda)$, which is, due to the derivative, only known up to order $m-1$, i.e., $L + M \leq m - 1$. The resulting Dlog-Padé approximants of $F(\lambda)$ are then defined by

$$dP[L/M]_F(\lambda) = \exp\left(\int_0^\lambda P[L/M]_D \quad \mathrm{d}\lambda'\right) \tag{4.47}$$

and represent physically grounded extrapolants in the case of a second-order phase transition. The poles of $P[L/M]_D(\lambda)$ can either indicate a critical value λ_c or be spurious. In practice, this is decided essentially by the location of these poles. The corresponding critical exponent of a pole λ_c is given by

$$\alpha = \left.\frac{P_L(\lambda)}{\frac{\mathrm{d}}{\mathrm{d}\lambda} Q_M(\lambda)}\right|_{\lambda=\lambda_c}. \tag{4.48}$$

If the exact value of λ_c is known, one can obtain better estimates of the critical exponent by defining

$$\begin{aligned} \alpha^*(\lambda) &:= (\lambda_c - \lambda) D(\lambda) \\ &\approx \alpha + O(\lambda - \lambda_c), \end{aligned}$$

where $D(\lambda)$ is given by Eq.(4.46). Then

$$P[L/M]_{\alpha^*}\big|_{\lambda=\lambda_c} = \alpha \tag{4.49}$$

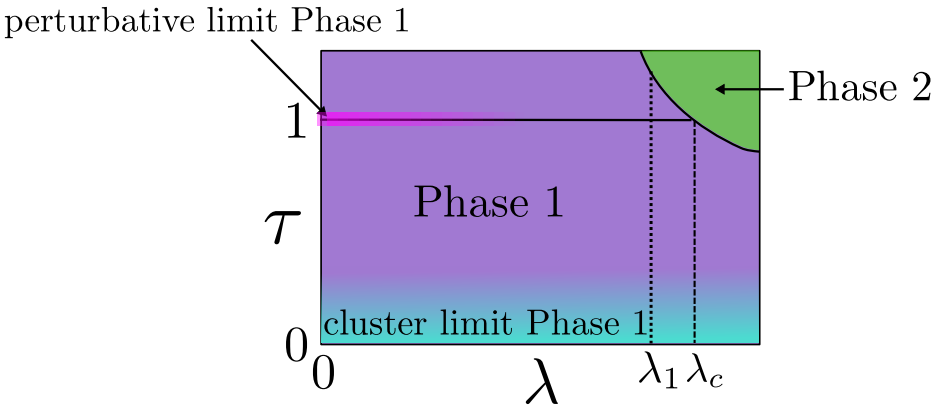

Figure 4.8: Sketch of the anticipated phase diagram in the parameters λ and τ. The perturbative series expansion is carried out from the $\lambda = 0$ limit on the physical axis ($\tau = 1.0$). The NLCE expansion in τ is carried out for an arbitrary but fix value of λ from the $\tau = 0$ limit. The phase transition from Phase 1 to Phase 2 can be induced by increasing λ or τ.

yields a (biased) estimate of the critical exponent.
Finally, it should be noted that Dlog-Padé extrapolants can also prove to be proper extrapolants if *no* phase-transition is described. In the next section, we describe how these extrapolation schemes can be applied to numerical data sequences obtained via NLCEs.

4.3.2 Non-perturbative linked-cluster expansion

In contrast to the purely perturbative LCE approaches, NLCEs yield numerical data sequences for a defined value of λ. Since each cluster is treated non-perturbatively, no perturbative parameter limiting the applicablity exits. Yet, only a finite set of clusters can be treated numerically which sets a characteristic length scale $\mathcal{L}$ of quantum fluctuations captured. Consequently, if the physical system has a finite correlation length, the NLCE converges as long as $\xi \sim \mathcal{L}$. Specifically at quantum critical points with $\xi \to \infty$, one must rely on extrapolation techniques. One form of extrapolation of NLCE results relies on an appropriate scaling in $\mathcal{L}$ [65]. A challenge of these scalings is the assignment of a length scale to a given cluster in more than one dimension. It is possible to extract universal properties relying on scaling arguments. It seems, at least in principle, possible to extract the critical exponent ν in a similar fashion. The other extrapolation relies on the ε-Wynn and related methods [59, 62]. This method does not require a length scale, yet, this approach does not provide any critical exponents.
In a work of Bernu and Misguich [134], the expansion for entropy in the inverse-temperature variable is converted to an expansion for entropy in the internal energy, allowing to build the ground-state energy and low-temperature power-law behavior into the extrapolation of high-temperature expansion. Our considerations are in a similar direction.
We suggest a scheme, addressing specifically the power-law behavior close to quantum criticality. The fundamental idea behind the approach is a reformulation of the data sequences as a series expansion in a pseudo parameter, allowing to utilize standard series expansion extrapolation techniques to extract critical properties. The reformulation does not rely on a length scale, yet, the series extrapolation schemes can be physically motivated. Most importantly, in addition to

critical points, this scheme provides access to critical exponents.
Let $K_{N,\lambda}$ denote the quantity of interest (e.g. excitation gaps, spectral weights) obtained via an NLCE calculation including up to N supersites for the coupling strength λ. The values of $K_{N,\lambda}$ are, in principle, expected to converge with increasing N as long as $\lambda < \lambda_c$. Next, we introduce the parameter

$$b_{N-1,\lambda} = K_{N,\lambda} - K_{N-1,\lambda}, \tag{4.50}$$

representing the contributions specific to N-site clusters ($K_{0,\lambda} \equiv 0$). We can simply rewrite

$$K_{N,\lambda} = \sum_{n\geq 0}^{N-1} b_{n,\lambda} = b_{0,\lambda} + b_{1,\lambda} + \cdots + b_{N-1,\lambda}. \tag{4.51}$$

With this, we can define the function

$$G_\lambda(\tau) = \sum_{n\geq 0}^{m} b_{n,\lambda}\tau^n = b_{0,\lambda} + b_{1,\lambda}\tau + \cdots + b_{m,\lambda}\tau^m, \tag{4.52}$$

with $m = N_{\max} - 1$. The pseudo parameter τ functions as a substitute for the missing expansion parameter and one aims at $\tilde{G}_\lambda(\tau = 1) = \lim_{n\to\infty} G_\lambda(\tau = 1)$. It is therefore possible to apply the wide range of series expansion extrapolation techniques in τ.
Indeed, the exptrapolation techniques applied to data sequences in Ref.[59] and Ref.[62] are identical to Padé extrapolations evaluated at $\tau = 1.0$. However, as we argue in the following, *Dlog* Padé extrapolations are perfectly suited for this purpose if the system is close to quantum criticality.
Following Eq.(4.52), the results of an NLCE expansion can be interpreted as an expansion in τ from the local cluster limits $\tau = 0$. But in addition to that, the cases $\tau = 1$ and $\tau \neq 1$ can be identified with the same physical system in an extended parameter space as visualized in figure 4.8. In NLCEs, the local cluster limit is closely related to the perturbative limit and the expansion is carried out starting from a specific phase.[4].Due to the close relation between the limit $\tau \to 0$ and $\lambda \to 0$, it is suggestive that the same phase transition from Phase 1 to Phase 2 is induced by increasing λ and τ respectively and no intermediate phases occur in τ. (If this assumption does not hold, the NLCE approach seems overall problematic.)
For values of λ close to criticality, one expects that τ_c is close to one, i.e., $G_\lambda(\tau)$ must be evaluated close to criticality and it is therefore reasonable to apply Dlog Padè extrapolations to obtain approximations of $\tilde{G}_\lambda(\tau = 1)$. If the extrapolation yields $\tau_c < 1.0$ ($\tau_c > 1.0$), one deduces $\lambda > \lambda_c$ ($\lambda < \lambda_c$). Thus, a scheme of the form $\lambda_{i+1} = \frac{\lambda_i}{\tau_{c,i}}$ allows an iteration to determine λ_c.
Most importantly, due to the universality of the critical exponents, it is possible to extract the critical exponent by applying Eq.(4.48) or Eq.(4.49) ($G_\lambda(\tau) \hat{=} F(\lambda)$), at least if λ is in the vicinity of λ_c.
We stress that this extrapolation scheme does not require any additional numerical overhead and relies solely on the data available. Moreover, the same argumentation can be applied to other numerical techniques which yield converging sequences of numerical data points with a similar relation between the limit $\tau \to 0$ and $\lambda \to 0$. A prototypical example for this is deepCUT [47], a numerical CUT approach which relies on a quasi-perturbative truncation.

[4]See for instance discussion of low-field NLCE and high-field NLCE in Ref.[65]

4.4 Applications

In this section, we discuss the applications of the modified gCUT schemes, illustrating the different methodological developments. We begin with a discussion of the general scheme and the treatment of pseudo decay for the two-leg spin 1/2 Heisenberg ladder in 4.4.1. Afterwards, gCUTs are applied to describe the quantum phase transition between the dimerized and the isotropic spin 1/2 Heisenberg chain, relying on the extrapolation scheme introduced in 4.4.2. Finally, we discuss the treatment of quasiparticle decay in the thermodynamic limit using a modified gCUT scheme in 4.4.3.

4.4.1 Two-leg Heisenberg ladders - pseudo decay

In this section, we discuss the application of the (optimized) gCUT scheme with respect to the general scheme and the treatment of pseudo decay, focussing on one-particle properties. Particularly suited for this purpose are isolated two-leg spin 1/2 Heisenberg ladders. The model is depicted in figure 4.9(a).
Two-leg spin 1/2 Heisenberg ladders represent a prototypical example of a one-dimensional valence-bond solid [135], i.e., the ground state does not break any symmetry and possesses no magnetic order. Interestingly, this system stays gapped for all values of the leg-coupling λ [136, 137] and the elementary excitations can be understood in terms of dressed triplets called triplons [10]. Being additionally relevant for superconductivity [138], the two-leg ladder system became of massive theoretical [42, 54–57, 139–142] and experimental interest [143–157]. Note, that the system can be modified by an additional ring exchange to match experiments on cuprate ladders [57, 158, 159]. Essential for the low-energy physics of this system are also characteristic two-triplon bound states [54–57, 140, 141].
For a large parameter intervall, the two-leg ladder exhibits large interactions without quasiparticle decay [47]. However, as we demonstrate in the following, depending on the coupling strength, the system can exhibit pseudo decay on finite clusters. Consequently, this system provides a perfect play-ground for gCUTs. Moreover, results of deepCUT [47] and CORE [99] for the one-triplon dispersion are available, allowing to compare our results with related techniques. Moreover, DMRG data [157, 160] allow for an unbiased check.

The model

The considered Hamiltonian of the two-leg Heisenberg ladder is given by

$$\mathcal{H} = \underbrace{\sum_{\langle i,j\rangle} S_i S_j}_{\mathcal{H}_0} + \lambda \underbrace{\sum_{\langle i,j\rangle'} S_i S_j}_{\mathcal{V}} , \tag{4.53}$$

where the first (second) sum represents the intra-dimer (inter-dimer) couplings. The different couplings are illustrated in figure 4.9(a).
The dimers form the supersites of the expansion. For $\lambda = 0$, the ground state is given by a product state of singlets $|s\rangle$ on these dimers and the excitations are local triplets $|t^\alpha\rangle$ with $\alpha = \{\pm 1, 0\}$ and an energy gap $\Delta = 1.0$. This defines a quasiparticle picture in terms of triplets, i.e., the local excitations are identified with the presence of a hardcore boson with falvour α and the ground state is given by a vacuum. We aim at an effective description in terms of these quasiparticles.

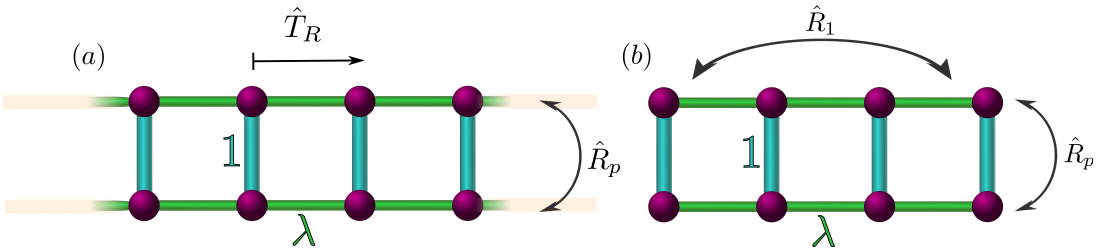

Figure 4.9: (a) Illustration of the considered model. The Hamiltonian is studied from the dimerized limit $\lambda = 0$. The system exhibits a translational symmetry $\hat{T}_R$ and the reflection symmetry $\hat{R}_p$ splits the Hamiltonian into a channel with even (odd) number of triplons. (b) Illustration of a ladder segment ($N = 4$). The reflection symmetry $\hat{R}_1$ is also exploited during the CUT calculations.

To this end, the Hamiltonian Eq.(4.53) must be represented in terms of triplets. The degeneracy of the local triplets leaves a degree of freedom for the local basis. In this context, it is advisable to sort the triplets with respect to the magnetization in S_z-direction in order to efficiently exploit S^z_{tot}. Consequently, the local basis of a dimer is given by

$$|s\rangle = \tfrac{1}{\sqrt{2}}\left(|\uparrow\downarrow\rangle - |\downarrow\uparrow\rangle\right) \tag{4.54}$$

$$|t^0\rangle = \tfrac{1}{\sqrt{2}}\left(|\uparrow\downarrow\rangle + |\downarrow\uparrow\rangle\right) \tag{4.55}$$

$$|t^1\rangle = |\uparrow\uparrow\rangle \tag{4.56}$$

$$|t^{-1}\rangle = |\downarrow\downarrow\rangle. \tag{4.57}$$

Since the system displays a reflection symmetry $\hat{R}_p$ around the center of the dimers, the system is divided into a channel of even and odd numbers of triplets, i.e., the Hamiltonian is expressed in terms of these triplets by

$$\mathcal{H} = \tfrac{3}{4}N + \mathcal{H}_0 + \lambda\left(T_{-2} + T_0 + T_2\right), \tag{4.58}$$

where N is the total number of dimers, $\mathcal{H}_0$ counts the number of triplets and T_m (T_{-m}) creates (annihilates) in total m triplets on neighboring dimers. The local matrix elements are shown in table 4.1.

Our objective is to derive a quasiparticle conserving effective Hamiltonian. The quasiparticles in the targeted effective description are dressed versions of the initial triplets and are referred to as triplons [10]. In particular, we aim at the one-triplon subspace, i.e., the desired effective Hamiltonian takes then the form

$$\mathcal{H}_{\text{eff}} \quad = \quad \tilde{E}_0(\lambda) + \sum_{i,\delta,\alpha} \tilde{a}_\delta(\lambda)\, \hat{\tilde{t}}^\dagger_{i+\delta,\alpha} \hat{\tilde{t}}_{i,\alpha} + \text{h.c.} \tag{4.59}$$

where $\hat{\tilde{t}}^\dagger_{i,\alpha}$ ($\hat{\tilde{t}}_{i,\alpha}$) creates (annihilates) a triplon with magnetization α on dimer i. Due to the $SU(2)$ invariance, the hopping elements $a_\delta(\lambda)$ are independent of the triplon flavor α. A Fourier transformation yields the one-triplon dispersion $\omega(k)$.

Finally, the clusters of the two-leg ladder correspond to simple ladder segments of length $\mathcal{L}$, as sketched in figure 4.9(b). The gCUT calculation is performed up to $N_{\text{max}} = 12$ dimers. One

$2\tau_0$		
$\|t^{0,\pm1},s\rangle$	$\leftrightarrow$	$\|s,t^{0,\pm1}\rangle$
$\|t^{0},t^{\pm1}\rangle$	$\leftrightarrow$	$\|t^{\pm1},t^{0}\rangle$
$\|t^{\pm1},t^{\pm1}\rangle$	$\leftrightarrow$	$\|t^{\pm1},t^{\pm1}\rangle$
$\|t^{\pm1},t^{\mp1}\rangle$	$\leftrightarrow$	$\|t^{0},t^{0}\rangle - \|t^{\pm1},t^{\mp1}\rangle$
$\|t^{0},t^{0}\rangle$	$\leftrightarrow$	$\|t^{1},t^{-1}\rangle + \|t^{-1},t^{1}\rangle$
$2\tau_2$		
$\|s,s\rangle$	$\rightarrow$	$-\|t^{1},t^{-1}\rangle + \|t^{0},t^{0}\rangle - \|t^{-1},t^{1}\rangle$

Table 4.1: Two-leg ladder: Representation of the local operators τ_n, which act on the links of the super lattice, in the considered triplet basis.

observes a strong even-odd effect with respect to $\mathcal{L}$ for the two-leg ladder. This can be traced back to the antiferromagnetic ordering wave vector of the gap $\Delta(k = \pi)$. We reduce this effect by averaging the results via $\omega^{\mathcal{L}}(k) \rightarrow \frac{1}{2}(\omega^{\mathcal{L}}(k) + \omega^{\mathcal{L}-1}(k))$.
Before going into details of the obtained results, we briefly discuss the symmetries exploited for the finite-cluster calculations. We implement the magnetization S^z_{tot} and the triplet-parity simultaneously using Lin tables. Due to the $SU(2)$ symmetry, we can restrict the calculation to the $S^z_{\text{tot}} = 0$ channel. Then, a global spin inversion mapping $S^z \rightarrow -S^z$ splits the Hamiltonian into a symmetric and an anti-symmetric channel. Note, that the respective channel depends on the targeted low-energy states but also on the number of dimers of the considered cluster. For instance, for N even (odd) the singlet product state is symmetric (anti-symmetric) with respect to the spin inversion.
Finally, we exploit the reflection symmetry $\hat{R}_1$ on each cluster, separating the calculation of the effective one-particle model into an symmetric (anti-symmetric) part.

General scheme

In the following, we want to discuss the results derived via gCUTs, relying on the general scheme described in 4.1. Before discussing the calculation for a specific value of λ in detail, we briefly discuss the resulting one-particle dispersions qualitatively.
Up to intermediate values of λ ($\lambda \leq 1.0$), one obtains sound results for the one-particle dispersion, as depicted in figure 4.10(a). With respect to the considered energy scales, the results are converged in N. For small values of λ, the form of $\omega(k)$ corresponds roughly to a cosine band. However, for intermediate values of λ, the form changes qualitatively and the dispersion exhibits a maximum at $k \approx \frac{\pi}{2}$ and the gap $\Delta = \omega(k = \pi)$ remains relatively large. In addition to that, one observes a characteristic dip at $k \sim 0$, reflecting the proximity of the three-triplon continuum due to large triplon-triplon interactions [142].
In contrast, for slightly larger values of λ ($\lambda = 1.25$, $\lambda = 1.5$), the results obtained via the general scheme become abruptly erratic, as shown in figure 4.10(b). The results do *not* converge with N, quite the contrary, the erratic effects become even more severe with increasing N. This behavior can be traced back to pseudo decays on finite clusters.
The treatment of pseudo decay via an optimized version of gCUTs is addressed in 4.4.1. First, we want to describe the general scheme and focus on the isotropic ladder with $\lambda = 1.0$. In this case, the system does not exhibit pseudo nor genuine decay for the one-particle states and it is suited to demonstrate the general gCUT scheme while the proper description of the one-particle dispersion is not trivial.

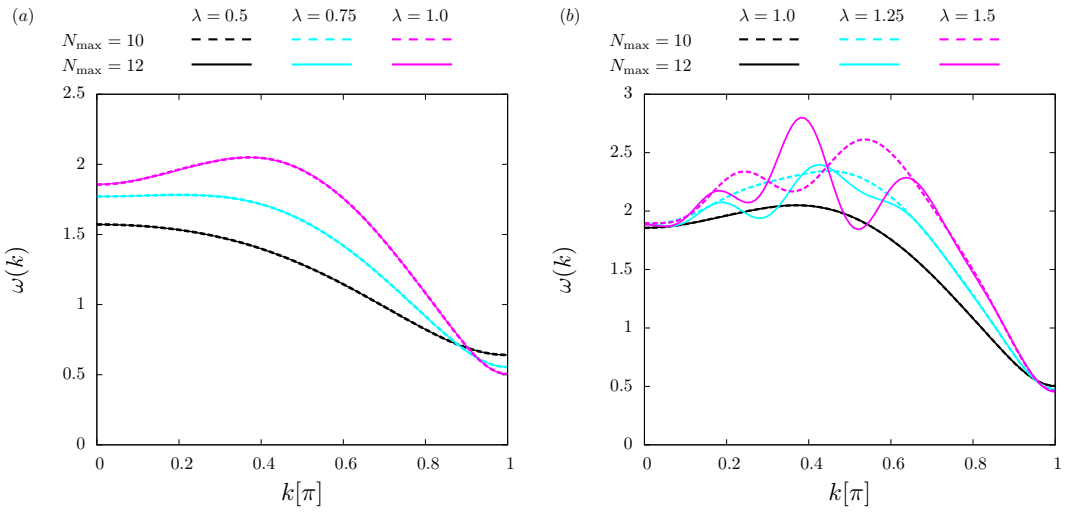

Figure 4.10: The one-particle dispersion $\omega(k)$ is shown for different values of the coupling λ. The solid (dashed) line shows ω obtained using the maximal cluster size $N_{\max} = 12$ ($N_{\max} = 10$.) (a) The one-particle dispersion is depicted for $\lambda = 0.5$ (black), $\lambda = 0.75$ (cyan) and $\lambda = 1.0$ (magenta). (b) The one-particle dispersion is depicted for $\lambda = 1.0$ (black), $\lambda = 1.25$ (cyan) and $\lambda = 1.5$ (magenta).

We begin with a brief exemplary discussion of the behavior of the characteristic quantities on a single cluster, to provide a picture of these quantities if no decay is present. Then, we discuss the resulting one-particle dispersion with respect to the convergence of both the cluster expansion and the truncation schemes applied on finite clusters.

CUTs on finite clusters We begin by discussing exemplarily the CUT on an intermediate sized $N = 10$ ladder segment on the basis of the characteristic quantities. The subblock energies $\varepsilon_i(\ell)$ are depicted in figure 4.11(a). For small values of ℓ, one observes that the subblock energies decrease, which reflects the renormalization effect of the interaction on the low-energy states. Moreover, for $\ell \sim 1.3$, one observes a sharp anticrossing in ℓ within the 1QP block.
Physically, this behavior is related to the maximum of the one-particle dispersion at $k_{\max} \approx \frac{\pi}{2}$, arising due to the interaction with the three-particle continuum. To illustrate this, we denote the dispersion of first-order perturbation theory in λ by $\omega^{(1)}(k)$ and the actual dispersion by $\omega(k)$. The first-order perturbation theory does not account for this interaction effect and, therefore, $\omega^{(1)}(k)$ is given by a cosine and does not exhibit a dip. Consequently, one finds $\omega^{(1)}(k_1) > \omega^{(1)}(k_{\max})$ and $\omega(k_1) < \omega(k_{\max})$ for the momenta $k_1 < k_{\max}$ suppressed by the three-particle continuum.
This behavior in the thermodynamic limit is also reflected by the physics on finite clusters. For $\ell = 0$, the subblock diagonalization corresponds to first-order perturbation theory in λ, i.e., the subblock energies $\varepsilon_i^n(\ell = 0)$ are identical to the first-order eigenenergies ($\rightarrow \omega^{(1)}(k)$). During the integration, the interactions with higher QP-blocks are continuously integrated, resulting in a decoupled one-QP block ($\rightarrow \omega(k)$). Since the finite-cluster states can be associated with different momenta in the thermodynamic limit, the order of the corresponding states is switched during the integration. In analogy to anticrossings associated with decay, one observes sharp anticrossings in ℓ within the one-QP subblock.

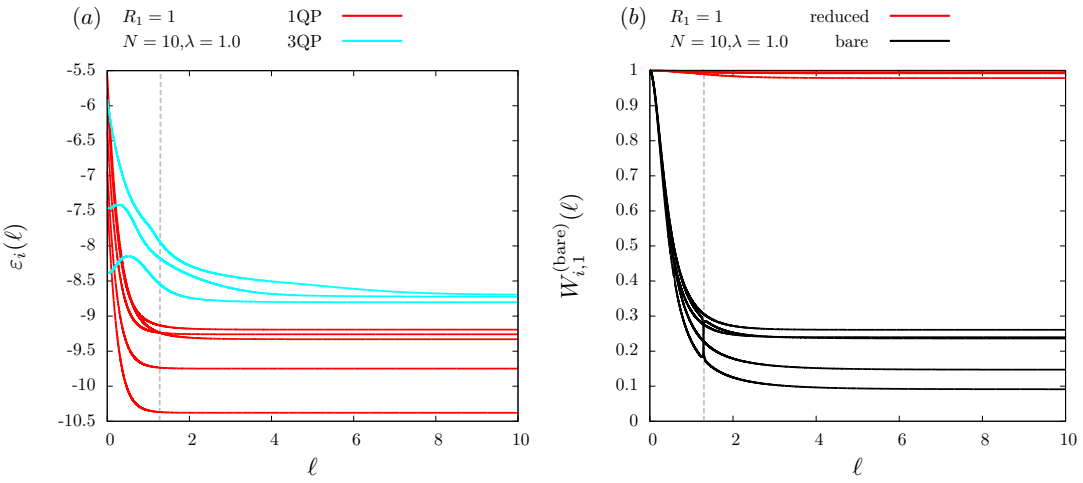

Figure 4.11: The behavior of the characteristic quantities of the basis states in dependence of ℓ is shown for $N = 10$-cluster and the symmetry channel $R_1 = 1$ for the coupling $\lambda = 1.0$. (a) The subblock energies $\varepsilon_i(\ell)$ are shown for the 1QP basis states (red) and the lowest 2QP basis states (cyan). (b) The reduced 1-QP weights $W_{i,1}(\ell)$ (red) and bare 1-QP weights $W_{i,1}^{\mathrm{bare}}(\ell)$ (black) are shown for the 1QP basis states. The vertical dashed line illustrates $\ell_{\mathrm{cross}} \approx 1.3$.

For larger values of ℓ, the subblock energies converge and the 1QP subblock energies represent the smallest energies of the system ($q_i = 1, q_j > 1 \Rightarrow \varepsilon_i(\ell) < \varepsilon_j(\ell)$), i.e., no pseudo decay is present.
To further illustrate the CUT performed on finite cluster, we introduce the bare one-particle weights $W_{i,1}^{\mathrm{bare}}(\ell) = \langle i(\ell)|\hat{P}_1|i(\ell)\rangle$. Here, the operator $\hat{P}_1$ projects onto the one-particle subspace, i.e., $W_{i,1}^{\mathrm{bare}}(\ell)$ measures the part of the bare one-particle states of the dressed state $|i(\ell)\rangle$. The reduced one-particle weights $W_{i,1}(\ell)$ and the bare one-particle weights $W_{i,1}^{\mathrm{bare}}(\ell)$ are shown in figure 4.11(b). One observes that the bare one-particle weights drop fast, indicating that the system is in a non-perturbative regime.[5] In contrast, the reduced one-particle weights remain large up to $\ell \to \infty$, indicating that the reduced one-QP weights are a distinguished quantity to identify the disentangled one-particle states.
This finishes the finite-cluster discussion. We remark that the behavior of these quantities is prototypical for this parameter regime. However, this changes qualitatively, if decay is present.

Convergence In the following, we want to discuss the convergence of the results. The initial gCUT scheme relies on the standard basis [46, 63] (see 4.1.2) without any form of truncation. Consequently, convergence relates only to the maximal number of sites considered in the calculation. However, the size of the matrices defining the flow equation grows exponentially fast, becoming the bottle neck of the calculation. Therefore, it is reasonable to introduce truncations of the basis on each cluster to reach significantly larger cluster sizes (see 4.1.3). Then, the convergence with respect to this truncation scheme must also be considered. As we demonstrate, it is possible to obtain accurate results with a truncated basis extremely smaller than the original one. This gives access to substantially larger cluster sizes $N_{\mathrm{max}} = 12$.

[5] The bare one-particle weights become almost evenly distributed over the states forming the low-energy spectrum, i.e., the bare weights are not suited to identify the disentangled one-particle states.

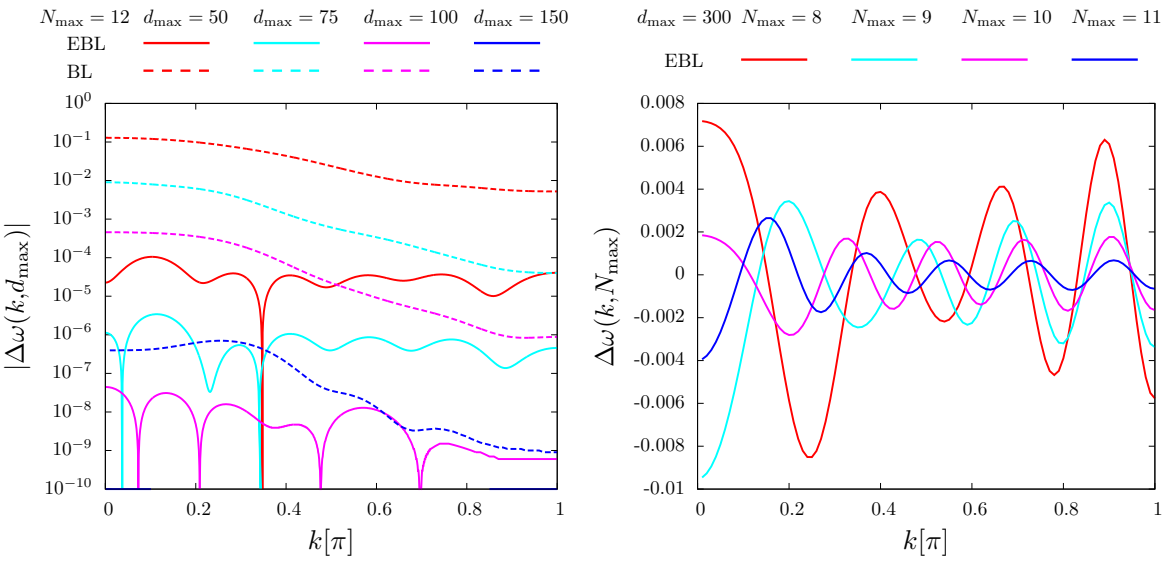

Figure 4.12: Left panel: For $\lambda = 1.0$, the error of the one-triplon dispersion $\Delta\omega(k,d_{\max})$ induced by the truncation of the basis is shown in dependence of the momentum k for various values of the basis size $d_{\max}$ ($d_{\max} = 50$ (red), $d_{\max} = 75$ (cyan), $d_{\max} = 100$ (magenta), $d_{\max} = 150$ (blue)). Solid (dashed) lines refer to the extended block lanzcos truncation (block lanzcos truncation). Right panel: For $\lambda = 1.0$, the difference of the one-particle dispersion $\Delta\omega(k,N_{\max})$ between the $\mathcal{L} = N_{\max}$ and $\mathcal{L} = 12$ calculation is shown in dependence of the momentum k for various values of $N_{\max}$ ($N_{\max} = 8$ (red), $N_{\max} = 9$ (cyan), $N_{\max} = 10$ (magenta), $N_{\max} = 11$ (blue)).

To discuss the convergence, the obtained one-particle dispersion $\omega(k,d_{\max},N_{\max})$ is viewed as a function of the maximal basis size $d_{\max}$ and the maximal number of dimers $N_{\max}$. Then, either $d_{\max}$ or $N_{\max}$ are fixed to the maximal value and the other parameter is varied to estimate the convergence in this parameter.
We start by discussing the convergence with respect to $d_{\max}$ for the block-Lanczos truncation (BLT) and the extended block-Lanczos truncation (EBLT). To this end, we define

$$\Delta\omega(k,d_{\max}) = \omega(k,d_{\max},N_{\max} = 12) - \omega(k,d_{\max} = 300,N_{\max} = 12), \tag{4.60}$$

where the results of $\omega(k,d_{\max} = 300,N_{\max} = 12)$ are obtained via EBLT and are numerically converged. The behavior of $\Delta\omega(k,d_{\max})$ is depicted in figure 4.12(a) for both truncation schemes and different values of $d_{\max}$.
One observes that the results obtained with EBLT converge considerably faster than the results obtained via BLT. It is noticeable that the convergence of the BLT becomes slow for small momenta. For these momenta, the one-particle dispersion is high in energy and close to the three-particle continuum. As expected, the accurate determination of corresponding high-energetic one-particle states on finite clusters via BLT is problematic. In contrast, the EBLT enforces an accurate low-energy spectrum on the cluster. Therefore, the convergence of the dispersion does not show such a characteristic behavior and converges more robust and faster than the BLT scheme. This relates specifically to the energetically challenging regimes, where the EBLT guarantees a more robust approach. In the following applications, we therefore

use the EBLT scheme.
Nevertheless, both truncation schemes converge with $d_{\max}$. For $d_{\max} = 150$, the results obtained via BLT are converged up to $\varepsilon < 10^{-6}$ and the results obtained via EBLT are even converged up to $\varepsilon < 10^{-10}$ which is sufficiently small.
The maximal number of dimers treated in gCUTs using the standard basis is given by $N_{\max} = 6$ [161] and the corresponding Hilbert space dimension in the S^z_{tot}=0-channel is given by $D_{\mathfrak{H}} = \frac{12!}{6!6!} = 924$. Consequently, the number of manageable supersites via gCUTs is practically doubled, which is a major improvement with regard to the exponential growth of the Hilbert space. The treatment of $N_{\max} = 12$ dimers via the standard basis is obviously infeasible, since it would require the treatment of $D_{\mathfrak{H}} \times D_{\mathfrak{H}}$ matrices with $D_{\mathfrak{H}} = \frac{24!}{12!12!} = 2704156$. Moreover, it is noticeable that the matrices involved in the truncated $N_{\max} = 12$ calculation are even *smaller* than the matrices of the initial $N_{\max} = 6$ calculation. Therefore, the *computational* challenge of the gCUT procedure generically shifts away from the actual CUT the clusters towards the truncation scheme.
Next, we investigate the convergence with $N_{\max}$. Accordingly, we define

$$\Delta\omega(k,N_{\max}) = \omega(k,N_{\max},d_{\max} = 300) - \omega(k,N_{\max} = 12,d_{\max} = 300). \tag{4.61}$$

The behavior of $\Delta\omega(k,N_{\max})$ is shown in figure 4.12(b). One observes, that the results converge with increasing $N_{\max}$. Moreover, $\Delta\omega(k,N_{\max})$ is dominated by an oscillation. To be precise, one observes $\frac{N_{\max}-1}{2}$ oscillations for the intervall $k = [0,\pi]$. The cluster expansion up to $N_{\max}$ dimers involves hopping elements over maximally $(N_{\max} - 1)$ sites. The contribution of this hopping element to the dispersion is consequently responsible for the oscillation, reflecting that boundary effects are stronger for this hopping element. As a consequence, $\Delta\omega(k,N_{\max})$ alternates for $k = 0$, while it converges slowly for $k = \pi$.
Finally, it should be noted that the errors related to the truncation in $N_{\max}$ are significantly larger than the errors induced by the basis truncation in $d_{\max}$. Consequently, we drop the additional parameter $d_{\max}$ and guarantee that the truncation errors induced by the basis truncation are negligible compared to the errors induced by the finite cluster sizes. Yet, if extrapolations in $N_{\max}$ are applied, the influence of $d_{\max}$ may become more relevant. It is therefore advisable to investigate the convergence of the *final* result with respect to $d_{\max}$.
The considerations with respect to the convergence clearly indicate, that the description by means of the standard gCUT scheme does not fail due to the finite cluster sizes or the basis truncation. Since no effects for these parameter regimes are present in the thermodynamic limit, the break down of the approach is purely caused by artifacts of the finite-cluster approach. This issue is clearly unsatisfying and will be addressed next.

Pseudo decay

In the following, we want to describe the treatment of pseudo decay using gCUTs. Relying on the reduced-weight generator scheme, the results are fully cured from the artifacts stemming of the finite-cluster approach.
To test these results, a comparison to other methods is reasonable. To this end, we discuss two different values of λ, namely $\lambda = 2.0$ and $\lambda = 5.0$. For $\lambda = 2.0$, deepCUT [47] and CORE results [99] for the one-particle dispersion are available. For $\lambda = 5.0$, we compare our results of the one-triplon dispersion to DMRG results for the dynamic structure factor. The gCUT calculations are performed using $d_{\max} = 250$ with $\Delta_{\text{vicinity}} = 0.1$ ($\lambda = 2.0$) and $\Delta_{\text{vicinity}} = 0.2$ ($\lambda = 5.0$) respectively.
We begin by discussing the behavior of the characteristic quantities exemplarily for the quasi-

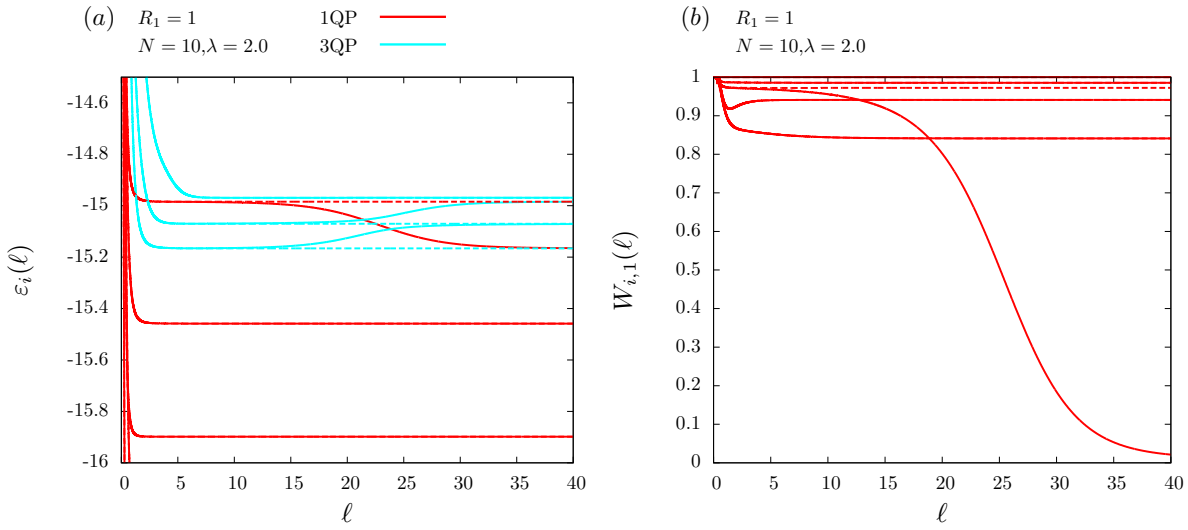

Figure 4.13: The characteristic quantities of the CUT are depicted for $N = 10$, $R_1 = 1$ and $\lambda = 2.0$. (a) The subblock energies $\varepsilon_i(\ell)$ of the one-particle (red) and two-particle (cyan) are shown in dependence of ℓ for the quasiparticle generator scheme (solid line) and the reduced-weight generator scheme (dashed line). (b) The reduced one-particle weights $W_{i,n}(\ell)$ are shown for the quasiparticle generator scheme (solid red line) and the reduced-weight generator scheme (dashed cyan line).

particle generator scheme and the reduced-weight generator scheme to give insights into the underlying physics. Subsequently, we discuss and compare the obtained one-triplon dispersion.

CUTs on finite clusters To demonstrate the difference between the deficient quasiparticle generator scheme Eq.(4.9) and the reduced-weight generator scheme (see 4.2.3) in the case of pseudo decay, we discuss the corresponding CUT on a finite cluster by means of the subblock energies $\varepsilon_i(\ell)$ and the reduced 1QP-weights $W_{i,1}(\ell)$. We choose a suited combination $N = 10$ and $R_1 = 1$ with $\lambda = 2.0$.
The results of the subblock energies $\varepsilon_i(\ell)$ are shown in figure 4.13(a). Up to intermediate values of ℓ, the qualitative behavior of the subblock energies is similar to the case $\lambda = 1.0$ and both generator schemes yield equivalent results and the subblock energies seemingly converge.
Yet, a fundamental difference is that the subblock energies are not sorted with respect to the number of QPs, i.e., $\varepsilon_i(\ell) > \varepsilon_j(\ell)$ with $q_i = 1$ and $q_j = 3$. The 1QP subspace overlaps energetically with the three-particle subspace and one observes pseudo decay. Consequently, the subblock energies are resorted by the quasiparticle generator at large ℓ-scales ($\ell_{\text{crit}} \sim 20$). In contrast, the reduced-weight generator scheme detects the pseudo decay and eliminates the respective element from the generator leading to a physically more reasonable development of the subblock energies.
The artificial nature of this overlap is supported by the behavior of the reduced 1QP-weights $W_{\nu,1}$ depicted for the one-particle basis states in figure 4.13(b). For small and intermediate values of ℓ, the reduced weights are large and close to one for both generator schemes. At $\ell \sim \ell_{\text{crit}}$, the reduced weight of the one-particle state involved in the resorting drops virtually to zero, indicating that states associated with different momenta are switched by the quasiparticle

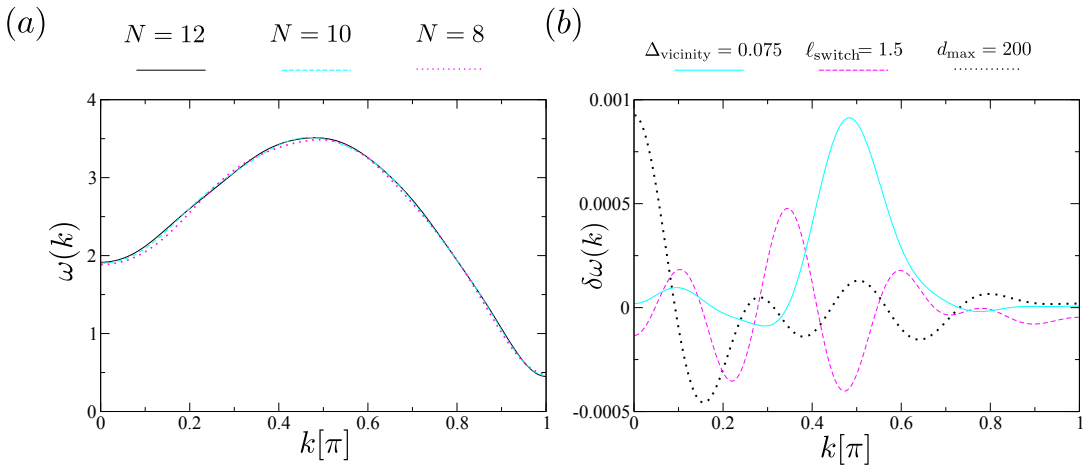

Figure 4.14: (a) Results obtained for the one-triplon dispersion $\omega(k)$ obtained for $\lambda = 2.0$ and different values of N: $N = 12$ (black solid line), $N = 10$ (cyan dashed line), $N = 8$ (magenta dotted line). (b) Deviations $\delta\omega(k)$ induced by setting $\Delta_{\text{vicinity}} = 0.075$ (cyan solid line), $\ell_{\text{switch}} = 1.5$ (magenta dashed line), $d_{\max} = 200$ (black dotted line)

generator scheme. By construction, the reduced-weight generator scheme fully prevents this artificial resorting leading to robust results in the thermodynamic limit.
We stress that the behavior of these characteristic quantities is qualitatively identical for all systems exhibiting pseudo decay. Consequently, the reduced-weight generator scheme provides a possibility to treat pseudo decay. Finally, to benchmark our approach, a comparison to other methods is performed next.

Comparison to other methods In the following, we want to discuss the resulting one-triplon dispersion for $\lambda = 2.0$, relying on the optimized version of gCUT. It should be recalled that this parameter regime is fully inaccessible using the general scheme relying on the quasiparticle generator. The one-triplon dispersion using the reduced-weight generator scheme is depicted for different values of $N_{\max}$ in figure 4.14(a). The qualitative form of the dispersion and the convergence with N indicate a robust scheme without artifacts stemming from the finite-cluster approach being noticeable. The gap of the dispersion is located at $k = \pi$ and, moreover, the dispersion exhibits a prominent maximum at $k \approx \frac{\pi}{2}$.
The results are obtained using the reduced-weight generator scheme with $\ell_{\text{switch}} = 1.0$, $\Delta_{\text{vicinity}} = 0.1$ and $d_{\max} = 250$. To estimate the uncertainty connected to the approach, one can vary each parameter and investigate the resulting deviations $\delta\omega(k)$, as depicted in figure 4.14(b). One finds $\delta\omega(k) \leq 10^{-3}$, which is considerably smaller than the uncertainty induced by the truncation in $N_{\max}$. Moreover, it is noticeable that the low-energy physics at $k \approx \pi$ is barely affected.
In the following, we want to compare the results of the one-triplon dispersion obtained via the modified gCUT scheme with results of the one-triplon dispersion available for deepCUT and CORE. The truncation parameter in gCUTs and CORE is given by the maximal cluster size N, the truncation parameter in deepCUT relates to the order in the perturbation parameter used to set up the differential equation system and is in the following also denoted by N.

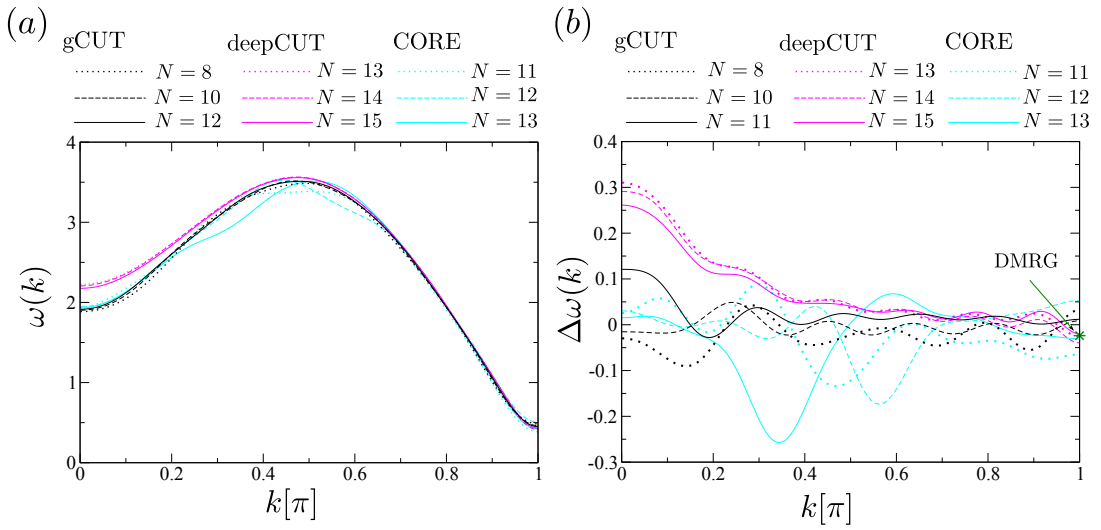

Figure 4.15: (a) The one-triplon dispersion $\omega(k)$ obtained via gCUT, deepCUT [47] and CORE [99] is shown for $\lambda = 2.0$ and different values of N. (b) The corresponding shifted one-triplon dispersion $\Delta\omega(k)$ is depicted to provide a better energetic resolution. The green symbol denotes the according value of DMRG [160].

All three methods yield, qualitatively, the same behavior of the dispersion, as shown in figure 4.15(a). To compare the results quantitatively, we define the difference

$$\Delta\omega(k) = \omega(k) - \omega_{\mathrm{gCUT,N=12}}(k), \tag{4.62}$$

where $\omega_{\mathrm{gCUT,N=12}}(k)$ denotes the result obtained via gCUT using $N = 12$ dimers. Note that $\omega_{\mathrm{gCUT,N=12}}(k)$ is not the exact result and that subtraction is only performed to increase the energetic resolution. In figure 4.15(b), $\Delta\omega(k)$ is shown for different methods and different values of the truncation parameter N. The (shifted) DMRG data at $k = \pi$ is provided by Nase [160]. For large values of k, the results of all three methods converge to similar results which are all in accordance with the DMRG data.[6]
For intermediate values of k, the gCUT and deepCUT results are similar and consistent with each other. In contrast, for these intermediate momenta, one observes bumps in the dispersion obtained via CORE. The form of the dispersions suggests that these deviations stem from artifacts of the finite-cluster approach in CORE. The CORE method relies on the exact eigenvectors of the finite clusters, i.e., the generalized cluster additivity is violated in Region II (see figure 4.4). This should not lead to a full break down of the approach, yet, one expects erratic but moderate deviations consistent with the obtained behavior. Nevertheless, it cannot be completely ruled out that the deviations are simply due to missing convergences of the applied diagonalization method.
For small values of k, CORE and gCUT yield converging results. In contrast, the dispersion obtained via deepCUT is significantly larger, yet, with increasing order, the results become closer to the results of gCUT and CORE. This behavior is consistent with the convergence of the truncation scheme. The physics at $k \approx 0$ is caused by strong interaction processes which is

[6] At $k = \pi$, one can perform a scaling in $\mathcal{N}$ for the gCUT, yielding results in full agreement with DMRG [70].

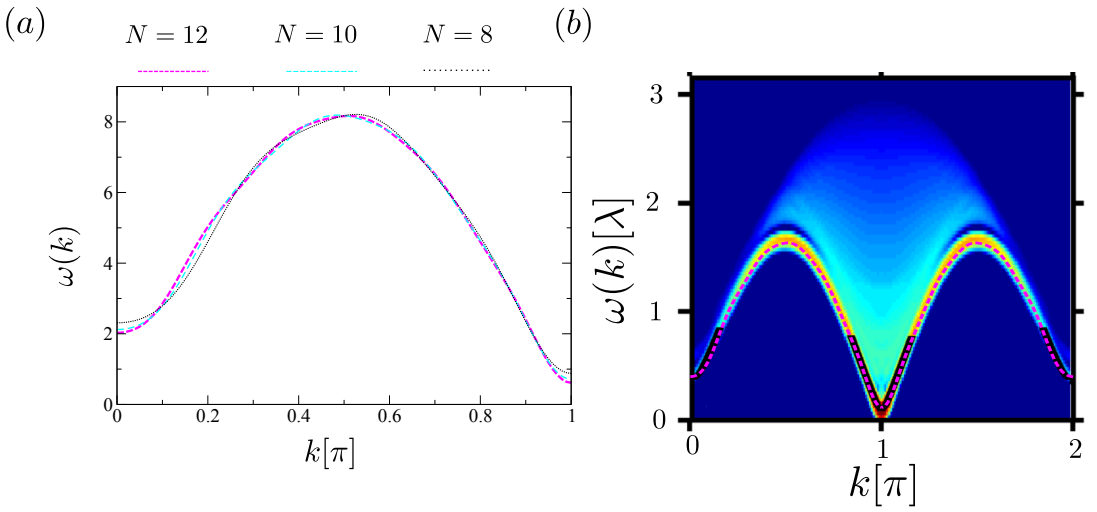

Figure 4.16: (a) The one-triplon dispersion $\omega(k)$ is depicted for $\lambda = 5.0$ and different values of N: $N = 12$ (black solid line), $N = 10$ (cyan dashed line), $N = 8$ (magenta dotted line). (b) The one-triplon dispersion $\omega(k)$ for $\lambda = 5.0$ ($N = 12$) is plotted on top of the corresponding dynamic structure factor obtained via DMRG [157].

difficult to capture adequately by a perturbative truncation. Unfortunately, no DMRG data for $\lambda = 2.0$ are available, but a comparison to DMRG data for $\lambda = 1.72$ and $\lambda = 5.0$ [157] suggests, that gCUT and CORE converge indeed to the correct value.
We note that the optimized gCUT scheme yields robust results for the whole momentum axis and no artifacts of the finite-cluster approach are observable on the relevant energy scales.

Finally, we investigate the results obtained via the optimized gCUT scheme for $\lambda = 5.0$. For this value in λ, DMRG data for the dynamic structure factor are available [157]. In figure 4.16(a), the results obtained via gCUTs for the one-particle dispersion are depicted for different values of $N_{\max}$. One observes a robust convergence with $N_{\max}$ even for this very large value of λ. The maximum at $k \approx \frac{\pi}{2}$ is very large ($\omega(k = \frac{\pi}{2}) \sim 8$). Interestingly, the gap at $k = \pi$ and the value at $k = 0$ are approximately constant, which is fully consistent with gapless spinon excitations spectrum for decoupled chains, as discussed in 4.4.2.
In figure 4.16(b), the one-triplon dispersion ($N_{\max} = 12$) is plotted with the corresponding DMRG data for the dynamic structure factor. Note that the DMRG results are plotted in units of λ because λ becomes the dominant energy scale, i.e., the results can also be interpreted as (weakly) coupled Heisenberg chains.
The one-triplon dispersion is located at the resonance of the dynamic structure factor obtained via DMRG, indicating agreement between both methods. This also implies that the quasiparticle interpretation in terms of triplons is valid for all momenta even in the weakly coupled chain limit. Our method therefore yields even in challenging regimes with very large values of the coupling constants correct results and the artifacts of the finite-cluster expansion are fully eliminated. Next, we investigate the most demanding case of quasiparticle condensation, where the triplon quasiparticle picture breaks down and a quantum phase transition occurs. For two-leg Heisenberg spin 1/2 ladders no such phase transition occurs for any value of λ, because a finite coupling between two Heisenberg spin 1/2 chains directly leads to a finite energy gap [136, 137]. In contrast, isolated Heisenberg chains are gapless. Indeed, one can study isolated

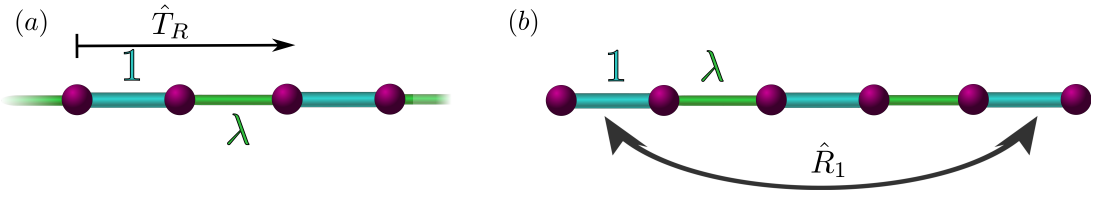

Figure 4.17: (a) Illustration of the considered model. The Hamiltonian is studied from the dimerized limit $\lambda = 0$. The system exhibits a translational symmetry $\hat{T}_\mathrm{R}$. (b) Illustration of a chain segment ($N = 3$). The reflection symmetry $\hat{R}_1$ is exploited during the CUT calculations.

Heisenberg chains starting from a limit of isolated dimers, i.e., the translational symmetry is broken on the level of the Hamiltonian. At the isotropic point, the translational symmetry is restored and the triplons condense inducing a quantum phase transition. Here, we focus specifically on the novel extrapolation technique introduced in 4.3.

4.4.2 Dimerized Heisenberg chain - quantum phase transition

To demonstrate the applicability of the extrapolation techniques, we study the (dimerized) Heisenberg spin 1/2 chain, which is depicted in figure 4.17(a). At the isotropic point $\lambda = 1.0$, the model is exactly solveable by Bethe Ansatz [162–164, 164]. Moreover, the corresponding excitation spectrum is exactly known [165] and is constituted by fractional spinon excitations carrying a spin 1/2 [166].
The ground state at finite dimerization $\lambda < 1$ is adiabatically connected to the product state of singlets on the dimers. For $\lambda \to 1$, one observes a quantum phase transition between the valence bond solid and the gapless Heisenberg chain. Here, the triplon quasiparticle picture breaks down and the spinon description is appropriate [167]. The one-triplon exciations closes with a critical exponent $\nu z = 2/3$ [168, 169].
The regime $\lambda < 1$ is accessible via an effective description in terms of triplons [10, 39, 170]. Interestingly, a spectral weight analysis using high-order series expansion shows that the one-triplon weight vanishes at criticality while almost all of the weight is shifted to the two-triplon channel [10, 171]. This indicates that a discription in terms of triplons is still valid even at criticality.
Finally, it should be noted that a large number of compounds is succesfully described by (frustated) Heisenberg chains at finite [172–175] and without dimerization [176–178].

The Model

The Hamiltonian is given by

$$\mathcal{H} = \underbrace{\sum_{\langle i,j\rangle} S_i S_j}_{\mathcal{H}_0} + \lambda \underbrace{\sum_{\langle i,j\rangle'} S_i S_j}_{\mathcal{V}} , \tag{4.63}$$

	$4\tau_0$	
$\lvert t^{0,\pm1},s\rangle$	$\leftrightarrow$	$-\lvert s,t^{0,\pm1}\rangle$
$\lvert t^{0},t^{\pm1}\rangle$	$\leftrightarrow$	$\lvert t^{\pm1},t^{0}\rangle$
$\lvert t^{\pm1},t^{\pm1}\rangle$	$\leftrightarrow$	$\lvert t^{\pm1},t^{\pm1}\rangle$
$\lvert t^{\pm1},t^{\mp1}\rangle$	$\leftrightarrow$	$\lvert t^{0},t^{0}\rangle - \lvert t^{\pm1},t^{\mp1}\rangle$
$\lvert t^{0},t^{0}\rangle$	$\leftrightarrow$	$\lvert t^{1},t^{-1}\rangle + \lvert t^{-1},t^{1}\rangle$
	$4\tau_1$	
$\lvert s,t^{1}\rangle,\lvert t^{1},s\rangle$	$\rightarrow$	$\lvert t^{1},t^{0}\rangle - \lvert t^{0},t^{1}\rangle$
$\lvert s,t^{0}\rangle,\lvert t^{0},s\rangle$	$\rightarrow$	$\lvert t^{1},t^{-1}\rangle - \lvert t^{-1},t^{1}\rangle$
$\lvert s,t^{-1}\rangle,\lvert t^{-1},s\rangle$	$\rightarrow$	$\lvert t^{0},t^{-1}\rangle - \lvert t^{-1},t^{0}\rangle$
	$4\tau_2$	
$\lvert s,s\rangle$	$\rightarrow$	$\lvert t^{1},t^{-1}\rangle - \lvert t^{0},t^{0}\rangle + \lvert t^{-1},t^{1}\rangle$

Table 4.2: Dimerized chain: Representation of the local operators τ_n, which act on the links of the super lattice, in the considered triplet basis.

where the first (second) sum represents the intra-dimer (inter-dimer) couplings. The different couplings are illustrated in figure 4.17(a). In contrast to the two-leg ladder, there is no reflection symmetry separating the system into channels of even- and odd-triplet number. Consequently, the Hamiltonian takes the form

$$\mathcal{H} = \tfrac{3}{4}N + \mathcal{H}_0 + \lambda\left(T_{-2} + T_{-1} + T_0 + T_1 + T_2\right), \tag{4.64}$$

where N denotes the number of dimers, $\mathcal{H}_0$ counts the number of triplets and T_m (T_{-m}) creates (annihilates) in total m triplets on neighboring dimers. The local matrix elements are shown in table 4.2.
The objective is to derive an effective low-energy Hamiltonian of the form

$$\mathcal{H}_{\text{eff}} \quad = \quad \tilde{E}_0(\lambda) + \sum_{i,\delta,\alpha} \tilde{a}_\delta(\lambda)\, \hat{\tilde{t}}^\dagger_{i+\delta,\alpha} \hat{\tilde{t}}_{i,\alpha} + \text{h.c.} \tag{4.65}$$

where $\hat{\tilde{t}}^\dagger_{i,\alpha}$ ($\hat{\tilde{t}}_{i,\alpha}$) creates (annihilates) a triplon with magnetization α on dimer i. Due to the $SU(2)$ invariance, the hopping elements $a_\delta(\lambda)$ are independent of the triplon flavor α. Again, a Fourier transformation yields the one-triplon dispersion $\omega(k)$. Here, we are specifically interested in the one-triplon gap Δ at the critical point $\lambda = 1$.
The gCUT is carried out using chain segments of dimers as depicted exemplarily in figure 4.17(b). The calculation is performed up to $N_{\max} = 12$ dimers.
The reflection symmetry $\hat{R}_1$ divides the calculation on each cluster into a symmetric and an anti-symmetric channel. The implementation of this reflection symmetry is straightforward in the spin-S_z basis. However, in the dimer basis, additional signs occur since each singlet is anti-symmetric under this reflection symmetry. As a result, the phase alternates for the n-QP channels in the dimer basis, which must be regarded in the implementation.

Results

In the following, we investigate the one-dispersion $\omega(k)$ at the critical point $\lambda = 1$ obtained via gCUTs up to clusters with $N = 12$ dimers and compare it to the exactly known spinon

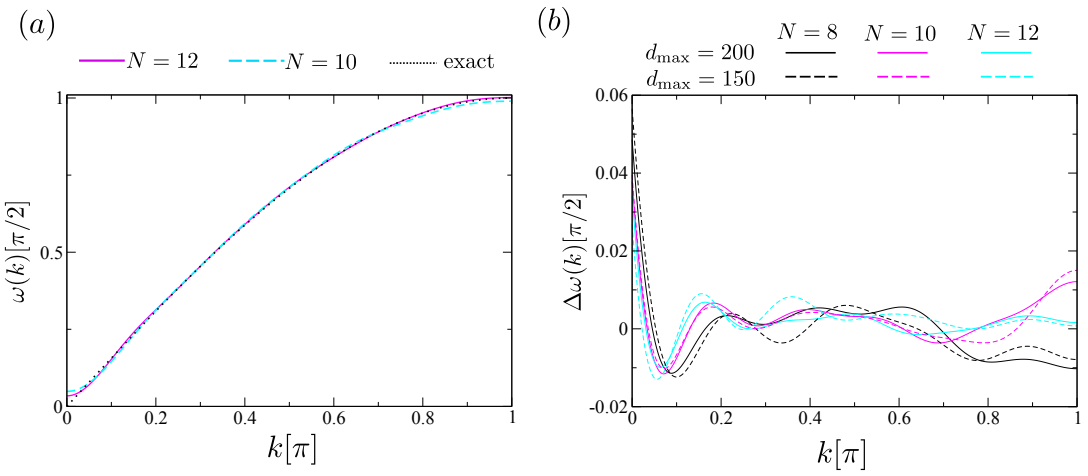

Figure 4.18: (a) The one-triplon dispersion $\omega(k)$ obtained via gCUT using clusters up to N dimers is shown with the exact spinen dispersion. (b) The difference $\Delta\omega(k)$ (see Eq.(4.67)) is plotted for various values of N and different basis truncations $d_{\max}$.

dispersion. Afterwards, we investigate the corrresponding one-triplon gap Δ derived via gCUTs, to determine the critical exponent νz, providing a proof of principle for the novel extrapolation technique introduced in section 4.3. In addition to that, the scheme is applied to analyze deepCUT data for Δ up to perturbative order $n = 12$, kindly provided by Mohsen Hafez and Götz Uhrig.[7]

One-triplon dispersion The gCUT is performed at the critical point $\lambda = 1.0$, making a proper description of the system very challenging. On a single cluster, a lot of states merge with the low-energy spectrum and distinction between genuine and defective interactions becomes difficult.
We choose $\Delta_{\text{vicinity}} = 0.2$ and additionally implement Eq.(4.28) with $\Delta_{\text{skalar}} = 0.5$. While the latter clearly stabilizes the calculation, one still observes a noticeable uncertainty. This can be illustrated by investigating different basis truncations $d_{\max}$.[8]
For $\lambda = 1.0$, the exact one-spinon dispersion [165] is given by

$$\omega_{\text{spinon}}(k) = \tfrac{\pi}{2}\sin(2k). \tag{4.66}$$

Here, k denotes the momentum with respect to the dimerized chain. Consquently, it is scaled by a factor two to account for the doubled unit cell size in the dimerized case. It should be noted, that spinons can only be created in pairs. Consequently, the triplon corresponds to the lower band edge, also given by Eq.(4.66). The resulting one-triplon dispersion $\omega(k)$ is plotted for $N = 10$ and $N = 12$ together with the exact spinon dispersion in figure 4.66(a). One finds good agreement between both dispersions. To increase the energetic resolution, we define the difference

$$\Delta\omega(k) = \omega(k) - \omega_{\text{spinon}}(k) \quad , \tag{4.67}$$

[7] It should be noted that orders $n > 12$ are in principle accessible by implementing symmetries.
[8] With increasing values of $d_{\max}$, the number of states merging with the low-energy spectrum becomes even larger, aggravating the problem of a distinction.

which is shown for different values of N and different basis truncations $d_{\max}$. The influence induced by the uncertainty of the elimination process is observable. Nevertheless, for $N = 12$, the obtained one-triplon dispersion is very close to the spinon dispersion for $k \gtrsim 0.3\pi$. However, for smaller values of k and specifically close to zero momentum, the approximation becomes poor. This is expected, since the correlation length diverges at $\lambda = 1$, leading to a gapless excitation spectrum. Consequently, one must rely on additional extrapolation techniques which help to extract the critical behavior, as we discuss in the following.

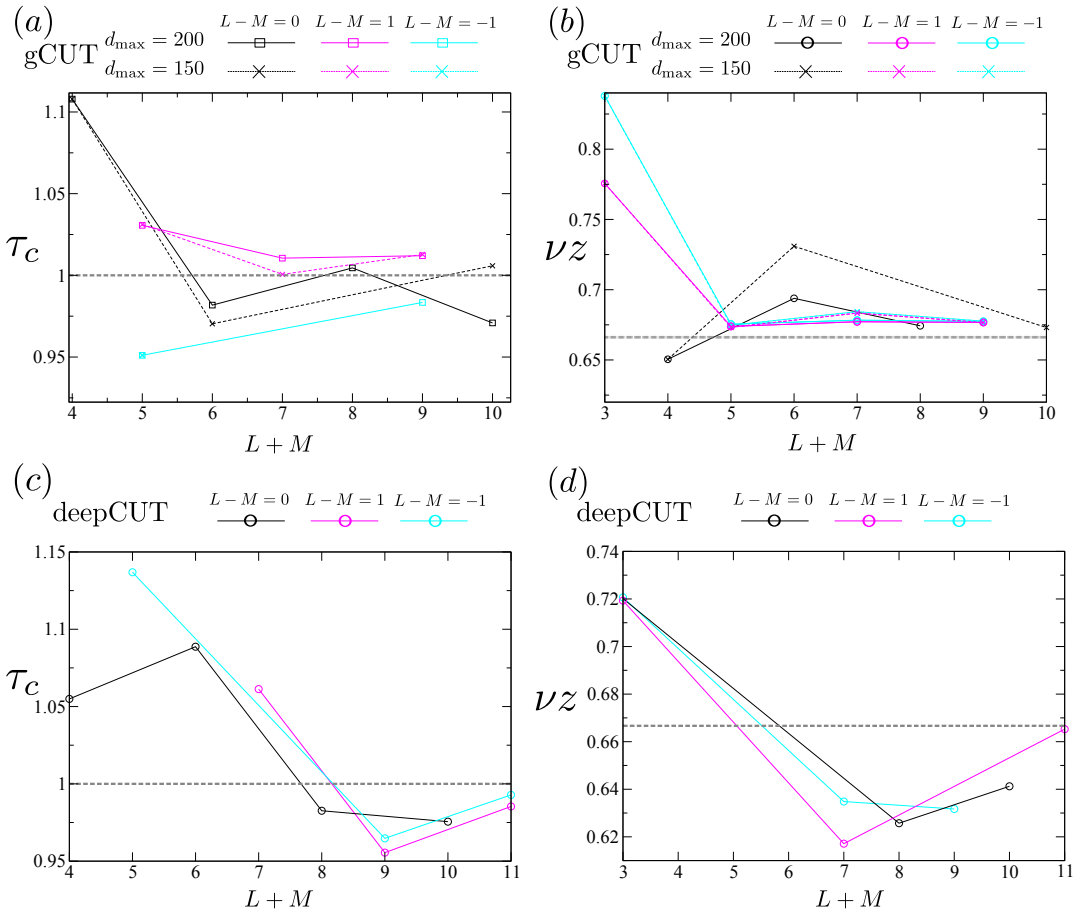

Figure 4.19: (a) Critical points τ_c of $\Delta_{\lambda=1.0}(\tau)$ obtained via Dlog Padè extrapolations of the gCUT results. (b) Critical exponents νz of $\Delta_{\lambda=1.0}(\tau)$ obtained via biased Dlog Padè extrapolations of the gCUT results. The dashed grey line represents the analytical result. (c) Critical points τ_c of $\Delta_{\lambda=1.0}(\tau)$ obtained via Dlog Padè extrapolations of the deepCUT results. (d) Critical exponents νz of $\Delta_{\lambda=1.0}(\tau)$ obtained via biased Dlog Padè extrapolations of the deepCUT results. The dashed grey line represents the analytical result.

One-triplon gap To perform an extrapolation of the one-triplon gap, we formulate the gap as an expansion in τ (see Eq.(4.52)). The aim is to extrapolate the resulting series $\Delta_\lambda(\tau)$ to infinite order. We argue that the series should vanish like $\Delta_\lambda \propto (\tau_c - \tau)^{\nu z}$, making Dlog Padè

extrapolations the method of choice.
The resulting critical values τ_c obtained via Dlog Padè extrapolations of $\Delta_\lambda(\tau)$ ($\lambda = 1$) are shown for gCUT in figure 4.19(a) and for deepCUT in figure 4.19(c). Defective extrapolants are omitted and we consider only the three families with $|L - M| \leq 1$. Since the calculation is performed at the critical point, one expects $\tau_c \approx 1.0$. Indeed, this is consistent with the convergence of the obtained critical values.
Next, we consider the extraction of critical exponents. To this end, we implement Eq.(4.49) with $\tau_c = 1$. The resulting critical exponents are depicted in figure 4.19(b) for gCUTs and in figure 4.19(d) for deepCUT. Indeed, the results are consistent with the critical exponent of the system and one reaches the actual value by two percent (gCUT) and five percent (deepCUT), which is for a sophisticated quantity like the critical exponent fairly accurate.
In gCUTs, the critical value is approached with increasing order from above, which corresponds to the typical behavior obtained in high-order series expansions. This is the opposite for deepCUT data and it would be interesting to investigate this behavior for other systems.

Following the investigation of quasiparticle condensation, we consider a very different scenario in the next section. We focus on a situation where the quasiparticle is not stable for all momenta and the challenge of finding an adequate effective low-energy model is tackled relying on the spectral weight generator.

4.4.3 Four-leg Heisenberg ladder - genuine decay

In this section we demonstrate the treatment of quasiparticle decay via gCUTs. In particular, we investigate four-leg spin-1/2 Heisenberg tubes from a dimerized limit with an additional asymmetry parameter, allowing to tune between fully periodic tubes and open four-leg Heisenberg ladders (see figure 4.20(a)). The system exhibits both, strong interaction effects and quasiparticle decay. The strength of the quasiparticle decay is controlled by the asymmetry parameter ζ. Therefore, the system is perfectly suited to examine the properties of the modified gCUT scheme. In contrast to the preceding discussions, the objective is to determine the low-energy part of the dynamic structure factor. This is done by the spectral weight generator and a subsequent diagonalization of the coupled one- and two-triplon sector.
The investigation of n-leg ladders ($n > 2$) is generically interesting, since it allows to study the transition from one-dimensional to two-dimensional systems. Fascinatingly, one finds surprises on the way [179] since even-leg and odd-leg spin 1/2 ladders behave fundamentally different: Even-leg spin 1/2 ladders are gapped while odd-leg spin 1/2 ladders are not [180, 181]. For odd-leg ladders, this relates to the Lieb-Schultz-Mattis theorem [182–184] while the gap of even-leg ladders can be interpreted in support of Haldanes conjecture [185].
It should be noted that the systems considered in this chapter can be interpreted in this context: spin 1/2 Heisenberg chains are gapless (see 4.4.2) and two-leg spin ladders exhibit a finite spin gap (see 4.4.1). The two-leg ladder exhibits a reflection symmetry with respect to the centers of the dimers, resulting in a parity conservation of the triplons. The four-leg ladder exhibits such a reflection symmetry with respect to the centers of the dimers only for $\zeta = 0$. For $\zeta \neq 0$, this symmetry is absent. Overall, the four-leg spin ladder is significantly closer to the two-dimensional system than the two-leg Heisenberg ladder.
We focus the discussion on four-leg ladders, which is motivated by the compound $La_2Cu_2O_5$ [186–188]. The system is considered to be a potential realization of isolated (open) four-leg spin ladders [189]. Structurally, the system is related to two-leg Heisenberg ladders ($La_xCa_{14-x}Cu_{24}O_{41}$, $x \in$ 4,5,5.2 and 6 [149, 151]) as well as to the undoped high-temperature super conductors La_2CuO_4, which is well described by the Heisenberg model on the square lattice [190]. Therefore, this system is a perfect platform to investigate the dimensional crossover from one to two

dimensions experimentally.
The ground state of the Heisenberg four-leg ladder can be understood as a short-range resonant valence bond [181, 191]. The ground state is adiabatically connected to the product state of singlets on the dimers (see figure 4.20(a) for $\lambda = 0$) and in this sense, the term valence bond solid also seems appropriate.
Numerous calculations were performed to estimate the spin gap Δ for isotropic couplings ($\lambda = 1$, $\zeta = 0$) from extrapolations of finite-cluster calculations to the infinite system. Exact diagonalization calculations on periodic systems up to $\mathcal{L} = 4$ rungs yield the estimate $\Delta \approx 0.245$ [192] while calculations up to $\mathcal{L} = 6$ rungs yields $\Delta \approx 0.27$ [193]). In contrast, density-matrix renormalization group calculations [181] determined the excitation gap to be $\Delta \approx 0.19$ with a ground-state correlation length $\xi \approx 4 - 6$ ($\mathcal{L} \approx 24$, open). Most recently, Ramos et al. determined the excitation gap via density-matrix renormalization group as $\Delta \approx 0.15$ [194] ($\mathcal{L} = 40$, open). In addition to that, we performed exact-diagonalization calculations up to clusters of length $\mathcal{L} = 8$ (periodic), which yields an estimate for the spin gap $\Delta \approx 0.16$. While these calculations give a good estimation of the spin gap, little is known of the spectral properties of open four-leg ladders like the dispersion of the elementary excitation, bound states or the dynamic structure factor $S(k,\omega)$.
For the sake of completeness, it should be noted that inelastic neutron scattering on the compound $Cu_2Cl_4 \cdot D_8C_4SO_2$ [195] induced rather recent investigations of fully frustrated four-leg tubes [196–198].
Here, we focus on *un*frustrated four-leg ladders. While most of the research focuses on ground state properties and the excitation gap, we aim at the dynamic structure factor in terms of triplon excitations. Our non-perturbative approach is not restricted to small values of λ, yet, a complete quasiparticle description in terms of triplons is challenging, since one observes quasiparticle decay for certain momenta. This issue is addressed and solved by the modified gCUT scheme.
We begin this section by introducing the model and the basics of the approach. Afterwards, the CUTs on finite clusters are discussed exemplarily for the quasiparticle and the new spectral weight generator scheme. Following this, the resulting spectral properties are reviewed and interpreted.

The model

We want to investigate four-leg Heisenberg tubes starting from the dimerized limit. The corresponding Hamiltonian is given by

$$\mathcal{H} = \sum_{\langle i,j \rangle} \boldsymbol{S}_i \boldsymbol{S}_j + \lambda \sum_{\langle i,j \rangle'} \boldsymbol{S}_i \boldsymbol{S}_j + \lambda(1-\zeta) \sum_{\langle i,j \rangle''} \boldsymbol{S}_i \boldsymbol{S}_j \quad . \tag{4.68}$$

The different couplings are illustrated in figure 4.20(a). The first sum runs over the dimers of the model, constituting the quasiparticle picture in terms of triplons and the second sum introduces the inter-dimer couplings of an open four-leg ladder. Consequently, the additional third sum runs over the periodic links closing the four-leg tubes, i.e., the parameter ζ allows to tune between periodic ($\zeta = 0$) and open ($\zeta = 1$) boundary conditions.
The system displays a reflection symmetry $\hat{R}_2$, dividing the system into a symmetric and an anti-symmetric channel. In the case $\zeta = 0$, the system exhibits an additional reflection symmetry $\hat{R}_\mathrm{p}$ with respect to the center of the dimers.[9] This reflection symmetry divides the

[9] The 180°-rotational symmetry associated with the periodic boundary conditions is given by the product of both reflection symmetries, which thus provides no additional information.

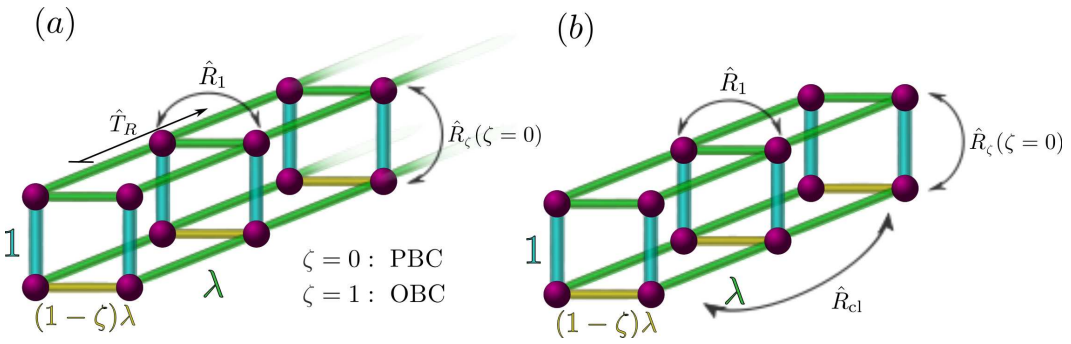

Figure 4.20: (a) Illustration of the considered model. The Hamiltonian is studied from the dimerized limit $\lambda = 0$. Besides the translational symmetry $\hat{T}_R$, the system exhibits a reflection $\hat{R}_1$. The parameter ζ allows to tune between periodic boundary conditions ($\zeta = 0$) and open boundary conditions ($\zeta = 1$). For $\zeta = 0$, another reflection symmetry $\hat{R}_\zeta$ is present. (b) Example of a cluster with $\mathcal{L} = 3$ super rungs. The clusters considered in the expansion exhibit two reflection symmetries $\hat{R}_{\mathrm{cl}}$ and $\hat{R}_1$ exploited in the calculation.

system into channels of even and odd number of triplets similar to the two-leg ladder. To be precise, the Hamiltonian Eq.(4.68) takes the form

$$\begin{aligned}\mathcal{H} = \tfrac{3}{4}N + \mathcal{H}_0 + \lambda\left(T^{\mathrm{leg}}_{-2} + T^{\mathrm{leg}}_{0} + T^{\mathrm{leg}}_{2}\right) + \lambda(1+\zeta)\left(T^{\mathrm{rung}}_{-2} + T^{\mathrm{rung}}_{0} + T^{\mathrm{rung}}_{2}\right) \\ + \lambda\zeta\left(T^{\mathrm{rung}}_{-1} + T^{\mathrm{rung}}_{1}\right) \quad ,\end{aligned} \tag{4.69}$$

where N denotes the number of dimers, $\mathcal{H}_0$ counts the number of triplets and $T^{\mathrm{leg/rung}}_n$ ($T^{\mathrm{leg/rung}}_{-n}$) creates (annihilates) n triplets by acting on the rungs/legs of the four-leg tube. Heisenberg links which couple identical dimers aggregate to a single link in the super lattice. While the super lattice of the two-leg ladder is given by a chain of dimers, the effective lattice of the four-leg tube is given by a two-leg ladder of these supersites (dimers).
The operators are again decomposed via

$$T^{\mathrm{leg/rung}}_n = \sum_l \tau^{\mathrm{leg/rung}}_{n,l} \tag{4.70}$$

into operators acting on the leg-links/rung-links l of the effective lattice. The Hamiltonian in terms of triplets is defined by the action of these operators on a single link in the triplet-basis (see table 4.3).
To respect as many symmetries of the model in the thermodynamic limit as possible, we perform the cluster expansion using super rungs, i.e., the two dimers of the unit cell build the elementary piece of the expansion. Therefore, the considered clusters can be viewed as chains in these super rungs. Such a cluster is exemplified for $N = 6$ dimers, i.e., $\mathcal{L} = 3$ superrungs, in figure 4.20(b). While the translational symmetry is broken, the reflection symmetries $\hat{R}_1$ and $\hat{R}_2$ devide the calculation on each cluster into four different symmetry sectors. Similar to the two-leg ladder, a strong even-odd effect is present and it is reasonable to reduce this effect again by averaging the obtained effective model for $\mathcal{L}$ and $\mathcal{L} - 1$.
A fundamental difference to the two-leg ladder is the asymmetry ζ, which induces processes between the odd-triplet and even-triplet channels. The Hamiltonian corresponds to the form

	$4\tau_0^{\text{rung}}$	
$\lvert t^{0,\pm1},s\rangle$	$\leftrightarrow$	$\lvert s,t^{0,\pm1}\rangle$
$\lvert t^{0},t^{\pm1}\rangle$	$\leftrightarrow$	$\lvert t^{\pm1},t^{0}\rangle$
$\lvert t^{\pm1},t^{\pm1}\rangle$	$\leftrightarrow$	$\lvert t^{\pm1},t^{\pm1}\rangle$
$\lvert t^{\pm1},t^{\mp1}\rangle$	$\leftrightarrow$	$\lvert t^{0},t^{0}\rangle - \lvert t^{\pm1},t^{\mp1}\rangle$
$\lvert t^{0},t^{0}\rangle$	$\leftrightarrow$	$\lvert t^{1},t^{-1}\rangle + \lvert t^{-1},t^{1}\rangle$
	$4\tau_1^{\text{rung}}$	
$\lvert s,t^{1}\rangle$,-$\lvert t^{1},s\rangle$	$\rightarrow$	$\lvert t^{1},t^{0}\rangle - \lvert t^{0},t^{1}\rangle$
$\lvert s,t^{0}\rangle$,-$\lvert t^{0},s\rangle$	$\rightarrow$	$\lvert t^{1},t^{-1}\rangle - \lvert t^{-1},t^{1}\rangle$
$\lvert s,t^{-1}\rangle$,-$\lvert t^{-1},s\rangle$	$\rightarrow$	$\lvert t^{0},t^{-1}\rangle - \lvert t^{-1},t^{0}\rangle$
	$4\tau_2^{\text{rung}}$	
$\lvert s,s\rangle$	$\rightarrow$	$\lvert t^{1},t^{-1}\rangle - \lvert t^{0},t^{0}\rangle + \lvert t^{-1},t^{1}\rangle$
	$2\tau_0^{\text{leg}}$	
$\lvert t^{0,\pm1},s\rangle$	$\leftrightarrow$	$\lvert s,t^{0,\pm1}\rangle$
$\lvert t^{0},t^{\pm1}\rangle$	$\leftrightarrow$	$\lvert t^{\pm1},t^{0}\rangle$
$\lvert t^{\pm1},t^{\pm1}\rangle$	$\leftrightarrow$	$\lvert t^{\pm1},t^{\pm1}\rangle$
$\lvert t^{\pm1},t^{\mp1}\rangle$	$\leftrightarrow$	$\lvert t^{0},t^{0}\rangle - \lvert t^{\pm1},t^{\mp1}\rangle$
$\lvert t^{0},t^{0}\rangle$	$\leftrightarrow$	$\lvert t^{1},t^{-1}\rangle + \lvert t^{-1},t^{1}\rangle$
	$2\tau_2^{\text{leg}}$	
$\lvert s,s\rangle$	$\rightarrow$	$-\lvert t^{1},t^{-1}\rangle + \lvert t^{0},t^{0}\rangle - \lvert t^{-1},t^{1}\rangle$

Table 4.3: Four-leg ladder: Representation of the local operators τ_n^{rung} (τ_n^{leg}), which act on the rungs (legs) of the super lattice in the considered triplet basis.

Eq.(2.19), indicating that one may observe quasiparticle decay and the strength of the decay can be varied with ζ.
The term Eq.(4.69) induces an interaction between the one- and two-triplon channels already in first order in λ. However, it should be noted that the resulting two-triplet state is anti-symmetric with respect to $\hat{R}_2$. Consequently, this process only occurs in first order in the anti-symmetric channel while it is absent in the symmetric channel for the *initial* Hamiltonian. Nevertheless, these terms are generated during the CUT. Accordingly, the resulting interaction between the one- and two-triplon states is expected to be considerably weaker in the symmetric channel compared to the anti-symmetric one.
The objective is to implement a modified gCUT scheme to derive an effective description in terms of triplons which allows to describe quasiparticle decay. The approach is defined by the spectral weight generator, relying on the spectral weight of an appropriate observable as guidance for the transformation. Of course, it is always possible to simply define an observable which consists of the suited creation operators and annihilation operators. However, here a natural candidate is given by the observables

$$\mathcal{O}^{\gamma}_{1,\text{left}}(k) = \frac{1}{\sqrt{\mathcal{N}}} \sum_{j\in \text{ left dimers}} \exp(\mathrm{I}kr_j) S^{\gamma}_{j,1} \tag{4.71}$$

$$\mathcal{O}^{\gamma}_{2,\text{right}}(k) = \frac{1}{\sqrt{\mathcal{N}}} \sum_{j\in \text{ right dimers}} \exp(\mathrm{I}kr_j) S^{\gamma}_{j,2} \tag{4.72}$$

$$\mathcal{O}^{\gamma}_{1,\text{left}}(k) = \frac{1}{\sqrt{\mathcal{N}}} \sum_{j\in \text{ left dimers}} \exp(\mathrm{I}kr_j) S^{\gamma}_{j,1} \tag{4.73}$$

$$\mathcal{O}^{\gamma}_{2,\text{right}}(k) = \frac{1}{\sqrt{\mathcal{N}}} \sum_{j\in \text{ right dimers}} \exp(\mathrm{I}kr_j) S^{\gamma}_{j,2} \quad , \tag{4.74}$$

where the sum runs over the left (right) dimers of the system and $\mathcal{N}$ denotes the number of unit cells. The parameter k represents the momentum of the observable in ladder direction and, correspondingly, r_j denotes the coordinate of dimer j in ladder direction. Here, $S^{\gamma}_{j,1}$ ($S^{\gamma}_{j,2}$) with $\gamma \in x,y,z$ acts on the upper (lower) spin of dimer j. The choice of this observable guiding the transformation is motivated by the corresponding dynamic structure factor relevant for neutron scattering experiments.
Due to the $SU(2)$ invariance of the system, we can choose $\gamma = z$. This choice is advisable, since the action of the observable flips the eigenvalue of the spin-flip symmetry $S_z \to -S_z$ while the magnetization is unchanged. This allows the exploitation of both symmetries during the calculation.
The local observables are expressed in terms of triplets by

$$S^z_{j,1} = \tfrac{1}{2}\left(\hat{t}^{\dagger}_{j,0} + \hat{t}_{j,0} + \hat{t}^{\dagger}_{j,1}\hat{t}_{j,1} - \hat{t}^{\dagger}_{j,-1}\hat{t}_{j,-1}\right) \tag{4.75}$$

$$S^z_{j,2} = \tfrac{1}{2}\left(-\hat{t}^{\dagger}_{j,0} - \hat{t}_{j,0} + \hat{t}^{\dagger}_{j,1}\hat{t}_{j,1} - \hat{t}^{\dagger}_{j,-1}\hat{t}_{j,-1}\right), \tag{4.76}$$

where $\hat{t}^{\dagger}_{i,\alpha}$ ($\hat{t}_{i,\alpha}$) creates (annihilates) a triplet of magnetization $S^z = \alpha$ on site j. To satisfy Eq.(4.29) and Eq.(4.30), the observables are (anti-)symmetrized with respect to $\hat{R}_{\zeta}$

$$\mathcal{O}_{\pm,\text{left}}(k) := \tfrac{1}{\sqrt{2}}\left(\mathcal{O}^z_{1,\text{left}}(k) \pm \mathcal{O}^z_{2,\text{left}}(k)\right) \tag{4.77}$$

$$\mathcal{O}_{\pm,\text{right}}(k) := \tfrac{1}{\sqrt{2}}\left(\mathcal{O}^z_{1,\text{right}}(k) \pm \mathcal{O}^z_{2,\text{right}}(k)\right). \tag{4.78}$$

Finally, it is reasonable to (anti-)symmetrize the observables also with respect to $\hat{R}_2$, which allows to investigate the response of each symmetry channel independently:

$$\mathcal{O}_{\pm,+}(k) = \tfrac{1}{\sqrt{2}}\left(\mathcal{O}_{\pm,\text{left}}(k) + \mathcal{O}_{\pm,\text{right}}(k)\right) \tag{4.79}$$

$$\mathcal{O}_{\pm,-}(k) = \tfrac{1}{\sqrt{2}}\left(\mathcal{O}_{\pm,\text{left}}(k) - \mathcal{O}_{\pm,\text{right}}(k)\right). \tag{4.80}$$

Using the modified gCUT scheme, an effective description in terms of triplons is derived for the Hamiltonian and the observables in order to determine the effective spectral density Eq.(2.16) for the coupled one- and two-triplon sector. The resulting effective Hamiltonian takes the form

$$\mathcal{H}_{\text{eff}} = \tilde{E}_0(\lambda,\zeta) + \sum_{i,\delta,\alpha} \tilde{a}_{i,j}(\lambda,\zeta)\, \hat{\tilde{t}}^{\dagger}_{i,\alpha}\hat{\tilde{t}}_{j,\alpha} + \text{h.c.} \tag{4.81}$$

$$+ \sum_{S\in\{0\ldots2\}} \sum_{\alpha\in\{-S\ldots S\}} \sum_{i,j,m,n} b^{S}_{i,j,m}(\lambda,\zeta)\mathfrak{T}^{S,\alpha\dagger}_{i,j}\mathfrak{T}^{S,\alpha}_{n,m} \tag{4.82}$$

$$+ \sum_{\alpha\in\{-1\ldots1\}} \sum_{i,m,n} c_{i,j,m}(\lambda,\zeta)\mathfrak{T}^{S,\alpha\dagger}_{i,j}\hat{\tilde{t}}_{m,\alpha} + \text{h.c.} \quad , \tag{4.83}$$

where $\hat{\tilde{t}}^{\dagger}_{i,\alpha}$ ($\hat{\tilde{t}}_{i,\alpha}$) creates (annihilates) a triplon of magnetization α on site i and the operator $\mathfrak{T}^{S,\alpha\dagger}_{i,j}$ ($\mathfrak{T}^{S,\alpha}_{i,j}$) creates (annihilates) two triplons on sites i and j with total spin S and magnetization

$S^z_{\text{tot}} = \alpha$. We restrict the considerations to $S = 1$ with $\alpha = 0$, which is sufficient to determine the dynamic structure factor. In this case, one has

$$\mathfrak{T}^{1,0^\dagger}_{i,j} = \frac{1}{\sqrt{2}}\left(\hat{\tilde{t}}^\dagger_{i,1}\hat{\tilde{t}}^\dagger_{j,-1} - \hat{\tilde{t}}^\dagger_{i,-1}\hat{\tilde{t}}^\dagger_{j,1}\right) \quad . \tag{4.84}$$

In the effective Hamiltonian, the first term (4.81) describes the one-triplon dynamics, the second term (4.82) denotes the two-triplon irreducible operator (two-triplon interaction) and (4.83) is a one-triplon irreducible operator inducing interactions between adjacent quasiparticle channels ($n \geq 1$). We consider specifically the interactions between the one- and the two-triplon channel, which moderate the quasiparticle decay of the one-triplon mode. Higher triplon interactions are neglected in the effective description.
To determine the dynamic structure factor at zero temperature, one must determine all operators of $\mathcal{O}_{\text{eff}}$ creating particles out of the vacuum. The effective observable takes the form

$$\mathcal{O}_{\text{eff},\circ,\bullet}(k) = \frac{1}{\sqrt{\mathcal{N}}}\sum_i \tilde{p}_i(\lambda,\zeta,k,\circ,\bullet)\hat{\tilde{t}}^\dagger_{i,0} + \text{h.c.} \tag{4.85}$$

$$+ \frac{1}{\sqrt{\mathcal{N}}}\sum_{i,j} \tilde{q}_{i,j}(\lambda,\zeta,k,\circ,\bullet)\mathfrak{T}^{1,0^\dagger}_{i,j} + \text{h.c.} \tag{4.86}$$

with $\circ = \pm$ and $\bullet = \pm$. All operators creating more than two triplons are neglected.
The observable $\mathcal{O}_{\text{eff},\circ,+}$ is symmetric with respect to the reflection symmetry $\hat{R}_2$, while $\mathcal{O}_{\text{eff},\circ,-}$ is anti-symmetric. Therefore, the action of $\mathcal{O}_{\text{eff},\circ,+}$ does not change the eigenvalues of $\hat{R}_2$ while $\mathcal{O}_{\text{eff},\circ,-}$ flips the eigenvalue of $\hat{R}_2$.
While the reflection symmetry $\hat{R}_\zeta$ is broken by ζ, one still expects $\mathcal{O}_{\text{eff},-,\bullet}|0\rangle$ to contribute mainly to the one-triplon sector while $\mathcal{O}_{\text{eff},+,\bullet}|0\rangle$ contributes mainly to the two-triplon sector. To determine the effective spectral density $I_{\text{eff}}(k,\omega)$ (see Eq.(2.16)), the effective Hamiltonian is Fourier transformed and Eq.(2.16) is analysed for the different sectors ($\hat{R}_2 = \pm 1$) via a continued fraction analysis (see for instance [29, 73, 74]). In this thesis, only the (coupled) one- and two-triplon channel is considered, i.e., contributions of higher QP channels are neglected. To estimate the validity of the approach, one can determine the total spectral weight captured in the considered one- and two-triplon channels. Let the spectral weight within the n-triplon channel be denoted by $W_{\text{tot},n}$ with

$$W_n^{\mathcal{O}_{\circ,\bullet}} = \frac{1}{\pi}\int_{k=0}^{\pi} \sum_{i\in n\text{QP}} |\langle i|\mathcal{O}_{\text{eff},\circ,\bullet}(k)|0\rangle|^2 \tag{4.87}$$

$$W_{\text{tot},n} = W_n^{\mathcal{O}_{-,-}} + W_n^{\mathcal{O}_{-,+}} + W_n^{\mathcal{O}_{+,-}} + W_n^{\mathcal{O}_{+,+}} \tag{4.88}$$

$$\sum_n W_{\text{tot},n} = 2. \tag{4.89}$$

The latter is often referred to as the sum rule. The proportion of the considered one- and two-triplon states

$$I_{1\&2} = \frac{W_{\text{tot},1} + W_{\text{tot},2}}{\sum_n W_{\text{tot},n}} \tag{4.90}$$

$$= \frac{W_{\text{tot},1} + W_{\text{tot},2}}{2} \tag{4.91}$$

gives an estimate of the relevant low-energy physics captured in the current description.
It should be noted that a Fourier transformation of the terms in Eq.(4.81) yields two almost

decoupled one-triplon dispersions $\tilde{\omega}_+(k)$ with $R_1 = 1$ and $\tilde{\omega}_-(k)$ with $R_1 = -1$.[10] Both one-triplon dispersions define the two-triplon continua. In the $R_1 = -1$ channel, the relevant continuum is defined by

$$\omega_{+,-}(k) = \tilde{\omega}_+(k - k_1) + \tilde{\omega}_-(k_1). \tag{4.92}$$

In the $R_1 = 1$ channel, two relevant continua exist, which are defined by

$$\omega_{-,-}(k) = \tilde{\omega}_-(k - k_1) + \tilde{\omega}_-(k_1) \tag{4.93}$$

$$\omega_{+,+}(k) = \tilde{\omega}_+(k - k_1) + \tilde{\omega}_+(k_1). \tag{4.94}$$

The objective of the modified gCUT scheme is to derive an effective Hamiltonian, such that:
i) if no quasiparticle decay is present, $\tilde{\omega}_\circ(k)$ corresponds to the actual one-triplon dispersion, i.e., all coefficients $c_{i,j,m}(\lambda,\zeta)$ are zero.
ii) if quasiparticle decay exists for certain momenta k, $\tilde{\omega}(k)$ should lay on top of the corresponding resonance in the dynamic structure factor, indicating the decaying one-triplon mode.
Naturally, both objectives are not exactly fulfilled when the modified gCUT scheme is applied to determine spectral densities. However, the subsequent evaluation process relies on a simultaneous analysis of the one- and two-triplon subspace including these interaction terms, which therefore renormalizes the almost decoupled one-triplon dispersions. The renormalized one-triplon dispersion is then identified either with i) the (shifted) delta-function or with ii) the (shifted) resonance in the continuum. Note, that the two-triplon continua are not renormalized by the current scheme and the upper and lower bounds of these continua are only constituted by the almost decoupled one-triplon dispersions. Therefore, it is essential, that the renormalization effects are not too large so that the bare one-triplon dispersions are already good approximations.
Overall, the size of the renormalization effects can be viewed as a measure for the quality of the approach. For the considered parameter sets, one finds that the one-triplon mode in the anti-symmetric channel does not decay. Consequently, it is possible to calculate the dispersion $\omega_-(k)$ via the quasiparticle generator scheme, allowing to estimate the quality of the approach via a fully independent check.
It should be noted that it is not possible to simply perform the calculation in the anti-symmetric channel with the quasiparticle generator and in the symmetric channel with the spectral weight generator, because the subtraction scheme performed for the two-triplons states (see A.1) couples both channels. This would yield erratic behavior including artifacts like pseudo bound states.

CUT on finite clusters

To give insights into the behavior of the spectral weight generator and the resulting CUT, we discuss the qualitative behavior of the characteristic quantities during the CUT for both the quasiparticle and the spectral weight generator scheme examplary for a finite system. These characteristic quantities are the subblock energies $\varepsilon_i^n(\ell)$, the reduced one-QP weights $W_{i,1}(\ell)$ and the spectral weights on finite clusters $I_i^{\mathcal{O}^C_{+/-,\bullet}}(\ell)$, defined in full correspondence to Eq.(4.32). We restrict the discussion to an intermediate system size ($N = 6$), since this system already exhibits non-trivial physics while the small number of low-QP states allows a convenient discussion of the relevant quantities.

[10] Here, $\tilde{\omega}_-(k)$ is generically lower than $\tilde{\omega}_+(k)$, as can be seen already in first-order perturbation theory.

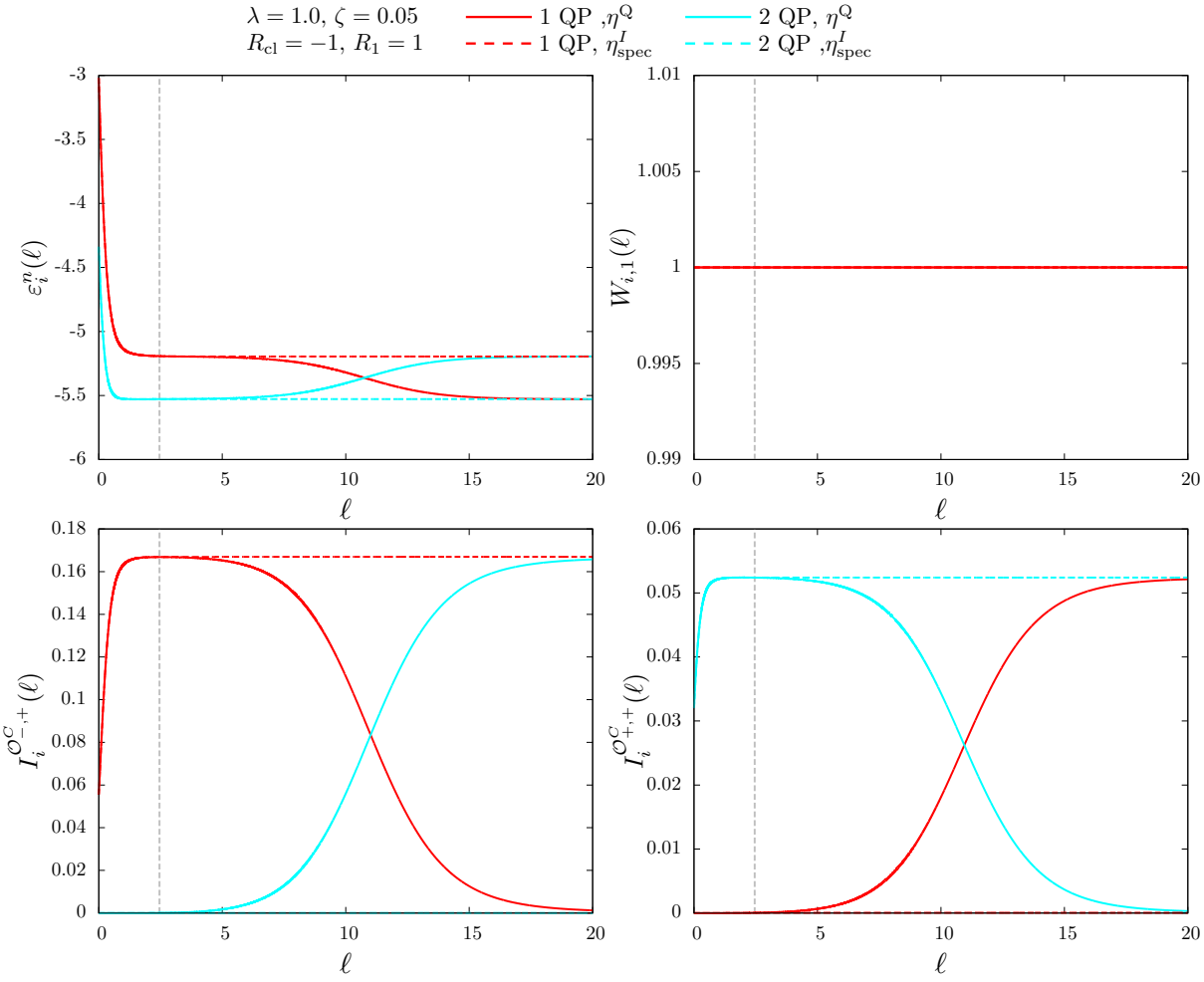

Figure 4.21: Illustration of the CUT performed for the $N = 6$-cluster ($L = 3$ super rungs), the symmetry channel $R_{\mathrm{cl}} = -1$, $R_1 = 1$ and the parameters $\lambda = 1.0$ and $\zeta = 0.05$. The behavior of the subblock energies $\varepsilon_i(\ell)$, the reduced one-particle weight $W_{i,1}(\ell)$, the anti-symmetric spectral weights $I_i^{\mathcal{O}^C_{-,+}}(\ell)$ and the symmetric spectral weights $I_i^{\mathcal{O}^C_{+,+}}(\ell)$ of the basis states are depicted in dependence of ℓ. The red (cyan) lines refer to 1QP (2QP) basis state. Solid lines show the behavior for the quasiparticle generator while the dashed lines refer to the corresponding behavior for the spectral weight generator. The vertical grey dashed line illustrates $\ell_{\mathrm{switch}} \approx 2.46$ of the spectral weight generator.

One-particle decay We begin the discussion by focussing on a prototypical example of quasiparticle decay. To this end, we choose $\lambda = 1$ with a relatively small asymmetry $\zeta = 0.05$ and the symmetry channel $R_{\mathrm{cl}} = -1$, $R_1 = 1$. Note, that the symmetry associated with $\hat{R}_\zeta$ is only present for $\zeta = 0$ and cannot be exploited. In the considered symmetry channel, only a single one-QP state exists and we restrict the discussion to this one-QP state and the lowest two-QP state. The corresponding characteristic quantities are depicted in figure 4.21.

One observes that both subblock energies $\varepsilon_i^n(\ell)$ decrease for small values of ℓ. This behavior is generic and reflects the repulsive interaction with higher QP channels. Both subblock energies seemingly converge, yet, the two-particle state is energetically below the one-particle state. Because the interaction between both states is associated with the small asymmetry induced by ζ, it relates to large ℓ-scales. Indeed, for intermediate values of ℓ, both subblock eigenvalues are switched by the quasiparticle generator scheme. In contrast, the spectral weight generator prevents this unphysical behavior. Qualitatively, the behavior of the subblock energies is very similar to the scenario of pseudo decay. However, the underlying physics in the thermodynamic limit differ fundamentally, which is also reflected in the reduced weights.
Both states represent the lowest states in the respective QP sector, i.e., $W_{i,1} = 1$. In other words, pseudo decay can simply not occur for the one-particle mode on this cluster in the considered symmetry channel. The reason for this behavior is therefore fundamentally different. The relevant weights to detect quasiparticle decay are the respective spectral weights. As intended, the spectral weight $I_i^{\mathcal{O}^C_{-},+}(\ell)$ of the one-particle state is large while it is basically zero for the two-particle state. Furthermore, as anticipated, one finds that the spectral weight of the one-particle state increases for small values of ℓ, indicating that the 'naked' low-energy states contain less spectral weight than the actual low-energy states. Therefore, the transformation increases the spectral weight of the basis states. For the quasiparticle generator, the spectral weight of the one-particle mode reaches a maximum at $\ell_{\text{switch}} \approx 2.46$ and the resorting of these states switches the associated spectral weights. The spectral weight of the one-particle state drops to zero while the weight is shifted to the two-particle state. In contrast, the spectral weight generator detects the decrease of the spectral weight and eliminates the corresponding matrix element from the generator, i.e., the spectral weight shift is fully prevented.
By construction, the symmetric spectral weight $I_i^{\mathcal{O}^C_{-},+}(\ell)$ is mainly contained in the two-particle sector. The weight of the two-particle states increases for small values of ℓ. In analogy to the symmetric spectral weight, the resorting of the quasiparticle generator switches both spectral weights, resulting in an unphysical weight distribution. This is prevented by the spectral weight generator.
One can conclude, that the modified generator scheme is suited to treat quasiparticle decay in the intended way if it is caused by a small asymmetry. Physically more demanding and more interesting is the treatment of large asymmetries, which we discuss in the following. For this purpose, we choose a large asymmetry $\zeta = 1$ and the same symmetry channel $R_{\text{cl}} = -1$, $R_1 = 1$ and set $\lambda = 1.0$. The characteristic quantities are depicted in figure 4.22.
The terms induced by the asymmetry are much larger and affect the transformation already for smaller values of ℓ. In particular, one does not observe a quasi-converged region in ℓ of the subblock energies for the quasiparticle generator. The resorting takes place at relatively small ℓ-scales, as indicated by the minimum of the two-particle subblock energy. Moreover, the subblock energies are not only sorted by the quasiparticle generator, but the interaction results in a noticeable level repulsion. In contrast, the spectral weight generator yields a qualitative different development of the subblock energies by eliminating the corresponding generator element for $\ell > \ell_{\text{switch}}$ with $\ell_{\text{switch}} = 1.42$. The resulting subblock energies are not sorted with respect to the number of QPs, indicating an energetic overlap of the QP channels.
Again, the reduced one-QP weight does not provide any information and more insight is gained by the spectral weights. For small values of ℓ, the behavior of the anti-symmetric spectral weights $I_i^{\mathcal{O}^C_{-},+}(\ell)$ is qualitatively identical to the case of small asymmetries. The weight of the one-particle state increases while the weight of the two-particle subblock energy is (relatively) small. For the quasiparticle generator, the resorting of the subblock energies leads to a large drop of the spectral weight of the one-QP state, which is shifted to the two-QP state. Finally,

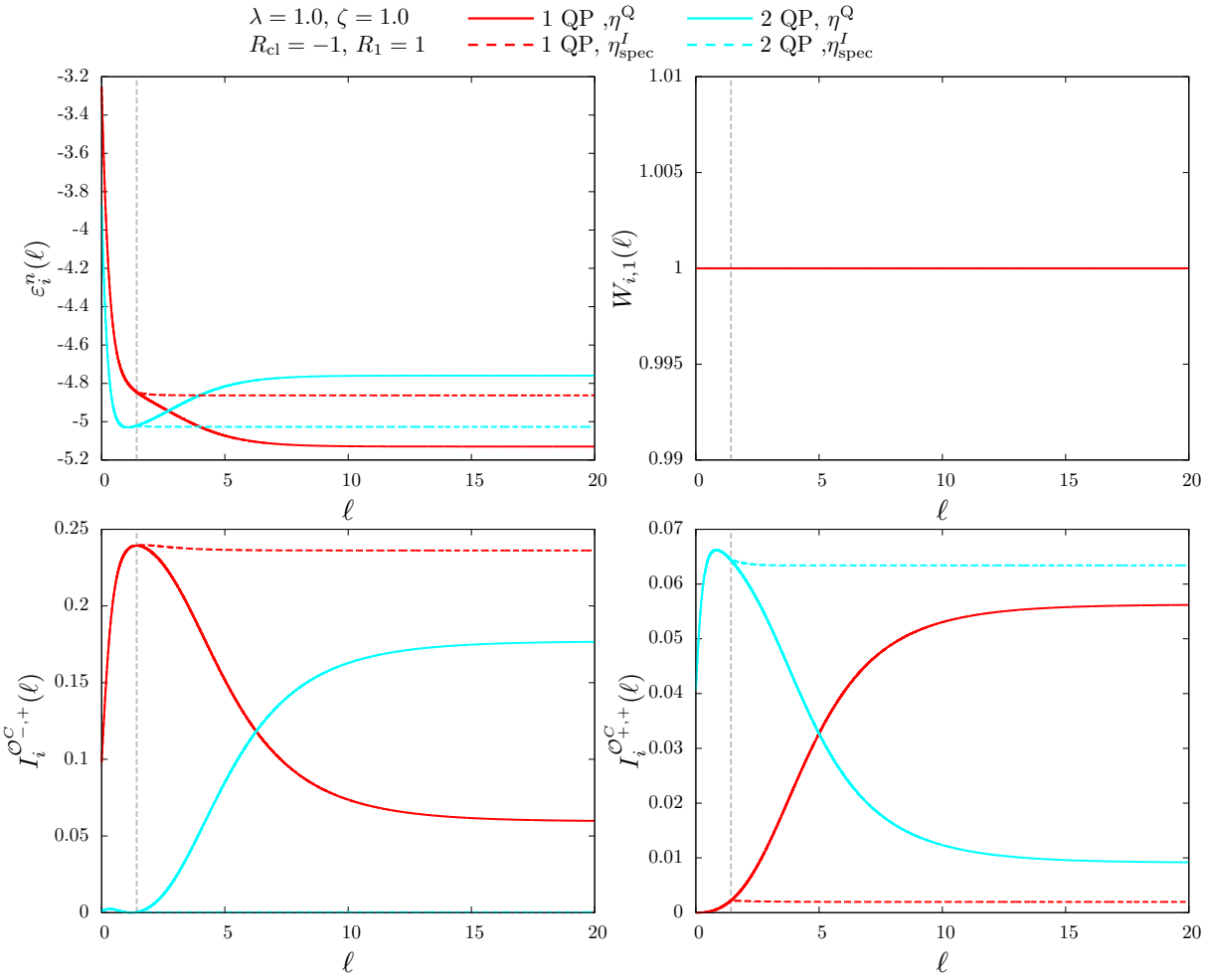

Figure 4.22: Illustration of the CUT performed for the $N = 6$-cluster ($L = 3$ super rungs), the symmetry channel $R_{\mathrm{cl}} = -1$, $R_1 = 1$ and the parameters $\lambda = 1$ and $\zeta = 1$. The behavior of the subblock energies $\varepsilon_i(\ell)$, the reduced one-particle weight $W_{i,1}(\ell)$, the anti-symmetric spectral weights $I_i^{\mathcal{O}^C_{-,+}}(\ell)$ and the symmetric spectral weights $I_i^{\mathcal{O}^C_{+,+}}(\ell)$ of the basis states are depicted in dependence of ℓ. The red (cyan) lines refer to 1QP (2QP) basis state. Solid lines show the behavior for the quasiparticle generator while the dashed lines refer to the corresponding behavior for the spectral weight generator. The vertical grey dashed line illustrates $\ell_{\mathrm{switch}} \approx 1.42$ of the spectral weight generator.

the spectral weight of the one-QP state converges to a finite value. Surprisingly, the spectral weight generator is able to prevent this shift of spectral weight to a great extent. Basically, the same features are present for the symmetric spectral weights $I_i^{\mathcal{O}^C_{+,+}}(\ell)$, only the roles are interchanged.
The spectral weight distribution obtained with the spectral weight generator is surprisingly sharp and justifies the elimination of the corresponding matrix element during the flow. It should

be noted that this behavior is again prototypical. Let us also remark that the corresponding features are also present for the decay of two quasiparticles.

Level repulsion Let us investigate an example where the corresponding system in the thermodynamic limit does *not* exhibit quasiparticle decay. As demonstrated in the applications, the anti-symmetric one-triplon mode is stable for the whole momentum axis for $\lambda = 1.0$ and $\zeta = 1.0$, i.e., the interactions induced by ζ result in a level repulsion pushing the one-particle mode below the two-particle continuum. We examine the corresponding CUT on a finite cluster for the symmetry channel $R_{\mathrm{cl}} = 1$, $R_1 = -1$ setting $\lambda = 1.0$ and $\zeta = 1.0$. The characteristic quantities are depicted in figure 4.23.

The subblock energies $\varepsilon_i^n(\ell)$ of the one-particle and two-particle block decrease for small values of ℓ. For the quasiparticle generator, one observes a minimum in ℓ for the lowest two-particle subblock energy. This effect is clearly non-perturbative and would not be captured by a perturbative approach. The corresponding matrix element is eliminated from the spectral weight generator and, consequently, the minimum caused by the level repulsion is absent; the interactions are misidentified as defective.

The reduced one-QP weights $W_{i,1}(\ell)$ become relatively small for both generator schemes indicating a highly non-perturbative and challenging parameter regime. The level repulsion also affects the behavior of the spectral weight. The level repulsion results in a drop of the anti-symmetric spectral weight $I_i^{\mathcal{O}^C_{-,-}}(\ell)$ of the corresponding one-particle state while the spectral weight is gained by the two-particle states. This weight shift is absent for the spectral weight generator scheme.

While the resulting symmetric spectral weight $I_i^{\mathcal{O}^C_{+,-}}(\ell)$ is mainly contained in the two-QP channel for the spectral weight generator, the level repulsion results in a shift between the different channels for the quasiparticle generator scheme.

In this sense, the spectral weight generator achieves the objectives on the finite-cluster calculation. There is no *qualitative* difference of the behavior of the characteristic quantities. It is (so far) not possible to decide on a cluster if the corresponding one-particle mode is stable or decays. Unfortunately, a counterpart similar to Eq.(4.28) is missing. If an interaction is viewed as artificial or proper is, ultimately, decided by the ℓ-scale of the respective interaction. For large level repulsions, this can lead to a scenario where the corresponding mode in the thermodynamic limit is stable while generator elements are eliminated, leaving finite proper interactions after the CUT on the cluster. However, it should be noted that the subsequent evaluation process allows to retroactively integrate these interactions.

Dynamic structure factor

In order to both demonstrate the properties of the modified gCUT scheme and provide an understanding of the spectral properties of the four-leg ladder in dependence of the two parameters λ and ζ, we investigate three prototypical points of the system:

1. moderate couplings, open system ($\lambda = 0.5$, $\zeta = 1.0$)
2. large couplings, quasi-periodic system ($\lambda = 1.0$, $\zeta = 0.05$)
3. large couplings, open system ($\lambda = 1.0$, $\zeta = 1.0$) ,

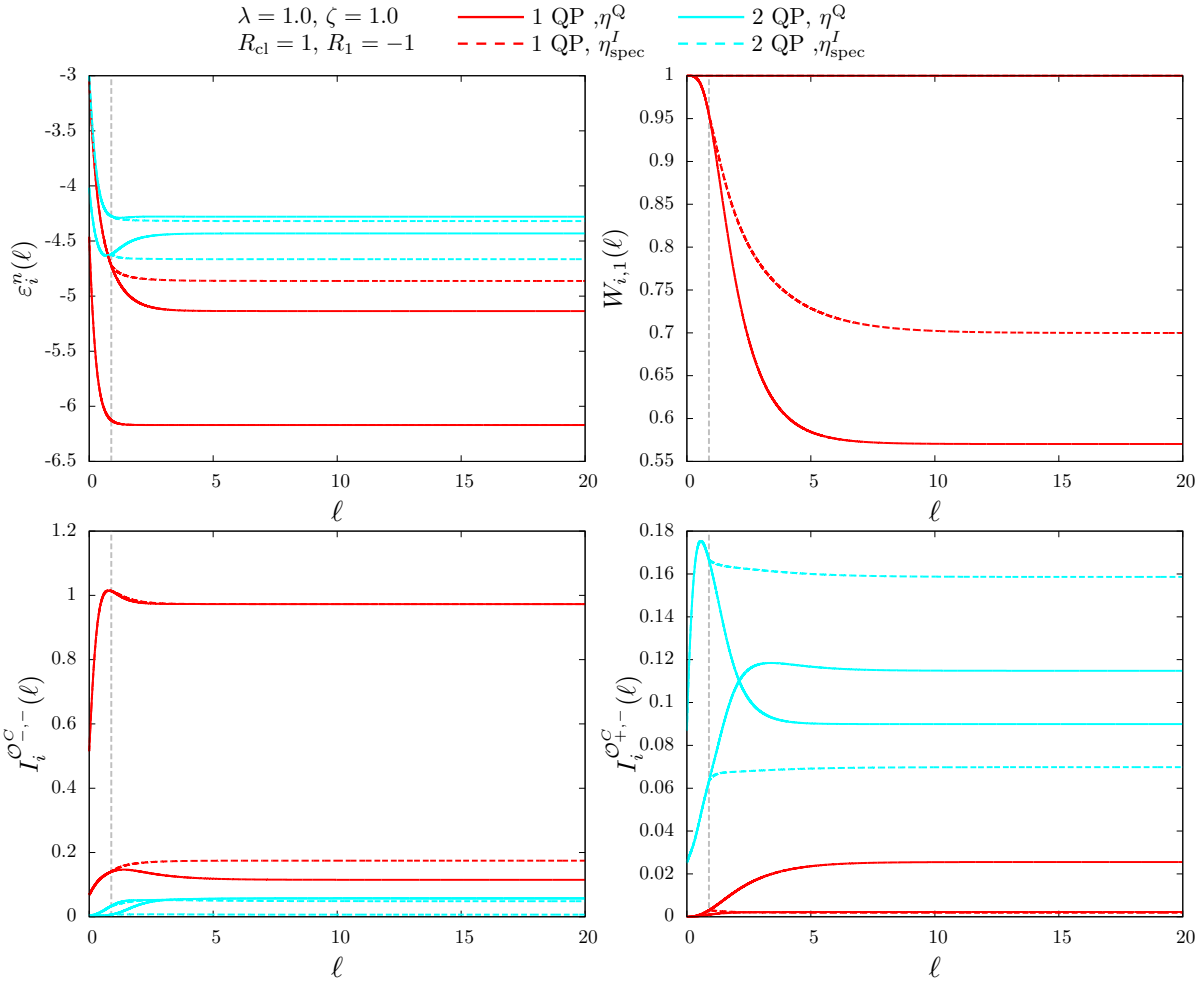

Figure 4.23: Illustration of the CUT performed for the $N = 6$-cluster ($L = 3$ super rungs), the symmetry channel $R_{\mathrm{cl}} = 1$, $R_1 = -1$ and the parameters $\lambda = 1$ and $\zeta = 1$. The behavior of the subblock energies $\varepsilon_i(\ell)$, the reduced one-particle weight $W_{i,1}(\ell)$, the anti-symmetric spectral weights $I_i^{\mathcal{O}^C_{-,-}}(\ell)$ and the symmetric spectral weights $I_i^{\mathcal{O}^C_{+,-}}(\ell)$ of the basis states are depicted in dependence of ℓ. The red (cyan) lines refer to 1QP (2QP) basis state. Solid lines show the behavior for the quasiparticle generator while the dashed lines refer to the corresponding behavior for the spectral weight generator. The vertical grey dashed line illustrates $\ell_{\mathrm{switch}} \approx 0.89$ of the spectral weight generator.

which provides a good overview of the underlying physical effects. The calculations are performed with $\Delta_{\mathrm{vicinity}} = 1.0\lambda$ and $d_{\mathrm{max}} = 350$. The basis truncation suffices to capture the relevant low-energy physics of the dynamic structure factor. The relatively large value of $\Delta_{\mathrm{vicinity}}$ accounts for much larger interactions in comparison to pseudo decay. If $\Delta_{\mathrm{vicinity}}$ is chosen too small, it becomes erratic if an interaction is switched of or not, impeding the convergence of the cluster expansion.

Open four-leg ladders ($\lambda = 0.5$) We begin by discussing the spectral weights for the open four-leg ladder ($\zeta = 1.0$) and moderate dimer-couplings $\lambda = 0.5$. The system already exhibits several interesting features even for this moderate value of λ. The spectral densities are shown for $N = 8$ in figure 4.24 and for $N = 12$ in figure 4.25.
The results are essentially converged with N with respect to the considered energy scales. While there are still some small shifts of the spectral density within the two-triplon continuum from $\mathcal{L} = 4$ to $\mathcal{L} = 6$, the results allow for a quantitative analysis.
One obtains $I_{1\&2} \approx 98\%$, indicating, that the spectral weight is captured accurately by the current description. The distribution is given by $W_{1\&2}^{\mathcal{O}_{-,-}} = 1.05$, $W_{1\&2}^{\mathcal{O}_{-,+}} \approx 0.75$, $W_{1\&2}^{\mathcal{O}_{+,-}} = 0.10$ and $W_{1\&2}^{\mathcal{O}_{+,+}} = 0.08$, i.e., the spectral weight is mainly contained in the anti-symmetric $\hat{R}_\zeta$-sector associated primarily with the one-particle mode.
First, we focus on the $R_1 = 1$ channel. As previously mentioned, the interaction between the one-triplon and the two-triplon sector is expected to be significantly smaller in this symmetry channel. In accordance with that, one observes that the interactions do not lead to a depression of the almost decoupled one-triplon dispersion $\tilde{\omega}_+(k)$ by the two-triplon continuum but lead to quasiparticle decay instead. The almost decoupled one-triplon dispersion $\tilde{\omega}_+(k)$ becomes minimal at $k = \pi$ and maximal at $k = 0$, while merging with the continuum for $k < k_c$ ($k_c \approx \frac{\pi}{2}$). Moreover, for momenta $k \gtrsim 0.6\pi$, a bound state emerges from the two-triplon continuum $\omega_{-,-}(k)$ and exhibits a small binding energy. In addition to that, for $k \gtrsim 0.8\pi$, the two-particle continuum $\tilde{\omega}_{+,+}(k)$ lies completely above the lower two-particle continuum $\tilde{\omega}_{-,-}(k)$ and another bound state is formed.
For $I^{\mathcal{O}_{-,+}}(k,\omega)$, the spectral weight for $k > k_c$ is contained mainly in the one-triplon sector. For $k < k_c$, the one-triplon dispersion merges with the continuum and the delta-function is replaced by a resonance. Interestingly, close to k_c, the resonance is broad and becomes more pronounced for $k \to 0$, which is generically observed for this system. Following the argumentation given in [29], this behavior is caused by the two-particle interactions, i.e., the bound state plays an important role in this mechanism. Notably, the almost decoupled one-triplon dispersion $\tilde{\omega}_+(k)$ lies on top of the resonance as intended by the modified generator scheme.
By contrast, the spectral density $I^{\mathcal{O}_{+,+}}(k,\omega)$ is dominated by the two-particle continuum while the spectral weight gathered by the one-triplon mode is very small. The spectral weight is mainly located at larger values of k and vanishes for $k \to 0$. The reason for this is that the corresponding observable at $k = 0$ corresponds to the total magnetization, i.e., $\mathcal{O}_{+,+}(k = 0) \propto S^z_{\text{tot}}$. Accordingly, the action of the observable on the ground state ($S^z_{\text{tot}} = 0$) vanishes. The spectral density is mainly located at the low edge of the lower two-particle continuum $\tilde{\omega}_{-,-}(k)$ as well as both bound states.
Next, we discuss the $R_1 = -1$ channel. The almost decoupled one-triplon dispersion $\tilde{\omega}_-(k)$ becomes maximal at $k = 0$ and minimal at $k = \pi$, defining the gap of the system $\Delta \approx 0.43(1)$. One observes that the almost decoupled one-triplon dispersion $\tilde{\omega}_-(k)$ merges with the continuum for small momenta. This overlap is just an artifact of the spectral weight generator wrongly eliminating matrix elements, since the renormalized one-particle dispersion does not merge with the continuum and is pushed out of the two-particle continuum. The one-triplon dispersion $\omega_-(k)$, which is determined via the quasiparticle generator scheme, is in full agreement with the renormalized one-triplon dispersion. The terms connecting the one-triplon mode with the two-triplon states are therefore properly included by the coupled Lanczos analysis leading to the correct renormalization.
In $I^{\mathcal{O}_{-,-}}(k,\omega)$, the spectral weight from the one-triplon mode is transferred into the two-particle

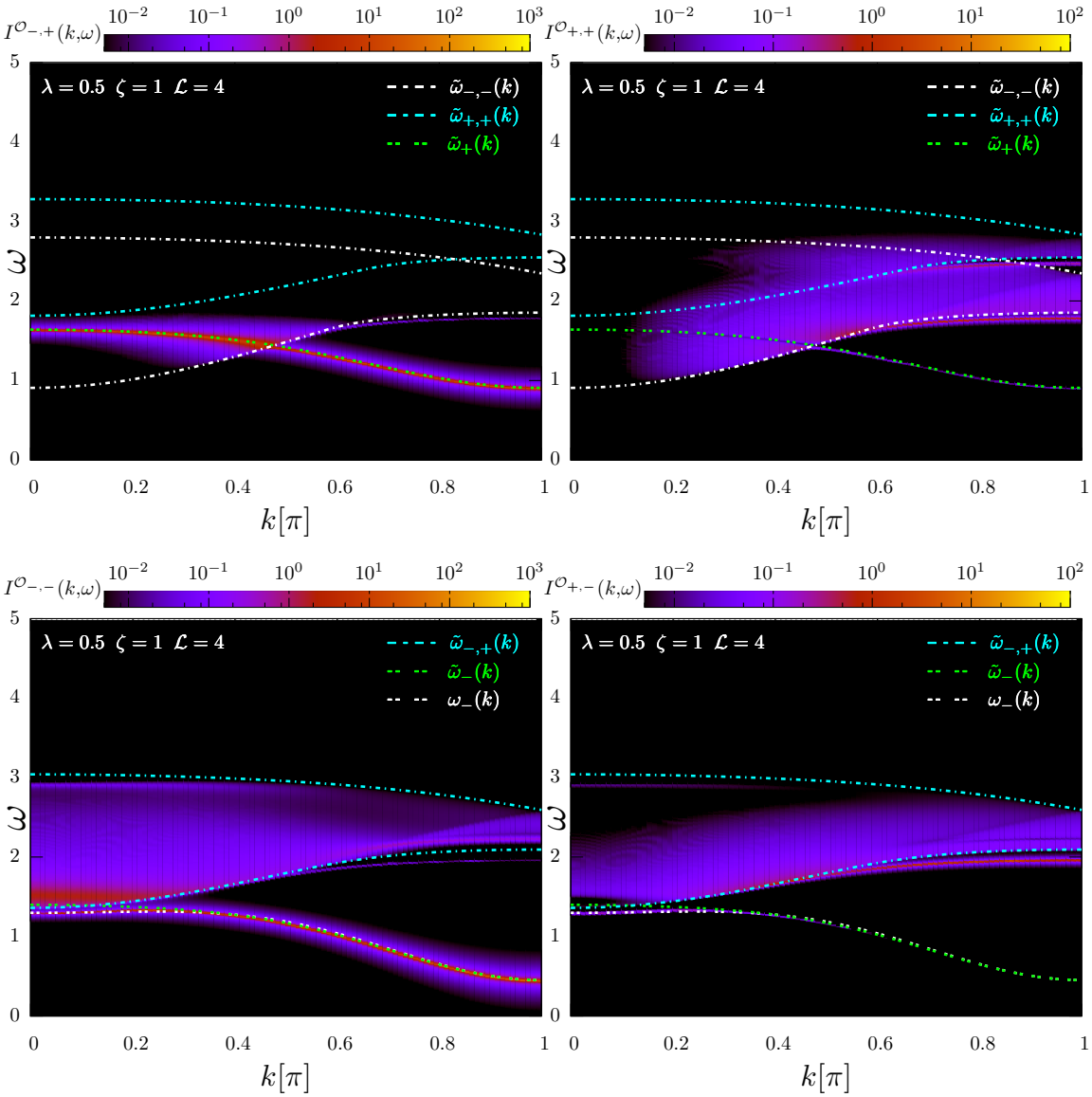

Figure 4.24: The spectral densities $I^{\mathcal{O}_{-,+}}(k,\omega)$, $I^{\mathcal{O}_{+,+}}(k,\omega)$, $I^{\mathcal{O}_{-,-}}(k,\omega)$ and $I^{\mathcal{O}_{+,-}}(k,\omega)$ derived via gCUTs with $\mathcal{L} = 4$ are depicted for $\lambda = 0.5$, $\zeta = 1.0$. The dashed lines refer to the corresponding (almost decoupled) one-triplon dispersion and upper- and lower bounds of the two-triplon continua, respectively.

continuum for $k \lesssim 0.4\pi$. Vice versa, for $I^{\mathcal{O}_{+,-}}(k,\omega)$, one observes a spectral-weight shift from the two-particle bound state/two-particle continuum to the one-particle mode, carrying a finite spectral weight for $k \lesssim 0.4\pi$. Similar to the investigation of the anti-symmetric two-leg ladders in Ref. [29, 33] , we find, that boundstate and triplon-triplon interactions play a fundamental role for the low-energy physics and the behavior of the one-triplon mode.

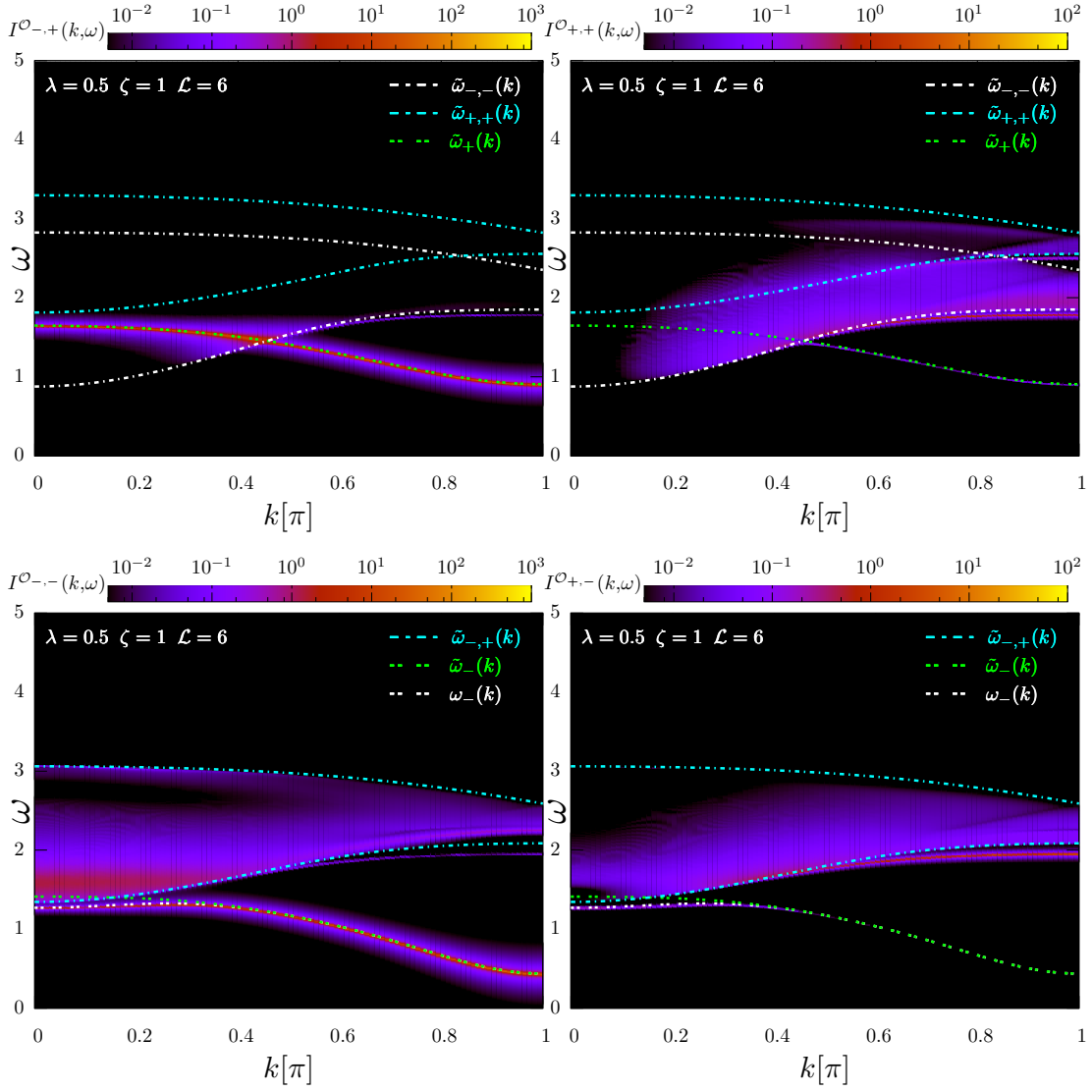

Figure 4.25: The spectral densities $I^{\mathcal{O}_{-,+}}(k,\omega)$, $I^{\mathcal{O}_{+,+}}(k,\omega)$, $I^{\mathcal{O}_{-,-}}(k,\omega)$ and $I^{\mathcal{O}_{+,-}}(k,\omega)$ derived via gCUTs with $\mathcal{L} = 6$ are depicted for $\lambda = 0.5$, $\zeta = 1.0$. The dashed lines refer to the corresponding (almost decoupled) one-triplon dispersion and upper- and lower bounds of the two-triplon continua, respectively.

Overall, one observes very different physics with respect to the one-triplon mode in both symmetry channels. In the anti-symmetric channel, the one-triplon dispersion is depressed by the two-triplon continuum and does not merge with the continuum. A comparison to the one-triplon dispersion obtained via the quasiparticle generator scheme is in full agreement with the renormalized one-triplon dispersion. In the symmetric channel, the one-triplon dispersion does merge with the continuum and one observes decay. Here, the one-triplon dispersion $\tilde{\omega}_{+}(k)$

lies exactly on top of the resonance. The modified gCUT scheme is capable of deriving an effective model which describes both cases *simultaneously*.

Quasi-periodic four-leg ladders ($\lambda = 1.0$) Next, we discuss the system for large inter-dimer couplings $\lambda = 1.0$ with a small asymmetry. For $\lambda = 1.0$, the system is in a non-perturbative regime and an effective description is challenging. For the fully symmetric case $\zeta = 0$, the $\hat{R}_\zeta$-symmetry divides the system into an channel of even and odd number of triplons. Therefore, the quasiparticle generator scheme is identical to the spectral weight generator and no quasiparticle decay exists. The system is already treated adequately by the standard gCUT scheme. However, for any finite value of ζ, the results obtained via the quasiparticle generator scheme change abruptly and reasonable results for the dynamic structure factor are only accessible via the spectral weight generator.

The spectral densities are shown for $\mathcal{L} = 4$ in figure 4.26 and for $\mathcal{L} = 6$ in figure 4.27. While the value of the dimer-coupling is large, the small asymmetry facilitates the description, resulting in a robust convergence with $\mathcal{L}$.

One obtains $I_{1\&2} \approx 93\%$, indicating, that the spectral weight is captured mainly by the current description. It is reasonable to assume, that most of the remaining weight is in the three-particle continuum. The distribution is given by $W_{1\&2}^{\mathcal{O}_{-,-}} = 1.05$, $W_{1\&2}^{\mathcal{O}_{-,+}} \approx 0.32$, $W_{1\&2}^{\mathcal{O}_{+,-}} = 0.33$ and $W_{1\&2}^{\mathcal{O}_{+,+}} = 0.16$, i.e., the spectral weight is *not* mainly contained in the anti-symmetric sector. The reason for this will become clear in the following.

Again, we begin focussing on the $R_1 = 1$ channel. As before, one observes quasiparticle decay for the almost decoupled one-triplon dispersion $\tilde{\omega}_+(k)$, which is located inside the two-triplon continuum for momenta $k < k_c$ ($k_c \approx 0.6\pi$). The dispersion is relatively flat and symmetric with respect to the maximum located at $k \approx \frac{\pi}{2}$. Additionally, one observes a bound state with a small binding energy emerging for $k \gtrsim 0.6\pi$.

Due to the small asymmetry $\zeta = 0.05$, the spectral density $I^{\mathcal{O}_{-,+}}(k)$ is clearly dominated by the one-triplon sector. The almost decoupled one-triplon dispersion $\tilde{\omega}_+(k)$ enters the continuum at $k_c \approx 0.6\pi$ and a very pronounced resonance is observable for $k < k_c$ since the decay induced by ζ is very weak.

Accordingly, the spectral density $I^{\mathcal{O}_{+,+}}(k)$ is dominated by the two-particle continuum and the bound state while the spectral weight carried by the one-triplon dispersion $\omega_+(k)$ is basically zero. As aforementioned, due to S^z_{tot} conservation, the spectral weight vanishes for $k \to 0$. The spectral weight is mainly located at the lower edge of the lower two-particle continuum $\tilde{\omega}_{-,-}(k)$ and in the corresponding bound states.

In the anti-symmetric channel $R_1 = -1$, one does not observe quasiparticle decay. The almost decoupled one-triplon dispersion $\tilde{\omega}_-(k)$ exhibits a minimum at $k = \pi$ and a maximum at $k = 0$ which is located close to the two-triplon continuum $\omega_{2,-,+}(k)$ but $\tilde{\omega}_-(k)$ does not merge with the two-triplon continuum. However, one observes a sharp (anti-)crossing at $k_{\text{crossing}} \approx 0.2\pi$ with a two-particle bound state, and it is a matter of interpretation if the renormalized one-triplon mode is the lower or the upper state for $k < k_{\text{crossing}}$. The almost decoupled one-triplon dispersion obtained via the spectral weight generator replaces the anti-crossing with a crossing and we adapt this interpretation. The two-triplon bound state involved in the crossing is rather flat, exhibits a maximum at $k_{\max} = \frac{\pi}{2}$ and is symmetric with respect to the maximum located at $k_{\max}$. The binding energy $\Delta_{\text{binding}} \sim 0.3$ is relatively large.

The one-triplon dispersion $\omega_-(k)$ is also determined via the quasiparticle generator scheme. In principle, the resulting one-triplon dispersion should correspond to $\tilde{\omega}_-(k)$ for $k > k_{\text{crossing}}$ and to the two-triplon bound state for $k < k_{\text{crossing}}$. However, one observes clear deviations from

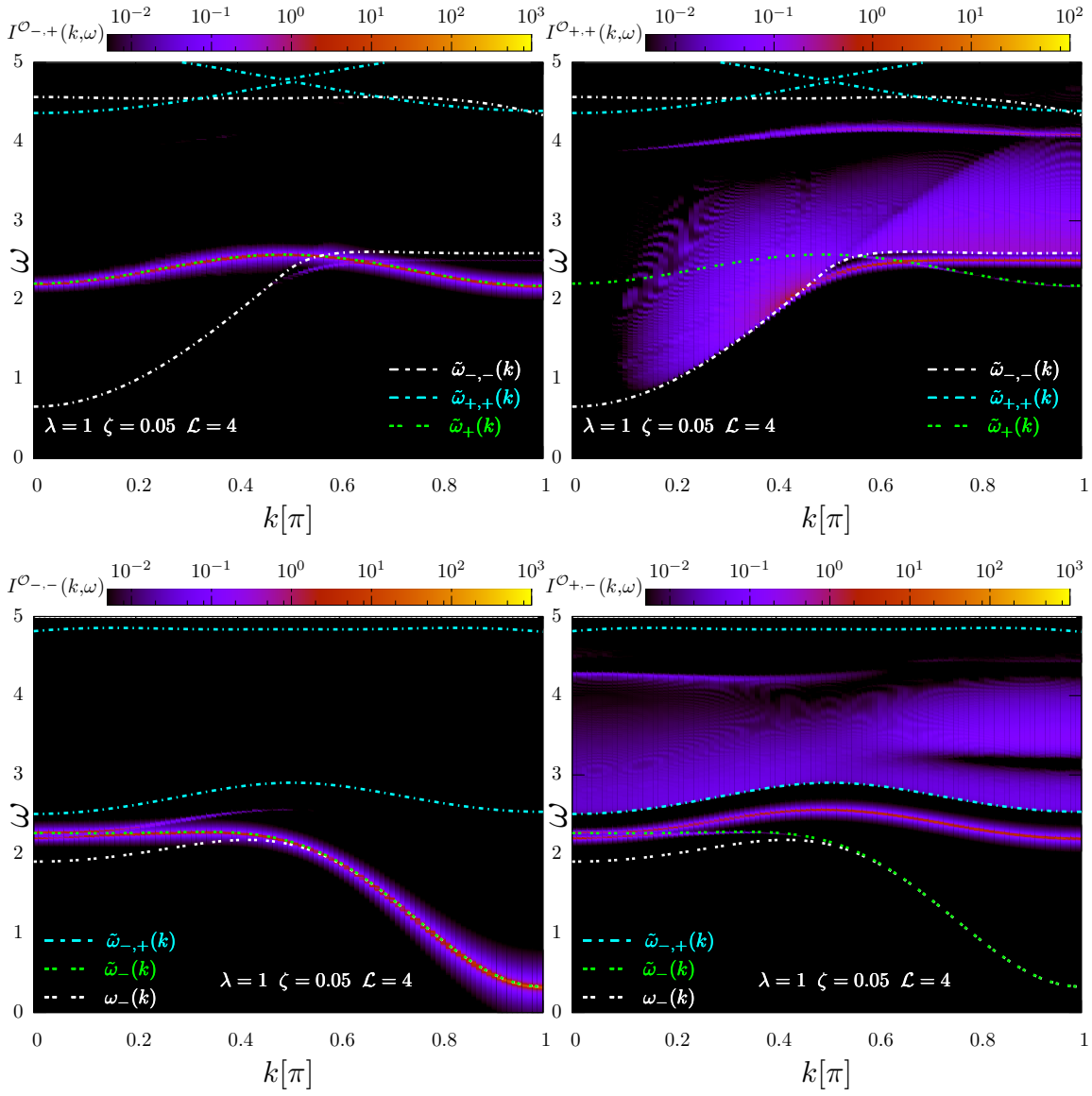

Figure 4.26: The spectral densities $I^{\mathcal{O}_{-,+}}(k,\omega)$, $I^{\mathcal{O}_{+,+}}(k,\omega)$, $I^{\mathcal{O}_{-,-}}(k,\omega)$ and $I^{\mathcal{O}_{+,-}}(k,\omega)$ derived via gCUTs with $\mathcal{L} = 4$ are depicted for $\lambda = 1.0$, $\zeta = 0.05$. The dashed lines refer to the corresponding (almost decoupled) one-triplon dispersion and upper- and lower bounds of the two-triplon continua, respectively.

this behavior for small values of k, caused by an impeded convergence due to the violation of the generalized cluster additivity. The impact is rather moderate, since the two-particle bound state and $\tilde{\omega}_{-}(k)$ are energetically very close. In the symmetric channel, the violation of the generalized cluster additivity is more severe and leads to a complete breakdown of the approach and it is not possible to obtain a reasonable one-triplon dispersion by the quasiparticle

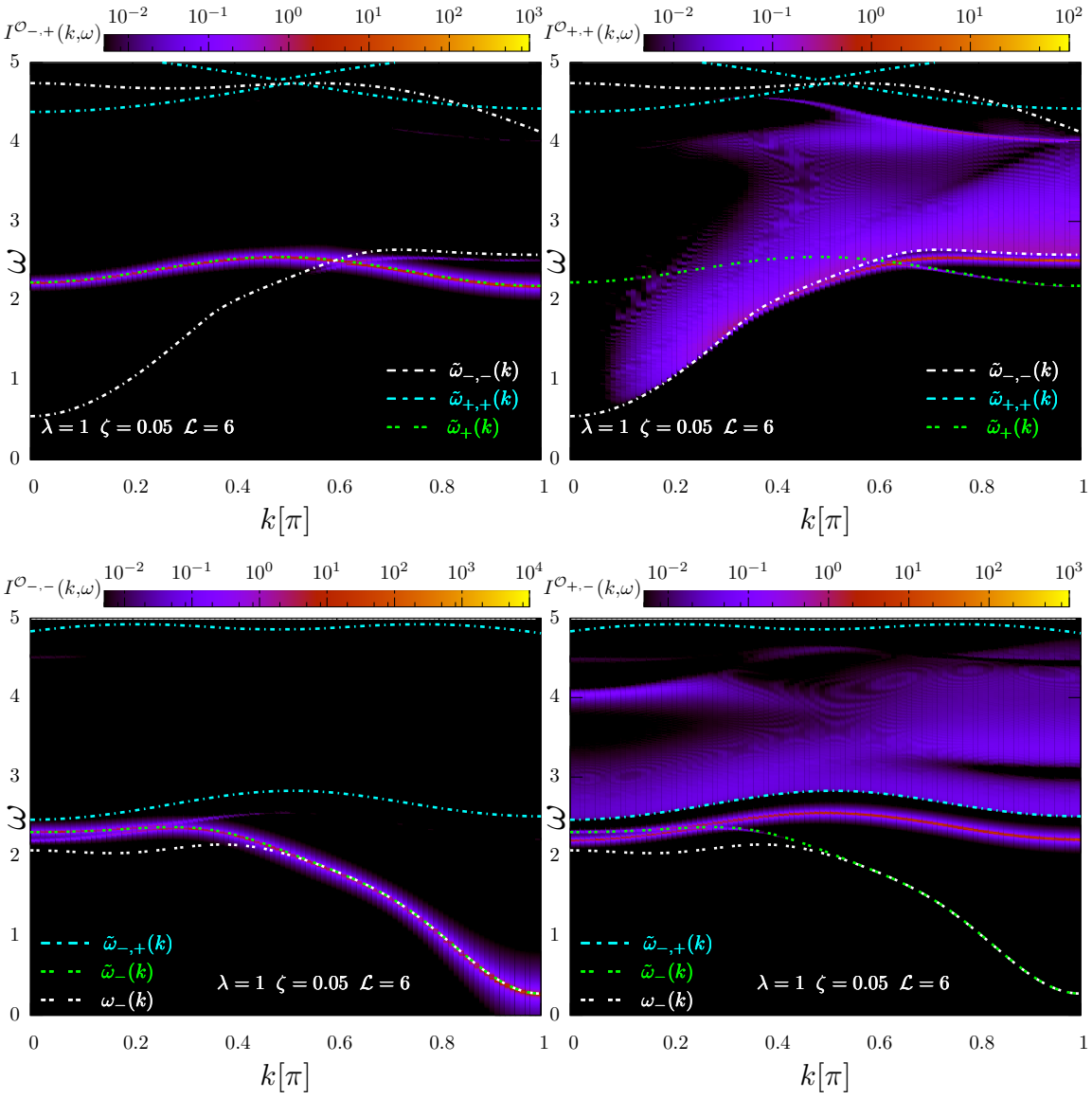

Figure 4.27: The spectral densities $I^{\mathcal{O}_{-,+}}(k,\omega)$, $I^{\mathcal{O}_{+,+}}(k,\omega)$, $I^{\mathcal{O}_{-,-}}(k,\omega)$ and $I^{\mathcal{O}_{+,-}}(k,\omega)$ derived via gCUTs with $\mathcal{L} = 4$ are depicted for $\lambda = 1.0$, $\zeta = 0.05$. The dashed lines refer to the corresponding (almost decoupled) one-triplon dispersion and upper- and lower bounds of the two-triplon continua, respectively.

generator.
As expected, the symmetry is only broken weakly by the small asymmetry and therefore the (anti-)symmetrized observables essentially divide the spectral density into parts of even and odd number of quasiparticles. Consequently, the spectral density $I^{\mathcal{O}_{-,-}}(k,\omega)$ is dominated by the one-particle dispersion while $I^{\mathcal{O}_{-,+}}(k,\omega)$ is dominated by the two-triplon bound state. For

$k \lesssim 0.25\pi$, small parts of the spectral weights are shifted between the quasiparticle sectors due to the (anti-)crossing.
The remarkable resemblance between the spectral densities $I^{\mathcal{O}_{+,-}}(k,\omega)$ and $I^{\mathcal{O}_{-,+}}(k,\omega)$ is not a coincidence. For $\zeta = 0.0$, the system exhibits a 90° rotational symmetry and the spectral densities $I^{\mathcal{O}_{+,-}}(k)$ and $I^{\mathcal{O}_{-,+}}(k)$ must be equivalent. By construction, the symmetry is not regarded in the ansatz since the quasiparticles are located at the dimers. If one compares the results for $\zeta = 0.05$, the anti-symmetric *two*-triplon $S = 1$ bound state can be identified with the symmetric *one*-triplon mode. This explains the weight distribution discussed above. Note, that the spectral density of the two-triplon continuum in $I^{\mathcal{O}_{-,+}}(k,\omega)$ would correspond to the three-triplon continuum in $I^{\mathcal{O}_{-,+}}(k)$ and is therefore not included in the description.
We conclude that the modified gCUT scheme is perfectly suited for the effective description for small asymmetries ζ. Following this, we discuss the open isotropic four-leg ladder having couplings and large asymmetries.

Open isotropic four-leg ladders ($\lambda = 1.0$) Finally, we discuss the case of large inter-dimer couplings $\lambda = 1.0$ with a large asymmetry ($\zeta = 1.0$, open system). For these parameter values, the interaction effects induced by ζ become considerable and soften the distinction between the one- and two-triplon sector via the respective observables. This parameter regime is very challenging and inaccessible by high-order series expansion or the quasiparticle generator scheme. Still, while the results obtained via the optimized gCUT scheme are not yet fully converged on the considered energy scales, one obtains a robust convergence with increasing $\mathcal{L}$. The results are shown for $\mathcal{L} = 4$ in figure 4.28 and for $\mathcal{L} = 6$ in figure 4.29. One observes many substructures within the two-particle continuum and it should be noted that the spectral densities of these structures are often very small and only visible due to the logarithmic scaling in the colorplot, i.e., they can possibly be irrelevant artifacts of the approach.
One obtains $I_{1\&2} \approx 92\%$, indicating, that the spectral weight is again captured in this parameter regime mainly by the current description. The distribution is given by $W_{1\&2}^{\mathcal{O}_{-,-}} = 0.96$, $W_{1\&2}^{\mathcal{O}_{-,+}} \approx 0.44$, $W_{1\&2}^{\mathcal{O}_{+,-}} = 0.26$ and $W_{1\&2}^{\mathcal{O}_{+,+}} = 0.19$.
As before, we start with a discussion of the symmetric channel ($R_1 = 1$). In accordance with the previous considerations, one observes quasiparticle decay of the symmetric almost decoupled one-triplon dispersion $\tilde{\omega}_+(k)$. For large momenta k, the two-triplon continuum $\omega_{-,-}(k)$ is energetically very close to the one-triplon mode $\tilde{\omega}_+(k)$. Depending on N, one even observes an energetic overlap. Yet, since the interactions of the one-triplon dispersion and the two-triplon continuum are weak, the results of the almost decoupled one-triplon dispersion $\tilde{\omega}_+(k)$ are still very robust.
For the spectral density $I^{\mathcal{O}_{-,+}}(k,\omega)$, we find that the renormalized one-triplon dispersion is depressed by the continuum and loses all spectral weight for smaller momenta k. The almost decoupled one-triplon dispersion $\tilde{\omega}_+(k)$ enters the continuum at $k_c \approx 0.6\pi$. In the vicinity of k_c, the spectral density stemming from the one-triplon dispersion results in a broader signature in the two-triplon continuum. However, for smaller values of k, this resonance becomes more pronounced and can be exactly identified with $\tilde{\omega}_+(k)$.
The spectral density $I^{\mathcal{O}_{+,+}}(k,\omega)$ exhibits no resonance associated with $\tilde{\omega}_+(k)$. Moreover, one observes that the suppressed renormalized one-triplon dispersion does not lose all its weight before entering the continuum leading to local increase of the spectral density. In addition to that, a broad structure inside the two-particle continuum is obtained for $k \gtrsim 0.5\pi$, which could indicate traces of the two-triplon bound state present for the other considered parameter sets.
In the anti-symmetric channel ($R_1 = -1$), one does not observe quasiparticle decay. Instead,

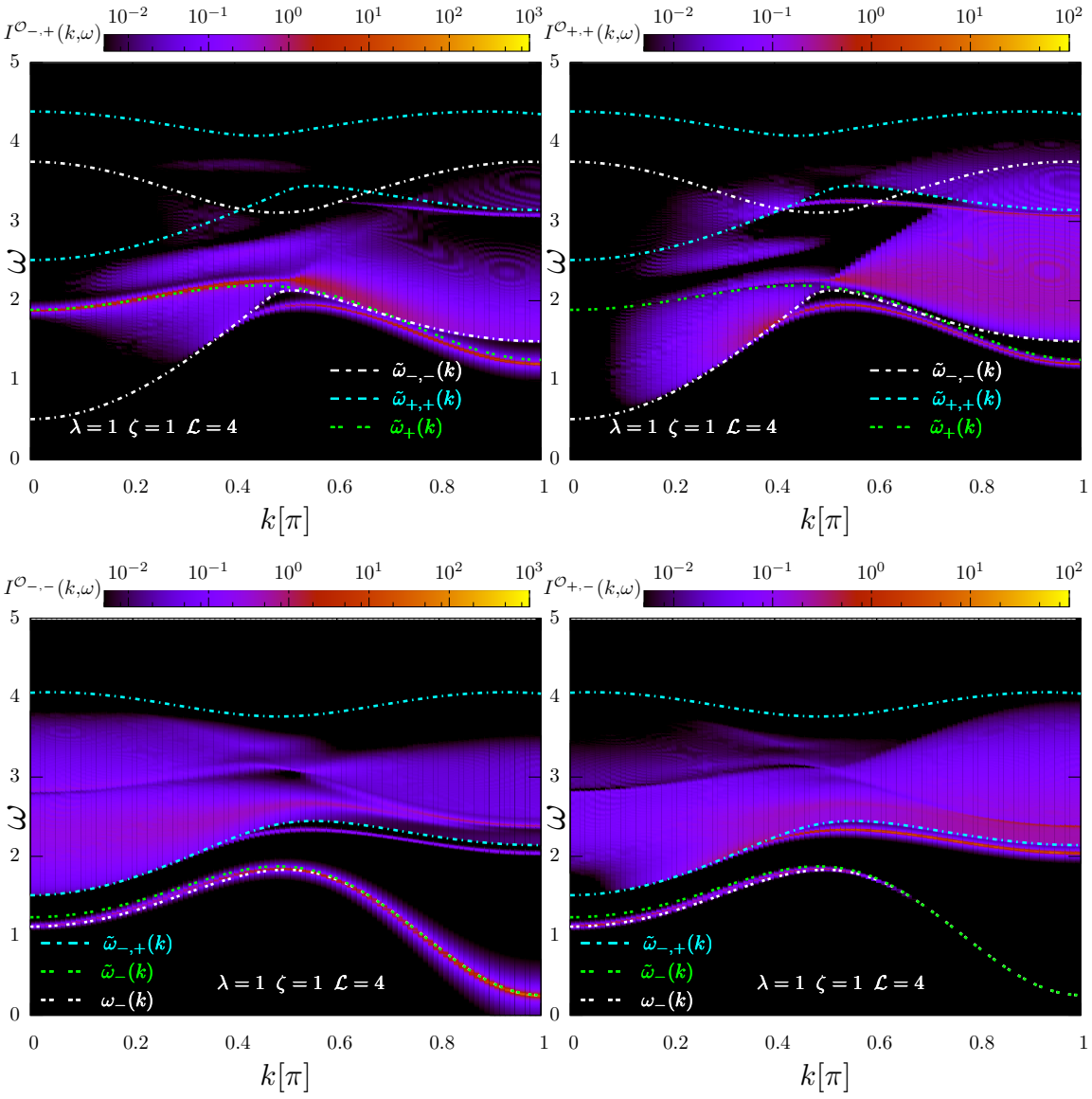

Figure 4.28: The spectral densities $I^{\mathcal{O}_{-,+}}(k,\omega)$, $I^{\mathcal{O}_{+,+}}(k,\omega)$, $I^{\mathcal{O}_{-,-}}(k,\omega)$ and $I^{\mathcal{O}_{+,-}}(k,\omega)$ derived via gCUTs with $\mathcal{L} = 4$ are depicted for $\lambda = 1.0$, $\zeta = 1.0$. The dashed lines refer to the corresponding (almost decoupled) one-triplon dispersion and upper- and lower bounds of the two-triplon continua, respectively.

the almost decoupled one-triplon dispersion $\tilde{\omega}_{-}(k)$ is pushed by the two-triplon continuum for small values of k and the dispersion exhibits a maximum at $k \approx \frac{\pi}{2}$. The renormalization effects of remaining inter-block interactions lead to a further (moderate) depression of the one-triplon dispersion for $k \lesssim \frac{\pi}{2}$. In addition to that, a two-triplon bound state is formed for large values of k, merging into the continuum at $k_c \approx \frac{1}{2}\pi$.

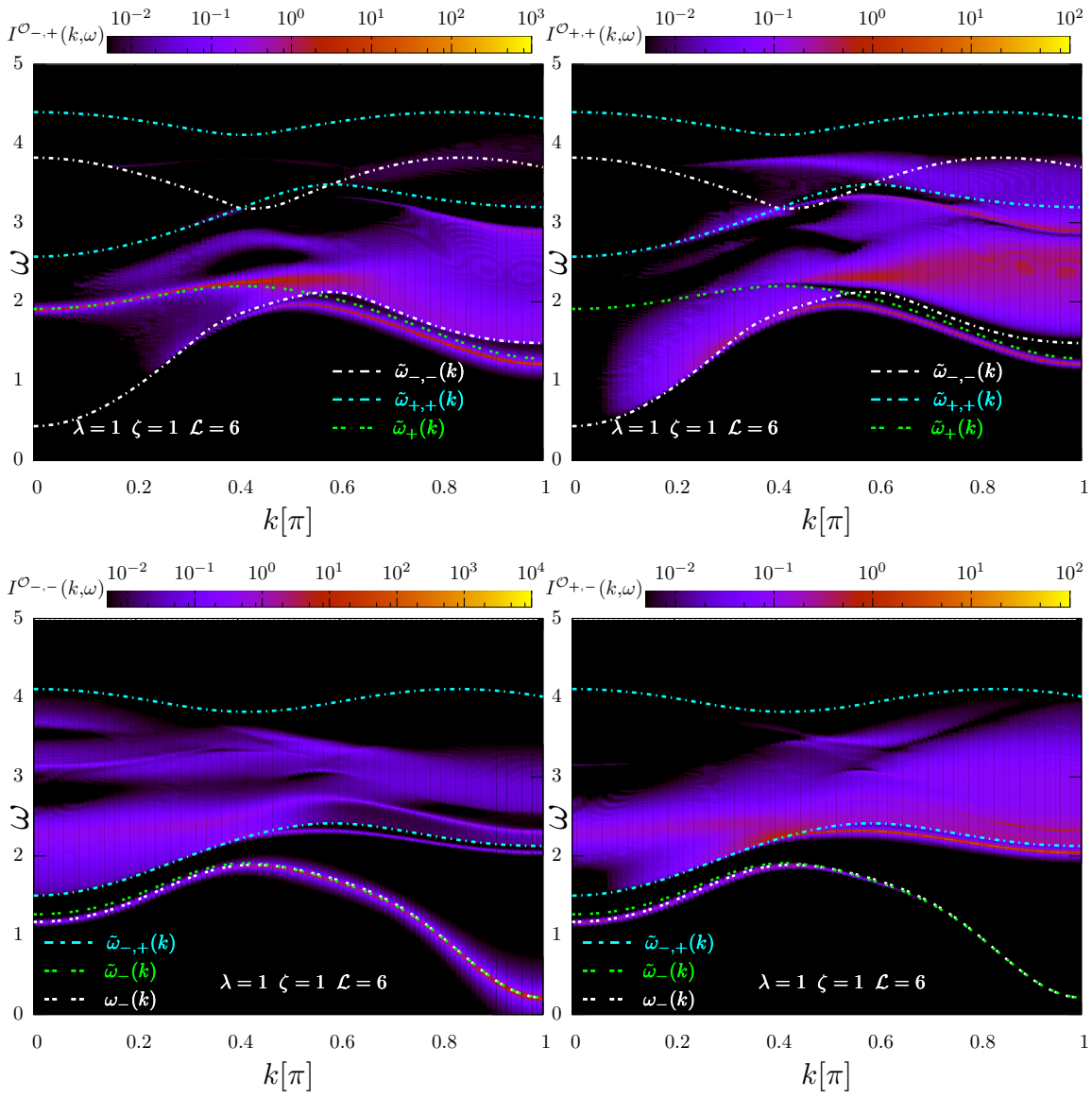

Figure 4.29: The spectral densities $I^{\mathcal{O}_{-,+}}(k,\omega)$, $I^{\mathcal{O}_{+,+}}(k,\omega)$, $I^{\mathcal{O}_{-,-}}(k,\omega)$ and $I^{\mathcal{O}_{+,-}}(k,\omega)$ derived via gCUTs with $\mathcal{L} = 4$ are depicted for $\lambda = 1.0$, $\zeta = 1.0$. The dashed lines refer to the corresponding (almost decoupled) one-triplon dispersion and upper- and lower bounds of the two-triplon continua, respectively.

For $I^{\mathcal{O}_{-,-}}(k,\omega)$, much of the spectral weight is located for $k \gtrsim \frac{1}{2}\pi$ at the one-triplon dispersion. However, for $k \gtrsim \frac{1}{2}\pi$, significant parts of the spectral weight are transferred to the two-triplon continuum leading to signatures of this interaction in the continuum, indicating traces of the $\zeta = 0$ one-triplon mode, which are only observable for $\mathcal{L} = 6$.
In contrast, for $I^{\mathcal{O}_{+,-}}(k,\omega)$, one obtains the opposite effect that the spectral weight is located

for $k \gtrsim \frac{1}{2}\pi$ mainly at the two-triplon continuum and the bound state. For $k \gtrsim \frac{1}{2}\pi$, significant parts of the spectral weight are shifted from the bound state to the one-triplon mode, carrying significant weight for $k \lesssim 0.5\pi$.
Let us close this discussion with some final remarks. The optimized gCUT scheme allows for a (semi) quantitative discussion of the spectral density even at challenging parameter values, which is considered to be relevant for the experimental realization of $La_2Cu_2O_5$. In the anti-symmetric channel, the one-triplon dispersion is suppressed by the continuum and in the symmetric channel, the one-triplon dispersion decays. We stress that this was not even qualitatively predictable by high-order series expansion [121]. Our modified gCUT scheme is able to treat both scenarios in a single effective description. In addition to that, we find first evidence of bound states within the framework of the approximation. Note, that quasiparticle decay between two-triplon and three-triplon states is not captured by the current description. In the near future, a comparison to quantum Monte Carlo [199] data can be utilized to benchmark the results with an unbiased method. The combination of both complementary techniques together with experiments represents a promising route for future research.

4.5 Chapter summary and conclusion

In this section, we summarize the methodological developments of gCUTs achieved in the scope of this thesis. The gCUT method combines CUTs and NLCEs and represents a non-perturbative tool to determine effective low-energy models if at least one degree of freedom is gapped [46]. Several methodological developments are introduced, addressing a wide range of challenges in NLCEs and non-perturbative CUTs in general.

4.5.1 General scheme

The first important development concerns the truncation of the basis for the finite-cluster calculations. The truncation scheme introduced in 4.1.3 is highly efficient and can be identified with a block Lanzcos algorithm complemented by the exact low-energy spectrum. The latter enforces the exact low-energy spectrum on the cluster which is shown to significantly increase the convergence. Furthermore, the truncation of the basis is combined with the exploitation of symmetries on finite clusters similar to exact diagonalization techniques, making the approach both more robust and efficient.
The efficiency of this truncation scheme is demonstrated for the one-triplon dispersion of the isotropic two-leg ladder (see 4.4.1). We conclude that the new approach is vastly superior to the untruncated standard basis, since the truncated basis allows to double the number of maximally manageable supersites. While these developments are rather technical, they are highly relevant for the applicability of gCUTs, making the method a competitive tool, specifically in comparison to CORE.

4.5.2 Generalized cluster additivity

However, it turns out that a simple enhancement of the considered fluctuation length is insufficient. When deriving effective low-energy models via gCUTs, one often finds a hard boundary separating a parameter regime where the low-energy physics is, at least in principle,

accessible via the standard gCUT scheme from a regime where this is rigorously not the case. The latter can be traced back to an energetic overlap of different quasiparticle sectors on finite clusters, which is absent in the thermodynamic limit due to the momentum conservation. In other words, this overlap ist just an artifact of the approach, inherently breaking the translational symmetry. This energetic overlap is identified with pseudo decay on finite clusters. The quasiparticle generator applied in gCUTs sorts the states energetically ascending with the quasiparticle number. Consequently, the wrong fluctuations are considered in the calculation leading to a breakdown of the approach. While the cluster additivity is in fact satisfied by the approach, the underlying principles connected to this concept are violated. We introduce the concept of generalized cluster additivity, which provides insights into the underlying mechanisms of this breakdown in the context of NLCEs and provides a guideline to possible solutions. Interestingly, this scheme demands to go beyond the paradigm of using the exact eigenvectors on clusters.
A physically entirely different scenario is present, if the energetic overlap on finite clusters corresponds to an energetic overlap also present in the thermodynamic limit, i.e., one observes true quasiparticle decay. Then, the energetic overlap on finite clusters is identified as genuine decay. In contrast to pseudo decay, the implementation does not inevitably lead to a break down of the approach, yet, the convergence of the approach is affected. Again, the generalized cluster additivity allows to understand convergence problems that can occur and defines possible remedies.
While the underlying physics differs fundamentally, the reasons for the convergence problems and solutions are related. The basic idea is to ignore the defective interactions which are responsible for the breakdown of the approach when deriving the effective model. In the case of pseudo decay, these interactions must annihilate when the translational invariance is restored by the embedding procedure, while, in the case of genuine decay, the interactions are part of the effective description and moderate the quasiparticle decay.
We introduce two modified versions of gCUTs relying on two different generator schemes to treat pseudo and genuine decay, respectively. The modified generator schemes are designed to cure the quasiparticle picture on the finite clusters restoring the convergence of the approach. To ignore an interaction during the transformation, the corresponding element must be eliminated from the generator. The defective interactions are very small and therefore affect the transformation mainly on large ℓ-scales of the transformation, i.e., it suffices to identify these interactions at intermediate values of ℓ. Another central element of the modification is the subblock basis, in which each defective interaction can be identified with a single element. Finally, the elimination relies on suited weights which are designed to uniquely identify the proper low-energy states.

4.5.3 Pseudo decay

In the case of pseudo decay, the reduced weights $W_{\nu,i}$ are perfectly suited to identify and understand this breakdown. The transformation is performed by the quasiparticle generator up to a value ℓ_{switch} and then possibly defective interactions are eliminated from the generator scheme by relying on energetic considerations and the influence on the reduced weights.
To demonstrate the validity of the treatment of pseudo decay, the modified gCUT scheme is applied to determine the one-triplon dispersion of the two-leg Heisenberg spin 1/2 ladder. Up to leg-couplings $\lambda \lesssim 1$, the standard gCUT scheme gives proper results. However, for larger values of λ, the obtained results become erratic due to pseudo decay. By contrast, the results obtained via the modified gCUT scheme are completely cured from any finite cluster artifacts. A comparison of our results to deepCUT [47] and CORE [96] clearly indicates, that

the gCUT method becomes compatible even in the previously inaccessible parameter regime. Furthermore, the modified gCUT scheme is applied to determine one-triplon dispersion for $\lambda = 5.0$. The resulting one-triplon dispersion is robust and in full agreement with corresponding dynamic structure factors obtained via DMRG [157]. To conclude, even in the regime of large leg-couplings, the new approach yields robust and proper results, demonstrating the validity of the approach. The uncertainty induced by the elimination process is negligible in these cases.

4.5.4 Quantum criticality

The optimized gCUT scheme allows to treat systems close to or even at quantum criticality. At quantum criticality, one generically expects pseudo decay since the multi-particle continua become energetically extremely close, which is also reflected by the physics of the finite cluster. A large number of states merges with the low-energy spectrum and the optimized gCUT scheme allows to treat this behavior in principle. However, it becomes difficult to distinguish between possibly defective interactions and genuine interactions relying on energetic considerations (Eq.(4.18)). In these cases, the approach can be made more robust by additionally regarding momentum-related considerations (Eq.(4.28)).
To investigate the modified gCUT scheme at quantum phase transitions, we investigate the one-triplon dispersion of the dimerized Heisenberg chain. At quantum criticality, the obtained one-triplon dispersion is surprisingly close to the exactly known dispersion. This supports the general treatment of pseudo decay. Still, one observes a noticeable uncertainty of the approach as illustrated by the comparison of different basis truncation parameters. While such effects are expected, other criteria, which render the approach more robust, even at quantum criticality, are desirable for future applications.
Of special interest close to or at quantum criticality is the excitation gap. Critical behavior is associated with a divergence of the correlation length $\xi \to \infty$ and one must rely on extrapolation techniques to obtain gapless behavior. Yet, in current literature, only few extrapolation techniques for NLCEs exist and no extrapolation scheme providing critical exponents exists so far. We introduce a novel scheme to extrapolate the results obtained via NLCEs and related numerical techniques giving access to critical points and critical exponents. The applicability of the extrapolation scheme is tested for the one-triplon gap of the dimerized Heisenberg chain with a known critical exponent $\nu = 2/3$. The extrapolation scheme is applied to the one-triplon gap yielding critical exponents, which are indeed in good agreement with the actual value. This result supports the validity of the new extrapolation technique.

4.5.5 Genuine decay

To treat quasiparticle decay, one cannot rely on the reduced weights suited to detect pseudo decay. Instead, the spectral weights of (anti-)symmetrized observables are applied to identify the proper low-energy states during the CUT. Interactions which are considered to lead to quasiparticle decay are not integrated out and are part of the effective description. These terms are regarded in a subsequent evaluation process of the coupled quasiparticle sectors and describe the quasiparticle decay in the thermodynamic limit, similar to the approach introduced by Fischer and Uhrig [33].
However, in contrast to the latter, the CUT is performed on finite clusters and not in operator space. Another conceptual difference is that the matrix elements between the one- and two-particle sector are included in the CUT and all states which do not overlap energetically are

separated by the transformation. Here, the energetic overlap refers to intermediate points of the continuous renormalization process defined by the flow-parameter ℓ. Due to the structure of the underlying CUT, this allows to distinguish between large and small interactions. As a result, the approach is designed to describe systems where the one-particle mode decays inside the continuum and the opposite scenario where the quasiparticle mode is depressed by the continuum.
We apply the modified gCUT scheme to the four-leg spin 1/2 Heisenberg ladder to demonstrate the possibility to treat quasiparticle decay within an NLCE approach. An effective description in terms of triplons is derived to determine the dynamic structure factor up to two triplons. Generically, one observes quasiparticle decay of the one-triplon mode in the symmetric channel while the one-triplon dispersion in the anti-symmetric channel is depressed by the two-triplon continuum. Both cases are captured by our approach and even in challenging parameter regimes, the method gives reasonable and consistent results.
While the low-energy spectrum of the isotropic open four-leg is inaccessible to standard (N)LCE schemes, our modified approach provides an interpretation in terms of (decaying) triplons and two-triplon bound states. These predictions are relevant for neutron scattering experiments of the compound $La_2Cu_2O_5$.
Overall, we conclude, that considerable progress has been achieved for gCUTs and NLCEs in general. There is potential for improvement with respect to the elimination processes in the treatment of both pseudo and genuine decay. Still, substantial understanding of both phenomena, pseudo and genuine decay, is gained and modified versions of gCUTs provide valid results for systems inaccessible by standard NLCEs.

Chapter 5

Conclusion and outlook

In this section, we revise the investigations considered this thesis and provide an outlook for future studies. The main focus of this thesis is the further development of two methods suited to derive effective low-energy Hamiltonians. The approaches can be viewed as a combination of LCEs with CUTs and NLCEs with CUTs, respectively. A generic aspect of these developments is the exploitation of properties provided by the CUT approach on the cluster. Moreover, both modifications can also be understood as a change of perspective. The calculation on finite clusters is considered in the context of the determination of the effective system in the thermodynamic limit.
For linked-cluster expansions, this leads to a reordering of the calculation process where the calculation on finite clusters is kept rather general to extract as much information as possible from a single cluster calculation. Our approach is specifically useful when the microscopic model under consideration has several expansion parameters. This case usually represents a major challenge for any kind of linked-cluster expansion, due to the proliferating number of linked graphs, as each expansion parameter corresponds to a distinct color in the graph expansion. The white-graph expansion overcomes this challenge to a great extent, since the actual calculation is performed on white graphs and the *coloring* is done after the calculation as a final step in the embedding procedure.
This is especially relevant for the comparison with experimental data where typically different coupling strengths are important and have to be determined [117]. This also includes demanding frustrated systems in three dimensions with multiple couplings [200]. In addition to that, the white-graph expansion opens up a new perspective of the applicability of high-order series expansions. If the couplings of the calculation can be easily matched with the couplings of the lattice, it is suggestive to apply white-graph expansions to systems with disorder, for instance by embedding the white graphs into (large) finite systems and an evaluation of the resulting effective model similar to the bond-operator approach in [201]. Moreover, one can apply the white-graph expansion to systems with long-range interactions [202] being notoriously complicated for linked-cluster expansions. In both cases, similar to calculations in d dimensions [92], the actual challenge of the calculation is expected to shift away from the calculation of the graphs and towards the embedding procedure.
The white-graph expansion relates ultimately to the efficiency of the approach. For the non-perturbative counterpart called gCUT, more fundamental challenges are addressed. Since gCUTs are both a non-perturbative CUTs with a finite cluster truncation and an NLCEs relying on a CUT for the finite cluster results, the challenges of gCUTs concern both classes of methods. One issue present for both classes of methods is the lack of a strong extrapolation scheme similar to high-order series expansions providing critical exponents. In this thesis, we introduce a novel scheme to extrapolate the results obtained via NLCEs and related numerical techniques. While the mapping of the data sequences to a series in a pseudo parameter changes the perspective, our approach is specifically designed to describe systems close to or even at criticality. Most

importantly, the scheme allows to extract critical exponents, providing both classes of methods with a key to these fundamental physical quantities.
A transfer to other NLCE schemes, for instance to determine the entanglement entropy [65], is straight forward. The determination of critical exponents would be specifically interesting for the determination of possibly new universality classes for systems not described by Landau's theory similar to [90]. In addition to that, it is appealing to investigate if these considerations can be translated to time-dependent properties calculated via NLCEs [66] or many-body (de)localization [68].
The central issue addressed in this thesis concerns the proper derivation of effective low-energy models. It is not as obvious as it may seem to identify the adequate low-energy model for a given truncation. As the name already indicates, the effective models are designed to describe the low-energy part of the spectrum. Consequently, in the standard NLCE approach, the low-energy parts of the system should form the effective description on the clusters which are then combined to define the effective model in the thermodynamic limit.
As a guiding principle, this approach is well-justified, yet, subtleties arise when the low-energy part of the system overlaps energetically with the remainder. The rigorous sorting property of the quasiparticle generator in the CUT follows exactly this standard notion and leads to unphysical effects resulting in a breakdown of the approach. In gCUTs, we have identified two quite distinct scenarios in which such an overlap can occur:
i) the energetic overlap is just an artifact of the broken translational symmetry of the finite clusters and
ii) the energetic overlap corresponds to an energetic overlap also present in the thermodynamic limit.
We have implemented two modified gCUT schemes which are suited to treat both cases adequately. In the case of energetic overlap, the issue of the proper low-energy model should *not* be answered by energetic considerations alone. In these cases, it is advisable to define reasonable quantities which help to identify the correct low-energy physics. Naturally, the effective low-energy model cannot be derived relying solely on these additional quantities and both aspects must be reconciled.
This challenge is at least partly solved by the CUT itself. In CUTs, the transformation is defined by a continuous flow parameter ℓ. With increasing values of ℓ, the initial system ($\ell = 0$) is transformed continuously into the effective description ($\ell = \infty$). Up to intermediate values of ℓ, the CUT is performed using the standard scheme relying on energetic considerations only; for larger values of ℓ, additional considerations are taken into account.
The issue of energetic overlap in the effective description relates to all non-perturbative methods suited to derive effective low-energy models. This effect observed in gCUTs can be viewed as a finite-cluster correspondence to divergencies which represent a fundamental challenge for other CUT approaches [33, 102]. It seems reasonable to assume that these issues concern possibly all non-perturbative derivations of effective low-energy models. Possibly, the underlying central notions constituted in this thesis can function as a platform for further CUT developments.
It should be noted that the occurrence of quasiparticle decay and the renormalization effects are of ongoing experimental interest [21, 24–26, 203, 204], affirming the importance of our developments.
Moreover, effective models are widely used in various fields of quantum physics [205–207], and their derivation often suffers from the appearance of intruder states in the low-energy spectrum which may cause either discontinuities or spurious behaviors [208, 209]. Thus, our algorithm might also be used in different fields, for instance quantum chemistry, in order to produce continuous physical results.
Finally, we want to stress the conceptual issues associated with pseudo decay. Our findings

are clearly important in a much more general manner, since the same kind of problem is expected to arise for any separation of degrees of freedom like for many-particle excitations, dynamical correlation functions, or the derivation of effective low-energy models using clusters with reduced symmetry, as done in any NLCE, CORE, or gCUT calculation. This applies e.g. to the derivation of effective spin models in the Mott phase of Hubbard models separating charge and spin degrees of freedom [63, 64].
It might be worth investigating whether similar problems are also present in high-temperature or non-equilibrium NLCEs as well as in cluster dynamical mean-field theory which all break translational symmetry on clusters. An NLCE study performed to determine the ground-state energy indicates similar finite cluster artifacts present even for such a well-defined quantity [126].
This thesis reveals not only challenges of NLCEs but also a central advantage of NLCE approaches over purely perturbative LCE approaches. While the final results obtained via high-order series expansions are unique, non-perturbative results are not. This allows an additional control over the results, making the approach more versatile. We believe that this freedom should be used in the future.

Appendix A

Appendix

A.1 Extracting the cluster additive quantities

It is physically intuitive to decompose the Hamilton operator $\mathcal{H}_{\text{eff}}$ as

$$\mathcal{H}_{\text{eff}} = \mathcal{H}_0 + \mathcal{H}_1 + \mathcal{H}_2 + \mathcal{H}_3 + \ldots, \tag{A.1}$$

where $\mathcal{H}_n$ is an n-particle irreducible operator. In the notation of the second quantization, the operators in real space read

$$\mathcal{H}_0 := E_0 \mathbb{1} \tag{A.2}$$

$$\mathcal{H}_1 := \sum_{i,j,\alpha,\beta} \tilde{a}_{i,j}^{\alpha\beta}(\lambda)\, \hat{\tilde{f}}_{i,\alpha}^{\dagger} \hat{\tilde{f}}_{j,\beta} \tag{A.3}$$

$$\mathcal{H}_2 := \sum_{i_1,i_2,j_1,j_2,\alpha_1,\alpha_2,\beta_1,\beta_2} \tilde{a}_{i_1,i_2,j_1,j_2}^{\alpha_1,\alpha_2,\beta_1,\beta_2}(\lambda)\, \hat{\tilde{f}}_{i_1,\alpha_1}^{\dagger} \hat{\tilde{f}}_{i_2,\alpha_2}^{\dagger} \hat{\tilde{f}}_{j_1,\beta_1} \hat{\tilde{f}}_{j_2,\beta_2} \tag{A.4}$$

$$\vdots \tag{A.5}$$

$$\mathcal{H}_n := \sum_{i_1\ldots i_n,j_1\ldots j_n,\alpha_1\ldots\alpha_n,\beta_1\ldots\beta_n} \tilde{a}_{i_1\ldots i_n,j_1\ldots j_n}^{\alpha_1\ldots\alpha_n,\beta_1\ldots\beta_n}(\lambda)\, \hat{\tilde{f}}_{i_1,\alpha_1}^{\dagger} \ldots \hat{\tilde{f}}_{i_n,\alpha_n}^{\dagger} \hat{\tilde{f}}_{j_1,\beta_1} \ldots \hat{\tilde{f}}_{j_n,\beta_n} \quad , \tag{A.6}$$

where $\mathbb{1}$ is the identity operator. The local operator $\hat{\tilde{f}}_{i,\alpha}^{\dagger}$ ($\hat{\tilde{f}}_{i,\alpha}$) creates (annihilates) a particle of flavor α at site i. Assuming $\mathcal{H}_{\text{eff}}$ is cluster additive, the reducible operators are also cluster additive:

$$\mathcal{H}_n^C = \mathcal{H}_n^A \otimes \mathbb{1}^B + \mathbb{1}^A \otimes \mathcal{H}_n^B \quad . \tag{A.7}$$

The operators directly accessible via the calculation on the cluster are, by contrast, not in the normal-ordered form Eq.(A.6) but are given as matrix elements of $\mathcal{H}_{\text{eff}}$. Let $M|_n$ denote that the operator M is restricted to the n-particle space. The elements extracted from the calculations on a single cluster are given by $\mathcal{H}_{\text{eff}}|_n$ as the matrix elements of $\mathcal{H}_{\text{eff}}$ in the n-particle subspace. The equation

$$\mathcal{H}_{\text{eff}}^C|_n = \mathcal{H}_{\text{eff}}^A|_n \otimes \mathbb{1}^B + \mathbb{1}^A \otimes \mathcal{H}_{\text{eff}}^B|_n \tag{A.8}$$

cannot be fulfilled, since the number of particles to which the identities $\mathbb{1}^A$ and $\mathbb{1}^B$ are applied is not fixed, i.e., $\mathcal{H}_{\text{eff}}|_n$ is *not* cluster additive. In this sense, the notation in second quantization is mandatory for the concept of cluster additivity and a proper normal ordering is imperative:

$$\mathcal{H}_0|_0 := \mathcal{H}_{\text{eff}}|_0$$

$$\mathcal{H}_1|_1 := \mathcal{H}_{\text{eff}}|_1 - \mathcal{H}_0|_1$$
$$\mathcal{H}_2|_2 := \mathcal{H}_{\text{eff}}|_2 - \mathcal{H}_0|_2 - H_1|_2$$
$$\vdots \tag{A.9}$$
$$\mathcal{H}_n|_n := \mathcal{H}_{\text{eff}}|_n - \sum_{i=0}^{n-1} H_i|_n \quad . \tag{A.10}$$

For $\mathcal{H}_n$, all the contributions of $\mathcal{H}_{\text{eff}}$ coming from the action on m particles ($m < n$) are subtracted and hence $\mathcal{H}_n|_m$ vanishes.

A.2 Contractor renormalization group

In this section, we give a brief discussion on the contractor-renormalization group (CORE) technique, specifically with respect to the cluster additivity. CORE was first introduced bei Morningstar and Weinstein in 1996 [210]. The essential idea of CORE is to derive an effective Hamiltonian that reproduces the low-energy spectrum of the original Hamiltonian. While the CORE approach can be used analytically, CORE can also be used as a sophisticated numerical tool [63, 95, 96, 211].
Similar to gCUT, the method is applied on finite clusters to determine an effective cluster-dependent Hamiltonian. These exact effective Hamiltonians are combined to define the effective description in the thermodynamic limit.
The numerical CORE method has been used mainly for effective low-energy descriptions or range-N interactions as outlined in Ref.[96]. Here, we discuss how CORE can be exploited to derive effective quasiparticle descriptions. The derivation of the effective particle Hamiltonians is achieved by modifying the CORE-algorithm outlined in Ref. [96] :

- Choose a small cluster (e.g., rung, plaquette, triangle, etc.) and diagonalize it. These small clusters build the effective sites of the quasiparticle picture. The lowest state of these effective sites is referred to as the vacuum while the excitations are identified with the quasiparticles (see also 2.1).

- For each connected clusters C consisting of N supersites obtain the low-energy spectrum of the full Hamiltonian $\mathcal{H}^C$ (the low-energy states $|i\rangle$ with eigenenergies ε_i).

- The eigenstates are projected on the subspace with dimension $d = N$ consisting of the tensor product states having one excitation only: $|\tilde{i}\rangle = \hat{P}_1|i\rangle$. The states are orthonormalized $|\tilde{i}\rangle \rightarrow |\tilde{i}_\perp\rangle$. The orthonormalized states define a basis of dimension d. It may happen that some of the eigenstates have a small projection or vanish after the orthogonalization it might be necessary to explicitly compute more than just the lowest d eigenstates.

- Next, the effective Hamiltonian for this cluster is built as

$$h_{\text{eff}}^C = \sum_{i \leq d} (\varepsilon_i - \varepsilon_0) |\tilde{i}_\perp\rangle\langle\tilde{i}_\perp|, \tag{A.11}$$

  where ε_0 is the ground-state energy of the system on cluster C. The Hamiltonian yields the one-particle hopping elements since the $|\tilde{i}_\perp\rangle$ only consist of one-particle states.

- Determine the reduced contributions of the cluster by subtracting the reduced contributions of all connected subclusters:

$$\hat{h}_{\mathcal{C}} = \hat{\tilde{h}}_{\mathcal{C}} - \sum_{\mathcal{C}_{\text{sub}}} \hat{h}_{\mathcal{C}_{\text{sub}}} \tag{A.12}$$

$$\tag{A.13}$$

- Finally, the effective Hamiltonian and the effective observable are given by a cluster expansion

$$H_{\text{eff}}^{\text{CORE}} = \sum_{\mathcal{C}} \hat{h}_{\mathcal{C}}$$

  where the sum runs over all clusters $\mathcal{C}$ of the lattice. The sum implies that all the operator coefficients are added up defining the effective Hamiltonian in the thermodynamic limit

It is essential that the effective Hamiltonian h_{eff}^{N} obeys the so-called cluster additivity. In the following, we argue that the CORE method in general does *not* yield a cluster additive effective Hamiltonian. Let us consider a disconnected cluster $C = A \cup B$ with $A \cap B = \emptyset$. By construction, the initial Hamiltonian is given by the cluster additive form in the form

$$\mathcal{H} = \mathcal{H}^A \otimes \mathbb{1}^B + \mathbb{1}^A \otimes \mathcal{H}^B. \tag{A.14}$$

We investigate, if the resulting effective Hamiltonian can also be written in a cluster additive form. First, we discuss the cluster additivity for standard CORE applications for deriving range-N interactions. Afterwards, we investigate the cluster additivity for the derivation of an effective quasi-particle description.

A.2.1 Low-energy descriptions

CORE is often applied to determine range-N interactions. Here, the first m states of a supersite are considered to be relevant for the low-energy physics. Consequently, the projection $\hat{P}$ projects on the subspace spanned by the truncated Hilbert space of dimension m^N, where N is the number of supersites on the considered cluster. A prototypical example for this is the derivation of an effective spin model starting from a Hubbard model. The projected low-energy states are the states without double occupancy defining a truncated Hilbert space. The resulting effective description corresponds to an effective spin model.
The eigenfunctions and eigenvalues of $\mathcal{H}^A$ ($\mathcal{H}^B$) are given by

$$\mathcal{H}^A|i\rangle_A = \varepsilon_{i,A}|i\rangle_A \tag{A.15}$$

$$\mathcal{H}^B|j\rangle_B = \varepsilon_{j,B}|j\rangle_B \quad . \tag{A.16}$$

The eigenfunctions of the full Hamiltonian $\mathcal{H}$ are given by the product states

$$\mathcal{H}|i\rangle_A|j\rangle_B = (\varepsilon_{i,A} + \varepsilon_{j,B})|i\rangle_A|j\rangle_B \quad , \tag{A.17}$$

and one finds

$$\hat{P}|i\rangle_A = |\tilde{i}\rangle_A \tag{A.18}$$

$$\hat{P}|j\rangle_B = |\tilde{j}\rangle_B \tag{A.19}$$

$$\hat{P}|i\rangle_A|j\rangle_B = |\tilde{i}\rangle_A|\tilde{j}\rangle_B. \tag{A.20}$$

Finally, these state are orthonormalized. This is done using Gram Schmidt orthonormalization and the order of the procedure is determined by the eigenenergies of the states starting with the lowest. The orthogonalization method should fulfill the following constraint: If the orthogonalized states on the single cluster A (B) be given by

$$|\tilde{i}\rangle_A \to |\tilde{i}_\perp\rangle_A \tag{A.21}$$

$$|\tilde{j}\rangle_B \to |\tilde{j}_\perp\rangle_B \quad , \tag{A.22}$$

then the orthogonalized states on the disconnected cluster should be given by

$$|\tilde{i}\rangle_A|\tilde{j}\rangle_B \to |\tilde{i}_\perp\rangle_A|\tilde{j}_\perp\rangle_B. \tag{A.23}$$

In Gram Schmidt, the eigenenergies are successively orthonormalized in ascending order with the energy. We believe that this step might violate the cluster additivity because the order of the procedure depends on the *sum* of both systems, which links two disconnected clusters. We consider scenario where an infinitesimal tuning of λ changes the order of two pairs:

$$\varepsilon_{i1,A}(\lambda) + \varepsilon_{j1,B}(\lambda) < \varepsilon_{i2,A}(\lambda) + \varepsilon_{j2,B}(\lambda) \tag{A.24}$$

$$\varepsilon_{i1,A}(\lambda+\delta_\lambda) + \varepsilon_{j1,B}(\lambda+\delta_\lambda) > \varepsilon_{i2,A}(\lambda+\delta_\lambda) + \varepsilon_{j2,B}(\lambda+\delta_\lambda) \tag{A.25}$$

Consequently, the resulting effective Hamiltonian derived on cluster C changes discontinuously while the effective Hamiltonian derived only on cluster A (B) is not affected. This indicates, that, in a rigorous sense, the cluster addivitiy might be violated. We stress, that the states are almost orthogonal before the orthogonalization process, suggesting, that the effect of the orthonormalization procedure is rather small. However, we believe that this issue can be solved by using overlap matrices to orthogonalize the respective states. For this procedure, one has to calculate the overlap matrix defined by

$$S_{i,j} = \langle i|j\rangle.$$

The orthogonal states are given by

$$|i_\perp\rangle = S_{i,j}^{-\frac{1}{2}}|j\rangle$$

In the case of the disconnected clusters, the overlap matrix is given by

$$S = S^A \otimes S^B \tag{A.26}$$

and the inverse matrix (and its square root) are given by

$$S^{-1} = (S^A)^{-1} \otimes (S^B)^{-1} \tag{A.27}$$

$$S^{-\frac{1}{2}} = (S^A)^{-\frac{1}{2}} \otimes (S^B)^{-\frac{1}{2}} \tag{A.28}$$

$$\tag{A.29}$$

and, thus, applying $S^{-\frac{1}{2}}$ yields

$$|\tilde{i}\rangle_A|\tilde{j}\rangle_B \to |\tilde{i}_\perp\rangle_A|\tilde{j}_\perp\rangle_B \quad . \tag{A.30}$$

Then, the effective Hamiltonian reads

$$\begin{aligned} H_{\text{eff}} &= \sum_{i,j} \left(\varepsilon_{i,A} + \varepsilon_{j,B}\right) |\tilde{i}_\perp\rangle_A |\tilde{j}_\perp\rangle_B \langle\tilde{i}_\perp|_A \langle\tilde{j}_\perp|_B \\ &= \sum_i \varepsilon_{i,A} |\tilde{i}_\perp\rangle_A \langle\tilde{i}_\perp|_A \mathbb{1}_B^{\text{sub}} + \sum_j \varepsilon_{j,B} |\tilde{j}_\perp\rangle_B \langle\tilde{j}_\perp|_B \mathbb{1}_A^{\text{sub}} \end{aligned}$$

with $\mathbb{1}_B^{\text{sub}} = \sum_j |\tilde{j}_\perp\rangle_B \langle\tilde{j}_\perp|_B$ and $\mathbb{1}_A^{\text{sub}} = \sum_i |\tilde{i}_\perp\rangle_B \langle\tilde{i}_\perp|_A$ which is the identity in the considered subspace. Hence, this is the desired cluster additive form. Next, we discuss the cluster additvity for effective quasiparticle descriptions.

A.2.2 Quasiparticle description

For the sake of simplicity, the investigation is restricted to the derivation of one-particle dispersions and a generalization is straightforward.
We consider a system with a unique ground state

$$\mathcal{H}^A |0\rangle_A = \varepsilon_{0,A} |0\rangle_A \tag{A.31}$$

$$\mathcal{H}^B |0\rangle_B = \varepsilon_{0,B} |0\rangle_B \tag{A.32}$$

$$\mathcal{H} |0\rangle_A |0\rangle_B = (\varepsilon_{0,A} + \varepsilon_{0,B}) |0\rangle_A |0\rangle_B. \tag{A.33}$$

For $\lambda = 0$ the ground state can be viewed as a vacuum and excitations can correspondingly be interpreted in terms of quasiparticles. Let the spectrum of the Hamiltonian $\mathcal{H}_0^A$ ($\mathcal{H}_0^B$) contain N (M) lowest degenerate excitations, namely the quasiparticles, which are (for sufficiently small values of λ) associated with the lowest excitations of the full Hamiltonian

$$\mathcal{H}^A |i\rangle_A = \varepsilon_{i,A} |0\rangle_A, \quad i = 1, \ldots, N \tag{A.34}$$

$$(\mathcal{H}^B |j\rangle_B = \varepsilon_{j,B} |j\rangle_B, \quad j = 1, \ldots, M) \tag{A.35}$$

The relevant $N + M$ low-energy states of the whole system are then given by

$$\mathcal{H} |i\rangle_A |0\rangle_B = (\varepsilon_{i,A} + \varepsilon_{0,B}) |i\rangle_A |0\rangle_B \quad i = 1, \ldots, N \tag{A.36}$$

$$\mathcal{H} |0\rangle_A |j\rangle_B = (\varepsilon_{0,A} + \varepsilon_{j,B}) |0\rangle_A |j\rangle_B \quad j = 1, \ldots, M \quad . \tag{A.37}$$

The action of the projector a critical part of the procedure. Let $\hat{P}_0$ denote the projector on the $\lambda = 0$ ground state and $\hat{P}_1$ is correspondingly the projector on the first excited states of $\mathcal{H}_0$. With these definitions the projection on the combined cluster is given by

$$\hat{P}_1 |i\rangle_A |0\rangle_B = (\hat{P}_1 |i\rangle_A)(\hat{P}_0 |0\rangle_B) + (\hat{P}_0 |i\rangle_A)(\hat{P}_1 |0\rangle_B) \tag{A.38}$$

$$\hat{P}_1 |0\rangle_A |j\rangle_B = (\hat{P}_1 |0\rangle_A)(\hat{P}_0 |j\rangle_B) + (\hat{P}_0 |0\rangle_A)(\hat{P}_1 |j\rangle_B). \tag{A.39}$$

To obtain a cluster additive Hamiltonian, $\hat{P}_0 |i\rangle_A$ ($\hat{P}_0 |j\rangle_B$) or $\hat{P}_1 |0\rangle_A$ ($\hat{P}_1 |0\rangle_B$) have to vanish. If the excited states are separated by a quantum number from the ground state, this is indeed true. In the scope of this thesis, CORE-data for the one-triplon dispersion of the two-leg spin 1/2 Heisenberg ladder are compared to gCUT data. Here, the one-triplon states ($S = 1$) a protected from the vacuum ($S = 0$) by the total spin S. We stress that the cluster additivity is violated if this is not the case.
If the states $|i\rangle_A |0\rangle$ and $|0\rangle_A |j\rangle_B$ are separated by the quantum numbers defined for each cluster A and B, it is easily shown that the Gram Schmidt orthogonalization yields

$$|\tilde{i}\rangle_A |\tilde{0}\rangle_B \to |\tilde{i}_\perp\rangle_A |\tilde{0}\rangle_B \tag{A.40}$$

$$|\tilde{0}\rangle_A|\tilde{j}\rangle_B \rightarrow |\tilde{0}_\perp\rangle_A|\tilde{j}_\perp\rangle_B \tag{A.41}$$

and the effective Hamiltonian reads (including the subtraction of the ground-state energy)

$$\mathcal{H}^{\mathrm{CORE}} = \sum_{i\leq N}(\varepsilon_{i,A}-\varepsilon_{0,A})|\tilde{i}_\perp\rangle_A\langle\tilde{i}_\perp|_A|\tilde{0}_\perp\rangle_B\langle\tilde{0}_\perp|_B \tag{A.42}$$

$$+\sum_{j\leq M}(\varepsilon_{j,B}-\varepsilon_{0,B})|\tilde{j}_\perp\rangle_B\langle\tilde{j}_\perp|_B|\tilde{0}_\perp\rangle_A\langle\tilde{0}_\perp|_A \quad , \tag{A.43}$$

which is the desired form.

Bibliography

[1] L.D. Landau. The Theory of a Fermi Liquid. *SOVIET PHYSICS JETP*, 3, January 1957.

[2] A. J. Schofield. Non-Fermi liquids. *Contemporary Physics*, 40:95–115, feb 1999.

[3] E G Brovman and Yurii M Kagan. Phonons in nontransition metals. *Soviet Physics Uspekhi*, 17(2):125, 1974.

[4] F. Schwabl, R. Hilton, and A. Lahee. *Advanced Quantum Mechanics*. Advanced Texts in Physics Series. Springer Berlin Heidelberg, 2008.

[5] S. W. Koch, M. Kira, G. Khitrova, and H. M. Gibbs. Semiconductor excitons in new light. *Nature Materials*, 5:523–531, 2006.

[6] T. Holstein and H. Primakoff. Field Dependence of the Intrinsic Domain Magnetization of a Ferromagnet. *Phys. Rev.*, 58:1098–1113, Dec 1940.

[7] Freeman J. Dyson. General Theory of Spin-Wave Interactions. *Phys. Rev.*, 102:1217–1230, Jun 1956.

[8] Chubukov A. V. A difference in the properties of one-dimensional antiferromagnets with integer and half-integer spins. *JETP Lett.*, 49:129, January 1989.

[9] Subir Sachdev and R. N. Bhatt. Bond-operator representation of quantum spins: Mean-field theory of frustrated quantum Heisenberg antiferromagnets. *Phys. Rev. B*, 41:9323–9329, May 1990.

[10] Kai P. Schmidt and Götz S. Uhrig. Excitations in One-Dimensional $S = \frac{1}{2}$ Quantum Antiferromagnets. *Phys. Rev. Lett.*, 90:227204, Jun 2003.

[11] J. Schlappa, K. Wohlfeld, K. J. Zhou, M. Mourigal, M. W. Haverkort, V. N. Strocov, L. Hozoi, S. Nishimoto, A. Singh, S. Revcolevschi, J.-S. Caux, L. Patthey, H. M. Ronnow, J. van den Brink, and T. Schmitt. Spin-orbital separation in the quasi-one-dimensional Mott insulator Sr_2CuO_3 . *Nature*, 485:82–85, 2012.

[12] Jindřich Kolorenč and Lubos Mitas. Applications of quantum monte carlo methods in condensed systems. *Reports on Progress in Physics*, 74(2):026502, 2011.

[13] Brian M. Austin, Dmitry Yu. Zubarev, and Jr. William A. Lester. Quantum monte carlo and related approaches. *Chemical Reviews*, 112(1):263–288, 2012. PMID: 22196085.

[14] Steven R. White. Density matrix formulation for quantum renormalization groups. *Phys. Rev. Lett.*, 69:2863–2866, Nov 1992.

[15] L. P. Pitaevskii. Phenomenological theory of superfluidity near the λ point. *Zh. Eksp. Teor. Fiz.*, 35:408–415, 1958.

[16] A J Smith, R A Cowley, A D B Woods, W G Stirling, and P Martel. Roton-roton interactions and excitations in superfluid helium at large wavevectors. *Journal of Physics C: Solid State Physics*, 10(4):543, 1977.

[17] H. R. Glyde, M. R. Gibbs, W. G. Stirling, and M. A. Adams. Excitations in superfluid 4 He beyond the roton. *EPL (Europhysics Letters)*, 43(4):422, 1998.

[18] Shaolong Ma, Collin Broholm, Daniel H. Reich, B. J. Sternlieb, and R. W. Erwin. Dominance of long-lived excitations in the antiferromagnetic spin-1 chain NENP. *Phys. Rev. Lett.*, 69:3571–3574, Dec 1992.

[19] I. A. Zaliznyak, S.-H. Lee, and S. V. Petrov. Continuum in the Spin-Excitation Spectrum of a Haldane Chain Observed by Neutron Scattering in $CsNiCl_3$. *Phys. Rev. Lett.*, 87:017202, Jun 2001.

[20] T. Masuda, A. Zheludev, H. Manaka, L.-P. Regnault, J.-H. Chung, and Y. Qiu. Dynamics of Composite Haldane Spin Chains in IPA-$CuCl_3$. *Phys. Rev. Lett.*, 96:047210, Feb 2006.

[21] Neil J. Robinson, Fabian H. L. Essler, Ivelisse Cabrera, and Radu Coldea. Quasiparticle breakdown in the quasi-one-dimensional Ising ferromagnet $CoNb_2O_6$. *Phys. Rev. B*, 90:174406, Nov 2014.

[22] Matthew B. Stone, Igor A. Zaliznyak, Tao Hong, Collin L. Broholm, and Daniel H. Reich. Quasiparticle breakdown in a quantum spin liquid. *Nature*, 440:187–190, 2006.

[23] T. Masuda, S. Kitaoka, S. Takamizawa, N. Metoki, K. Kaneko, K. C. Rule, K. Kiefer, H. Manaka, and H. Nojiri. Instability of magnons in two-dimensional antiferromagnets at high magnetic fields. *Phys. Rev. B*, 81:100402, Mar 2010.

[24] Joosung Oh, Manh Duc Le, Jaehong Jeong, Jung-hyun Lee, Hyungje Woo, Wan-Young Song, T. G. Perring, W. J. L. Buyers, S.-W. Cheong, and Je-Geun Park. Magnon Breakdown in a Two Dimensional Triangular Lattice Heisenberg Antiferromagnet of Multiferroic $LuMnO_3$. *Phys. Rev. Lett.*, 111:257202, Dec 2013.

[25] K. W. Plumb, Kyusung Hwang, Y. Qiu, Leland W. Harriger, G. E. Granroth, Alexander I. Kolesnikov, G. J. Shu, F. C. Chou, Ch. Ruegg, Yong Baek Kim, and Young-June Kim. Quasiparticle-continuum level repulsion in a quantum magnet. *Nat. Phys.*, 2015.

[26] J. Ma, Y. Kamiya, T. Hong, H. B. Cao, G. Ehlers, W. Tian, C. D. Batista, Z. L. Dun, H. D. Zhou, and M. Matsuda. Static and Dynamical Properties of the Spin-1/2 Equilateral Triangular-Lattice Antiferromagnet Ba_3CoSb_2O_9. *ArXiv e-prints*, July 2015.

[27] Alexei Kolezhuk and Subir Sachdev. Magnon Decay in Gapped Quantum Spin Systems. *Phys. Rev. Lett.*, 96:087203, Mar 2006.

[28] M. E. Zhitomirsky. Decay of quasiparticles in quantum spin liquids. *Phys. Rev. B*, 73:100404, Mar 2006.

[29] Tim Fischer. *Description of quasiparticle decay by continuous unitary transformations.* PhD thesis, TU Dortmund, 2011.

[30] A. L. Chernyshev and M. E. Zhitomirsky. Spin waves in a triangular lattice antiferromagnet: Decays, spectrum renormalization, and singularities. *Phys. Rev. B*, 79:144416, Apr 2009.

[31] M. Mourigal, W. T. Fuhrman, A. L. Chernyshev, and M. E. Zhitomirsky. Dynamical structure factor of the triangular-lattice antiferromagnet. *Phys. Rev. B*, 88:094407, Sep 2013.

[32] P. N. Bibikov. Magnon mode truncation in a rung-dimerized asymmetric spin ladder. *Phys. Rev. B*, 76:174431, Nov 2007.

[33] T. Fischer, S. Duffe, and G. S. Uhrig. Microscopic model for Bose-Einstein condensation and quasiparticle decay. *EPL (Europhysics Letters)*, 96(4):47001, 2011.

[34] Andreas Lüscher and Andreas M. Läuchli. Exact diagonalization study of the antiferromagnetic spin-$\frac{1}{2}$ Heisenberg model on the square lattice in a magnetic field. *Phys. Rev. B*, 79:195102, May 2009.

[35] Olav F. Syljuåsen. Numerical evidence for unstable magnons at high fields in the Heisenberg antiferromagnet on the square lattice. *Phys. Rev. B*, 78:180413, Nov 2008.

[36] Weihong Zheng, John O. Fjærestad, Rajiv R. P. Singh, Ross H. McKenzie, and Radu Coldea. Anomalous excitation spectra of frustrated quantum antiferromagnets. *Phys. Rev. Lett.*, 96:057201, Feb 2006.

[37] Weihong Zheng, John O. Fjærestad, Rajiv R. P. Singh, Ross H. McKenzie, and Radu Coldea. Excitation spectra of the spin-$\frac{1}{2}$ triangular-lattice Heisenberg antiferromagnet. *Phys. Rev. B*, 74:224420, Dec 2006.

[38] F. Wegener. Flow-equations for Hamiltonians. *Annalen der Physik*, 506:77–91, 1994.

[39] C. Knetter and G.S. Uhrig. Perturbation theory by flow equations: dimerized and frustrated $S = 1/2$ chain. *Eur. Phys. J. B*, 13(2):209–225, 2000.

[40] Christian Knetter, Alexander Bühler, Erwin Müller-Hartmann, and Götz S. Uhrig. Dispersion and Symmetry of Bound States in the Shastry-Sutherland Model. *Phys. Rev. Lett.*, 85:3958–3961, Oct 2000.

[41] Christian Knetter and Götz S. Uhrig. Triplet dispersion in $CuGeO_3$: Perturbative analysis. *Phys. Rev. B*, 63:094401, Jan 2001.

[42] C. Knetter, K.P. Schmidt, and G.S. Uhrig. High order perturbation theory for spectral densities of multi-particle excitations: S = 1/2 two-leg Heisenberg ladder. *The European Physical Journal B - Condensed Matter and Complex Systems*, 36(4):525–544, 2003.

[43] Christian Knetter and Götz S. Uhrig. Dynamic Structure Factor of the Two-Dimensional Shastry-Sutherland Model. *Phys. Rev. Lett.*, 92:027204, Jan 2004.

[44] Alexander Reischl, Erwin Müller-Hartmann, and Götz S. Uhrig. Systematic mapping of the Hubbard model to the generalized *t-J* model. *Phys. Rev. B*, 70:245124, Dec 2004.

[45] S. Duffe and G.S. Uhrig. Hole dispersions for antiferromagnetic spin-$\frac{1}{2}$12 two-leg ladders by self-similar continuous unitary transformations. *The European Physical Journal B*, 84(3):475–490, 2011.

[46] H. Y. Yang and K. P. Schmidt. Effective models for gapped phases of strongly correlated quantum lattice models. *EPL (Europhysics Letters)*, 94(1):17004, 2011.

[47] H. Krull, N. A. Drescher, and G. S. Uhrig. Enhanced perturbative continuous unitary transformations. *Phys. Rev. B*, 86:125113, Sep 2012.

[48] M. Powalski, G. S. Uhrig, and K. P. Schmidt. Roton minimum as a fingerprint of magnon-higgs scattering in ordered quantum antiferromagnets. *Phys. Rev. Lett.*, 115:207202, Nov 2015.

[49] L G Marland. Series expansions for the zero-temperature transverse Ising model. *Journal of Physics A: Mathematical and General*, 14(8):2047, 1981.

[50] A.C. Irving and C.J. Hamer. Methods in hamiltonian lattice field theory (II). Linked-cluster expansions. *Nuclear Physics B*, 230(3):361 – 384, 1984.

[51] Rajiv R. P. Singh, Roger G. Melko, and Jaan Oitmaa. Thermodynamic singularities in the entanglement entropy at a two-dimensional quantum critical point. *Phys. Rev. B*, 86:075106, Aug 2012.

[52] H X He, C J Hamer, and J Oitmaa. High-temperature series expansions for the (2+1)-dimensional Ising model. *Journal of Physics A: Mathematical and General*, 23(10):1775, 1990.

[53] Martin P. Gelfand. Series expansions for excited states of quantum lattice models. *Solid State Communications*, 98(1):11–14, 1996.

[54] Simon Trebst, Hartmut Monien, Chris J. Hamer, Zheng Weihong, and Rajiv R. P. Singh. Strong-Coupling Expansions for Multiparticle Excitations: Continuum and Bound States. *Phys. Rev. Lett.*, 85:4373–4376, Nov 2000.

[55] Weihong Zheng, Chris J. Hamer, Rajiv R. P. Singh, Simon Trebst, and Hartmut Monien. Linked cluster series expansions for two-particle bound states. *Phys. Rev. B*, 63:144410, Mar 2001.

[56] C. Knetter, K. P. Schmidt, M. Grüninger, and G. S. Uhrig. Fractional and Integer Excitations in Quantum Antiferromagnetic Spin 1/2 Ladders. *Phys. Rev. Lett.*, 87:167204, Oct 2001.

[57] K. P. Schmidt, C. Knetter, and G. S. Uhrig. Raman response in antiferromagnetic two-leg S = 1/2 Heisenberg ladders. *EPL (Europhysics Letters)*, 56(6):877, 2001.

[58] Marcos Rigol, Tyler Bryant, and Rajiv R. P. Singh. Numerical Linked-Cluster Approach to Quantum Lattice Models. *Phys. Rev. Lett.*, 97:187202, Nov 2006.

[59] Marcos Rigol, Tyler Bryant, and Rajiv R. P. Singh. Numerical linked-cluster algorithms. I. Spin systems on square, triangular, and kagomé lattices. *Phys. Rev. E*, 75:061118, Jun 2007.

[60] Marcos Rigol, Tyler Bryant, and Rajiv R. P. Singh. Numerical linked-cluster algorithms. II. t-J models on the square lattice. *Phys. Rev. E*, 75:061119, Jun 2007.

[61] Ehsan Khatami, Rajiv R. P. Singh, and Marcos Rigol. Thermodynamics and phase transitions for the Heisenberg model on the pinwheel distorted kagome lattice. *Phys. Rev. B*, 84:224411, Dec 2011.

[62] Baoming Tang, Ehsan Khatami, and Marcos Rigol. A short introduction to numerical linked-cluster expansions . *Computer Physics Communications*, 184(3):557 – 564, 2013.

[63] Hong-Yu Yang, A Fabricio Albuquerque, Sylvain Capponi, Andreas M Läuchli, , and Kai Phillip Schmidt. Effective spin couplings in the Mott insulator of the honeycomb lattice Hubbard model . *New Journal of Physics*, 11:115027, 2012.

[64] D. Ixert, F. F. Assaad, and K. P. Schmidt. Mott physics in the half-filled Hubbard model on a family of vortex-full square lattices. *Phys. Rev. B*, 90:195133, Nov 2014.

[65] Ann B. Kallin, Katharine Hyatt, Rajiv R. P. Singh, and Roger G. Melko. Entanglement at a Two-Dimensional Quantum Critical Point: A Numerical Linked-Cluster Expansion Study. *Phys. Rev. Lett.*, 110:135702, Mar 2013.

[66] M. Rigol. Quantum Quenches in the Thermodynamic Limit. *Phys. Rev. Lett.*, 112:170601, Apr 2014.

[67] Marcos Rigol. Quantum quenches in the thermodynamic limit. II. Initial ground states. *Phys. Rev. E*, 90:031301, Sep 2014.

[68] Trithep Devakul and Rajiv R. P. Singh. Early Breakdown of Area-Law Entanglement at the Many-Body Delocalization Transition. *Phys. Rev. Lett.*, 115:187201, Oct 2015.

[69] K. Coester and K. P. Schmidt. Optimizing linked-cluster expansions by white graphs. *Phys. Rev. E*, 92:022118, Aug 2015.

[70] K. Coester, S. Clever, F. Herbst, S. Capponi, and K. P. Schmidt. A generalized perspective on non-perturbative linked-cluster expansions. *EPL (Europhysics Letters)*, 110(2):20006, 2015.

[71] Daniel Huerga, Jorge Dukelsky, and Gustavo E. Scuseria. Composite Boson Mapping for Lattice Boson Systems. *Phys. Rev. Lett.*, 111:045701, Jul 2013.

[72] E. R. Gagliano and C. A. Balseiro. Dynamical Properties of Quantum Many-Body Systems at Zero Temperature. *Phys. Rev. Lett.*, 59:2999–3002, Dec 1987.

[73] Christian Knetter. *Perturbative Continuous Unitary Transformations: Spectral Properties of Low Dimensional Spin Systems*. PhD thesis, Köln, 2003.

[74] Kai P. Schmidt. *Spectral Properties of Quasi One-dimensional Quantum Antiferromagnets Perturbative Continuous Unitary Transformations*. PhD thesis, Cologne, 2004.

[75] A. J. A. James, F. H. L. Essler, and R. M. Konik. Finite-temperature dynamical structure factor of alternating heisenberg chains. *Phys. Rev. B*, 78:094411, Sep 2008.

[76] Fabian H. L. Essler and Robert M. Konik. Finite-temperature lineshapes in gapped quantum spin chains. *Phys. Rev. B*, 78:100403, Sep 2008.

[77] Benedikt Fauseweh, Joachim Stolze, and Götz S. Uhrig. Finite-temperature line shapes of hard-core bosons in quantum magnets: A diagrammatic approach tested in one dimension. *Phys. Rev. B*, 90:024428, Jul 2014.

[78] M. E. Zhitomirsky and A. L. Chernyshev. *Colloquium* : Spontaneous magnon decays. *Rev. Mod. Phys.*, 85:219–242, Jan 2013.

[79] Jaan Oitmaa, Christopher Hamer, and Weihong Zheng. Series expansion methods for strongly interacting lattice models. 2006.

[80] Martin P. Gelfand and Rajiv R. P. Singh. High-order convergent expansions for quantum many particle systems. *Advances in Physics*, 49(1):93–140, 2000.

[81] G S Rushbrooke and P J Wood. On the High-Temperature Susceptibility for the Heisenberg Model of a Ferromagnet. *Proceedings of the Physical Society. Section A*, 68(12):1161, 1955.

[82] G. S. Rushbrooke. On the Theory of Randomly Dilute Ising and Heisenberg Ferromagnetics. *Journal of Mathematical Physics*, 5(8):1106–1116, 1964.

[83] G.A. Baker, H.E. Gilbert, J. Eve, and G.S. Rushbrooke. On the heisenberg spin 12 ferromagnetic models. *Physics Letters*, 20(2):146 – 147, 1966.

[84] G.A. Baker Jr., H.E. Gilbert, J. Eve, and G.S. Rushbrooke. On the two-dimensional, spin-12 Heisenberg ferromagnetic models . *Physics Letters A*, 25(3):207 – 209, 1967.

[85] Zheng Weihong, J. Oitmaa, and C. J. Hamer. Square-lattice Heisenberg antiferromagnet at T =0. *Phys. Rev. B*, 43:8321–8330, Apr 1991.

[86] C. J. Hamer, Zheng Weihong, and J. Oitmaa. Spin-wave stiffness of the Heisenberg antiferromagnet at zero temperature. *Phys. Rev. B*, 50:6877–6888, Sep 1994.

[87] Christian Knetter, Kai P Schmidt, and Götz S Uhrig. The structure of operators in effective particle-conserving models. *Journal of Physics A: Mathematical and General*, 36(29):7889, 2003.

[88] Hong-Yu Yang, Andreas M. Läuchli, Frédéric Mila, and Kai Phillip Schmidt. Effective Spin Model for the Spin-Liquid Phase of the Hubbard Model on the Triangular Lattice. *Phys. Rev. Lett.*, 105:267204, Dec 2010.

[89] M. Powalski, K. Coester, R. Moessner, and K. P. Schmidt. Disorder by disorder and flat bands in the kagome transverse field Ising model. *Phys. Rev. B*, 87:054404, Feb 2013.

[90] Marc Daniel Schulz, Sébastien Dusuel, Kai Phillip Schmidt, and Julien Vidal. Topological Phase Transitions in the Golden String-Net Model. *Phys. Rev. Lett.*, 110:147203, Apr 2013.

[91] Marc Daniel Schulz, Sébastien Dusuel, Grégoire Misguich, Kai Phillip Schmidt, and Julien Vidal. Ising anyons with a string tension. *Phys. Rev. B*, 89:201103, May 2014.

[92] Darshan G. Joshi, Kris Coester, Kai P. Schmidt, and Matthias Vojta. Nonlinear bond-operator theory and $1/d$ expansion for coupled-dimer magnets. I. Paramagnetic phase. *Phys. Rev. B*, 91:094404, Mar 2015.

[93] B. Tang, D. Iyer, and M. Rigol. Thermodynamics of two-dimensional spin models with bimodal random-bond disorder. *ArXiv e-prints*, January 2015.

[94] E. M. Stoudenmire, Peter Gustainis, Ravi Johal, Stefan Wessel, and Roger G. Melko. Corner contribution to the entanglement entropy of strongly interacting O(2) quantum critical systems in 2+1 dimensions. *Phys. Rev. B*, 90:235106, Dec 2014.

[95] Sylvain Capponi and Didier Poilblanc. Charge density correlations in $t - J$ ladders investigated by the contractor-renormalization method. *Phys. Rev. B*, 66:180503, Nov 2002.

[96] Sylvain Capponi, Andreas Läuchli, and Matthieu Mambrini. Numerical contractor renormalization method for quantum spin models. *Phys. Rev. B*, 70:104424, Sep 2004.

[97] A. Abendschein and S. Capponi. Contractor-renormalization approach to frustrated magnets in a magnetic field. *Phys. Rev. B*, 76:064413, Aug 2007.

[98] Sébastien Dusuel, Michael Kamfor, Kai Phillip Schmidt, Ronny Thomale, and Julien Vidal. Bound states in two-dimensional spin systems near the Ising limit: A quantum finite-lattice study. *Phys. Rev. B*, 81:064412, Feb 2010.

[99] Sylvain Capponi. private communication.

[100] Stanisław D. Głazek and Kenneth G. Wilson. Renormalization of Hamiltonians. *Phys. Rev. D*, 48:5863–5872, Dec 1993.

[101] Jürgen Stein. Flow equations and the strong-coupling expansion for the Hubbard model. *Journal of Statistical Physics*, 88(1-2):487–511, 1997.

[102] Nils Alexander Drescher. *Variational and Perturbative Extensions of Continuous Unitary Transformations for Low-Dimensional Spin Systems*. PhD thesis, Dortmund, 2014.

[103] Michael Moeckel and Stefan Kehrein. Interaction Quench in the Hubbard Model. *Phys. Rev. Lett.*, 100:175702, May 2008.

[104] P. Wang and S. Kehrein. Flow equation calculation of transient and steady-state currents in the Anderson impurity model. *Phys. Rev. B*, 82:125124, Sep 2010.

[105] K. P. Schmidt and G. S. Uhrig. Hard-core magnons in the $S = 1/2$ Heisenberg model on the square lattice. *Phys. Rev. B*, 73:172407, May 2006.

[106] Jörn Krones and Götz S. Uhrig. Effective models for Anderson impurity and Kondo problems from continuous unitary transformations. *Phys. Rev. B*, 91:125102, Mar 2015.

[107] W. Hofstetter and S. Kehrein. Flow equation analysis of the anisotropic kondo model. *Phys. Rev. B*, 63:140402, Mar 2001.

[108] Dmitry Lobaskin and Stefan Kehrein. Crossover from nonequilibrium to equilibrium behavior in the time-dependent kondo model. *Phys. Rev. B*, 71:193303, May 2005.

[109] Sébastien Dusuel and Götz S Uhrig. The quartic oscillator: a non-perturbative study by continuous unitary transformations. *Journal of Physics A: Mathematical and General*, 37(39):9275, 2004.

[110] Andreas Mielke. Flow equations for band-matrices. *Euro. Phys. Jour. B*, 5:605–611, 1998.

[111] C.P. Heidbrink and G.S. Uhrig. Renormalization by continuous unitary transformations: one-dimensional spinless fermions. *The European Physical Journal B - Condensed Matter and Complex Systems*, 30(4):443–459, 2002.

[112] Alexander A. Reischl. *Derivation of Effective Models using Self-Similar Continuous Unitary Transformations in Real Space*. PhD thesis, Köln, 2006.

[113] Sebastian Duffe. *Effective Hamiltonians for Undoped and Hole-Doped Antiferromagnetic Spin-1/2 Ladders by Self-Similar Continuous Unitary Transformations in Real Space*. PhD thesis, Dortmund, 2011.

[114] M. Hafez Torbati, Nils A. Drescher, and Götz S. Uhrig. Dispersive excitations in one-dimensional ionic Hubbard model. *Phys. Rev. B*, 89:245126, Jun 2014.

[115] Mohsen Hafez-Torbati, Nils A. Drescher, and Götz S. Uhrig. From gapped excitons to gapless triplons in one dimension. *The European Physical Journal B*, 88(2), 2015.

[116] M. Hafez-Torbati and G. S. Uhrig. Orientational bond and N\'eel order in the two-dimensional ionic Hubbard model. *ArXiv e-prints*, September 2015.

[117] Magnetic ordering induced by interladder coupling in the spin-$\frac{1}{2}$ Heisenberg two-leg ladder antiferromagnet $C_9H_{18}N_2CuBr_4$, author = Hong, Tao and Schmidt, K. P. and Coester, K. and Awwadi, F. F. and Turnbull, M. M. and Qiu, Y. and Rodriguez-Rivera, J. A. and Zhu, M. and Ke, X. and Aoyama, C. P. and Takano, Y. and Cao, Huibo and Tian, W. and Ma, J. and Custelcean, R. and Zhou, H. D. and Matsuda, M. *Phys. Rev. B*, 89:174432, May 2014.

[118] J. Dorier, K. P. Schmidt, and F. Mila. Theory of Magnetization Plateaux in the Shastry-Sutherland Model. *Phys. Rev. Lett.*, 101:250402, Dec 2008.

[119] Julien Vidal, Sébastien Dusuel, and Kai Phillip Schmidt. Low-energy effective theory of the toric code model in a parallel magnetic field. *Phys. Rev. B*, 79:033109, Jan 2009.

[120] Onofre Rojas, C J Hamer, and J Oitmaa. A frustrated three-dimensional antiferromagnet: stacked J 1 – J 2 layers. *Journal of Physics: Condensed Matter*, 23(41):416001, 2011.

[121] Kris Coester. Series expansions for dimerized quantum spin systems. Master's thesis, TU Dortmmund, 2011.

[122] A. J. Guttmann. *Phase Transitions and Critical Phenomena*, volume 13. Academic, London, 1989.

[123] David A. Huse. Ground-state staggered magnetization of two-dimensional quantum Heisenberg antiferromagnets. *Phys. Rev. B*, 37:2380–2382, Feb 1988.

[124] Rajiv R. P. Singh and David A. Huse. Microscopic calculation of the spin-stiffness constant for the spin-(1/2 square-lattice Heisenberg antiferromagnet. *Phys. Rev. B*, 40:7247–7251, Oct 1989.

[125] M Takahashi. Half-filled hubbard model at low temperature. *Journal of Physics C: Solid State Physics*, 10(8):1289, 1977.

[126] Dominik Ixert, Tobias Tischler, and Kai P. Schmidt. Nonperturbative linked-cluster expansions for the trimerized ground state of the spin-one kagome Heisenberg model. *Phys. Rev. B*, 92:174422, Nov 2015.

[127] C. M. Dawson, J. Eisert, and T. J. Osborne. Unifying variational methods for simulating quantum many-body systems. *Phys. Rev. Lett.*, 100:130501, Mar 2008.

[128] G. H. Golub and R.Underwood. *The block Lanczos method for computing eigenvalues*. Academic Press, New York, 1977.

[129] Ernest R. Davidson. The iterative calculation of a few of the lowest eigenvalues and corresponding eigenvectors of large real-symmetric matrices. *Journal of Computational Physics*, 17(1):87 – 94, 1975.

[130] Gerard L. G. Sleijpen and Henk A. Van der Vorst. A Jacobi–Davidson Iteration Method for Linear Eigenvalue Problems. *SIAM Journal on Matrix Analysis and Applications*, 17(2):401–425, 1996.

[131] AndreasM. Läuchli. Numerical Simulations of Frustrated Systems. In Claudine Lacroix, Philippe Mendels, and Frédéric Mila, editors, *Introduction to Frustrated Magnetism*, volume 164 of *Springer Series in Solid-State Sciences*, pages 481–511. Springer Berlin Heidelberg, 2011.

[132] H. Q. Lin. Exact diagonalization of quantum-spin models. *Phys. Rev. B*, 42:6561–6567, Oct 1990.

[133] Sebastian Clever. Beschreibung kollektiver Anregungen mittels graphen-basierter kontinuierlicher unitärer Transformationen in zwei Dimensionen. Master's thesis, TU Dortmmund, 2014.

[134] B. Bernu and G. Misguich. Specific heat and high-temperature series of lattice models: Interpolation scheme and examples on quantum spin systems in one and two dimensions. *Phys. Rev. B*, 63:134409, Mar 2001.

[135] Ian Affleck, Tom Kennedy, Elliott H. Lieb, and Hal Tasaki. Rigorous results on valence-bond ground states in antiferromagnets. *Phys. Rev. Lett.*, 59:799–802, Aug 1987.

[136] T. Barnes, E. Dagotto, J. Riera, and E. S. Swanson. Excitation spectrum of Heisenberg spin ladders. *Phys. Rev. B*, 47:3196–3203, Feb 1993.

[137] D. G. Shelton, A. A. Nersesyan, and A. M. Tsvelik. Antiferromagnetic spin ladders: Crossover between spin S =1/2 and S =1 chains. *Phys. Rev. B*, 53:8521–8532, Apr 1996.

[138] Masatomo Uehara, Takashi Nagata, Jun Akimitsu, Hiroki Takahashi, Nobuo Môri, and Kyoichi Kinoshita. Superconductivity in the Ladder Material Sr0.4Ca13.6Cu24O41.84. *Journal of the Physical Society of Japan*, 65(9):2764–2767, 1996.

[139] Kedar Damle and Subir Sachdev. Spin dynamics and transport in gapped one-dimensional Heisenberg antiferromagnets at nonzero temperatures. *Phys. Rev. B*, 57:8307–8339, Apr 1998.

[140] O. P. Sushkov and V. N. Kotov. Bound States of Magnons in the $S = 1/2$ Quantum Spin Ladder. *Phys. Rev. Lett.*, 81:1941–1944, Aug 1998.

[141] Christoph Jurecka and Wolfram Brenig. Optical absorption of spin ladders. *Phys. Rev. B*, 61:14307–14310, Jun 2000.

[142] K. P. Schmidt and G. S. Uhrig. Spectral Properties of Magnetic Excitations in Cuprate Two-Leg Ladder Systems. *Modern Physics Letters B*, 19(24):1179–1205, 2005.

[143] K. Kojima, A. Keren, G. M. Luke, B. Nachumi, W. D. Wu, Y. J. Uemura, M. Azuma, and M. Takano. Magnetic Behavior of the 2-Leg and 3-Leg Spin Ladder Cuprates $Sr_{n-1}Cu_{n+1}O_{2n}$. *Phys. Rev. Lett.*, 74:2812–2815, Apr 1995.

[144] H. Schwenk, M. Sieling, D. König, W. Palme, S.A. Zvyagin, B. Lüthi, and R.S. Eccleston. Magnetic resonances and magnetization in the spin ladder compound (VO)2P2O7 . *Solid State Communications*, 100(6):381 – 384, 1996.

[145] R. S. Eccleston, M. Azuma, and M. Takano. Neutron-scattering and susceptibility study of spin chains and spin ladders in $(Sr_{0.8}Ca_{0.2})_{14}$ Cu_{24} O_{41}. *Phys. Rev. B*, 53:R14721–R14724, Jun 1996.

[146] Ken-ichi Kumagai, Sigenori Tsuji, Masatsune Kato, and Yoji Koike. NMR Study of Carrier Doping Effects on Spin Gaps in the Spin Ladder $Sr_{14-x}A_xCu_{24}O_{41}$ ($A = Ca$, Y, and La). *Phys. Rev. Lett.*, 78:1992–1995, Mar 1997.

[147] Philip R. Hammar, Daniel H. Reich, Collin Broholm, and Frans Trouw. Spin gap in a quasi-one-dimensional $S = \frac{1}{2}$ antiferromagnet: $Cu_2(1,4-\text{diazacycloheptane})_2Cl_4$. *Phys. Rev. B*, 57:7846–7853, Apr 1998.

[148] S. Sugai and M. Suzuki. Magnetic Raman Scattering in Two-Leg Spin Ladder Sr14—x—yCaxYyCu24O41. *physica status solidi (b)*, 215(1):653–659, 1999.

[149] M. Matsuda, K. Katsumata, R. S. Eccleston, S. Brehmer, and H.-J. Mikeska. Magnetic excitations and exchange interactions in the spin-$\frac{1}{2}$ two-leg ladder compound $La_6Ca_8Cu_{24}O_{41}$. *Phys. Rev. B*, 62:8903–8908, Oct 2000.

[150] M. J. Konstantinović, J. C. Irwin, M. Isobe, and Y. Ueda. Low-energy excitations in NaV_2O_5. *Phys. Rev. B*, 65:012404, Nov 2001.

[151] M Grüninger, M Windt, T Nunner, C Knetter, K.P Schmidt, G.S Uhrig, T Kopp, A Freimuth, U Ammerahl, B Büchner, and A Revcolevschi. Magnetic excitations in two-leg spin 1/2 ladders: experiment and theory . *Journal of Physics and Chemistry of Solids*, 63(12):2167 – 2173, 2002. Proceedings of the Conference on Spectroscopies in Novel Superconductors.

[152] S. Notbohm, P. Ribeiro, B. Lake, D. A. Tennant, K. P. Schmidt, G. S. Uhrig, C. Hess, R. Klingeler, G. Behr, B. Büchner, M. Reehuis, R. I. Bewley, C. D. Frost, P. Manuel, and R. S. Eccleston. One- and Two-Triplon Spectra of a Cuprate Ladder. *Phys. Rev. Lett.*, 98:027403, Jan 2007.

[153] Alexander Shapiro, and Christopher P. Landee, and Mark M. Turnbull, and Joaquim Jornet, and Mercè Deumal, and Juan J. Novoa, and Michael A. Robb, and and William Lewis. Synthesis, structure, and magnetic properties of an antiferromagnetic spin-ladder complex: Bis(2,3-dimethylpyridinium) tetrabromocuprate. *Journal of the American Chemical Society*, 129(4):952–959, 2007. PMID: 17243832.

[154] A. T. Savici, G. E. Granroth, C. L. Broholm, D. M. Pajerowski, C. M. Brown, D. R. Talham, M. W. Meisel, K. P. Schmidt, G. S. Uhrig, and S. E. Nagler. Neutron scattering evidence for isolated spin-$\frac{1}{2}$ ladders in $(C_5D_{12}N)_2CuBr_4$. *Phys. Rev. B*, 80:094411, Sep 2009.

[155] Tao Hong, Y. H. Kim, C. Hotta, Y. Takano, G. Tremelling, M. M. Turnbull, C. P. Landee, H.-J. Kang, N. B. Christensen, K. Lefmann, K. P. Schmidt, G. S. Uhrig, and C. Broholm. Field-Induced Tomonaga-Luttinger Liquid Phase of a Two-Leg Spin-1/2 Ladder with Strong Leg Interactions. *Phys. Rev. Lett.*, 105:137207, Sep 2010.

[156] D. Schmidiger, S. Mühlbauer, S. N. Gvasaliya, T. Yankova, and A. Zheludev. Long-lived magnons throughout the Brillouin zone of the strong-leg spin ladder $(C_7H_{10}N)_2CuBr_4$. *Phys. Rev. B*, 84:144421, Oct 2011.

[157] D. Schmidiger, S. Muehlbauer, A. Zheludev, P. Bouillot, T. Giamarchi, C. Kollath, G. Ehlers, and A. M. Tsvelik. Symmetric and asymmetric excitations of a strong-leg quantum spin ladder. *Phys. Rev. B*, 88:094411, Sep 2013.

[158] S. Brehmer, H.-J. Mikeska, M. Müller, N. Nagaosa, and S. Uchida. Effects of biquadratic exchange on the spectrum of elementary excitations in spin ladders. *Phys. Rev. B*, 60:329–334, Jul 1999.

[159] Nobuyasu Haga and Sei-ichiro Suga. Dynamical structure factors of $S = \frac{1}{2}$ two-leg spin-ladder systems. *Phys. Rev. B*, 66:132415, Oct 2002.

[160] Carsten Nase. private communication.

[161] Johannes Konstantin Splinter. Untersuchung der magnetischen Eigenschaften der antiferromagnetischen Spin S=1/2 Zweibeinleiter mittels graphen-basierter kontinuierlicher unitaerer Transformation. Master's thesis, TU Dortmmund, 2012.

[162] H. Bethe. Zur Theorie der Metalle. *Zeitschrift für Physik*, 71(3-4):205–226, 1931.

[163] L. Hulthén. Ueber das Austauschproblem eines Kristalles. *Arkiv foer Matematik, Astronomi och Fysik*, 26A(11):1–106, 1939.

[164] C. N. Yang and C. P. Yang. One-Dimensional Chain of Anisotropic Spin-Spin Interactions. I. Proof of Bethe's Hypothesis for Ground State in a Finite System. *Phys. Rev.*, 150:321–327, Oct 1966.

[165] Jacques des Cloizeaux and J. J. Pearson. Spin-Wave Spectrum of the Antiferromagnetic Linear Chain. *Phys. Rev.*, 128:2131–2135, Dec 1962.

[166] L.D. Faddeev and L.A. Takhtajan. What is the spin of a spin wave? *Physics Letters A*, 85(6):375 – 377, 1981.

[167] Rajiv R. P. Singh and Zheng Weihong. Dynamical transition from triplets to spinon excitations: A series expansion study of the $J_1{-}J_2 - \delta$ spin-$\frac{1}{2}$ chain. *Phys. Rev. B*, 59:9911–9915, Apr 1999.

[168] M. C. Cross and Daniel S. Fisher. A new theory of the spin-Peierls transition with special relevance to the experiments on TTFCuBDT. *Phys. Rev. B*, 19:402–419, Jan 1979.

[169] I Affleck, D Gepner, H J Schulz, and T Ziman. Critical behaviour of spin-s Heisenberg antiferromagnetic chains: analytic and numerical results. *Journal of Physics A: Mathematical and General*, 22(5):511, 1989.

[170] Kai P. Schmidt, Christian Knetter, and Götz S. Uhrig. Spectral properties of the dimerized and frustrated $S = 1/2$ chain. *Phys. Rev. B*, 69:104417, Mar 2004.

[171] Chris J. Hamer, Weihong Zheng, and Rajiv R. P. Singh. Dynamical structure factor for the alternating Heisenberg chain: A linked cluster calculation. *Phys. Rev. B*, 68:214408, Dec 2003.

[172] Masashi Hase, Ichiro Terasaki, and Kunimitsu Uchinokura. Observation of the spin-Peierls transition in linear Cu^{2+} (spin-1/2) chains in an inorganic compound $CuGeO_3$. *Phys. Rev. Lett.*, 70:3651–3654, Jun 1993.

[173] M. Nishi, O. Fujita, and J. Akimitsu. Neutron-scattering study on the spin-Peierls transition in a quasi-one-dimensional magnet $CuGeO_3$. *Phys. Rev. B*, 50:6508–6510, Sep 1994.

[174] José Riera and Ariel Dobry. Magnetic susceptibility in the spin-Peierls system $CuGeO_3$. *Phys. Rev. B*, 51:16098–16102, Jun 1995.

[175] G. Castilla, S. Chakravarty, and V. J. Emery. Quantum Magnetism of $CuGeO_3$. *Phys. Rev. Lett.*, 75:1823–1826, Aug 1995.

[176] S. E. Nagler, D. A. Tennant, R. A. Cowley, T. G. Perring, and S. K. Satija. Spin dynamics in the quantum antiferromagnetic chain compound $KCuF_3$. *Phys. Rev. B*, 44:12361–12368, Dec 1991.

[177] T. Ami, M. K. Crawford, R. L. Harlow, Z. R. Wang, D. C. Johnston, Q. Huang, and R. W. Erwin. Magnetic susceptibility and low-temperature structure of the linear chain cuprate Sr_2CuO_3. *Phys. Rev. B*, 51:5994–6001, Mar 1995.

[178] N. Motoyama, H. Eisaki, and S. Uchida. Magnetic Susceptibility of Ideal Spin 1 /2 Heisenberg Antiferromagnetic Chain Systems, Sr_2CuO_3 and $SrCuO_2$. *Phys. Rev. Lett.*, 76:3212–3215, Apr 1996.

[179] Elbio Dagotto and T. M. Rice. Surprises on the Way from One- to Two-Dimensional Quantum Magnets: The Ladder Materials. *Science*, 271(5249):618–623, 1996.

[180] T. M. Rice, S. Gopalan, and M. Sigrist. Superconductivity, Spin Gaps and Luttinger Liquids in a Class of Cuprates. *EPL (Europhysics Letters)*, 23(6):445, 1993.

[181] S. R. White, R. M. Noack, and D. J. Scalapino. Resonating Valence Bond Theory of Coupled Heisenberg Chains. *Phys. Rev. Lett.*, 73:886–889, Aug 1994.

[182] Elliott Lieb, Theodore Schultz, and Daniel Mattis. Two soluble models of an antiferromagnetic chain. *Annals of Physics*, 16(3):407–466, 1961.

[183] Ian Affleck and ElliottH. Lieb. A proof of part of Haldane's conjecture on spin chains. *Letters in Mathematical Physics*, 12(1):57–69, 1986.

[184] Ian Affleck. Spin gap and symmetry breaking in CuO_2 layers and other antiferromagnets. *Phys. Rev. B*, 37:5186–5192, Apr 1988.

[185] F. D. M. Haldane. Nonlinear Field Theory of Large-Spin Heisenberg Antiferromagnets: Semiclassically Quantized Solitons of the One-Dimensional Easy-Axis Néel State. *Phys. Rev. Lett.*, 50:1153–1156, Apr 1983.

[186] I V Golosovsky, A G Gukasov, V A Polyakov, D I Zhigunov, and I A Zobkalo. Magnetic structure of lanthanum copper oxide La 2 Cu 2 O 5. *Journal of Physics: Condensed Matter*, 11(36):6959, 1999.

[187] M Matsuda, I Watanabe, and K Nagamine. Magnetic ordering in La2Cu2O5. *Physica B: Condensed Matter*, 289–290:161 – 164, 2000.

[188] Kazutaka Kudo, Takashi Noji, Yoji Koike, Terukazu Nishizaki, and Norio Kobayashi. Thermal Conductivity of the Four-Leg Spin-Ladder System La2Cu2O5 Single Crystal. *Journal of Low Temperature Physics*, 131(3-4):725–729, 2003.

[189] Markus Grueninger. private communication.

[190] R. Coldea, S. M. Hayden, G. Aeppli, T. G. Perring, C. D. Frost, T. E. Mason, S.-W. Cheong, and Z. Fisk. Spin Waves and Electronic Interactions in La_2CuO_4. *Phys. Rev. Lett.*, 86:5377–5380, Jun 2001.

[191] N Flocke. Fully variational resonance-valence-bond results on two-, three- and four-legged spin-1/2 Heisenberg ladders. *Journal of Physics: Condensed Matter*, 11(36):6945, 1999.

[192] D. Poilblanc, H. Tsunetsugu, and T. M. Rice. Spin gaps in coupled t-J ladders. *Phys. Rev. B*, 50:6511–6514, Sep 1994.

[193] N Hatano, Y Nishiyama, and M Suzuki. A critical-amplitude relation for one-dimensional quantum transitions and determination of the exponent eta. *Journal of Physics A: Mathematical and General*, 27(18):6077, 1994.

[194] F. B. Ramos and J. C. Xavier. N-leg spin-S Heisenberg ladders: A density-matrix renormalization group study. *Phys. Rev. B*, 89:094424, Mar 2014.

[195] V. O. Garlea, A. Zheludev, L.-P. Regnault, J.-H. Chung, Y. Qiu, M. Boehm, K. Habicht, and M. Meissner. Excitations in a Four-Leg Antiferromagnetic Heisenberg Spin Tube. *Phys. Rev. Lett.*, 100:037206, Jan 2008.

[196] Marcelo Arlego and Wolfram Brenig. Series expansion analysis of a frustrated four-spin tube. *Phys. Rev. B*, 84:134426, Oct 2011.

[197] M. Arlego, W. Brenig, Y. Rahnavard, B. Willenberg, H. D. Rosales, and G. Rossini. Quantum phases of a frustrated four-leg spin tube. *Phys. Rev. B*, 87:014412, Jan 2013.

[198] F. A. Giomez Albarracin, M. Arlego, and H. D. Rosales. Magnetization plateaus and jumps in a frustrated four-leg spin tube under a magnetic field. *Phys. Rev. B*, 90:174403, Nov 2014.

[199] M. Lohoefer, T. Coletta, D. G. Joshi, F. F. Assaad, M. Vojta, S. Wessel, and F. Mila. Dynamical structure factors and excitation modes of the bilayer Heisenberg model. *ArXiv e-prints*, August 2015.

[200] Tycho S. Sikkenk, Kris Coester, Stefan Buhrandt, Kai P. Schmidt, and Lars Fritz. The transverse field Ising model on the three dimensional swedenborgite lattice: Disorder-by-disorder and an effective classical two dimensional dimer model. *to be published*, 2015.

[201] Matthias Vojta. Excitation Spectra of Disordered Dimer Magnets Near Quantum Criticality. *Phys. Rev. Lett.*, 111:097202, Aug 2013.

[202] Thomas Koffel, M. Lewenstein, and Luca Tagliacozzo. Entanglement Entropy for the Long-Range Ising Chain in a Transverse Field. *Phys. Rev. Lett.*, 109:267203, Dec 2012.

[203] M. E. Zayed, Ch. Rüegg, Th. Strässle, U. Stuhr, B. Roessli, M. Ay, J. Mesot, P. Link, E. Pomjakushina, M. Stingaciu, K. Conder, and H. M. Rønnow. Correlated Decay of Triplet Excitations in the Shastry-Sutherland Compound $SrCu_2(BO_3)_2$. *Phys. Rev. Lett.*, 113:067201, Aug 2014.

[204] Tao Hong, Y. Qiu, D. A. Tennant, K. Coester, K. P. Schmidt, F. F. Awwadi, and M. M. Turnbull. Spontaneous magnon decay and universal scaling behavior at nite magnetic fields in a spin-1/2 coupled two-leg ladder antiferromagnet $C_9H_{18}N_2CuBr_4$ with small Ising anisotropy. *submitted to Phys. Rev. Lett.*, 2015.

[205] B.H. Brandow. Perturbation theory of effective Hamiltonians. In B.R. Barrett, editor, *Effective Interactions and Operators in Nuclei*, volume 40 of *Lecture Notes in Physics*, pages 1–24. Springer Berlin Heidelberg, 1975.

[206] Vladir Kvasnicka. *Application of Diagrammatic Quasidegenerate Rspt in Quantum Molecular Physics*, pages 345–412. John Wiley and Sons, Inc., 2007.

[207] Philippe Durand and Jean-Paul Malrieu. *Effective Hamiltonians and Pseudo-Operators as Tools for Rigorous Modelling*, pages 321–412. John Wiley and Sons, Inc., 2007.

[208] J P Malrieu, P Durand, and J P Daudey. Intermediate Hamiltonians as a new class of effective Hamiltonians. *Journal of Physics A: Mathematical and General*, 18(5):809, 1985.

[209] S. Evangelisti, J. P. Daudey, and J. P. Malrieu. Qualitative intruder-state problems in effective Hamiltonian theory and their solution through intermediate Hamiltonians. *Phys. Rev. A*, 35:4930–4941, Jun 1987.

[210] Colin J. Morningstar and Marvin Weinstein. Contractor renormalization group technology and exact hamiltonian real-space renormalization group transformations. *Phys. Rev. D*, 54:4131–4151, Sep 1996.

[211] J. Piekarewicz and J. R. Shepard. Dynamic spin response for Heisenberg ladders. *Phys. Rev. B*, 57:10260–10263, May 1998.

Danksagung

Zuallererst gehört der größte Dank Dr. Kai Schmidt, der mich wirklich absolut vorbildlich betreut hat. Wir haben stets mit Begeisterung diskutiert und nicht nur die Physik verstanden. Darüber hinaus danke ich Prof. Dr. Frithjof Anders für die Begutachtung der Arbeit.
Natürlich danke ich auch meiner Familie. Ich danke demütig meinen beiden Eltern, die der Grundstein von allem sind und deren Liebe ich sehr zu schätzen weiß. Nicht unerwähnt sollte bleiben, dass das Buch *Wissen für Kinder - Forschung und Technik*, das Karl-Hans Neuhaus mir vor zwanzig Jahren geschenkt hat, mich in Bahnen gelenkt hat, dich mich nun zu diesem Punkt geführt haben. Außerdem danke ich der gesamten Arbeitsgruppe Schmidt, die mit dem höchsten Soja-Konsum pro Kopf an der gesamten TU Dortmund die Welt jeden Tag ein bisschen besser machen möchte.
In der Studienzeit bin ich so vielen beeindruckenden, interessanten und lieben Menschen begegnet, denen eine kurze Aufführung hier nicht gerecht werden würde. Ich bin deswegen redlich bemüht, mich im echten Leben dankbarer zu zeigen und auch wieder mehr Zeit für sie zu haben.
Der letze Dank gilt Nina Gausmann, meinem Lieblingsmenschen und meiner Zuflucht.